



Prediction of the Cancer Patients' Response to their Therapeutical Treatment with Non-linear Forecasting Techniques

Sotirios G. Liliopoulos

Submitted in partial fulfilment of the requirements for the Degree of
Master of Science in Electrical and Computer Engineering

in the

School of Electrical and Computer Engineering
(Research M.Sc. in ECE Subjects)

Examination Committee

Prof. George S. Stavrakakis (Advisor)

Prof. Michael Zervakis

Prof. Konstantinos Balas

December 2023



**Πρόγνωση της Απόκρισης Καρκινοπαθών στην Εκάστοτε
Χορηγούμενη Θεραπευτική Αγωγή με Τεχνικές Μη-
γραμμικής Πρόβλεψης**

Σωτήριος Γ. Λιλιόπουλος

Υποβλήθηκε για την μερική εκπλήρωση των απαιτήσεων για τη
λήψη του

**Διπλώματος Μεταπτυχιακών Σπουδών Ηλεκτρολόγου
Μηχανικού και Μηχανικών Υπολογιστών**

από τη

Σχολή Ηλεκτρολόγων Μηχανικών κ Μηχανικών Υπολογιστών
(Research M.Sc. in ECE Subjects)

Εξεταστική Επιτροπή

Καθ. Γεώργιος Σ. Σταυρακάκης (Επιβλέπων)

Καθ. Μιχαήλ Ζερβάκης, Καθ. Κωνσταντίνος Μπάλας

Δεκέμβριος 2023

Sotirios G. Liliopoulos

sliliopoulos@tuc.gr

ORCID iD: 0000-0002-7338-977X

© Sotirios G. Liliopoulos 2023

This work is licensed under a [Creative Commons Attribution 4.0 International License](https://creativecommons.org/licenses/by/4.0/)

Declaration

I hereby declare that the work presented in this thesis has not been submitted for any other degree or professional qualification, and that it is the result of my own independent work.

Sotirios G. Liliopoulos

4 December 2023

Date

Abstract

This thesis delves into the complexity of cancer, necessitating a multidisciplinary approach for effective understanding and treatment. Central to this exploration is the use of mathematical tumor modeling to understand and predict the growth of solid tumors under a variety of therapeutic interventions. First, an introduction to the key concepts underlying the dynamics of cancer and a thorough review of current treatment modalities is presented. A comprehensive review of state-of-the-art mathematical models that portray tumor growth in both unperturbed and perturbed scenarios, focusing on chemotherapy, immunotherapy, and their combination also takes place. A key part of this work is the application of optimal control theory to refine cancer therapy protocols. This includes a detailed examination of the clinically acclaimed Simeoni *et al.*'s tumor growth inhibition (TGI) model. That model is enhanced in this thesis with a novel formulation, the *augmented Simeoni et al.'s TGI* model, which also incorporates the drug pharmacokinetics. An optimal non-linear control problem is then introduced and solved, based on that novel formulation, using the state-dependent Riccati equation (SDRE) methodology to identify the most effective chemotherapy strategies for tumor eradication. Additionally, this thesis presents the Adaptive Neuro-Fuzzy Inference System (ANFIS) and introduces three *ANFIS TGI* model structures for mathematical modeling of tumor growth under chemotherapy. Further, a novel method for modeling TGI under the efficacy of single and in combination chemotherapy drugs is proposed. Specifically, two *autoregressive with exogenous inputs (ARX) TGI* models for solid tumor growth are identified and evaluated. The parameters of these models estimated using non-linear optimization and laboratory experimental data, have shown high accuracy in fitting experimental tumor growth data under chemotherapy effects, being a pioneering contribution of this work. The use of linear quadratic regulator (LQR) optimal control based on those *ARX TGI* models is then introduced and explored for determining optimal chemotherapy dosages under various periodic and intermittent treatment schedules. Finally, all the presented in this thesis TGI models' capability for short-term adaptive tumor growth predictions incorporating also moving (sliding) window techniques, is thoroughly investigated giving accurate and significant for the clinical practice and the

Prediction of the cancer patients' response to their therapeutical treatment with non-linear forecasting techniques

Abstract

new anticancer drug discovery research TGI prediction results. All the simulation results are presented and extensively discussed, leading to insightful conclusions.

Keywords: cancer, tumor growth inhibition (TGI), tumor growth mathematical modeling, tumor growth prediction, linear mathematical model, non-linear mathematical model, parameter estimation, step-ahead predictions, state-space representation, NNA, COMPLEX method of Box, ARX, ANFIS, optimal control, SDRE, LQR, chemotherapy, optimal drug dose administration, periodic chemotherapy, intermittent chemotherapy, metronomic chemotherapy.

Περίληψη

Ο καρκίνος είναι μια πολύπλοκη ασθένεια που απαιτεί διεπιστημονική προσέγγιση για την κατανόηση και τη θεραπεία της. Στην παρούσα εργασία, και με τη βοήθεια γραμμικών και μη-γραμμικών μαθηματικών μοντέλων, πραγματοποιείται μία προσπάθεια για την κατανόηση και την πρόβλεψη της ανάπτυξης συμπαγών καρκινικών όγκων υπό διαφορετικές θεραπευτικές προσεγγίσεις. Αρχικά, πραγματοποιείται μια εισαγωγή στις βασικές έννοιες που διέπουν τη «δυναμική» της ανάπτυξης-εξέλιξης του καρκίνου και μια διεξοδική ανασκόπηση των πιο ευρέως χρησιμοποιούμενων θεραπευτικών μεθόδων. Διεξάγεται επίσης μια ολοκληρωμένη ανασκόπηση των state-of-the-art μαθηματικών μοντέλων, που χρησιμοποιούνται για την περιγραφή ανάπτυξης όγκων υπό διαφορετικές μορφές θεραπείας, συμπεριλαμβανομένης της χημειοθεραπείας, της ανοσοθεραπείας και του συνδυασμού τους. Επιπλέον, γίνεται μια σύντομη εισαγωγή στη θεωρία βέλτιστου ελέγχου, ενώ παράλληλα τονίζεται η σημασία της στην ανάπτυξη και βελτιστοποίηση των πρωτοκόλλων (σχημάτων) αποτελεσματικής θεραπείας του καρκίνου. Με τη βοήθεια μη-γραμμικού μαθηματικού μοντέλου για την περιγραφή της εξέλιξης καρκινικών όγκων (*Simeoni et al.'s tumor growth inhibition – TGI model*) και την εισαγωγή επιπλέον φαρμακοκινητικών εξισώσεων στη δομή του (*augmented Simeoni et al.'s TGI model*) διαμορφώνεται ένα πρόβλημα βέλτιστου ελέγχου. Στόχος του είναι ο προσδιορισμός βέλτιστης στρατηγικής, με τη βοήθεια της μεθόδου SDRE (state-dependent Riccati equation), για τη χορήγηση βέλτιστων δόσεων χημειοθεραπείας με σκοπό την εξάλειψη της κακοήθειας με τις ελάχιστες παρενέργειες. Επιπλέον, αναπτύσσονται τρία νέα μοντέλα νευρο-ασαφούς λογικής (Adaptive Neuro-Fuzzy Inference System – ANFIS) για την περιγραφή της ανάπτυξης του καρκινικών όγκων υπό χημειοθεραπεία (*ANFIS TGI models*) και αξιολογείται η ικανότητά τους να μοντελοποιούν-αναπαριστούν με ακρίβεια τις πειραματικές καμπύλες ανάπτυξης του όγκου. Παρουσιάζεται επίσης μια νέα προσέγγιση για την περιγραφή της εξέλιξης ενός όγκου υπό την επίδραση ενός ή περισσότερων αντικαρκινικών φαρμάκων, που δίνονται σε συνδυασμό. Συγκεκριμένα, χρησιμοποιώντας αναδρομικές γραμμικές εξισώσεις διαφορών με εξωτερική είσοδο (autoregressive with exogenous inputs – ARX) δημιουργούνται και αξιολογούνται με τη χρήση εργαστηριακών δεδομένων από

Prediction of the cancer patients' response to their therapeutical treatment with non-linear forecasting techniques

Abstract

πειράματα σε ποντίκια δύο συστήματα μαθηματικής μοντελοποίησης καρκινικών όγκων (*ARX TGI models*). Παράλληλα, με τη χρήση ενός γραμμικού τετραγωνικού ρυθμιστή (linear quadratic regulator - LQR) διερευνώνται πιθανές βέλτιστες δοσολογίες χημειοθεραπείας, τόσο για περιοδικά (periodic) όσο και για διακοπτόμενα (intermittent) προγράμματα (σχήματα) θεραπείας. Τέλος, αξιολογείται η ικανότητα όλων αυτών των μοντέλων να πραγματοποιούν βραχυπρόθεσμες προβλέψεις της εξέλιξης μίας κακοήθους νεοπλασίας με την εφαρμογή μεθόδου «κινούμενου παραθύρου» (sliding window) στη χρονοσειρά των δεδομένων. Σημειωτέον, τα μοντέλα βραχυχρόνιας πρόβλεψης της εξέλιξης του καρκίνου, είτε υπόκειται, είτε όχι, σε θεραπεία, είναι μεγάλης σημασίας στην φαρμακευτική έρευνα ανάπτυξης νέων αντικαρκινικών φαρμάκων. Όλα τα αποτελέσματα των προσομοιώσεων παρουσιάζονται και αναλύονται λεπτομερώς.

Acknowledgements

With this thesis a journey of about 9 years of studying at the Technical University of Crete comes to an end. At this point I would like to acknowledge all the people who helped me and supported me during my studies in Chania.

Foremost, I would like to thank my supervisor Professor George Stavrakakis for his guidance throughout my undergraduate and postgraduate studies. His interest, enthusiasm and encouragement made the completion of this thesis possible. I have truly enjoyed our collaboration. I would also like to thank the members of the supervisory committee in charge, Professors Michael Zervakis and Konstantinos Balas for their thoughtful critiques and comments to improve the quality of my research.

I am also grateful to the Professor of Pharmacology at the Medical School of the University of Thessaly, Dr. Konstantinos Dimas not only for the valuable data he provided but also for his insightful feedback. Furthermore, I would like to thank Professor Anastasios Pouliezos (school of Production Engineering and Management of TUC, retired) for his suggestions and the interesting discussions on the optimal control issues. Our discussions were very useful for my research.

Last but not least, I thank my friends in Chania, my parents Eleni and George, my brother Vasilis and my sister Olympia, for their continuous encouragement, understanding and endless support over the years. I am deeply grateful to them!

Vergina, December 2023

Sotirios G. Liliopoulos

Table of contents

Declaration	i
Abstract	ii
Keywords	iii
Περίληψη	iv
Acknowledgements	vi
Table of contents	viii
List of figures	xii
List of tables	xvii
List of abbreviations	xix
Chapter 1: Introduction	1
1.1 Cancer – Solid tumor growth	1
1.2 Current strategies for cancer therapy.....	5
1.2.1 Surgical operation.....	6
1.2.2 Radiation.....	6
1.2.3 Chemotherapy	6
1.2.4 Immunotherapy.....	8
1.2.5 Chemo-immunotherapy	10
1.3 Key contributions and novelty of this Thesis	11
1.4 Thesis organization	12
Chapter 2: Mathematical frameworks in tumor growth and treatment	14
2.1 A survey of mathematical models for tumor growth.....	14
2.1.1 Mathematical frameworks for tumor-immune interactions	22
2.2 Foundations of pharmacokinetic (PK) modeling	25
2.2.1 Compartment models in drug kinetics	25
2.3 Application of optimal control theory in cancer treatment.....	28

Prediction of the cancer patients' response to their therapeutical treatment with non-linear forecasting techniques

Table of contents

2.3.1	Optimal control theory in tumor growth modeling and treatment strategies	30
Chapter 3: Material and methods.....		32
3.1	Human-to-mouse xenograft data.....	32
3.2	The inverse problem: parameters estimation in mathematical modeling.....	33
3.3	Adaptive short-term ahead predictions of tumor growth evolution	36
3.4	Performance evaluation metrics	39
PART I Mathematical modeling approaches for efficient tumor growth inhibition predictions.....		40
Chapter 4: Tumor growth inhibition (TGI) mathematical model.....		41
4.1	The Simeoni's et al. TGI mathematical model.....	41
4.2	Model identification – TGI model's parameters values estimation	44
4.3	Short-term ahead predictions of the tumor growth inhibition	47
Chapter 5: Time series approaches to tumor growth inhibition: ARX modeling and predictive analysis		50
5.1	ARX models background	50
5.2	Identification and parameters estimation of ARX models for TGI	51
5.2.1	A single-agent dynamics based ARX TGI model	51
5.2.2	ARX modeling of TGI in multi-drug chemotherapy scenarios	53
5.3	Adaptive short-term ahead prediction of TGI using ARX models.....	56
5.3.1	Predictions of TGI for single-agent scenarios.....	56
5.3.2	Multi-agent ARX-based predictions of tumor inhibition.....	58
Chapter 6: Tumor growth modelling using adaptive neuron-fuzzy inference system (ANFIS).....		61
6.1	Introduction to ANFIS.....	61
6.2	ANFIS models for tumor growth inhibition modelling	64

Prediction of the cancer patients' response to their therapeutical treatment with non-linear forecasting techniques

Table of contents

6.2.1	An ANFIS TGI model for single-agent chemotherapy	65
6.2.2	ANFIS TGI models for multi-agent chemotherapy treatments	68
6.3	Evaluation of ANFIS models short-term ahead predictions of TGI	72
6.3.1	Single-drug chemotherapy – Predictions of TGI under gemcitabine	73
6.3.2	Multi-drug chemotherapy – Predictions of TGI in combination chemotherapy scenarios	76
PART II Efficient tumor eradication based on optimal control methods		82
Chapter 7: Non-linear optimal control for efficient tumor growth eradication		83
7.1	Optimized chemotherapy dosages in periodic treatment scenarios using the augmented TGI model and SDRE optimal control	88
7.2	Optimized chemotherapy dosages in intermittent treatment cases using the augmented TGI model and SDRE optimal control	92
Chapter 8: Linear quadratic control (LQC) applied for effective tumor growth eradication		95
8.1	ARX and LQR-based gemcitabine dosage optimization for periodic treatment schedules	99
8.2	Optimal gemcitabine dosages for intermittent treatment schedules using ARX and LQR	103
8.3	Multi-agent chemotherapy optimal control of tumor growth: The case of CPT-11 administered in combination with drug C2	106
Chapter 9: Discussion and conclusions		109
References.....		116
Appendix		137
Appendix A: Neural Network Algorithm (NNA)		137
Appendix B: Complex method of Box.....		141
Appendix C: LQR optimal control		143
Appendix D: SDRE – State-Dependent Riccati Equation		145

Prediction of the cancer patients' response to their therapeutical treatment with non-linear forecasting techniques

Table of contents

D.1 SDC parameterization.....	146
D.2 Non-affine control	148
D.3 Selection of the Q and R weighting matrices.....	149
Appendix E: State-space realization in control systems	151
E.1 Definition and representation.....	151
E.2 Transfer function relationship	151
E.3 Minimal Realization	151

List of figures

Figure 1.1. Cancer progression. Adapted from [2], [4].	2
Figure 1.2. Natural killer (NK) cells (yellow) display a killer inhibitory receptor (red) that can recognize MHC I receptors on the surface of potential target cells (gray). In the absence of MCH I, NK cell attacks the target cell (right). Otherwise, the attack is declined (left). Adapted by [10].	4
Figure 1.3. (Left) Diagram showing CAR T-cell therapy. (Right) Diagram showing the T cell before and after genetic engineering. Adapted from [42].	10
Figure 2.1. Simulated time curves of tumor size from the linear (top left), exponential (top right), logistic (bottom left) and Gompertz (bottom right) tumor growth models [71].	18
Figure 2.2. One-compartment model representing the transfer of the drug to the central compartment (plasma, etc.). k_{01} and k_{10} represent the first-order fractional rates for absorption and excretion of the drug.....	27
Figure 2.3. Two-compartment model representing the transfer of the drug to and from the central and peripheral compartments. k_{01} , k_{10} , k_{12} and k_{21} represent the first-order fractional rates for absorption, excretion, distribution, and redistribution.	27
Figure 3.1. Gemcitabine treatment schedule: 100 mg/kg administered at days 19 and 26 post tumor inoculation.	32
Figure 3.2. 5-FU and drug C2 treatment schedule: 50 mg/kg of 5-FU administered q4dx3 from day 9 and 60 mg/kg of drug C2 on days 10, 11, 12 and 14, 15, 16 post tumor inoculation.....	33
Figure 3.3. CPT-11 and drug C2 treatment schedule: 45 mg/kg of CPT-11 administered q4dx3 from day 9 and 60 mg/kg of drug C2 on days 10, 11, 12 and 14, 15, 16 post tumor inoculation.....	33
Figure 3.4. A non-convex objective function with a global minimum and multiple local minima.....	35
Figure 3.5. A convex function with one global minimum.	35
Figure 3.6. Comparator procedure between the physical experimental process of xenografted mice and the under fitting to the experimental data tumor growth inhibition model.	36
Figure 3.7. Flowchart of the proposed procedure for the measurement and the model update, ensuring effective adaptive short-term ahead tumor growth prediction.....	38
Figure 4.1. Diagram of the PK-PD TGI state-space model introduced by Simeoni et al. [226]. k_1 : first-order rate constant of transit; k_2 : anti-tumor potency of the anticancer agent, $c(t)$: plasma concentration of the anticancer agent and $w(t)$: tumor weight at any time t	42

Prediction of the cancer patients' response to their therapeutical treatment with non-linear forecasting techniques

List of figures

Figure 4.2. Plasma concentration of gemcitabine (measured in mg/L). Gemcitabine administrated as repeated i.p. doses at 100 mg/kg, with 7-days interval [230]..... 46

Figure 4.3. Observed/interpolated (black dots) and best fitted TGI mathematical model tumor growth curves obtained in mice given i.p. doses of gemcitabine (100 mg/kg on days 19 and 26) using the median (continuous line) and the mean (dashed line) of the estimated values of each unknown parameter. 46

Figure 4.4. Observed and time period (1 to 5 days) ahead adaptive prediction curves of the tumor growth in mice given doses of gemcitabine (100 mg/kg on days 19 and 26). Predictions performed after the 25th day of the experiment. 48

Figure 5.1. Observed/interpolated (black dots) and best fitted ARX (3,3) model tumor growth curves obtained in mice given i.p. doses of gemcitabine (100 mg/kg on days 19 and 26). 53

Figure 5.2. Observed/interpolated (black dots) and best fitted ARX (4,4) model tumor growth curves obtained in mice given doses of CPT-11 in combination with drug C2.. 55

Figure 5.3. Observed and time period (1 to 5 days) ahead adaptive prediction curves of the tumor growth in mice given doses of gemcitabine (100 mg/kg on days 19 and 26). Predictions performed after the 25th day of the experiment using ARX (3,3) model... 57

Figure 5.4. Observed curve and time period (1 to 5 days) ahead adaptive predictions of the tumor growth in mice given doses of CPT-11 and drug C2 (45 mg/kg q4dx3 from day 9 and 60 mg/kg on days 10, 11, 12 and 14, 15, 16). Predictions performed after the 16th day of the experiment using ARX (4,4) model. 59

Figure 6.1. Representation of an adaptive neuro fuzzy inference system (ANFIS) structure with two rules, for a system of one output (f) and two inputs (x and y). 61

Figure 6.2. Illustration of the TSK fuzzy inference method..... 62

Figure 6.3. A generalized bell-shaped membership function for fuzzy sets [236]..... 63

Figure 6.4. Case 1 – (Left) Observed/interpolated (*) and ANFIS model fitted tumor growth curves (in g) obtained in mice given i.p. doses of gemcitabine (100 mg/kg on Days 19 and 26). (Right) Curve fitting error by iteration. 67

Figure 6.5. Case 2 – (Left) Observed/interpolated (*) and ANFIS model fitted tumor growth curves (in g) obtained in mice given i.p. doses of gemcitabine (100 mg/kg on Days 19 and 26). (Right) Curve fitting error by iteration. 67

Figure 6.6. Case 3 – (Left) Observed/interpolated (*) and ANFIS model fitted tumor growth curves (in g) obtained in mice given i.p. doses of gemcitabine (100 mg/kg on Days 19 and 26). (Right) Curve fitting error by iteration. 67

Figure 6.7. Case 1 – (Left) Observed/interpolated (*) and ANFIS model fitted tumor growth curves (in g) obtained in mice given doses of CPT-11 and drug C2 (45 mg/kg q4dx3 from day 9 and 60 mg/kg on days 10, 11, 12 and 14, 15, 16). (Right) Curve fitting error by iteration. 70

Prediction of the cancer patients' response to their therapeutical treatment with non-linear forecasting techniques

List of figures

Figure 6.8. Case 2 – (Left) Observed/interpolated (*) and ANFIS model fitted tumor growth curves (in g) obtained in mice given doses of CPT-11 and drug C2 (45 mg/kg q4dx3 from day 9 and 60 mg/kg on days 10, 11, 12 and 14, 15, 16). (Right) Curve fitting error by iteration. 70

Figure 6.9. Case 3 – (Left) Observed/interpolated (*) and ANFIS model fitted tumor growth curves (in g) obtained in mice given doses of CPT-11 and drug C2 (45 mg/kg q4dx3 from day 9 and 60 mg/kg on days 10, 11, 12 and 14, 15, 16). (Right) Curve fitting error by iteration. 70

Figure 6.10. Case 1 – (Left) Observed/interpolated (*) and ANFIS model fitted tumor growth curves (in g) obtained in mice given doses of 5-FU and drug C2 (50 mg/kg q4dx3 from day 9 and 60 mg/kg on days 10, 11, 12 and 14, 15, 16). (Right) Curve fitting error by iteration. 71

Figure 6.11. Case 2 – (Left) Observed/interpolated (*) and ANFIS model fitted tumor growth curves (in g) obtained in mice given doses of 5-FU and drug C2 (50 mg/kg q4dx3 from day 9 and 60 mg/kg on days 10, 11, 12 and 14, 15, 16). (Right) Curve fitting error by iteration. 72

Figure 6.12. Case 3 – (Left) Observed/interpolated (*) and ANFIS model fitted tumor growth curves (in g) obtained in mice given doses of 5-FU and drug C2 (50 mg/kg q4dx3 from day 9 and 60 mg/kg on days 10, 11, 12 and 14, 15, 16). (Right) Curve fitting error by iteration. 72

Figure 6.13. Observed and time period (1 to 5 days) ahead adaptive prediction curves of the tumor growth in mice given i.p. doses of gemcitabine (100 mg/kg on days 19 and 26). Predictions performed after the 25th day of the experiment using ANFIS model (3,100) without moving window. 74

Figure 6.14. Observed curve and time period (1 to 5 days) ahead adaptive predictions of the tumor growth in mice given i.p. doses of gemcitabine (100 mg/kg on Days 19 and 26). Predictions performed after the 25th day of the experiment using ANFIS model (3,50) with moving window of $l=20$ measurements. 75

Figure 6.15. Observed curve and time period (1 to 5 days) ahead adaptive predictions of the tumor growth in mice given i.p. doses of gemcitabine (100 mg/kg on Days 19 and 26). Predictions performed after the 25th day of the experiment using ANFIS model (3,50) with moving window of $l =15$ measurements. 76

Figure 6.16. Observed curve and time period (1 to 5 days) ahead adaptive predictions of the tumor growth in mice given doses of 5-FU and drug C2 (50 mg/kg q4dx3 from day 9 and 60 mg/kg on days 10, 11, 12 and 14, 15, 16). Predictions performed after the 16th day of the experiment using ANFIS model (3,100). 78

Figure 6.17. Observed curve and time period (1 to 5 days) ahead adaptive predictions of the tumor growth in mice given doses of CPT-11 and drug C2 (45 mg/kg q4dx3 from day 9 and 60 mg/kg on days 10, 11, 12 and 14, 15, 16). Predictions performed after the 16th day of the experiment using ANFIS model (5,100). 79

Prediction of the cancer patients' response to their therapeutical treatment with non-linear forecasting techniques

List of figures

Figure 6.18. Prediction errors (MAPE %) for the time period ahead tumor growth inhibition predictions in mice given 5-FU and drug C2: TGIadd and ANFIS models. One, two and three time periods ahead. 80

Figure 6.19. Prediction errors (MAPE %) for the time period ahead tumor growth inhibition predictions in mice given CPT-11 and drug C2: TGIadd and ANFIS models. One, two and three time periods ahead. 81

Figure 7.1. The absolute determinant of the state-dependent controllability matrix $MC(x)$ against $x_2 = z_1$ (g) state of the augmented Simeoni's TGI model for various free design parameters θ 86

Figure 7.2. Augmented TGI system's response (i.e., tumor weight) and optimal control input (i.e., dose level). Continuous treatment: daily dose administration (Case 1). 89

Figure 7.3. Augmented TGI system's response (i.e., tumor weight) and optimal control input (i.e., dose level). Periodic treatment: dose administration every 2 days (Case 2). 90

Figure 7.4. Augmented TGI system's response (i.e., tumor weight) and optimal control input (i.e., dose level). Periodic treatment: dose administration every 3 days (Case 3). 91

Figure 7.5. Augmented TGI system's response (i.e., tumor weight) and optimal control input (i.e., dose level). Periodic treatment: dose administration every 5 days (Case 4). 91

Figure 7.6. Augmented TGI system's response (i.e., tumor weight) and optimal control input (i.e., dose level). Periodic treatment: dose administration every 7 days (Case 5). 92

Figure 7.7. Augmented TGI system's response (i.e., tumor weight) and optimal control input (i.e., dose level). Intermittent: q3dx5, q5dx5 dose administrations with 7 days pauses (Case 6). 94

Figure 7.8. Augmented TGI system's response (i.e., tumor weight) and optimal control input (i.e., dose level). Intermittent: q3dx5, q5dx5 dose administrations with 10 days pauses (Case7). 94

Figure 8.1. ARX system's response (i.e., tumor weight) and optimal control input (i.e., dose level) utilizing the initial "good" Q and R weights. Continuous treatment (daily drug administration starting from day 19). 98

Figure 8.2. ARX system's response (i.e., tumor weight) and optimal control input (i.e., dose level). Continuous treatment: daily dose administration (Case 1). 101

Figure 8.3. ARX's response (i.e., tumor weight) and optimal control input (i.e., dose level). Periodic treatment: dose administration every 2 days (Case 2). 101

Figure 8.4. ARX's response (i.e., tumor weight) and optimal control input (i.e., dose level). Periodic treatment: dose administration every 3 days (Case 3). 102

Prediction of the cancer patients' response to their therapeutical treatment with non-linear forecasting techniques

List of figures

Figure 8.5. ARX's response (i.e., tumor weight) and optimal control input (i.e., dose level). Periodic treatment: dose administration every 5 days (Case 4).	102
Figure 8.6. ARX's response (i.e., tumor weight) and optimal control input (i.e., dose level). Periodic treatment: dose administration every 7 days (Case 5).	103
Figure 8.7. ARX's response (i.e., tumor weight) and optimal control input (i.e., dose level). Intermittent treatment: q3dx5, q5dx5 dose administrations with 7 days pauses (Case 6).	105
Figure 8.8. ARX's response (i.e., tumor weight) and optimal control input (i.e., dose level). Intermittent treatment: q3dx5, q5dx5 dose administrations with 10 days pauses (Case 7).	106
Figure 9.1. Prediction errors (MAPE %) for the time period ahead tumor growth inhibition predictions in mice given gemcitabine i.p.: A comparison of Simeoni et al.'s TGI, ANFIS (3,50) and ARX (3,3) TGI models. One, two, three, four and five time periods ahead.	112
Figure 9.2. Prediction errors (MAPE %) for the time period ahead tumor growth inhibition predictions in mice given CPT-11 and drug C2: A comparison of TGIadd, ANFIS (5,100) and ARX (4,4) TGI models. One, two and three time periods ahead.	113

List of tables

Table 2.1. DePillis model parameters [156].	24
Table 2.2. Description of the ADME stages [175].	25
Table 3.1. Average tumor masses registered in the experiment of [220] (i.e., gemcitabine given i.p. at 100 mg/kg on days 19 and 26).	32
Table 4.1. Pharmacodynamic (PD) parameters of the TGI model.	43
Table 4.2. Value range of the TGI mathematical model principal parameters.	45
Table 4.3. TGI mathematical model fitting errors to the tumor growth experimental curve obtained in mice administered i.p. doses of gemcitabine (100 mg/kg on days 19 and 26).	47
Table 4.4. Pharmacodynamic parameters values of the TGI model. Obtained by best fitting the Simeoni TGI model to the tumor growth curve of mice given gemcitabine i.p. injections.	47
Table 4.5. Prediction errors for the time period (1 to 5 days) ahead adaptive tumor growth inhibition prediction in mice given i.p. doses of gemcitabine (100 mg/kg on days 19 and 26).	49
Table 5.1. Single agent ARX models fitting errors to the tumor growth experimental curve obtained in mice given i.p. doses of gemcitabine (100 mg/kg on days 19 and 26).	53
Table 5.2. Multi-agent ARX models fitting errors to the tumor growth experimental curve obtained in mice given doses of CPT-11 in combination with drug C2.	55
Table 6.3. Prediction errors for the time period (1 to 5 days) ahead adaptive tumor growth inhibition prediction in mice given doses of gemcitabine (100 mg/kg on days 19 and 26). Predictions performed with ARX (3,3) model.	57
Table 6.4. Prediction errors for the time period (1 to 5 days) ahead adaptive tumor growth inhibition prediction in mice given doses of CPT-11 and drug C2 (45 mg/kg q4dx3 from day 9 and 60 mg/kg on days 10, 11, 12 and 14, 15, 16). Predictions performed with ARX (4,4) model.	59
Table 6.1. Inputs and outputs of the ANFIS tumor growth inhibition model for the case of single agent chemotherapy (gemcitabine i.p.).	65
Table 6.2. Configurations of the tested ANFIS structures for the case of single agent chemotherapy (gemcitabine i.p.).	66
Table 6.3. Evaluation (i.e., fitting errors to the tumor growth experimental curve) of the ANFIS model for different structure configurations for the case of single agent chemotherapy (gemcitabine i.p.).	66
Table 6.4. Inputs and outputs of the ANFIS tumor growth inhibition model for the case of multi-agent chemotherapy.	68

Prediction of the cancer patients' response to their therapeutical treatment with non-linear forecasting techniques

List of tables

Table 6.5. Configurations of the tested ANFIS structures ANFIS for the cases of multi-agent chemotherapy treatment.	69
Table 6.6. Evaluation (i.e., fitting errors to the tumor growth experimental curve) of the ANFIS model for different structure configurations for the case of CPT-11 given with drug C2.....	69
Table 6.7. Evaluation (i.e., fitting errors to the tumor growth experimental curve) of the ANFIS model for different structure configurations for the case of 5-FU given with drug C2.....	71
Table 6.8. Prediction errors for the time period (1 to 5 days) ahead adaptive tumor growth inhibition prediction in mice given i.p. doses of gemcitabine (100 mg/kg on days 19 and 26). Predictions performed with ANFIS model (3,100) without using moving window.	74
Table 6.9. Prediction errors for the time period (1 to 5 days) ahead adaptive tumor growth inhibition prediction in mice given i.p. doses of gemcitabine (100 mg/kg on Days 19 and 26). Predictions performed with ANFIS model (3,50) with moving window of $l = 20$ measurements.	75
Table 6.10. Prediction errors for the time period (1 to 5 days) ahead adaptive tumor growth inhibition prediction in mice given i.p. doses of gemcitabine (100 mg/kg on Days 19 and 26). Predictions performed with ANFIS model (3,50) with moving window of $l = 15$ measurements.	76
Table 6.11. Prediction errors for the time period (1 to 5 days) ahead adaptive tumor growth inhibition prediction in mice given 5-FU and drug C2 (50 mg/kg q4dx3 from day 9 and 60 mg/kg on days 10, 11, 12 and 14, 15, 16). Predictions performed with ANFIS model (3,100).	78
Table 6.12. Prediction errors for the time period (1 to 5 days) ahead adaptive tumor growth inhibition prediction in mice given CPT-11 and drug C2 (45 mg/kg q4dx3 from day 9 and 60 mg/kg on days 10, 11, 12 and 14, 15, 16). Predictions performed with ANFIS model (5,100).	79
Table 7.1. Sets of the free design parameters θ values. Tested against the augmented TGI model states to identify the vector $\theta = [\theta_1, \theta_2]$ which maximizes the pointwise controllable space.	85
Table 7.2. Periodic SDRE treatment results (dose schedules and metrics) across Cases 1 to 5.	89
Table 7.3. Intermittent SDRE treatment results (dose schedules and metrics) across Cases 6 and 7.	93
Table 8.1. Periodic LQR treatment results (dose schedules and metrics) across Cases 1 to 5.....	100
Table 8.2. Intermittent LQR treatment results (dose schedules and metrics) across Cases 6 and 7.....	105

List of abbreviations

5-FU	5-fluorouracil
ACT	adoptive cell transfer
ADME	absorption, distribution, metabolism, and excretion
AIC	Akaike's information criterion
ALL	acute lymphocytic leukemia
ANFIS	adaptive neuro-fuzzy inference system
ANNs	artificial neural network
AR	autoregressive
ARE	algebraic Riccati equations
ARMA	autoregressive moving average
ARX	autoregressive with exogenous inputs
BER	base-excision repair
CAR	chimeric-antigen receptor
CDX	cell line-derived xenograft
CPT-11	irinotecan
CSF	colony-stimulating factors
DC	dendritic cells
DNA	deoxyribonucleic acid
DP	dynamic programming
DRA	discrete-time realization algorithm
EEG	electroencephalogram
EFTA	European Free Trade Association
EU	European Union
GA	genetic algorithm
GI	gastrointestinal
H. pylori	helicobacter pylori
HBV	hepatitis B virus
HCV	hepatitis C virus
HIV-1	human immunodeficiency virus type 1
HJB	Hamilton-Jacobi-Bellman

Prediction of the cancer patients' response to their therapeutical treatment with non-linear forecasting techniques

List of abbreviations

HPV	human papilloma virus
HS	Harmony Search
i.m.	intramuscular
i.p.	intraperitoneal
IFN	Interferons
IFN γ	interferon gamma
Ig	immunoglobins
IL-2	interleukin 2
JRC	Ispra Joint Research Centre
LQC	linear quadratic control
LQR	linear quadratic regulator
LTI	linear time invariant
MA	moving average
mAbs	monoclonal antibodies
MAPE	mean absolute percentage error
mCHT	metronomic chemotherapy
MCTs	mouse clinical trials
MF	membership function
MHC I	major histocompatibility complex class I molecule
MIMO	multiple-input multiple-output
MISO	multi-input, single output
MPBVP	multi-point value boundary problem
MSE	mean square error
MTC	metronomic chemotherapy
MTD	maximum tolerated dose
NHL	non-Hodgkin lymphoma
NK	natural killer cells
NLP	non-linear programming problem
NNA	neural network algorithm
OCP	optimal control problem
OCT	optimal control theory

Prediction of the cancer patients' response to their therapeutical treatment with non-linear forecasting techniques

List of abbreviations

ODE	ordinary differential equation
OS	overall survival
PD	pharmacodynamics
PDE	partial differential equation
PDX	patient-derived xenograft
PK	pharmacokinetics
PMP	Pontryagin's maximum (minimum) principle
PSA	prostate-specific antigen
PSO	particle swarm optimization
q4dx3	three times at an interval of four days
QoL	quality of life
RMSE	root mean square error
RNA	ribonucleic acid
s.c.	subcutaneous
SA	simulated annealing
SCLC	small cell lung cancer
SDC	state dependent coefficient
SDRE	state dependent Riccati equation
CAR-T	chimeric antigen receptor T cell
TEI	time efficacy index
TGI	tumor growth inhibition
TGIadd	TGI additive model
TPBVP	two-point boundary value problem
TSK	Takaki-Sugeno-Kang

Chapter 1: Introduction

1.1 Cancer – Solid tumor growth

Despite the major improvements in medicine and health care technologies along with the increased access to high quality and up-to-date healthcare information, cancer remains one of the main causes of death. Based on projections by the European Commission – Joint Research Centre (JRC) in Ispra, Italy, the number of new cancer cases in the European Union (EU) and the European Free Trade Association (EFTA) countries is projected to increase by 21%, reaching 3.4 million in 2040. At the same time, the number of deaths due to cancer is expected to grow dramatically, from 1.3 million in 2020 to almost 1.7 million by 2040. An increase of this size equals a rise of 32.2% in 20 years' time. For the lower mortality scenario, this number can potentially increase up to 35.4% for the same time period.

In layman's terms, cancer is a collection of no less than 100 diseases that develop across time and involve the continual unregulated division of the body's cells. Even though each type of cancer has its very own unique features (e.g., different staging system, mutational signatures, etc.) and it is possible to be developed anywhere in the body, there are strong similarities amid the processes that produce cancer. When a normal cell bypasses the normal route and starts to follow its own proliferation rules, then it is when cancer begins (see Figure 1.1). The disease primarily results from genetic mutations in the cellular deoxyribonucleic acid (DNA) which interfere with the internal cellular control mechanisms [1], [2]. This allows the cells to evade the homeostatic controls that ordinarily suppress inappropriate proliferation and inhibit the survival of aberrantly proliferating cells outside their normal niches. The cells escape apoptosis and grow improperly with or without growth signals from the environment [3], [4]. Of course, cancer is not developed all at once. It is a multistage process which requires the accumulation of DNA damage (i.e., genetic mutations) in the genes whose role is to control cellular growth. A normal cell may undergo 60 or more genetic mutations to become abnormal [5]. The number of cell divisions that occur during this process can be astronomically large—human tumors often become apparent only after they have grown to a size of 10 billion to 100 billion cells [6]. External factors such as chemicals and environmental carcinogens, exposure to radiation, viruses, and smoking can cause

Prediction of the cancer patients' response to their therapeutical treatment with non-linear forecasting techniques

Chapter 1: Introduction

damages to DNA and lead to cell immortality [1], [7]. A small number of cancers can also occur due to genetic mutations inherited by the parents.

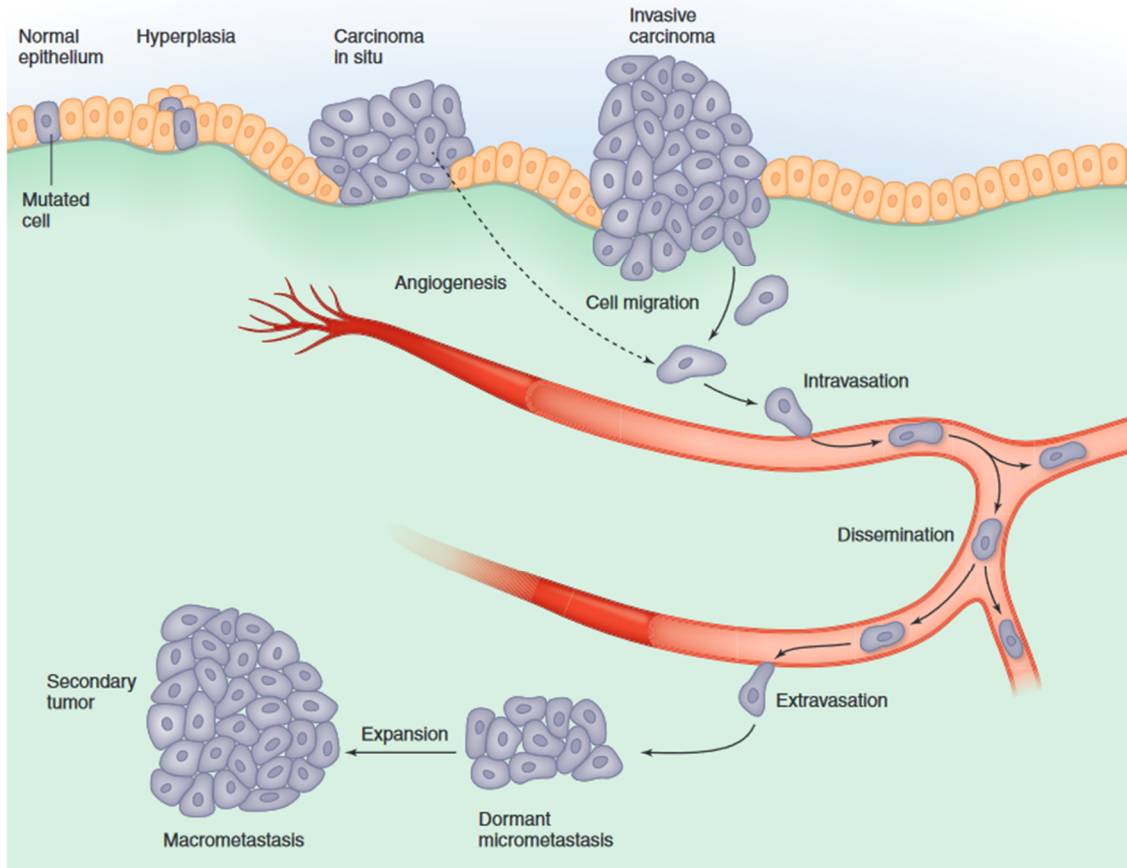


Figure 1.1. Cancer progression. Adapted from [2], [4].

The uncontrolled proliferation of these cells eventually leads to the development of a solid mass which is called a tumor or neoplasm. The location where the tumor occurred, the cell types, as well as the nutrition supply, are crucial for the growth of the neoplasm. The abnormal cells may remain in the original tumor (i.e., the primary site) a condition called in situ cancer or in the worst case, break off and invade other surrounding tissues in a condition called invasive cancer. In the latter case, the tumor is said to be malignant, and the cancer cells may spread through the bloodstream and the lymphatic system and establish metastases (i.e., new tumors) in other parts of the body. It has to be noted that in many cases the primary tumor and the secondary metastases do not progress at the same pace and in such an instance the primary tumor may manifest itself while the metastases do not cause symptoms. This way, they might not be detected on time and

threaten the patient's life when their growth disrupts the tissues and organs needed for survival.

As previously mentioned, carcinogenesis is a multistep process during which normal cells turn into cancer cells. To defend against cancer, the human body itself has developed a pool of various defense mechanisms. The DNA damage repair system is one of the most important mechanisms. Two of the main repair processes for DNA repair are nucleotide-excision repair and base-excision repair (BER) [8]. Once DNA damage is detected, the cell cycle is blocked in order to completely address the damage. Although, in most cases, the alterations in DNA are reversible, the repair process might fail, and the involved genetic mutations might introduce abnormality and transform a normal cell into a cancerous cell. Studies have found that genes belonging to anti-oncogene (i.e., tumor suppressor gene) and proto-oncogene classes, when mutated, can contribute to the development of cancer [8].

The immune system is the human's defense mechanism against pathogens (as well as its own cells that have been infected). It is a highly complex network of biological processes, mainly composed of white blood cells such as B and T lymphocytes (B and T cells), natural killer cells (NK), macrophages, dendritic cells (DC) etc. that acts as a shield against a variety of viruses, bacteria, foreign bodies, as well as tumor cells. Therefore, it has an important role to play in the fight against cancer. It is comprised of two arms which are in continuous interaction and interdependence, the innate and the adaptive immune system. NK cells, dendritic cells, and macrophages are part of the innate immune system and are the first line of defense against pathogens.

When antigens, molecular structures such as proteins and sugars that may be present on the surfaces of pathogens enter the body a series of reactions are carried out to stimulate an immune response and fight the threat off. More specifically, specific proteins called antibodies or immunoglobins (Ig) are produced as a result of the body's immune response. Then, these proteins recognize and stick to those of the pathogens and either directly destroy them or block them from infecting other cells of the host [9]. NK cells are maybe the first group of immune system cells to defend against intruders.

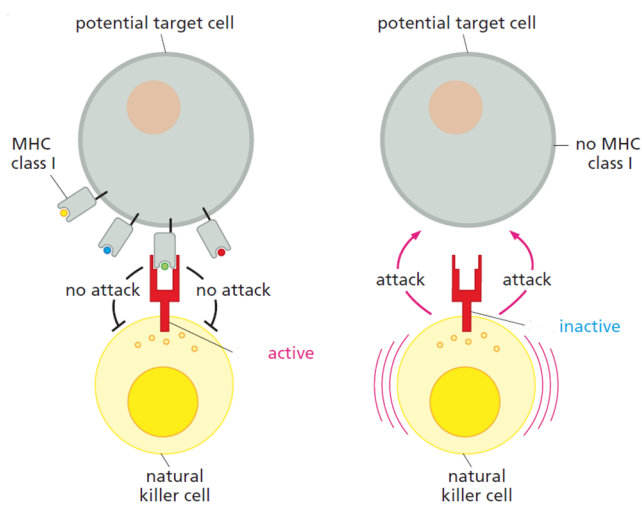


Figure 1.2. Natural killer (NK) cells (yellow) display a killer inhibitory receptor (red) that can recognize MHC I receptors on the surface of potential target cells (gray). In the absence of MCH I, NK cell attacks the target cell (right). Otherwise, the attack is declined (left). Adapted by [10].

They are lymphocytes equipped with a variety of receptors (e.g., activation receptors, see Figure 1.2 (adapted by [10]), which control their actions. Using such receptors, they can identify potential infectious agents and cancer (potential target cells) and attack them without any prior exposure to them. A way to do this is by the major histocompatibility complex class I (MHC I) molecules. The NK cell binds with the potential target

cell and then it checks whether MHC I molecules are present on it or not. In the absence of MHC I molecules, kill activating receptors are attached and an attack by the NK cell is possible. However, in the case where a target cell presents self-antigens in its MHC class I receptors then it avoids the attack and remains unharmed. Cancer cells are likely to develop such self-antigens in MHC I, like most of the healthy cells of the body, and therefore avoid the kill signal from the NK cell [10]. It is common for an infected or cancer cell to lose its MHC I. In this case, the cell is vulnerable to attacks by NK cells, which release special proteins and enzymes (perforin and granzymes), leading eventually to the death of it. This is also the case in the absence of self-antigens in the MHC I [10], [11]. Right after the innate immune response, the NK cells secrete some proteins called cytokines (e.g., interferon gamma (IFN γ)) which affect other cells such as dendritic cells and macrophages to boost the immune response [12].

In contrast to innate system cells that recognize abnormal cells, cells of the adaptive immune system must be “taught” how to recognize “hostile” cells. Nevertheless, they are more specific and more effective compared to those of the innate immune system. B and T lymphocytes such as CD4+ T helper and CD8+ T cytotoxic are included to this second arm. More specifically, CD8+ T cells are developed in the thymus and present T-

cell receptors on their surface through which they can identify a specific antigen (e.g., produced by cancer cells or viruses). If the specific antigen, e.g., tumor-specific-antigen, is recognized then it binds to the MHC I molecule – antigen complex of the specific-antigen-displaying target cell and a killing process is triggered (e.g., through secretion of perforin, granzymes, INF γ , etc.) [10], [13]. It is important to note that the bond of the two cells is achieved through a glycoprotein called CD8, which is present in the T-cell receptors [10], [13].

Despite the existence of these natural mechanisms, cancer cells can develop highly effective strategies, called immunoevasion strategies, in order to avoid immunological attacks, thus creating large, life-threatening tumors [10].

1.2 Current strategies for cancer therapy

Both primary and secondary prevention of cancer is of great importance for public health. In the former, lifestyle changes are crucial, as is prophylaxis against infectious agent-induced cancers. A large number of infectious agents, like human papilloma virus (HPV), hepatitis B virus (HBV), hepatitis C virus (HCV), human immunodeficiency virus type 1 (HIV-1) and helicobacter pylori (*H. pylori*) have been identified to cause or contribute to the development of specific human cancers [14]. According to [14], infections and the agents causing them are associated with 10% of the types of cancer. Vaccination, safe sex practices and treatments against microbes have been proven beneficial in the fight against these infections and can serve as preventive solutions.

In terms of secondary prevention, screening with mammography, colonoscopy, PAP-testing and other laboratory tests like prostate-specific antigen (PSA) has been shown to reduce mortality from the respective neoplasms. These screening techniques, when combined with significant therapeutic developments, may lead to further improvements in prognosis and increased survival rates. Therefore, the early detection and diagnosis of cancer, followed by an effective treatment, are crucial for the patient's outcome and overall survival (OS).

There are over 100 different kinds of cancer that can be developed in the human body [3]. However, despite the research efforts and the treatment modalities which have been developed, there is no specific therapy that treats all forms of cancer. For this

reason, different strategies are used in the clinical practice, with therapies given either alone (i.e., monotherapy) or in combination. Some of the most common approaches to treat cancer are **surgery**, **radiation** (or radiotherapy), **chemotherapy** and **immunotherapy** [15], [16].

1.2.1 Surgical operation

Surgical operations are the first method introduced in the battle against cancer. They aim to directly (i.e., physically) remove solid tumors. During the operation, a healthy, non-tumorous tissue around the tumor mass is also removed. This way it is ensured that the cancerous cells are fully removed from the area and the chance of local recurrence is minimized. This approach is called resection or surgical margin [17], [18]. Even though surgery reduces the tumor burden, it is a common practice to be followed by another treatment method such as radiation or chemotherapy in order to achieve better results and prevent local recurrence of the tumor.

1.2.2 Radiation

Radiation therapy is a non-invasive local treatment for cancer that uses ionizing radiation. Most of the time, it is used as the first treatment against cancer. It is also common practice to be applied after other treatment methods like chemotherapy and surgery to eradicate cancer cells which may have survived. In several cases, when cancer cannot be fully eradicated, radiation is used to reduce the tumor size, relieve pain, and improve the patient's quality of life (QoL). This kind of treatment is called palliative radiation [19].

1.2.3 Chemotherapy

Chemotherapy was introduced to cancer treatment in the 1940s when nitrogen mustard was administered to patients with non-Hodgkin's lymphoma [20]. It involves the use of single cytotoxic anticancer drugs or a combination of them, usually given intravenously and sometimes orally, to combat cancer growth. Unlike radiation and surgery which are local treatments, chemotherapy is considered a systemic treatment. Chemotherapy drugs travel through the bloodstream and interact with cells, cancerous or not, all over the host's body. This way, the abnormal cells that are present in other areas of the body, i.e., the metastasized cells are also affected and killed by.

Chemotherapeutic drugs normally inhibit mitosis or induce ribonucleic acid (RNA) or DNA damage to the cells which makes them unable to divide. The faster the cancer cells divide, the more likely it is that chemotherapy will kill the cells. Depending on the type of the drug used in the treatment, chemotherapy may be cell-cycle specific or cell-cycle non-specific. Drugs that are toxic to cancer cells while they are dividing are called cell-cycle specific. On the other hand, the drugs that are toxic to cancer cells at any point in their cell cycle are called cell-cycle non-specific. Chemotherapeutic antineoplastic agents can be classified based on several factors, including their chemical composition/structure and their action against cancerous cells. They include alkylating agents, antimetabolites, plant alkaloids, topoisomerase inhibitors, antibiotics, and others [21], [22].

- ❖ **Antimetabolites** are one of the most used and effective group of drugs against neoplasms. They are cell-cycle specific, meaning they are most effective during the DNA replication period (S-phase) of cell division. Specifically, antimetabolites act as substitutes for the actual metabolites that would be used in the normal metabolism, thereby preventing the synthesis of DNA, RNA, and subsequently, cell division [23], [24]. They include compounds such as 5-fluorouracil, gemcitabine, decitabine, 8-chloroadenosine and 6-mercaptopurine [22].
- ❖ **Alkylating agents:** Compared to antimetabolites, alkylating agents are cell-cycle phase nonspecific drugs that act on the DNA of the cells by preventing the strands of the double DNA helix from linking correctly. This causes DNA strand breaks which affect the ability of the cancerous cell to divide and ultimately leads to cell death. Examples include cyclophosphamide, temozolomide, cisplatin, carboplatin, busulfan and oxaliplatin [25], [26].
- ❖ **Topoisomerase inhibitors:** Drugs of this category interfere with topoisomerase enzymes, i.e., topoisomerase I and II. These enzymes play a pivotal role in DNA replication and transcription. By blocking them, it is possible to block the ligation step during either replication or transcription of the DNA, thus creating a single- and double-strand break which leads to necrosis or apoptosis. Agents in this group are irinotecan, topotecan (inhibitors of topoisomerase I), etoposide and teniposide (inhibitors of topoisomerase II) [25].

- ❖ **Cytotoxic antibiotics** are drugs made from natural products. They are considered cell-cycle non-specific as they act during multiple phases of the cell cycle. Some commonly used anti-tumor antibiotics in this group are anthracycline antibiotics, dactinomycin, mitomycin, bleomycin, and doxorubicin [22], [27].

Typically, chemotherapy is administered in cycles near or at the maximum tolerated dose (MTD). This means the drug is given at the highest dose that yields tolerable side effects. Although this strategy has been effective in many patients the excess use of chemotherapy drugs (i.e., the duration of the treatment) in combination with the high dosage levels may lead to short- and long-term toxicity and severe side effects. Depending on the drug type, dose and treatment schedule, these side effects can vary. Healthy cells with high proliferation rates, such those in the gastrointestinal (GI) tract, mouth, and throat, as well as blood cells are particularly susceptible. Nausea, vomiting, oral and GI mucositis and alopecia (loss of hair) are the most common possible adverse effects. [28], [29]. Fortunately, these side effects usually subside post-treatment.

To mitigate toxicity, an alternative therapeutic strategy involves administering chemotherapeutic drugs at significantly lower doses. This approach, known as metronomic chemotherapy (mCHT), differentiates from the conventional chemotherapy not only in terms of dose levels but also in terms of frequency of the anti-neoplastic drug administration [30]–[32]. Numerous studies suggest that smaller doses of chemotherapeutic drugs without extended drug-free time intervals can effectively manage the disease, lead to prolonged OS and reduce side effects [32]–[34].

1.2.4 Immunotherapy

Cancer immunotherapy, also called immuno-oncology, is described as a class of therapies designed to strengthen or stimulate the patient's immune system in the battle against malignant cells. This comes in contrast with other conventional treatments like chemotherapy which directly target the cancer cell. Immunotherapy usually involves the modulation of the immune system response, either by enabling or enhancing it to fight cancer. Common types of immunotherapies include cytokines, monoclonal antibodies, and adoptive cell transfer therapy.

- ❖ **Cytokines** are natural (i.e., found in the human body) or synthesized (in the lab) substances that affect the response of the immune system. Due to this reason, they are also known as immune system response modifiers. They are a group of proteins that boost the body's defense mechanism and its response against cancer. Interferons (IFN), interleukins and colony-stimulating factors (CSF) are included in this category [35]. Interleukin-2 (IL-2) stands out among the interleukins. It facilitates the proliferation and function of T-cells while augments the cytotoxic activity of NK cells. It is primarily produced by CD4⁺ T cells in response to antigen stimulation. Nevertheless, it is possible to be secreted also by CD8⁺ T cells and activated DC and NK cells [36], [37].
- ❖ **Monoclonal antibodies** (mAbs) were first introduced to the treatment of cancer back in 1980, when administered to a patient with non-Hodgkin lymphoma (NHL) [25]. In brief, these monoclonal antibodies for cancer are laboratory made proteins which can identify and trigger an immune response against cancer cells. They can also be used as a vehicle to deliver anticancer drugs or radiation directly to the malignant cells using radioactive particles called radionuclides [38], [39].
- ❖ An emerging and highly promising type of cancer immunotherapy is **adoptive cell transfer** (ACT). Here, T cells are isolated from the patient's blood and are in-vitro genetically modified to display high specificity on tumor cells. Once multiplied in vast numbers, these tailored T cells are re-infused back to the patient's bloodstream to attack the cancer cells without interfering with the normal cells [40]. A type of ACT therapy with promising results (e.g., 92% of end-stage patients with acute lymphocytic leukemia (ALL) were fully recovered [41]) is the chimeric-antigen receptor T-cell therapy (CAR). In CAR-T, the extracted T cells are modified to express chimeric antigen receptors in order to interact with cancer cells and kill them (see Figure 1.3 [42]) [43].

It is worth mentioning that by 2020 more than 75 anticancer immunotherapeutic agents had already been approved by the regulatory agencies. Numerous others are currently under investigation, either as standalone treatments or as adjunct to conventional therapies [25], [39], [44].

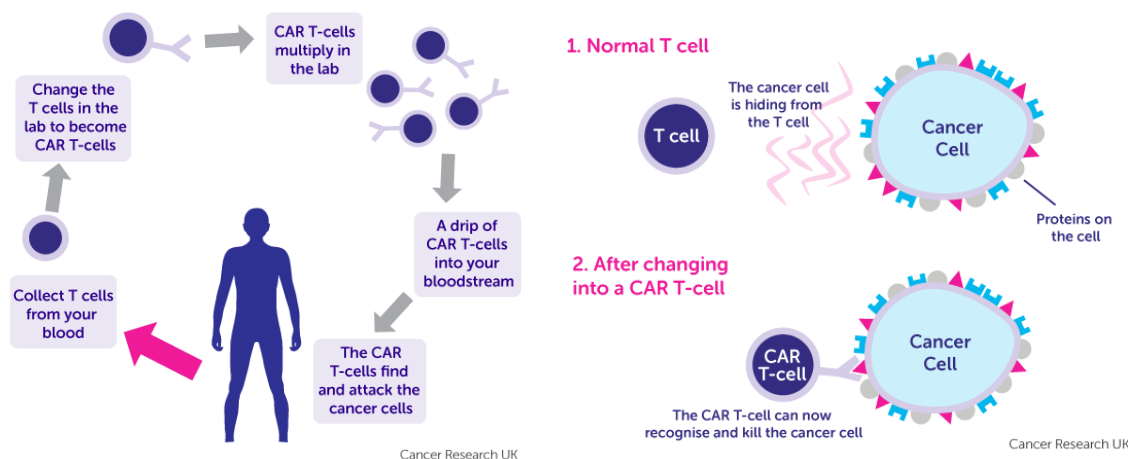


Figure 1.3. (Left) Diagram showing CAR T-cell therapy. (Right) Diagram showing the T cell before and after genetic engineering. Adapted from [42].

1.2.5 Chemo-immunotherapy

Even though both immunotherapy and chemotherapy may successfully inhibit the tumor growth progression, treatments failure remains a challenge in many cases. A significant reason for this is the ability of cancer cells to develop resistance to antineoplastic treatments due to continuous drug administration. Genetics and the tumor microenvironment are two of the many contributing factors [45]–[50]. It is estimated that drug resistance accounts for treatment failure in over 90% of the patients with metastatic cancer [51]. Tumor cells can also acquire specific mechanisms through which they evade immune surveillance and gradually develop resistance to immunotherapy [52].

Addressing a major problem like this could dramatically improve survival rates and may even lead to the treatment of the disease. Studies have shown that the use of combination chemotherapy (i.e., administration of two or more different drugs) can significantly help towards minimizing the effect of drug resistance [53]–[58]. Yet, identifying multiple drugs that can be co-administered to effectively arrest tumor growth and its progression is a challenging task that requires a lot of time and money.

Another rising strategy to deal with tumor resistance and disease progression is the combination of chemotherapy and immunotherapy. For a long time, most of the chemotherapy drugs were considered immunosuppressants. For this reason and due to antagonistic effects, the combination of anti-neoplastic drugs and immunotherapy was considered unapplicable. However, recent studies have shown that such combinations

can have positive effects and result in improved clinical outcomes than chemotherapy alone [59]–[61]. Chemotherapy not only has cytotoxic effects upon the cells but also can enable immune system's responses against tumors either by increasing the immunogenicity of the tumor antigens or by halting the production of immunosuppressive substances due to debulking of the tumor [59], [61]. Inhibiting the tumor growth and reducing its mass through chemotherapy, results in smaller population of cancer cells which is easier to be tackled by the immune system of the organism, enhanced by immunotherapy. Of course, such a thing also reduces the possibility of the tumor cells to develop immunoescape mechanisms.

Indeed, clinical trials combining chemotherapy and immunotherapy have reported enhanced OS. For example, OS prolonged by an average of 4.7 months for lung adenocarcinoma patients [62], by 3.7 months for breast cancer [63] and by 2.7 months for small cell lung cancer (SCLC) [64]. Furthermore, when immunotherapy was administered as a maintenance therapy post-chemotherapy, survival rates also improved. For instance, the median OS for metastatic urothelial carcinoma patients increased by nearly 7 months [65].

1.3 Key contributions and novelty of this Thesis

Mathematical modeling and *in silico* experiments in the field of oncology can optimize chemotherapy and/or immunotherapy treatments, offering personalized care while at the same time saving money. To this direction, the challenges of accurately describing tumor growth inhibition (TGI) under chemotherapy and the identification of optimal chemotherapy regimens are addressed. For this purpose, the Simeoni *et al.*'s TGI model is utilized. Two novel ARX-based mathematical models for describing the growth of solid tumors under the effect of chemotherapy, both for single and multiple anticancer drug treatment, using laboratory data from human-to-mouse xenografts are also developed and evaluated. Moreover, the feasibility of using ANFIS-based TGI models to accurately model tumor growth is investigated in this work and three new models are introduced. Lastly, the application of optimal control techniques is employed to extract optimal chemotherapy dosing schedules, both periodic and intermittent. However, it is worth mentioning that this research has some limitations, such as the small size of the dataset

used and the need for further validation in other types of cancer, which are suggested as potential future research directions.

1.4 Thesis organization

The organization of the thesis is described below:

In **Chapter 1**, a brief introduction to the complex world of cancer and solid tumor biology is provided, and some key concepts underlying the biomedical background for the anticancer treatments considered in this thesis are discussed. Additionally, a thorough review of the most widely used treatment modalities for cancer and solid tumors is conducted.

In **Chapter 2**, there is a comprehensive review of state-of-the-art mathematical models employed to depict both unperturbed and perturbed tumor growth under different therapeutic approaches including chemotherapy, immunotherapy, and their combination. The models are examined in increasing order of complexity, both in terms of their modeling and mathematical aspects. Furthermore, an introduction to optimal control theory is provided, and its significance in developing and optimizing cancer therapy protocols is highlighted.

In **Chapter 3**, the material and methods employed in this work are presented and discussed. Specifically, the dataset used in this work is described, followed by a detailed presentation of the estimation problem for the unknown parameters of mathematical models, be they linear or non-linear. Last but not least, the short-term ahead forecasting methodology is analytically described, and the evaluation metrics used are briefly presented.

In **Chapter 4**, the well-established in the clinical practice Simeoni *et al.*'s tumor growth inhibition mathematical model is presented and described. The model's parameters are presented and short-term step ahead predictions of the tumor growth (pancreatic adenocarcinoma) under the action of gemcitabine are presented and evaluated.

In **Chapter 5**, a new approach to describe the tumor growth inhibition under the effect of single and in combination anti-cancer drugs is introduced. Two novel linear systems of difference equations (autoregressive with exogenous inputs - ARX) which model the

growth of solid tumors under single and multi-agent chemotherapy treatments are identified and evaluated using laboratory data of experiments in mice.

In **Chapter 6**, a short introduction to Adaptive Neuro-Fuzzy Inference System (ANFIS) is provided and three ANFIS models for tumor growth inhibition under chemotherapy are introduced and fitted to experimental tumor growth curves. One model simulates the tumor growth inhibition under the action of a single chemotherapy agent, while the other two models describe tumor growth under the effect of two drugs given in combination. The chapter also includes short-term step ahead predictions of the tumor growth under the effect of chemotherapy treatment.

In **Chapters 7** and **8**, non-linear and linear optimal control methods are applied for efficient tumor growth eradication. First, a non-linear optimal control problem is formed to determine the best (i.e., optimal) chemotherapy treatment strategy for tumor eradication using advanced non-linear control method and by introducing an augmented form of the non-linear Simeoni *et al.*'s TGI model. Then, linear quadratic regulator (LQR)-based optimal control of tumor dynamics is used along with *ARX TGI* models to explore possible optimal chemotherapy dosages for both periodic and intermittent treatment schedules. Finally, the simulation results are presented, discussed, and conclusions are drawn.

The last chapter, **Chapter 9**, presents a thorough discussion about the achievements and the limitations of the present work. Analysis of the results obtained in this thesis is also performed, and concluding remarks are provided.

Chapter 2: Mathematical frameworks in tumor growth and treatment

2.1 A survey of mathematical models for tumor growth

Mathematical modelling is powerful tool to quantitatively describe the current knowledge of a system or a process through parameters and mathematical equations. It can be used not only to describe and simulate complex systems but also to test hypotheses and validate experiments. In addition, the enormous costs of designing and conducting laboratory experiments in order to simulate complex systems can be off-loaded through mathematical models which provide relatively fast and costless simulations.

In oncology particularly, mathematical models have been introduced about 60 years ago in an attempt to understand the highly complex dynamics of cancer. Using available clinical and experimental data cancer mathematical models can be built, calibrated, and validated. These data are usually collected through mouse clinical trials (MCTs). MCTs are population studies that use cell line-derived xenograft (CDX) or patient-derived xenograft (PDX) models (i.e., models of cancer where the tissue or cells from a patient's tumor are implanted into an immunodeficient or humanized mouse) to assess efficacy and predict drug responders in preclinical oncology drug development. The models' parameters, usually based on biological and physiological grounds, can be estimated and their prediction ability, i.e., how well a model can predict the tumor growth, can be explored. As predictive tools, cancer mathematical models can be used also to anticipate the outcome of new chemical entities and regimens used in treatment [66], [67] in an attempt to optimize the preclinical experimental design. Finally, the description of the relationships between treatment (i.e., chemotherapy drug pharmacokinetics (PK) and pharmacodynamics (PD), i.e., the drug effects), and tumor progression may provide new, valuable insights and offer several possibilities to understand better the cancer process and therefore its treatment.

To this day, a plethora of tumor growth mathematical models has been created. This kind of mathematical models can be classified as empirical (descriptive), mechanistic and large scale/system biology models [68]. However, this is not the only classification of the tumor growth models. They can also be grouped based on the scales of the desired mechanism as continuous (i.e., models that study cancer at the tissue scale),

discrete (i.e., models that study cancer at the cell scale) and hybrid [67], [69]. Moreover, there are also a lot of studies that group models based on the type of the equations they are structured, see [70]–[72]. Therefore, they are usually classified as ordinary differential equation (ODE), partial differential equation (PDE) and algebraic equation models.

Some of the first mathematical models for cancer were based on the von Bertalanffy tumor growth equation and functions like the linear, the exponential and the logistic. Even though such equations can describe the growth of several processes in living organisms, their parameters lack the biology relevant information. All these models are classified as continuous models with tumor to be considered as a set of cancerous cells and described as the density of volume fraction of these cells. Key benefit of continuous models is the small number of parameters they are composed of, which can be easily estimated from the available experimental model system. Continuous models can be further classified based on the heterogeneity of the cells forming the tumor including inter and intratumor heterogeneities [73]–[75]. Many of the mathematical models assume that tumor cells are similar, having common properties and undergo one-dimensional growth. These models belong to the class of homogenous models.

The linear and the exponential growth are the simplest homogenous models. The linear model assumes constant growth rate k_g of the tumor cells, while in the exponential model the number of the cancerous cells are increased exponentially with time (see Eqs. below).

Linear growth model
$$\frac{dT}{dt} = k_g \quad (2.1)$$

with $T(t) = k_g t + T_0$ where $k_g > 0$ and $T_0 = T(t = 0)$.

Exponential growth model
$$\frac{dT}{dt} = k_g T \quad (2.2)$$

with $T(t) = T_0 e^{t k_g}$ where $T_0 = T(t = 0)$ (i.e., the tumor size at inoculation time $t = 0$). Initial growth of solid tumors is rapid [76]. However, their growth rate decreases as the size of the tumor increases mainly due to limitations in nutrients, space and oxygen [77]. In the above two models all tumor cells are assumed to obtain ample growth

factors and nutrients, modelling an ideal scenario in which tumor cells proliferate endlessly. Therefore, the saturation and the reduced growth rate as the tumor size increases, is not captured.

These equations can be applied to model the initial stages of tumor expansion. For this reason, alternative model formations in which the rate of tumor growth does not remain constant have been explored. To capture the saturation of the tumor's size the logistic and the Von Bertalanffy models were introduced [66], [71]. In fact, both models describe the tumor growth in relationship with the host carrying capacity. For example, in logistic growth model the proliferation rate of the cancerous cells depends on and thus is limited by a carrying capacity. As long as the tumor size T is smaller than the carrying capacity T_{max} then its growth is nearly exponential. Things are a bit different as soon as the tumor cells population size converges to the carrying capacity, where the growth is inhibited, and the tumor size eventually reaches a plateau.

Logistic growth model
$$\frac{dT}{dt} = k_g T \left(1 - \frac{T}{T_{max}}\right) \quad (2.3)$$

Von Bertalanffy model
$$\frac{dT}{dt} = \alpha T^{\frac{2}{3}} - \beta T \quad (2.4)$$

It is worth to mention that in 1964, Anne Kane Laird formulated the Gompertz model of tumor [77]. Even though the model was introduced by Benjamin Gompertz in 1825 as a way to describe the human mortality curves [79], Laird was the first scientist to show that the growth of a tumor, in the absence of therapy (i.e., the unperturbed case) follows Gompertzian kinetics. This means the model assumes the growth rate of tumor decelerates over time. The model is described by the following equation:

Gompertz model
$$\frac{dT}{dt} = -k_g T \log\left(\frac{T}{T_{max}}\right) \quad (2.5)$$

Following Laird's work, a series of papers have been presented. Through the works of Norton and Simon [80]–[82] the Gompertz model was utilized in humans, modeling breast cancer growth. However, models based on the Gompertz-Laird equation may be problematic as the plateau is difficult to estimate. It is common, as a matter of ethics in mouse clinical trials, to kill the mice when tumor sizes exceed a certain threshold (e.g.,

Prediction of the cancer patients' response to their therapeutical treatment with non-linear forecasting techniques

Chapter 2: Mathematical frameworks in tumor growth and treatment

$T > 10^3 \text{ mm}^3$). Usually this happens before the appearance of the plateau, therefore it is not easy to estimate it.

The above models, i.e., (2.3), (2.4) and (2.5), are in fact special cases of a generalized empirical model, described by the following ODE [67]:

$$\frac{dT}{dt} = \frac{k_g}{a} T \left[1 - \left(\frac{T}{T_{max}} \right)^a \right] \quad (2.6)$$

with

$$T(t) = T_{max} \left(\frac{T_0^a}{T_0^a + (T_{max} - T_0^a)e^{-tk_g}} \right) \quad (2.7)$$

where $T_0 = T(t = 0)$ and a is a parameter which determines how fast the solid tumor will reach its maximum size (i.e., saturation). In the case where $a = 1$ the model is converted to the logistic model. On the other side, if a tends to 0^+ the generalized model is reduced to the Gompertzian model of (2.5). The time curves (simulations) of the tumor growth models described above are presented in Figure 2.1.

While it is useful to describe the time course of the unperturbed tumor growth, it is vital to know the effects of the applied treatment (e.g., chemotherapy, immunotherapy, etc.) upon the tumor cells. In light of this, classical models such as Gompertz have been modified to include anti-tumor treatments and new models have been introduced. In general, cancer treatment focuses on either reducing the overall size of the tumor (i.e., shrinking the tumor mass) by causing severe damage leading to the death of the proliferating cancer cells or by decreasing the tumor's ability to grow (i.e., reducing the carrying capacity). Treatment related tumor size reduction is typically described using empirical drug-induced shrinkage terms [70] introduced to models' equations as follows:

$$\frac{dT}{dt} = (\text{tumorGrowth}) - (\text{drugTreatment}) \quad (2.8)$$

where (tumorGrowth) denotes the net tumor growth:

$$(\text{tumorGrowth}) = (\text{natural tumor growth}) - (\text{natural tumor death}) \quad (2.9)$$

and (drugTreatment) the drug-induced decay processes.

Prediction of the cancer patients' response to their therapeutical treatment with non-linear forecasting techniques

Chapter 2: Mathematical frameworks in tumor growth and treatment

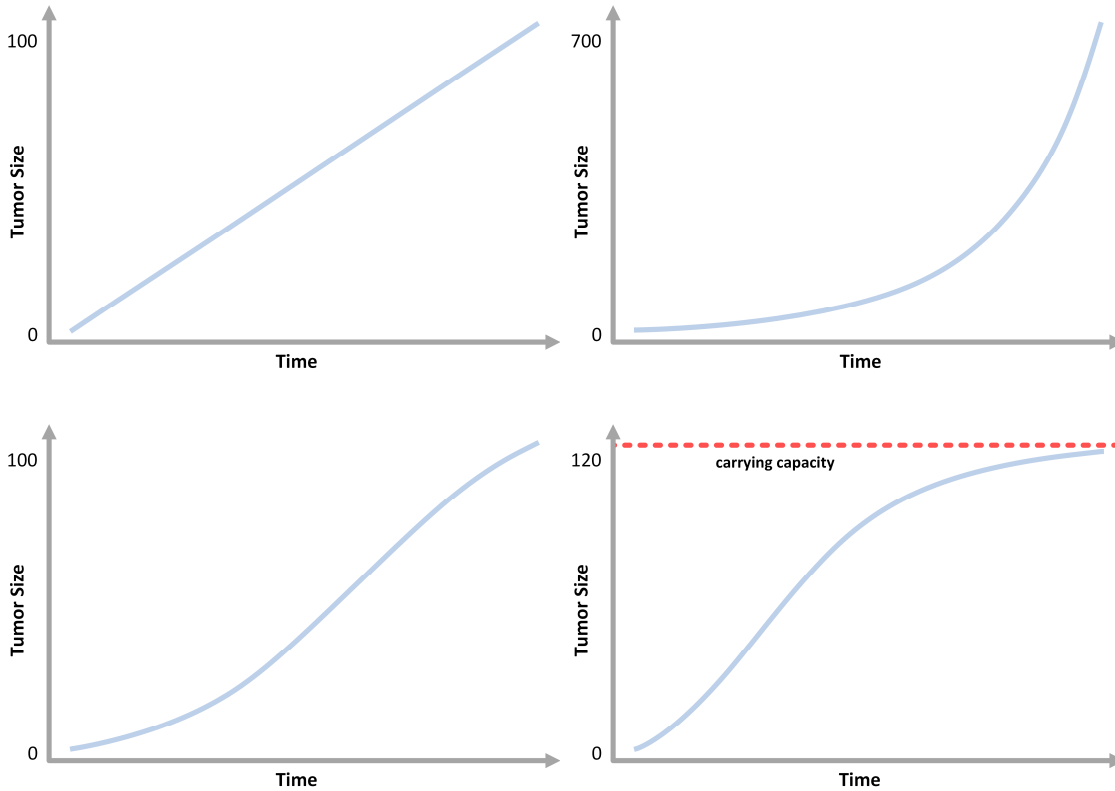


Figure 2.1. Simulated time curves of tumor size from the linear (top left), exponential (top right), logistic (bottom left) and Gompertz (bottom right) tumor growth models [71].

A standard approach to describe the anti-tumor treatment effect is through a log-kill pattern, based on the concept that the tumor's decay rate, due to treatment is proportional to its size:

$$(\text{drugTreatment}) = d_e T \tag{2.10}$$

where d_e is the drug-induced decay rate. In its simplest form d_e can be a constant however it often represents a function that reflects the drug exposure, such as the drug dose or the drug plasma concentration $u(t)$:

$$d_e = \beta u(t) T \tag{2.11}$$

with β to be a constant value or a time related function, describing the decay of the drug effect over time [83], [84]. There are also other more complicated forms (linear or non-linear) which describe the drug treatment effects upon tumor cells considering drug resistance and by in biomarkers [71], [84]–[91].

A large number of the studies on modeling drug treatment effects on malignant tumors incorporate the action of a single drug. However, the strategy of treating cancer with

multiple drugs has become widely adopted. This approach aims to maximize treatment effectiveness and reduce the risk of cancer cells developing resistance to the drugs being used. To this direction, several mathematical models have been introduced trying to model and explore possible interactions between the drugs in combination. Koch *et al.* [92] and Rossetti *et al.* [93] are some examples. An extension of [92] and [93] models, was presented and tested by Terranova *et al.* [94]. The model is based on the hypothesis that the co-administered drugs damage the tumor cell populations either alone or in combination which comes in contrast to [93] where no drug-drug interaction is modeled (drugs act without interacting to each other). The drug's effect on the tumor divides the cancer cells into two groups: to those that are damaged and those that are not. The cells that belong to the first group, i.e., the damaged ones, will eventually die through a transit compartment model that considers the delayed drug response. The rate of damage to the tumor cells is described by three terms: two terms proportional to the drug concentrations and one term that represents the interaction between the co-administered drugs, which is proportional to the product of the drug concentrations. For the case where treatment is based on a "cocktail" of two anticancer drugs a and b the interaction effect is formulated as follows:

$$v = \gamma u_a(t)u_b(t) T \quad (2.12)$$

where γ is the drug interaction related parameter, $u_a(t)$ and $u_b(t)$ are the concentrations for each drug a and b , respectively and, T is the fraction of the undamaged tumor cells [94].

Of course, the above equations model an ideal situation. Tumors may be comprised of blood vessels and other cells subpopulations with which they compete for oxygen and nutrients and interact not only with each other but also with normal cells such as immune system cells [74]. The continuous models that are trying to model tumor growth encapsulating the above theory belong to the family of heterogenous models. Usually, tumor mass is separated into subpopulations of cells based on their activity (e.g., proliferative, quiescent, and necrotic cells) [95], [96]. Other heterogeneous models are structured based on the assumption that tumor cells may have or acquire resistance to treatment (i.e., they are not affected) [97]–[103]. This phenomenon is one of the most

important factors that chemotherapy fails. In such models tumor cells are classified as drug sensitive and drug resistance cells based on their sensitivity to treatment. Cell proliferation takes place on both populations however, agents can only act upon and damage drug sensitive tumor cells. An example of such model is described by the following set of ODEs [104]:

$$\begin{aligned}\frac{dT_r}{dt} &= p_r(1 - (T_s + T_r))T_r + S_R(t)T_s \\ \frac{dT_s}{dt} &= (1 - (T_s + T_r))T_s - S_R(t)T_s - du(t)T_s\end{aligned}\tag{2.13}$$

with

$$S_R(t) = (\epsilon + au(t))\tag{2.14}$$

where T_r , T_s are the drug resistant and the drug sensitive tumor cell populations and u the drug dosage. The growth rate of the resistant cells (with respect to the population of the sensitive tumor cells) is described by a factor p_r while the term S_R models the sensitive to resistant transitions (ϵ accounts for the drug independent transition rate of the sensitive to resistant and $au(t)$ the drug related transition rate). Finally, the drug induced deaths of the sensitive tumor cells are described by $du(t)$ term, where d is the drug cytotoxicity parameter.

In addition to these forms of models there are other approaches that model how tumors grow, spread and metastasize [105]–[107] over time taking into account the availability of vital nutrients and how they can affect tumor cells. A tumor is often modeled through PDEs as a density of malignant cells in a spatial position (in single or multi-dimensional space) at the tumor microenvironment or as a fraction of the maximum available volume at this position. The studies of Burton [108], Casciari *et al.* [109] as well as the model of cancer invasion presented by Gatenby and Gawlinski [110], [111] are some of most important spatial models. For example, in [110] Gatenby describes the cancer cells growth over time along with the hydrogen ions (H^+) that are secreted during tumor's cells proliferation (anaerobic metabolism). The increase of H^+ creates an acidic environment which damages the normal host tissue. Furthermore, the model suggests that there is a space between tumor and the host, and it is one of the few mathematical

Prediction of the cancer patients' response to their therapeutical treatment with non-linear forecasting techniques

Chapter 2: Mathematical frameworks in tumor growth and treatment

models that have been tested and confirmed experimentally. Another example is the spatiotemporal model of presented by Papadogiorgaki *et al.* in [112]. In this work a continuous 3-dimensional mathematical model of a vascular glioma spatiotemporal evolution is introduced. The model describes the interactions between four heterogeneous glioma cell populations and their tissue microenvironment investigating how they can affect tumor growth and invasion. It also includes the effects taking place on concentration changes of important nutrients in the tumor microenvironment which lead to the creation of tumor cell populations with varying metabolic profiles and invasion capabilities. Such nutrients are glucose and oxygen. A brief review of this kind of mathematical models is presented in the work of Harris *et al.* [74].

The complexity of the disease and the need to understand in depth its mechanisms led to the creation of another category of models. Goal of these models is to provide a more detailed and realistic representation of the complex processes underlying tumor growth. To achieve this, they describe tumor growth as a series of discrete events scale taking into account genetic and specific biophysical rules that are involved in its processes. The mathematical models belonging to this category are classified as discrete models. However, to build models of this kind may be a challenging and time-consuming task as it may require significant amount of experimental data to parameterize the model. This includes data on biochemical pathways, cell cycle, cell division, cell death, and other intracellular events that control cell survival and death. Data can also be associated with the spatial and temporal heterogeneity of tumors, as well as the effects of therapy and the immune system on tumor growth. Obtaining such data often requires a multidisciplinary approach involving expertise in areas such as cell biology, genetics, and biochemistry. Despite the difficulties, these models can offer valuable understanding of the biology behind tumor growth. Examples of such models can be found in [113]–[119]. To overcome such limitations hybrid mathematical models for tumor growth have been introduced during the last years. Hybrid models or multiscale models – as they also called – are comprised by both discrete and continuous variables taking advantage of the strengths of both modeling techniques [120]–[123].

Accurate descriptions and predictions of the unperturbed and perturbed tumor growth can help towards understanding the underlying biology of cancer evolution, provide

predictions of response to treatments as well as inform treatment decisions leading to improved patient care and outcomes. The tumor growth models reviewed in this chapter comprise only a small portion of the total introduced number. A variety of mathematical modeling approaches for solid tumors are comprehensively analyzed and discussed in [67], [68], [70]–[72], [107], [124]–[127].

2.1.1 Mathematical frameworks for tumor-immune interactions

As mentioned in the previous chapter, the immune system is a fundamental unit in the fight against cancer. Recent progresses in cancer immunology and immunotherapy suggest that its use may be a key variable to prevent or even cure cancer [128]–[135]. To this direction, mathematical modeling has also been used to provide a means to describe and analyze the highly complex interactions between immune system cells populations and cancerous cells. During the past years several mathematical models describing the tumor-immune dynamics been developed. Immunotherapy, chemotherapy their combined action and their effects against cancer have also been explored and modelled. Some approaches that capture and model these dynamics and their interactions in the tumor immune microenvironment have been proposed in the works of [135]–[150]. By such systems clinicians have access to powerful insights into stimulating and modulating immune responses to prevent or even treat cancer, and therefore advance the development of tumor-immunotherapies.

One of the first systems that modeled tumor-immune interactions was introduced in 1994 by Kuznetsov *et al.* [137]. Based on the Lotka-Volterra predator-prey model [152] Kuznetsov created a system of two ODEs able to describe the interaction of two cell populations, the tumor cells (i.e., the prey) and the effectors' cells (i.e., the predator). The model is expressed by the following set of equations:

$$\begin{aligned} \dot{T} &= \alpha T(1 - bT) - nET \\ \dot{E} &= s - dE + p \frac{ET}{g + T} - mET \end{aligned} \tag{2.15}$$

where T represents the population of tumor cells (i.e., prey) and E represents the population of effector cells (i.e., predator). The $\alpha T(1 - bT)$ factor describes the growth of tumor cells population while the mass action form $-nET$ describes the fraction of

Prediction of the cancer patients' response to their therapeutical treatment with non-linear forecasting techniques

Chapter 2: Mathematical frameworks in tumor growth and treatment

tumor cells eliminated by the action of the effector cells. a is the maximum growth rate of the tumor cell population and b^{-1} the maximum carrying capacity of the tumor. The size of the effector cells population is described by a constant rate s , and d is the natural death rate of the effector cells. The term $p \frac{ET}{g+T}$ is a Michaelis-Menten form which describes the growth of the immune system cells due to the presence of the tumor. Finally, a fraction of the effector cells population is eliminated due to its interaction with the cancerous cells. This decay is described by the mass action form $-mET$.

Several mathematical models have then been built on Kuznetsov's model, either by extending the model by adding more cell populations or by modifying terms. For example, Roesch *et al.* [153] added first order loss terms, to include chemotherapy damage to both tumor and immune system cells. Based also on Kuznetsov model, Kirschner and Panetta introduced a three-population model that encapsulates IL-2 (Interleukin-2) dynamics, describing the interactions not only between tumor cells and the activated immune system cells such as NK cells and cytotoxic T-cells but also with cytokine [138]. In a more recent study, Dong *et al.* [154] used a simpler version of Kuznetsov's (as proposed by Gallach [155]) combined with the treatment modelling approach proposed by Kirschner and Panetta including to the system treatments such as TIL injections that boost the immune activity against the tumor cell population.

In 2001, De Pillis and Radunskaya [156] introduced a competition model of tumor growth that includes both the immune system response and chemo drug therapy. It is a four-population model based on aspects of previously developed models such as the Kuznetsov model that includes malignant tumor cells, healthy host cells, immune system cells as well as drug interaction. It incorporates immune response to tumor growth along with chemotherapy. The growth of the immune cells may be stimulated by the presence of the tumor and that can destroy tumor cells through a kinetic process. Both normal cells and tumor cells compete for available resources, while immune cells and tumor cells compete in a predator-prey fashion (competition terms). The model was used to analyze the stability of the drug-free equilibria with respect to the immune response and to simulate qualitatively the asynchronous tumor-drug interaction, i.e., the "Jeff's Phenomenon" [156].

Prediction of the cancer patients' response to their therapeutical treatment with non-linear forecasting techniques

Chapter 2: Mathematical frameworks in tumor growth and treatment

A set of four non-linear differential equations describes the system:

$$\begin{aligned}
 \dot{I} &= s + \frac{\rho IT}{\alpha + T} - c_1 IT - d_1 I - \alpha_I (1 - e^{-u}) I \\
 \dot{T} &= r_T T (1 - b_T T) - c_2 IT - c_3 TN - \alpha_T (1 - e^{-u}) T \\
 \dot{N} &= r_N N (1 - b_N N) - c_4 TN - \alpha_N (1 - e^{-u}) N \\
 \dot{u} &= v(t) - d_2 u
 \end{aligned} \tag{2.16}$$

where I , T and N denote the immune cells (such as CD8+ T cells), the tumor and the normal cells populations, respectively and u is the concentration of the chemotherapy.

The model parameters are presented in the table below:

Table 2.1. Description of the De Pillis model parameters [156].

Parameter	Description	Unit
α_I	Fraction immune cell kill by chemotherapy	L/mg
α_T	Fraction tumor cell kill by chemotherapy	L/mg
α_N	Fraction normal cell kill by chemotherapy	L/mg
α	Immune threshold rate	cells
b_T	Tumor cell carrying capacity	cells ⁻¹
b_N	Normal cell carrying capacity	cells ⁻¹
s	Immune source rate	cells/day
ρ	Immune response rate	day ⁻¹
c_1	Competition term	cells ⁻¹ day ⁻¹
c_2	Competition term	cells ⁻¹ day ⁻¹
c_3	Competition term	cells ⁻¹ day ⁻¹
c_4	Competition term	cells ⁻¹ day ⁻¹
d_1	Per capita death rate of immune cells	day ⁻¹
d_2	Per capita decay rate of the drug	day ⁻¹
r_T	Per unit growth rate of tumor cells	day ⁻¹
r_N	Per unit growth rate of normal cells	day ⁻¹

Cell populations are damaged by constant rates a_i , $i = I, T, N$ which differ for each cell type. Normal cells are being damaged at the lowest rate. On the contrary, tumor cells are damaged with the highest rate. With treatment terms included in the model, simulations with hypothetical dosing schedules are possible. This fact along with the simplicity of the model have made easy to apply optimal control theory and search for improved treatment protocols. Based on this model, several other, more advanced

tumor-immune models have been created [142], [35], [157], [52], [158]–[161]. In addition to that, numerous studies on the optimal control theory for chemotherapy have been published and used to identify and design practical treatment protocols that could improve the standard regimens [149], [162]–[169]. Detailed reviews of tumor-immune interaction models can be found on the works of Adam and Bellomo (1997) [170], Eftimie *et al.* (2011) [171], de Pillis *et al.* (2014) [172], Altrock *et al.* (2015) [173] and Mahlbacher *et al.* (2019) [174].

2.2 Foundations of pharmacokinetic (PK) modeling

Most mathematical models for tumor growth incorporate the effects of chemotherapy on cancer cells. To do that, the drug plasma concentrations of each dosing regimen are inputs to the pharmacodynamic model. While it is vital to know how the administered drug affects the host, it is equally important to know how the body interacts with the drug. Pharmacokinetics (PK) is defined as a branch of pharmacology that focuses on how therapeutic agents (i.e., drugs) move during their passage through the body (i.e., in the blood and subsequently in the tissues), reach their site(s) of action and excreted from the body.

As soon as a chemical enters the body a series of quite complicated processes begins. Absorption, distribution, metabolism, and excretion (ADME) are the four processes which govern the rate of drug accumulation and elimination. A summary of the ADME stages is presented in Table 2.2.

Table 2.2. Description of the ADME stages [175].

Stage	Description
Absorption	The drug enters the body and the systemic circulation.
Distribution	The drug is distributed to the peripheral tissues.
Metabolism	The drug is transformed to other chemical compounds called metabolites.
Excretion	The drug is excreted from the body (through kidneys and urine).

2.2.1 Compartment models in drug kinetics

Through mathematical modelling, PK can describe the time course of the drug concentration in the different areas of the body. However, due to the complexity of the ADME processes some simplifications are essential. A common approach to do this is by

Prediction of the cancer patients' response to their therapeutical treatment with non-linear forecasting techniques

Chapter 2: Mathematical frameworks in tumor growth and treatment

simulating the body and its processes through compartmental models. More specifically, the body is divided into discrete parts, i.e., compartments where the drug kinetics are similar. For example, in organs such as the heart and the liver the drug kinetics follow a similar pattern, thus they may group into a single compartment. The concentration of the drug is measured usually in the plasma. For this reason, plasma and organs like the kidneys, the lungs and the liver are grouped into the same compartment which is called central or highly blood-perfused compartment [176].

At this point it is important to define drug concentration. Concentration is defined as amount of the drug per volume, e.g., in mg/L and it is calculated as:

$$C = \frac{\text{amount of the drug } \left(\frac{\text{mg}}{\text{kg}}\right)}{V_d \left(\frac{\text{L}}{\text{kg}}\right)}, \quad (2.17)$$

where V_d in L/kg is the volume of distribution. The volume of distribution is basically the apparent volume which the chemical compound must be dissolved as soon as it enters the body in order to reach the measured concentration C [177].

The properties of the administered drug along with its observed concentrations in the plasma over time can define the number of the compartments required to accurately describe the PK of the drug. In general, there are one-compartment, two-compartment and multi-compartment models which can be used to model the concentration of an agent in the organism over time. The simplest form of such model includes just the central compartment (see Figure 2.2). In this case both tissues and fluids of the body are included in the compartment while the drug the drug is assumed to be delivered instantly. On the contrary, advanced models like two and multi-compartment models include not only the central, but also other compartments such peripheral and absorption (see Figure 2.3) in the case of extravascular administration of the drug, i.e., intramuscular (i.m.), subcutaneous (s.c.), intraperitoneal (i.p.), oral, etc. A peripheral compartment may include tissues (e.g., muscles and fat) and fluids such as cerebrospinal where the distribution of the drug is slower compared to plasma [178], [179].

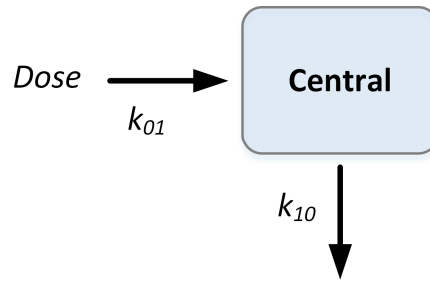


Figure 2.2. One-compartment model representing the transfer of the drug to the central compartment (plasma, etc.). k_{01} and k_{10} represent the first-order fractional rates for absorption and excretion of the drug.

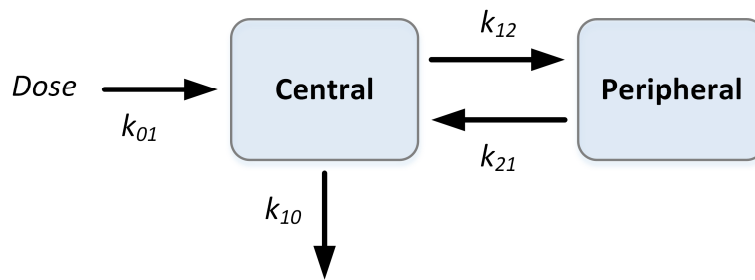


Figure 2.3. Two-compartment model representing the transfer of the drug to and from the central and peripheral compartments. k_{01} , k_{10} , k_{12} and k_{21} represent the first-order fractional rates for absorption, excretion, distribution, and redistribution.

It is also essential to model the changes in the amount of the drug across the body, i.e., in the tissues, the blood (plasma), the organs and the fluids and how it transfers between the different compartments. For this reason, transfer rates of the drug have been introduced. For instance, the transfer rate of the drug (over time) between two compartments is usually described by two first-order rates k_{12} (h^{-1}) and k_{21} (h^{-1}). In most PK models the elimination of the drug takes place in the central compartment where it is excreted from the body at a constant rate k_{10} (h^{-1}). A two-compartment model for bolus administration can be described by a system of differential equations, as follows:

$$\begin{aligned}
 \dot{q}_1(t) &= -k_{10}q_1(t) - k_{12}q_1(t) + k_{21}q_2(t) + k_{01}u(t) \\
 \dot{q}_2(t) &= k_{12}q_1(t) - k_{21}q_2(t) \\
 C_1(t) &= \frac{q_1(t)}{V_1} \\
 C_2(t) &= \frac{q_2(t)}{V_2}
 \end{aligned} \tag{2.18}$$

where k_{01} , k_{10} , k_{12} and k_{21} , in h^{-1} , represent the first-order transfer rates for absorption, excretion, distribution, and redistribution, u is the drug dose in mg/kg, q_1 , q_2 are the amounts of the drug in the central and peripheral compartments, and C_1 and C_2 in mg/L are the drug concentrations, respectively. The drug concentration in the central compartment C_1 is equal to the concentration in the plasma. Finally, V_1 and V_2 in L/kg are the volumes of distribution for each of the two compartments. More details about these and other pharmacokinetics parameters can be found on [176], [180].

2.3 Application of optimal control theory in cancer treatment

Optimal control theory (OCT) is a mathematical framework for analyzing dynamic systems and determining the best control signal overtime that will lead a process to satisfy certain constraints while at the same time will maximize or minimize (i.e., optimize) a predefined performance index. To determine the optimal control signal, it is necessary to define an optimal control problem (OCP). This involves, in the simplest case, the optimization of an integral equation J_D subject to a set of ODEs describing the dynamics of the in-study dynamic system D :

$$\begin{aligned} \text{Minimize } J_D(\underline{x}, \underline{u}, t) &= \int_0^{t_f} F(\underline{x}, \underline{u}, t) dt \\ \text{Subject to: } \frac{d\underline{x}}{dt} &= D(\underline{x}, \underline{u}, t) \\ \text{with } \underline{x}(0) &= \underline{x}_0, \quad 0 = t_0 \leq t \leq t_f \end{aligned} \tag{2.19}$$

Where t is the time, $\underline{x} \in \mathbb{R}^n$ is the system's state variables (e.g., tumor mass, cell populations at time t), $\underline{u} \in \mathbb{R}^m$ is the control vector (e.g., drug doses at time t) which affect the behavior of the system, \underline{x}_0 is the system's states vector values at $t = t_0 = 0$, while t_f is the simulation end-time.

Once the OCP is formulated, there is a variety of numerical methods that can be used to solve it. There are two broad categories in which they are fall into: the direct and the indirect methods [181]. In a direct method a process called "direct transcription" takes place. The OCP is transformed into a discrete constrained minimization problem. The system's states and control variables are discretized to get a non-linear programming problem (NLP). Then, the NLP problem is solved using iterative non-linear optimization

algorithms. However, methods of this type can be sensitive to initial conditions making difficult to find the global optimal solution. Even though they are generally robust they can also be computationally expensive especially in where the number of the system states and the control variables is large. Direct Collocation (e.g., Hermite-Simpson), Direct Single Shooting and Direct Multiple Shooting are some commonly used direct methods [181].

On the other hand, in indirect methods the problem is transformed into another type of problem, which then can be solved using numerical methods. Based on the nature of the given optimal control problem, the optimality conditions typically lead to a two-point boundary value problem (TPBVP) or a multi-point value boundary problem (MPBVP). The optimal solution is determined by satisfying optimality conditions rather than directly minimizing a cost function, as in direct methods. Pontryagin's maximum (or minimum) principle (PMP), dynamic programming (DP) and Hamilton-Jacobi-Bellman (HJB) equation are some of the most well-known indirect methods [182]–[184]. More information about direct, indirect, and other type of methods can be found on [185]–[190].

The solution of the optimal control problem of dynamical systems is well-established for Linear Time Invariant (LTI) systems subjected to a linear quadratic functional. The solution of algebraic Riccati equations (ARE) produces necessary information to compute the optimal feedback gain(s). Hence, the regulation (stabilization) problem of LTI systems, which is known as linear quadratic regulator (LQR), is solved in optimal way. The optimal control for non-linear systems, on the other hand, cannot – in general – be handled in a way similar to LTI systems as the solutions of HJB equations do not yield a straightforward procedure. Analytical solutions for the optimal control may be obtained for only a few restricted cases since the governing equations for optimality are also non-linear and their solutions should satisfy the terminal conditions. It is well known [24] that even numerical solutions for the optimal control cannot be obtained with precision for non-linear systems as the number of possible candidates for the optimal solution is not known [186]. This difficulty brings out many different approaches to approximate solutions to the HJB equation which are regarded as suboptimal solutions to the optimal control problem of non-linear dynamical systems.

One of the approaches to the optimal control of non-linear systems is the use of the State-Dependent Riccati Equation (SDRE) [191]. In brief, SDRE provides a systematic approach to design non-linear feedback controllers that can approximate the solution of the infinite time horizon optimal control problem. It gives time responses of the non-linear mathematical model in real-time, making it possible to implement the controllers online. Essentially, SDRE allows for the design of controllers that can control non-linear systems in real-time by approximating the optimal control solution [192]–[194]. This is achieved by factoring the non-linearity of the state equations as product of a state-dependent matrix with the state vector (i.e., the non-linear system of equations is transformed to a linear structure comprised of state-dependent coefficient matrices). The simplicity of the algorithm along with its effectiveness make SDRE the ideal tool for the design of non-linear controllers. In contrast to other strategies which try to solve Hamilton-Jacobi-Bellman partial differential equations and non-linear two-point boundary value problems, the SDRE method involves only the factorization of the non-linear dynamics to a linear structure and an ARE. A detailed description of the LQR and SDRE methods is presented in Appendix D.

2.3.1 Optimal control theory in tumor growth modeling and treatment strategies

Despite the significant increase in the number and types of cancer treatments during the last decades, the precise dosing and timing of administration of the drug remains imprecise. Treatment regimens are determined through costly and lengthy clinical trials, which first determine the MTD and then assess the expected effectiveness for the average patient. However, this approach, within the clinical trial system does not allow for a systematic evaluation of all possible dosing schemes, leaving the optimal scheduling of radiation and systemic therapies, such as chemotherapy, largely unknown.

In the context of tumor growth modeling, OCT can be used to determine the optimal treatment strategy for a given patient. This involves finding the best immunotherapy and/or chemotherapy drug dose levels and treatment schedules, taking into account the predicted growth of the tumor and the potential risks and benefits of different treatment options [195]. Once a tumor growth model has been developed, using patient-specific data, optimal control theory can be used to determine the optimal

Prediction of the cancer patients' response to their therapeutical treatment with non-linear forecasting techniques

Chapter 2: Mathematical frameworks in tumor growth and treatment

treatment strategy which may lead to tumor eradication while minimizing any potential risks or side effects of treatment. In literature, some of the first applications of optimal control theory to mathematical models of cancer biology and tumor treatment date back to 1970s [196], [197]. Specifically, the work of Swan and Vincent in 1977 [197] was the first to apply optimal control in human IgG multiple myeloma. Till this day a plethora of works on optimal control for mathematical models of cancer therapies such as chemotherapy and/or immunotherapy have been published. A small pool of such works can be found on [156], [162], [163], [172], [195], [168], [198]–[217], [218], [219].

Usually, a tumor receiving some kind of treatment, such as chemotherapy, can be viewed as a control system. The state of the system is given by the population(s) of cancer cells or the tumor mass(es) at time t , while the control signal(s) at that time t , u . Typically, the variable u represents the amount of the administered drug or its impact on healthy tissue and cancer cells. Since chemotherapy can affect both types of cells (normal & cancer cells) the goal of the control problem is to minimize the number of cancer cells while also maintaining a safe level of toxicity for normal tissue. Overall, optimal control theory can be a useful tool for optimizing treatment decisions in the context of tumor growth modeling, helping to improve patient outcomes and increase survival rates.

Chapter 3: Material and methods

3.1 Human-to-mouse xenograft data

Experimental data from human-to-mouse cancer xenografts were used in the present study. The data were obtained from the experimental studies reported by Bilalis *et al.* [220] and Rocchetti *et al.* [93].

In the first case (i.e., data from Bilalis *et al.*), AsPC-1 human pancreatic cancer cell line was xenografted subcutaneously at the rear flank of male NOD SCID mice. All mice received intraperitoneal injections of gemcitabine twice, in a week interval (the days 19 and 26 after the inoculation of the tumor cells). The dose of the drug was at 100 mg/kg/injection/mouse (see Figure 3.1). The pharmacodynamic (PD) data after the two i.p. injections of 100 mg/kg on days 19 and 26 after the inoculation are given in Table 3.1 below:

Table 3.1. Average tumor masses registered in the experiment of [220] (i.e., gemcitabine given i.p. at 100 mg/kg on days 19 and 26).

Day	Tumor masses (g)	
	Unperturbed	Under gemcitabine
15	0.22	0.22
19	0.41	0.43
22	0.83	0.64
26	1.16	0.80
32	1.41	1.00
35	1.34	0.98
39	1.65	1.25

It must be noted that linear interpolation was used to estimate the “unobserved” tumor masses in the time instants that an observation (tumor measurement) was not carried out (e.g., at days 0-14, 16-18, 20-21, etc.).

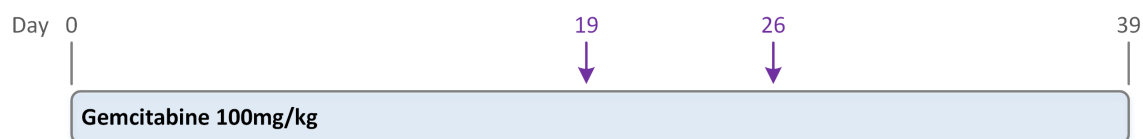


Figure 3.1. Gemcitabine treatment schedule: 100 mg/kg administered at days 19 and 26 post tumor inoculation.

In the second case (data from Rocchetti *et al.* [93]), HT29 human colon cancer cell lines were implanted subcutaneously at the left flank of mice. All mice of the experiments received intravenous injections of irinotecan (CPT-11) and 5-fluorouracil (5-FU) in combination with an under development anticancer agent C2 (see Figure 3.2 and Figure 3.3).

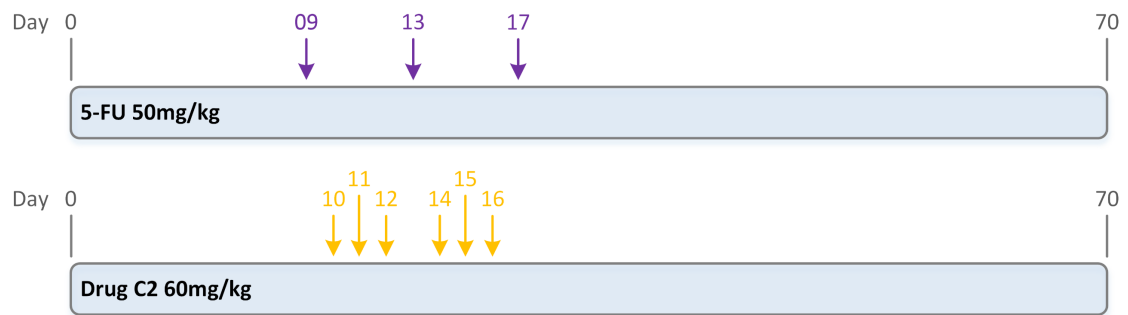


Figure 3.2. 5-FU and drug C2 treatment schedule: 50 mg/kg of 5-FU administered q4dx3 from day 9 and 60 mg/kg of drug C2 on days 10, 11, 12 and 14, 15, 16 post tumor inoculation.

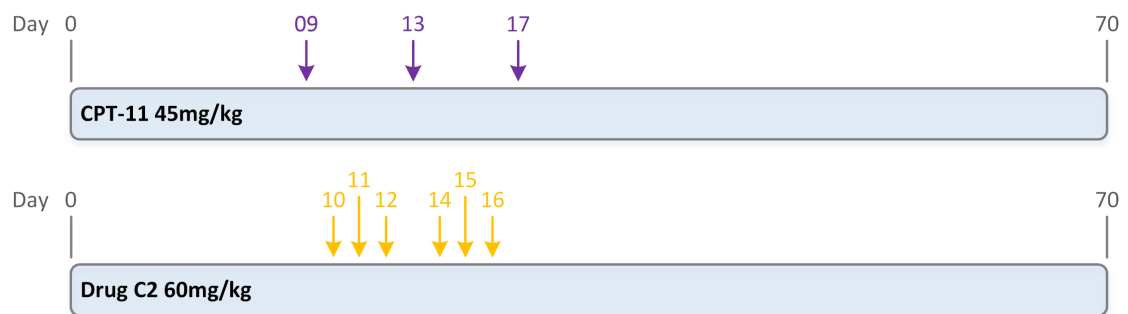


Figure 3.3. CPT-11 and drug C2 treatment schedule: 45 mg/kg of CPT-11 administered q4dx3 from day 9 and 60 mg/kg of drug C2 on days 10, 11, 12 and 14, 15, 16 post tumor inoculation.

5-FU and CPT-11 were given iv at doses of 50 mg/kg and 45 mg/kg respectively, three times at an interval of four days (q4dx3), starting from day 9. On the other hand, drug C2 was administered orally at 60 mg/kg on days 10, 11, 12 and 14, 15, 16 after the tumor inoculation.

3.2 The inverse problem: parameters estimation in mathematical modeling

In many mathematical modeling cases of physical processes, the model parameters are unknown. Therefore, they must be estimated using the available input-output experimental observations. This type of problem is often called the “inverse problem”. It is called “inverse” since it uses the results of actual observations to infer (i.e.,

calculate) the casual factors that produced them (i.e., the numerical values of the parameters of the linear/non-linear mathematical model).

Observations → Casual factors (model parameters)

A way to address this is by defining and solving an optimization problem. An optimization problem is a computational problem in which the object is to select the optimal solution from among the set of candidate solutions [221]. In order to quantify and evaluate the goodness of a possible solution an objective/cost function is used. To be more specific, a set of arguments that minimizes the value of the cost function subject to a number of constraints is explored. The set which gives the global minimum value (i.e., the minimal cost function value) is the solution to the optimization problem. This vector of values is also the solution to the parameter estimation problem.

A standard mathematical representation of the general optimization problem is shown below [222]:

$$\begin{aligned} \text{Let } J & \mathbb{R}^n \rightarrow \mathbb{R} \\ \text{Find } \hat{\underline{x}} & = \operatorname{argmin} J(\underline{x}), \quad \underline{x} \in \mathbb{R}^n \\ \text{Subject to: } & g_i(\underline{x}) \leq 0, \quad i = 1, \dots, m \\ & h_j(\underline{x}) \leq 0, \quad j = 1, \dots, p \\ & x_{r,\min} \leq x_r \leq x_{r,\max} \quad r = 1, \dots, n \end{aligned} \quad (3.1)$$

where J is the objective function, $\hat{\underline{x}}$ is the unique minimizer and the solution to the problem, $g_i(\underline{x})$ is an inequality constraint and $h_j(\underline{x})$ an equality constraint function. The vector $\underline{x} = [x_1, \dots, x_n]$ represents the design variables. The adjustment of these variables inside the design space defined by the constraints leads to the global optimum.

Ideally, for each cost function there is a set of parameters' values which provides an optimal solution to the problem. However, in many cases it is very difficult to find a unique vector of values that provides a global solution to the problem (see Figure 3.4 and Figure 3.5 below). In many applications the objective function can have both a global minimum and several local minimizers. Hence, it may be hard for optimization algorithms to identify an optimal solution to the problem. Among optimization approaches, linear and non-linear, metaheuristic optimization methods have proven capable of finding near optimal solutions to various problems. In contrast, analytical

approaches may not detect the optimal solution within a reasonable computational time, especially when the global minimum is surrounded by many local minima.

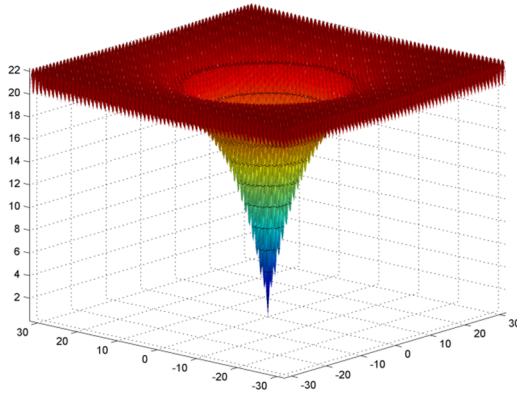


Figure 3.4. A non-convex objective function with a global minimum and multiple local minima.

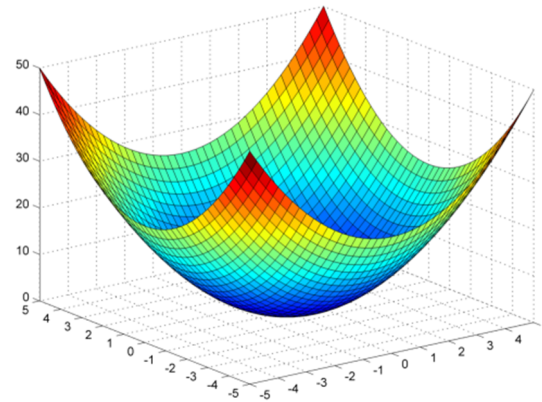


Figure 3.5. A convex function with one global minimum.

Metaheuristic algorithms are usually inspired by observations of phenomena and rules found in nature, such as the Genetic Algorithm (GA), Simulated Annealing (SA), Particle Swarm Optimization (PSO), Harmony Search (HS), and so on. A relatively new metaheuristic optimization algorithm capable of finding solutions to complex constrained and unconstrained optimization problems is the Neural Network Algorithm (NNA) [223]. This method is based on the biological nervous system and the structure/configuration of artificial neural networks (ANNs). A detailed description of the algorithm is given in Appendix A.

In the cases of the experimental data, such as those of Bilalis *et al.* [220] and Rocchetti *et al.* [93], which are studied in this work, the tumor growth curve (i.e., the model output) in combination with the delivered chemotherapy dosing (i.e., the model input) are used to estimate the values of the parameters of each model from the experimental observations (i.e., the physical process). More specifically, an objective function J , which depends on the model's unknown parameters values and time, created by the comparator of Figure 3.6, must be minimized with respect to the vector of the model's unknown parameters \underline{x} .

The vector that minimizes the cost function $J(\underline{x}, t)$, is the solution to the model parameters estimation problem.

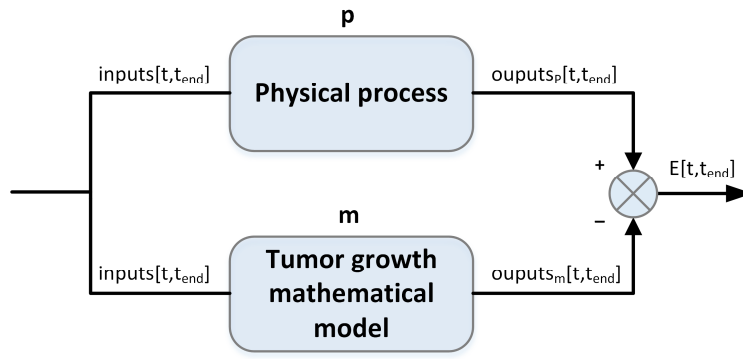


Figure 3.6. Comparator procedure between the physical experimental process of xenografted mice and the under fitting to the experimental data tumor growth inhibition model.

A commonly used objective function, described by the equation below, is the sum of square errors:

$$J(\underline{x}, t) = \sum_{t=0}^{N \cdot \Delta T} E^2(\underline{x}, t), \text{ where } t = i \cdot \Delta T, i = 0, 1, \dots, N \quad (3.2)$$

where $E(\underline{x}, t)$ is calculated as the difference between the measured (observed) tumor mass at each time point t and the tumor mass estimated by the model simulation at the same time point t .

$$E(\underline{x}, t) = output_{physical}(t) - output_{model}(\underline{x}, t) \quad (3.3)$$

with $output_{physical}$ to be the observed tumor mass and $output_{model}(\underline{x}, t)$ the tumor mass estimated by the model.

Of course, introducing extra terms in J , such as the regularization term:

$$L_2 = \lambda \sum_{r=1}^n x_r^2 \quad (3.4)$$

where λ is the regularization strength, can help in preventing overfitting, especially in cases where a model has a large number of parameters. This term penalizes large values of parameters to avoid overfitting, with the strength of this penalty determined by λ . A larger value of λ results in stronger regularization.

3.3 Adaptive short-term ahead predictions of tumor growth evolution

Accurate (statistically) forecasting of tumor evolution is essential for evaluating treatment efficacy. A methodology for statistically robust predictions of tumor growth

in the near future, based on available experimental data up to a given time instant is described here. The proposed approach utilizes the parameter estimation of a mathematical model, linear or non-linear, to simulate and predict tumor growth inhibition.

Firstly, the parameters of a mathematical model representing tumor growth are estimated using a subset of experimental data available from day 0 up to a specific time instant, denoted as t_e , $t_e \leq t_{end}$, t_{end} being the last day of the experiment. For this purpose, methods such as NNA and Complex method of Box can be used. Once its parameters are estimated, the model is numerically integrated (i.e., simulated) using the available inputs, i.e., the anticancer agent dosing of the experiment delivered up to time t_e (model inputs) for the time periods $[0, t_e + i]$, $i \in \mathbb{N}$, i being the forecasting horizon, i.e., the number of steps (e.g., days) ahead. This simulation aims to predict tumor growth inhibition for different time horizons, such as $i = 1, 2, 3, 4$, or 5 days ahead, leading to $[0, t_e + 1]$, $[0, t_e + 2]$, $[0, t_e + 3]$, $[0, t_e + 4]$, and $[0, t_e + 5]$ time periods, respectively. To assess the accuracy of the predictions, commonly used metrics, such as the root mean square error (RMSE) and the mean absolute percentage error (MAPE), are utilized for each step ahead. More information on the metrics used can be found in the Section 3.4. Following prediction evaluation, the model parameters are updated for the "new" time period $[0, t_{e,new} = t_e + 1]$. Specifically, the model parameters are re-estimated based on a new, extended subset of the experimental data, available until day $t_{e,new} = t_e + 1$, acting as an extended window. The time instant $t_{e,new}$ is assigned as the new "time index" t_e , and the procedure re-starts and repeated, iteratively updating the model parameters and predicting tumor growth until the final experimental day, $t_{e,new} = t_{end}$. The above methodology can be understood through the simple flow diagram, shown in Figure 3.7.

To improve prediction accuracy and computational efficiency, a moving (rolling/sliding) window technique can also be applied to the experimental data, instead of the extended window. This technique involves selecting subsets of time-dependent measurements by considering the most recent l time instants' measurements ($t = n \cdot \Delta T$, where $n = 0, 1, \dots, N$, and $l \ll N$). The length of the moving window can be determined either by trial and error or by using metrics, such as the Akaike's information criterion (AIC) [221].

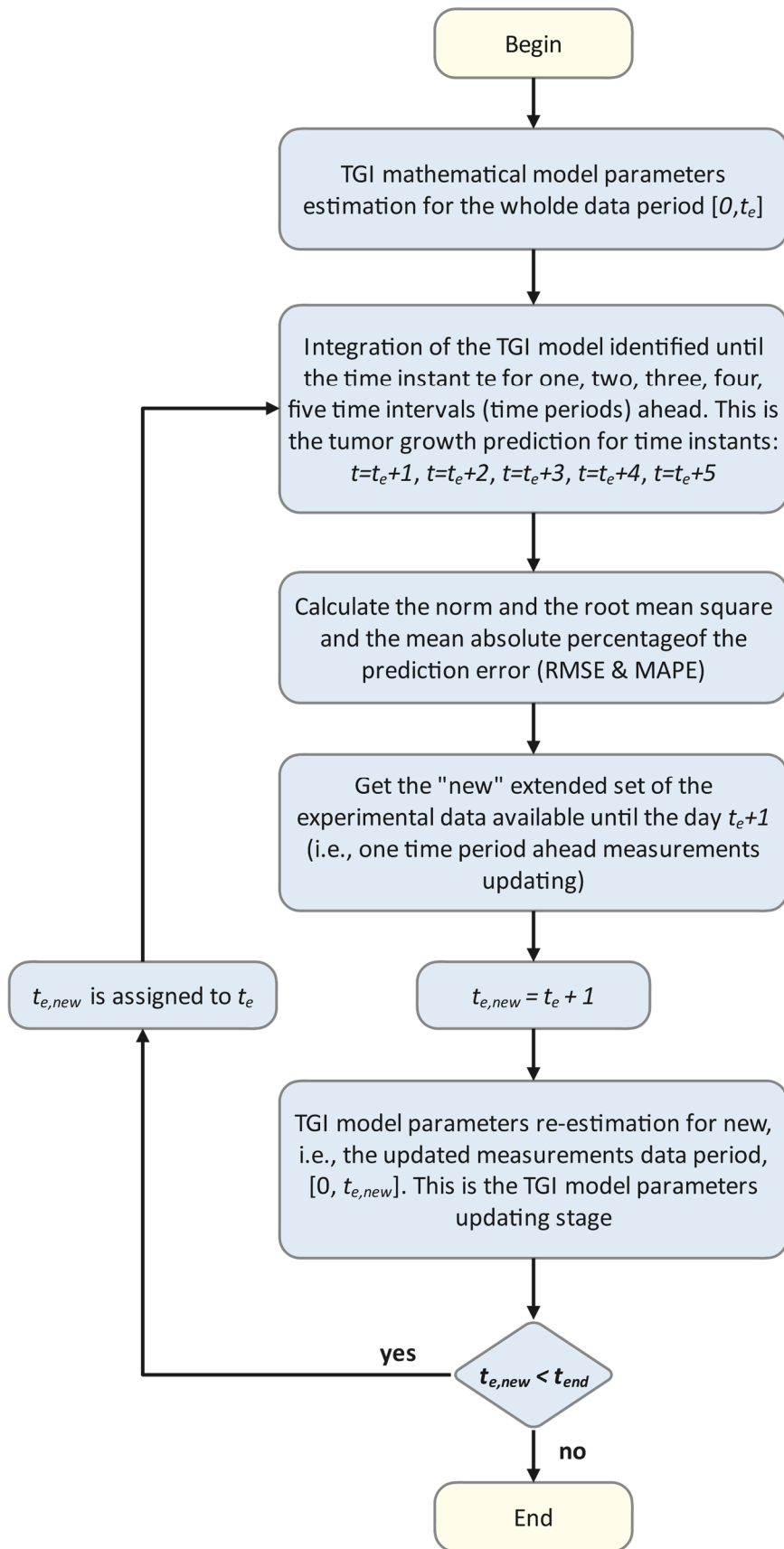


Figure 3.7. Flowchart of the proposed procedure for the measurement and the model update, ensuring effective adaptive short-term ahead tumor growth prediction.

By continually updating the mathematical model parameters based on the "input-output" measurements within the moving window formed at each time instant, the methodology may efficiently capture the changing slopes of the experimental data curves. This iterative parameter update process enables the model to adapt and align more closely with the observed tumor growth dynamics, which may result in improved predictive accuracy. The inclusion of the moving window approach ensures that recent data points have a stronger influence on parameter estimation, which potentially may enhance the model's ability to capture temporal variations in tumor evolution.

3.4 Performance evaluation metrics

The performance of the models, their fitting to the tumor growth data as well as the tumor growth predictions were evaluated using statistical parameters. More specifically, commonly used scale-dependent and scale-independent metrics such as the mean square error (MSE), the root mean square error (RMSE) [224] and the mean absolute percentage error (MAPE) [225] were calculated to measure the fitting error:

$$\text{MSE (units}^2\text{)} = \frac{1}{d} \sum_{i=1}^d (P_i - O_i)^2 \quad (3.5)$$

$$\text{RMSE (units)} = \sqrt{\frac{1}{d} \sum_{i=1}^d (P_i - O_i)^2} \quad (3.6)$$

$$\text{MAPE (\%)} = \frac{1}{d} \sum_{i=1}^d \left(\frac{|P_i - O_i|}{O_i} \times 100 \right) \quad (3.7)$$

where d is the number of the data points in the dataset (e.g., the tumor mass at each time point (e.g., day)) and P_i denotes the prediction (estimation) of the actual measurement (observation) O_i . The smaller the value of the statistic is (i.e., closer to 0), the better the identified model performs.

PART I

Mathematical modeling approaches for efficient tumor growth inhibition predictions

Chapter 4: Tumor growth inhibition (TGI) mathematical model

4.1 The Simeoni *et al.*'s TGI mathematical model

A first order differential equations (i.e., state-space) mathematical model based on a few biologically pertinent parameters, with only requirement the data collected in preclinical studies such as the pharmacokinetics (PK) of the anticancer drugs, linking the progress (i.e., evolution) of the tumor mass with the administrated anticancer agent during treatment, is the one first presented by Simeoni *et al.* in 2004 [226], [227]. The pharmacokinetic-pharmacodynamic (PK-PD) state-space mathematical model (TGI model, in brief) is described by the set of the non-linear first order differential equations (4.1) shown below:

$$\begin{aligned} \frac{dz_0(t)}{dt} &= \frac{\lambda_0 \cdot z_0(t)}{\left[1 + \left(\frac{\lambda_0}{\lambda_1} \cdot w(t)\right)^\psi\right]^{\frac{1}{\psi}}} - k_2 \cdot c(t) \cdot z_0(t) \\ \frac{dz_1(t)}{dt} &= k_2 \cdot c(t) \cdot z_0(t) - k_1 \cdot z_1(t) \\ \frac{dz_2(t)}{dt} &= k_1 \cdot [z_1(t) - z_2(t)] \\ \frac{dz_3(t)}{dt} &= k_1 \cdot [z_2(t) - z_3(t)] \\ w(t) &= z_0(t) + z_1(t) + z_2(t) + z_3(t) \end{aligned} \tag{4.1}$$

with

$$z_0(0) = w_0 \text{ and } z_1(0) = z_2(0) = z_3(0) = 0$$

And $c(t) = 0$, before any treatment administration.

The unperturbed growth of the tumor in xenograft models is characterized by two phases [226], [228]: a rapid or exponential growth at the early stages of the tumor development, followed by a linear one, when the tumor mass overcomes a certain threshold. This behavior is accurately described by the equations of TGI model shown above. It has been observed that the value $\psi = 20$ allows the (4.1) system to pass from the first order to the zero-order growth sharply enough, during the unperturbed tumor growth phase. The parameters λ_0 and λ_1 represent the growth rates of the two phases described above, i.e., the exponential and the linear growth rate, respectively.

Prediction of the cancer patients' response to their therapeutical treatment with non-linear forecasting techniques

Chapter 4: Tumor Growth Inhibition (TGI) mathematical model

w_0 represents the tumor mass at the inoculation time, defined as $t = 0$. In treated animals, the administrated anticancer agent concentration $c(t)$ (in mg/L) is not zero and thus its effect impinges upon the cycling (proliferating) cancer cells, i.e., the perturbed tumor growth phase. Due to the action of the anticancer treatment, a portion of these cells stops proliferation and after passing through three progressive stages of damage they finally die. At each time instant t ($t \geq 0$) the total tumor mass $w(t)$ (i.e., the output of the model) is calculated as the sum of all state-space variables z . More specifically, $z_0(t)$ is the mass of the proliferating tumor cells and z_i , $i = 1,2,3$ is the mass of the damaged (by chemotherapy) tumor cells in each stage of damage. The plasma concentration of the antineoplastic agent is indicated by the variable $c(t)$ (i.e., the input to the model). The portion of the tumor cells damaged by an anticancer drug is increased by a parameter k_2 , which is a measure of the drug's potency. In case a cancer cell is affected by the agent action, cell division stops, and it proceeds through three different states z_1 , z_2 and z_3 , each one defined by different progressive stages of damage. The transition from a state to another, i.e., the kinetics of cancerous cell death, is described by a first order rate constant k_1 , which is inversely proportional to the mean time-to-death of the tumor cells. In brief, the set of the two parameters (k_1, k_2) describe the effects of the anticancer drug to inhibit the tumor growth while $(w_0, \lambda_0, \lambda_1)$ describe the tumor kinetics in absence of treatment (i.e., the unperturbed case). It is important to note that in the unperturbed case where $c(t) = 0$ the total tumor growth mass is calculated as $w(t) = z_0(t)$. A diagram, adapted from Simeoni *et al.* [226] that describes the TGI model can be seen in Figure 4.1 below:

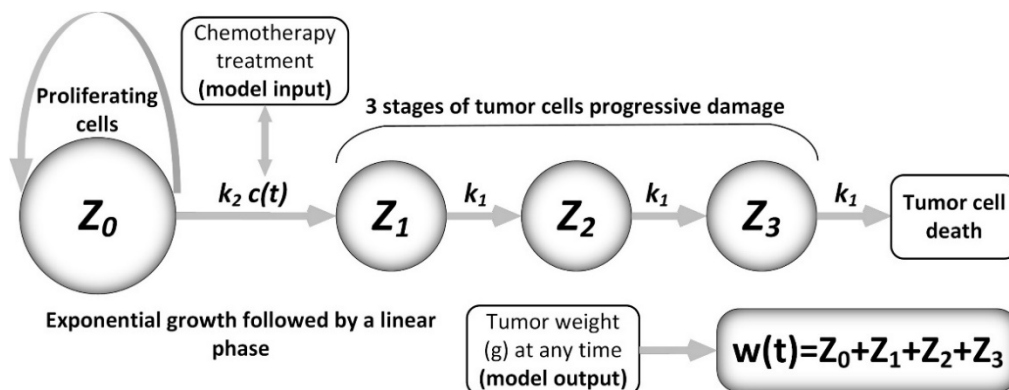


Figure 4.1. Diagram of the PK-PD TGI state-space model introduced by Simeoni *et al.* [226]. k_1 : first-order rate constant of transit; k_2 : anti-tumor potency of the anticancer agent, $c(t)$: plasma concentration of the anticancer agent and $w(t)$: tumor weight at any time t .

Prediction of the cancer patients' response to their therapeutical treatment with non-linear forecasting techniques

Chapter 4: Tumor Growth Inhibition (TGI) mathematical model

The set of the above non-linear differential equations (4.1), can be also written in the following form:

$$\dot{\underline{z}}(t) = \underline{f}(\underline{z}(t), \underline{x}) + \underline{B}(\underline{z}(t)) u(t) \quad (4.2)$$

where $z_i(t)$, $i = 0,1,2,3$, are the four state variables, $\underline{x}^T \triangleq [k_1, k_2, \lambda_0, \lambda_1, w_0]$ is a vector of the five biologically relevant principal parameters and $u(t) \triangleq c(t)$ is the input (i.e., chemotherapy drug plasma concentration) to the model. A short description of each parameter of the model is presented in Table 4.1 [226], [227].

Table 4.1. Pharmacodynamic (PD) parameters of the TGI model.

Parameter	Description	Unit
k_1	First-order rate constant of transit	1/day
k_2	Anti-tumor potency of the anticancer agent	ml/ng day
λ_0	Exponential tumor growth rate	1/day
λ_1	Linear tumor growth rate	g/day
w_0	Tumor mass at the inoculation time	g

Apart from the five principal pharmacodynamic (PD) parameters described above, two important and biologically relevant parameters, also called “secondary TGI parameters” can be obtained from the TGI mathematical model [227]. The first one is a time efficacy index (TEI) which can be calculated using the following equation:

$$TEI = \frac{k_2 \cdot AUC}{\lambda_0}, \quad (4.3)$$

where AUC is the area under the plasma concentration-time curve of the administered anticancer agent. TEI is a time metric that measures the efficacy of a chemo treatment using the achieved tumor growth delay, i.e., the time-lag required to achieve a predetermined tumor mass between treated and untreated animals during the linear phase of the tumor growth.

C_T is another parameter which can be calculated. It describes a threshold of the delivered anticancer agent's concentration in order to achieve tumor eradication. Treatment schedules with concentrations exceeding C_T for at least some period of time,

may be capable of delaying significantly the tumor growth and reducing correspondingly the tumor mass. The threshold concentration can be calculated as follows:

$$C_T = \frac{\lambda_0}{k_2}. \quad (4.4)$$

4.2 Model identification – TGI model's parameters values estimation

The tumor growth inhibition model presented above has been extensively used to describe the dynamics of the growth of several cancer cells lines (see [226], [227], [229]) under the effects of different chemotherapy compounds administrated in several different schedules. As in many mathematical modeling cases of physical processes, the mathematical model parameters are unknown, and they must be estimated using the available input-output experimental observations. In the case of the experimental data of Bilalis *et al.* [220], the gemcitabine regimen (i.e., the TGI model input) in combination with the tumor growth curve (i.e., the TGI model output) were used in order to estimate the Simeoni *et al.*'s model's principal parameters values from the tumor mass observations (the physical process).

A cost function J depending on time and the TGI model's unknown parameters values, created by the comparator procedure of Figure 3.6 and (3.2) and (3.3), was minimized with respect to the vector of the unknown parameters of the model, $\underline{x}^T = [k_1, k_2, \lambda_0, \lambda_1, w_0] \triangleq [x_1, \dots, x_n]$ ($n = 5$ in the present case) to be to best fit of the TGI state-space mathematical model to the experimental data. For any given set (i.e., vector \underline{x}) of the unknown parameters' values, the non-linear TGI model, when solved numerically for the same time period as that of the experiments, simulates the tumor growth for the same time period. The vector of the unknown parameters' values that minimizes the cost function $J(\underline{x}, t)$ is the solution to the TGI mathematical model's unknown primary parameters k_1, k_2, w_0, λ_0 and λ_1 estimation problem. The function $J(\underline{x}, t)$ formed by the sum of square errors during the xenografted mice experiment period was minimized using the non-linear optimization algorithm NNA. Further details on the working principles of NNA can be found in the Appendix A. To achieve the best fit to the experimental data some hard bounds on the model's primary parameters

Prediction of the cancer patients' response to their therapeutical treatment with non-linear forecasting techniques

Chapter 4: Tumor Growth Inhibition (TGI) mathematical model

values was defined. The lower and upper physically imposed bounds for the values of each parameter are presented in Table 4.2 below.

Table 4.2. Value range of the TGI mathematical model principal parameters.

	Parameters				
	k_1	k_2	λ_0	λ_1	w_0
Units	1/day	ml/ng day	1/day	g/day	g
Value Range	(0, 1)	(0, 10E-3)	(0, 1)	(0, 1)	(0, 1)

The pharmacokinetic data of gemcitabine were obtained and depicted from the almost identical experiments found in the literature, i.e., Veerman *et al.* [230]. The PKs (i.e., the drug plasma concentration) attained after the i.p. administration of gemcitabine were described by applying a single-compartment model. The compartmental model is described by the below set of differential equations:

$$\begin{aligned} \dot{q}(t) &= -k_{10}q(t) + k_{01}u(t) \\ c(t) &= \frac{q(t)}{V} \end{aligned} \tag{4.5}$$

where k_{01} in h^{-1} is a first-order transfer rate, u is the anticancer agent dose in mg/kg, q is the amount of the drug in the central compartment, and c in mg/L is the drug concentration in plasma. V is the volume of distribution in L/kg. The *in-silico* plasma concentration of gemcitabine after two intraperitoneal (i.p.) injections at 100 mg/kg (in a 7-day interval) resulted from the above equations is shown in Figure 4.2 below.

As it is shown in Figure 4.3 the identified TGI model could describe with accuracy the tumor growth experimental curves, with fitting statistical errors to be less than 10% (see Table 4.3). Using the estimated TGI model's primary parameters values (Table 4.4), a threshold concentration C_T for the tumor eradication of ~ 336 ng/ml (0.336 mg/l) was estimated, which means that any drug concentration over this value eventually may lead to a delayed tumor growth and hence can be considered effective. The TEI value, i.e., the efficacy of a treatment measured using the achieved delay of the tumor growth, was estimated to be approximately 7.2 days which means that the tumor growth was inhibited in this experiment by gemcitabine for about 7 days.

Prediction of the cancer patients' response to their therapeutical treatment with non-linear forecasting techniques

Chapter 4: Tumor Growth Inhibition (TGI) mathematical model

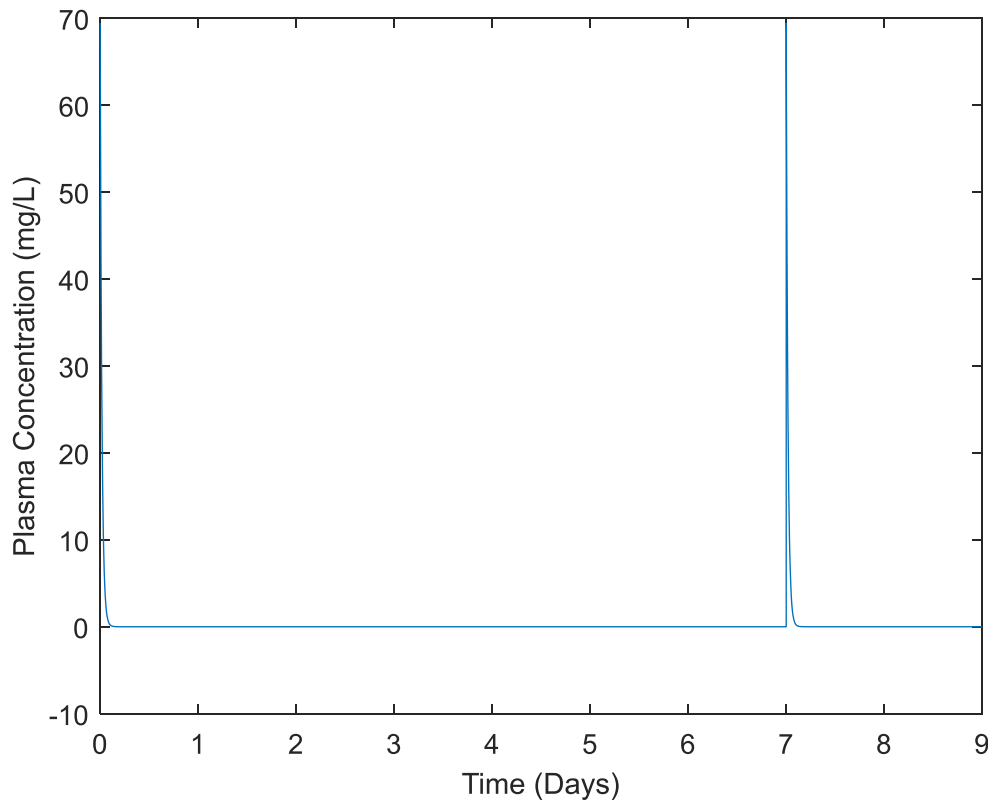


Figure 4.2. Plasma concentration of gemcitabine (measured in mg/L). Gemcitabine administrated as repeated i.p. doses at 100 mg/kg, with 7-days interval [230].

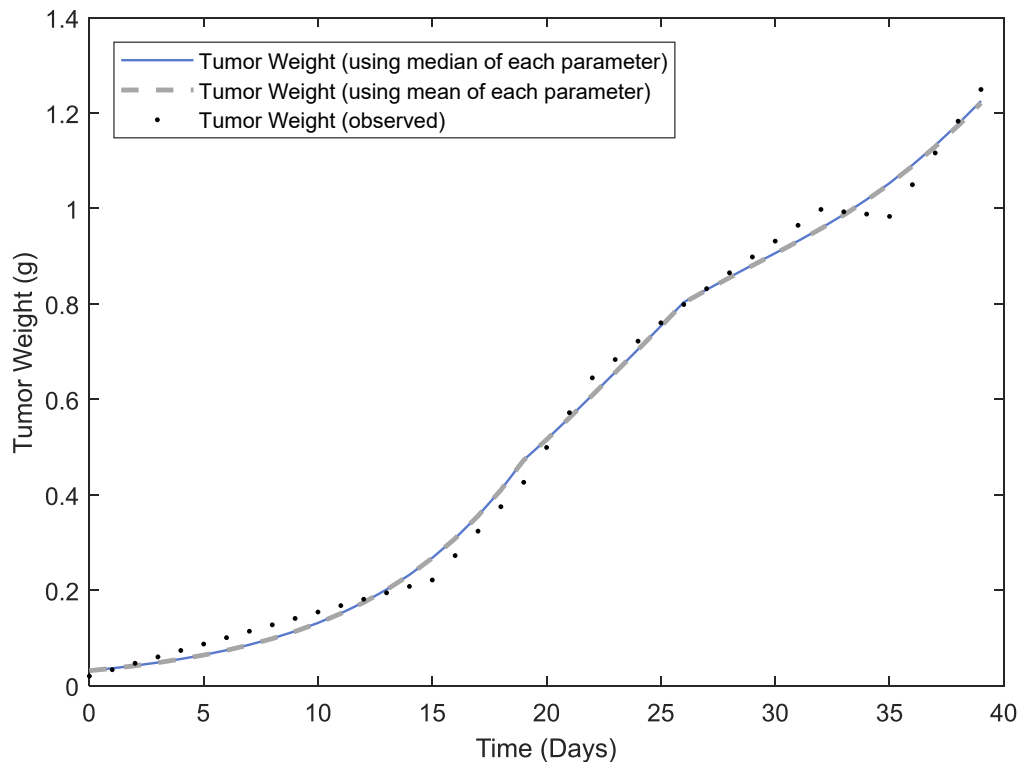


Figure 4.3. Observed/interpolated (black dots) and best fitted TGI mathematical model tumor growth curves obtained in mice given i.p. doses of gemcitabine (100 mg/kg on days 19 and 26) using the median (continuous line) and the mean (dashed line) of the estimated values of each unknown parameter.

Table 4.3. TGI mathematical model fitting errors to the tumor growth experimental curve obtained in mice administered i.p. doses of gemcitabine (100 mg/kg on days 19 and 26).

Evaluation metrics	Median of each estimated parameter	Mean of each estimated parameter
RMSE(g)	0.02663	0.02661
MAPE (%)	9.93	9.97

Table 4.4. Pharmacodynamic parameters values of the TGI model. Obtained by best fitting the Simeoni TGI model to the tumor growth curve of mice given gemcitabine i.p. injections.

TGI model's estimated parameters values					
	k_1	k_2	λ_0	λ_1	w_0
Units	1/day	ml/ng/day	1/day	g/day	g
Median	0.23810	4.22e-4	0.14202	0.07618	0.03147
Mean	0.23294	4.23e-4	0.14225	0.07573	0.03131
SD	0.01069	0.00003	0.00193	0.00199	0.00104
CV (%)	4.59	6.20	1.35	2.63	3.31

SD: Standard deviation; CV: coefficient of variation; k_1 , first-order rate constant of tumor growth transit; k_2 , measure of anticancer drug potency; λ_0 , first-order rate constant of tumor growth; λ_1 , zero-order rate constant of tumor growth; w_0 , tumor weight at the inoculation time.

4.3 Short-term ahead predictions of the tumor growth inhibition

Using the NNA algorithm (see Appendix A00), the TGI model was first identified using the experimental input-output data until the 25th day ($t_e = 25$, initially). Then it was integrated for one, two, three, four, five time periods ahead to predict the tumor's growth at the 26th, 27th, 28th, 29th, and 30th day respectively. On the 26th day, a dose of 100 mg/kg gemcitabine was administrated in mice. An optimal length $l = 5$ (i.e., the last l time instants measurements) of the moving window was applied based on the AIC criterion. Thus, the TGI model parameters were re-estimated using the TGI data from the 22nd day to the 26th day of the experiment, i.e., $t_{e,new} = t_e + 1 = 26$. Next, the prediction error was determined using the predicted value and the corresponding actual value, known by the laboratory experiments. Starting from the new $t_e = t_{e,new} = 26$, the tumor growth was predicted again for one, two, three, four, five time periods (days) ahead, i.e. for the days $t = 27, 28, 29, 30$ and 31 . Subsequently, the model's parameters were re-estimated using the TGI data from the 23rd to the 27th day of the experiment, i.e., $t_{e,new} = t_e + 1 = 27$ (moving the window) and the prediction errors were

Prediction of the cancer patients' response to their therapeutical treatment with non-linear forecasting techniques

Chapter 4: Tumor Growth Inhibition (TGI) mathematical model

calculated. The whole procedure of the measurement update, of the re-estimation of the TGI model's parameters following each measurement update (based on the last $l = 5$ time instants measurements) and of the adaptive tumor growth prediction is continued step by step until the end of the experiment, $t_{end} = 39$.

The tumor growth prediction curves for one, two, three, four and five time periods ahead, are shown in Figure 4.4.

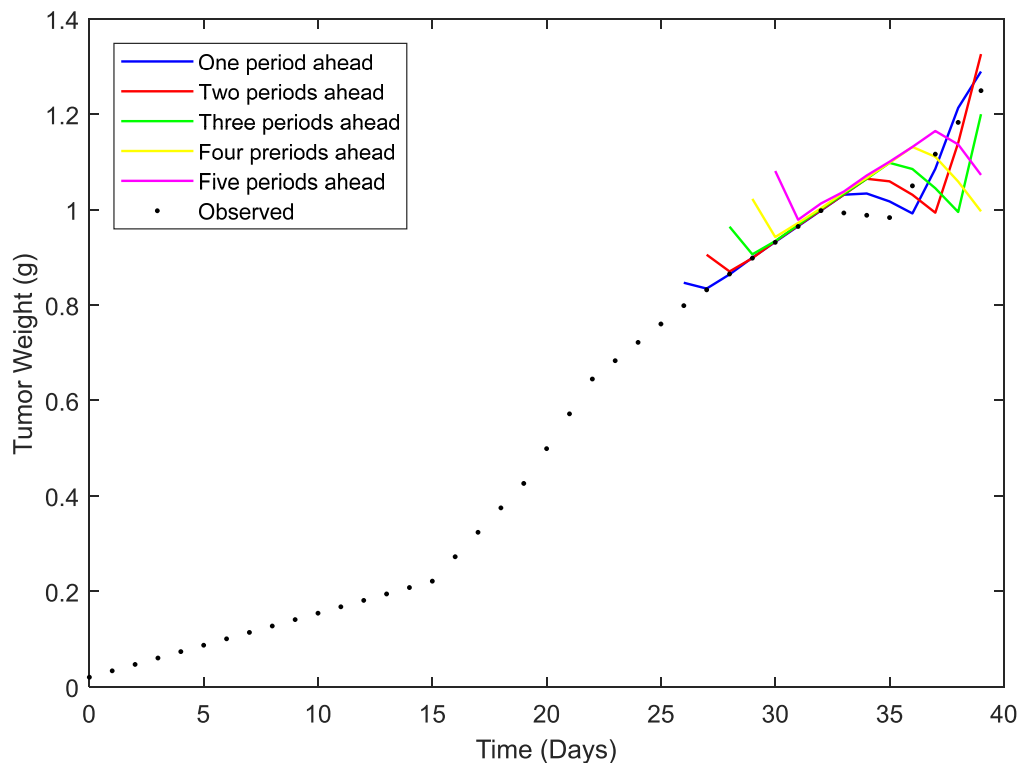


Figure 4.4. Observed and time period (1 to 5 days) ahead adaptive prediction curves of the tumor growth in mice given doses of gemcitabine (100 mg/kg on days 19 and 26). Predictions performed after the 25th day of the experiment.

The model demonstrated a high level of statistical accuracy in predicting the future course of tumor progression when gemcitabine was administered, as evidenced by the close alignment of the predicted and experimental tumor growth curves. Notably, the calculated prediction errors were small, with MAPE ranging from 2.3% for the one time period ahead predictions to 7.4% for the five time periods ahead predictions. However, as the prediction period of the tumor growth extends, the convergence between the predicted and the experimental tumor growth curves decreases, resulting in a decrease in prediction accuracy and an increase to the prediction errors. This is due to the increasing uncertainty introduced while the predictions time frame increases.

Prediction of the cancer patients' response to their therapeutical treatment with non-linear forecasting techniques

Chapter 4: Tumor Growth Inhibition (TGI) mathematical model

Moreover, the model may also be more affected by changes in the underlying data (e.g., gemcitabine dosages) or by inaccuracies in the model itself, leading to even greater errors. More on prediction errors are presented in Table 4.5 below.

Table 4.5. Prediction errors for the time period (1 to 5 days) ahead adaptive tumor growth inhibition prediction in mice given i.p. doses of gemcitabine (100 mg/kg on days 19 and 26).

Evaluation metrics	# Time periods ahead				
	1	2	3	4	5
RMSE (g)	0.03142	0.05662	0.07880	0.10566	0.09368
MAPE (%)	2.33	3.99	5.52	7.20	7.40

Chapter 5: Time series approaches to tumor growth inhibition: ARX modeling and predictive analysis

Even though mathematical models provide good approximations of tumor's growth, they can be complex and challenging to understand and apply. Their complexity arises not only from the large number of biologically relevant parameters they based on, but also from their attempts to model specific processes and phenomena that take place in the microenvironment of a malignant tumor. An alternative approach is to model tumor progression as a time series. Time series models, such as difference equations and Autoregressive Moving Average (ARMA) models, are some of the most popular tools to analyze data [231]. They are relatively simple to implement and have been widely used for forecasting in various fields, including electricity load forecasting [232], electroencephalogram (EEG) analysis [233] and economics [231]. A special version of such models is the Autoregressive with eXogenous inputs model [231]. In the context of tumor growth analysis, they can be used to model the evolution of the tumor over time and to make predictions about the future tumor growth. By modeling the relationship between the current size of the tumor and its past growth under the effect of the applied treatment such as chemotherapy, they provide a useful tool not only to analyze the tumor progression but also make informed decisions about treatment. In summary, an ARX model provides a flexible and effective way to model time series data.

This chapter introduces a new approach to describe tumor growth inhibition under chemotherapy. ARX systems modeling tumor growth under single, or combination chemotherapy are identified and evaluated using laboratory data from TGI experiments in mice.

5.1 ARX models background

An ARX model is a combination of two linear models, the autoregressive (AR) and the eXogeneous (X) input models, respectively [231]. It can be defined as a linear input-output model that uses a weighted linear combination of past input values and data observations (i.e., back fit to historical data) to perform predictions. An ARX model can be generally described as:

Prediction of the cancer patients' response to their therapeutical treatment with non-linear forecasting techniques

Chapter 5: Time series approaches to tumor growth inhibition: ARX modeling and predictive analysis

$$w_k = - \sum_{i=1}^p a_i w_{k-i} + \sum_{j=1}^q b_j u_{k-j}, \quad k \in \mathbb{Z}, \quad (5.1)$$

where w_k is the prediction (output of the model), w_{k-i} , $i \leq p$ are the past observations and u_{k-j} , $j \leq q$ are the past inputs, with $p \leq q$.

For example, in the case of tumor growth analysis, w and u correspond to the tumor weight observations and the chemotherapy drug dosages, respectively. Parameters $a_i \in \mathbb{R}$ and $b_j \in \mathbb{R}$ are weights associated with each previous observation and input, respectively while the set of parameters (p, q) defines the order of the ARX model. It is important to note that the order of the model can significantly impact the accuracy of the predictions made by the ARX model. Therefore, careful consideration and experimentation is required when selecting these parameters, to ensure the best possible results.

5.2 Identification and parameters estimation of ARX models for TGI

ARX models have a long history in forecasting and time series analysis. However, In the case of tumor growth analysis they have not extensively been used. Toward this, ARX models describing the dynamics of tumor growth under single and multi-agent chemotherapy (*ARX TGI* modes) were developed. Again, the data used to identify the ARX models were derived from the experimental studies in human-to-mouse cancer xenografts reported by Bilalis *et al.* [220] and Rocchetti *et al.* [93] and described in Chapter 3.

5.2.1 A single-agent dynamics based ARX TGI model

It is prominent that the essential step in developing a predictor for a process (e.g., tumor growth under chemotherapy) is the identification of a model. Of course, a crucial step in fitting an ARX model to data is determining its order (p, q) . In the single agent case of the tumor growth inhibition under gemcitabine, ARX models of all possible order (p, q) , where $1 < p \leq 5$ and $1 < q \leq 5$, were fitted to the observed tumor growth data of [220] as described in the *Material and Methods* section. The weights a_i and b_j of the ARX model were estimated by using the Complex Method, while the order of the model

Prediction of the cancer patients' response to their therapeutical treatment with non-linear forecasting techniques

Chapter 5: Time series approaches to tumor growth inhibition: ARX modeling and predictive analysis

was selected based on the Akaike criterion. To measure the quality of fit and the accuracy of the models RMSE and MAPE were also calculated.

Based on AIC, an ARX model of order ($p = 3, q = 3$) was selected, as described by the following equation:

$$w_k = -a_1 w_{k-1} - a_2 w_{k-2} - a_3 w_{k-3} + b_1 u_{k-1} + b_2 u_{k-2} + b_3 u_{k-3} \quad (5.2)$$

where $a_i = \begin{bmatrix} a_1 \\ a_2 \\ a_3 \end{bmatrix} = \begin{bmatrix} -2.9653 \\ 2.9456 \\ -0.9851 \end{bmatrix}$ and $b_j = \begin{bmatrix} b_1 \\ b_2 \\ b_3 \end{bmatrix} = \begin{bmatrix} 6.7573 \\ -5.8769 \\ -8.7736 \end{bmatrix}$, are the estimated ARX model coefficients.

In Figure 5.1, the model-fitted tumor weight curve is plotted against the observed tumor growth curve. It can be observed that the ARX (3,3) model was able to accurately describe the observed tumor growth under gemcitabine treatment, as evidenced by the close agreement between the model and the observed curves. This finding is further supported by the evaluation metrics presented in Table 5.1, which show that the ARX (3,3) model exhibited both low RMSE of 0.0148 g and MAPE of 2.45%.

Moreover, the AIC value of -323.09 indicates that the ARX (3,3) model provides the best trade-off between model complexity and goodness of fit compared to the other models considered. Thus, the selection of the (3,3) model is supported by both statistical criteria and measures of accuracy.

Overall, the results suggest that the ARX (3,3) model is the most appropriate and reliable model (among the tested) for describing the observed tumor growth under gemcitabine treatment. However, it is important to note that while these results are promising, further validation and exploration are necessary. Additional data from diverse cohorts and treatment regimens would be valuable to thoroughly establish the ability of such models to describe tumor growth evolution under chemotherapy. Robust evidence from larger and more varied datasets would enhance the confidence in the reliability and generalizability of these models in clinical practice.

Prediction of the cancer patients' response to their therapeutical treatment with non-linear forecasting techniques

Chapter 5: Time series approaches to tumor growth inhibition: ARX modeling and predictive analysis

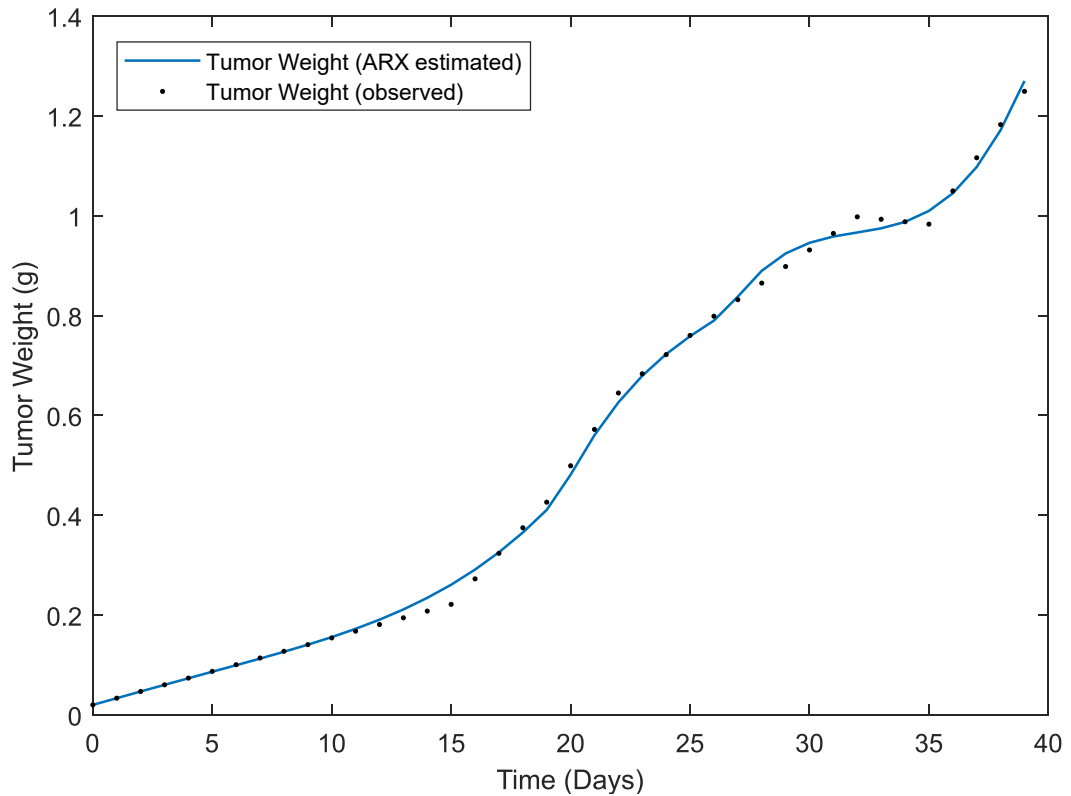


Figure 5.1. Observed/interpolated (black dots) and best fitted ARX (3,3) model tumor growth curves obtained in mice given i.p. doses of gemcitabine (100 mg/kg on days 19 and 26).

Table 5.1. Single agent ARX models fitting errors to the tumor growth experimental curve obtained in mice given i.p. doses of gemcitabine (100 mg/kg on days 19 and 26).

Model order (p,q)	AIC	RMSE (g)	MAPE (%)
(2,2)	-249.48	0.0390	8.32
(3,3)	-323.09	0.0148	2.45
(4,4)	-320.79	0.0145	2.42
(5,5)	-312.09	0.0154	2.34

5.2.2 ARX modeling of TGI in multi-drug chemotherapy scenarios

In addition to investigating the tumor growth inhibition under single-agent chemotherapy, it is also crucial to explore the effects of combination chemotherapy. This section focuses on the multi-drug case involving CPT-11 and drug C2, aiming to identify an appropriate multi-input ARX model that describes the tumor growth under combination treatment.

Similar to the single-agent case of gemcitabine, ARX models of various orders (p_m, q_m) with $1 < p_m \leq 7$ and $1 < q_m \leq 7$ with were fitted to the observed tumor growth data

Prediction of the cancer patients' response to their therapeutical treatment with non-linear forecasting techniques

Chapter 5: Time series approaches to tumor growth inhibition: ARX modeling and predictive analysis

from experimental studies conducted by Rocchetti *et al.* [93]. To determine the most suitable ARX model AIC was used. The models parameters (weights) were estimated using the Complex Method while the accuracy and the fitness of each model to the observed tumor growth curve were evaluated using RMSE and MAPE.

Based on AIC, an ARX model of $p_m = 4$ and $q_m = 4$ was selected. The model is described by the following equation:

$$w_{m_k} = -a_{m1}w_{m_{k-1}} - a_{m2}w_{m_{k-2}} - a_{m3}w_{m_{k-3}} - a_{m4}w_{m_{k-4}} + U_{d_1} + U_{d_2} \quad (5.3)$$

with

$$U_{d_1} = b_{1,1}u_{1,k-1} + b_{1,2}u_{1,k-2} + b_{1,3}u_{1,k-3} + b_{1,4}u_{1,k-4}$$

$$U_{d_2} = b_{2,1}u_{2,k-1} + b_{2,2}u_{2,k-2} + b_{2,3}u_{2,k-3} + b_{2,4}u_{2,k-4}$$

where w_{m_k} is the prediction (output of the multi-input model), $w_{m_{k-i}}$ are the past observations and U_{d_1} and U_{d_2} are the past inputs factors (one for each of the drugs).

$$a_m = \begin{bmatrix} a_{m1} \\ a_{m2} \\ a_{m3} \\ a_{m4} \end{bmatrix} = \begin{bmatrix} -1.6640 \\ 0.2182 \\ 0.1082 \\ 0.3594 \end{bmatrix}, \quad b_{1,j} = \begin{bmatrix} b_{1,1} \\ b_{1,2} \\ b_{1,3} \\ b_{1,4} \end{bmatrix} = \begin{bmatrix} -9.1822 \\ 10.8916 \\ -9.9531 \\ 5.0423 \end{bmatrix} \quad \text{and} \quad b_{2,j} = \begin{bmatrix} b_{2,1} \\ b_{2,2} \\ b_{2,3} \\ b_{2,4} \end{bmatrix} = \begin{bmatrix} -20.1489 \\ 1.9032 \\ 1.9030 \\ 24.1672 \end{bmatrix},$$

are the estimated multi-input ARX coefficients.

Figure 5.2 displays the model-fitted tumor weight curve plotted against the observed tumor growth curve for the CPT-11 and Drug C2 combination treatment. Among the range of tested models, the ARX (4,4) model emerges as a strong contender, as it demonstrates a good fit to the observed tumor growth data, closely aligning with the measured tumor growth curve. The metrics presented in Table 5.2 further support the suitability and the effectiveness of the ARX (4,4) model, as it exhibits a low RMSE of 0.0159 g and MAPE of 11.54%.

Furthermore, the AIC value of -562.2 indicates that the (4,4) model offers a favorable balance between model complexity and goodness of fit compared to the other models considered. This statistical criterion, along with the RMSE and MAPE metrics, supports

Prediction of the cancer patients' response to their therapeutical treatment with non-linear forecasting techniques

Chapter 5: Time series approaches to tumor growth inhibition: ARX modeling and predictive analysis

the selection of the ARX (4,4) model as the most appropriate and reliable model for describing tumor growth inhibition under CPT-11 and drug C2.

In summary, the ARX (4,4) model offers a robust framework for accurately describing tumor growth inhibition under the combination of CPT-11 and Drug C2. Its ability to capture the dynamic nature of tumor growth in response to this specific combination treatment highlights its potential as a valuable tool for analyzing and predicting tumor progression.

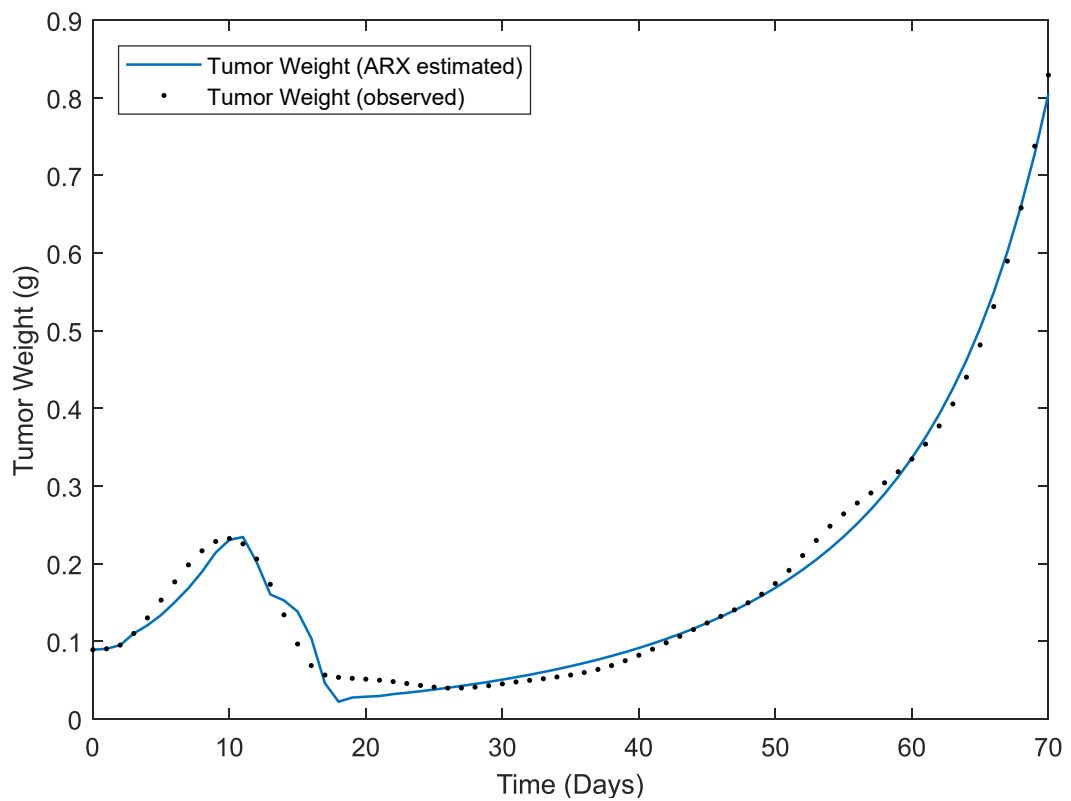


Figure 5.2. Observed/interpolated (black dots) and best fitted ARX (4,4) model tumor growth curves obtained in mice given doses of CPT-11 in combination with drug C2.

Table 5.2. Multi-agent ARX models fitting errors to the tumor growth experimental curve obtained in mice given doses of CPT-11 in combination with drug C2.

Model order (p,q)	AIC	RMSE (g)	MAPE (%)
(2,2)	-514.99	0.0241	15.71
(3,3)	-559.14	0.0169	15.66
(4,4)	-562.20	0.0159	11.54
(5,5)	-547.90	0.0168	12.04
(6,6)	-547.79	0.0162	7.10
(7,7)	-552.39	0.0150	12.34

5.3 Adaptive short-term ahead prediction of TGI using ARX models

Understanding the nuances of tumor growth dynamics, especially under treatment, goes beyond merely noting its current state. Delving into predictive analyses can offer a comprehensive outlook on how a tumor might evolve over time, thereby guiding clinical decisions more proactively. This section dives into the predictive capabilities of the ARX models. Drawing from the methodologies detailed in the *Materials and Methods* section, it echoes the short-term adaptive prediction process featured in Chapter 4, but through the lens of ARX. The ARX's prowess in forecasting short-term tumor growth is explored, under varying treatment conditions: single chemotherapy drug administration (gemcitabine i.p.), and combination drug therapy (CPT-11 and 5-FU with drug C2). In each of these cases, the predictions span one to five consecutive time periods (days) to gauge the models' accuracy and relevance in oncological applications.

5.3.1 Predictions of TGI for single-agent scenarios

The efficacy of the ARX (3,3) model, described before, for forecasting short-term tumor weight evolution was examined specifically for the gemcitabine single-agent treatment. Starting from day 26 of the experiment, step-ahead predictions were carried out using the ARX (3,3) model. Predictions were made for one, two, three, four, and five time periods ahead. After each prediction, the model was recalibrated by integrating the most recent observed data, encompassing the latest tumor weight measurements. This approach aligns with the adaptive prediction technique delineated in the preceding chapters.

The projected tumor growth trajectories for one, two, three, four, and five time periods ahead are illustrated in Figure 5.3. These are compared with the actual measured tumor weights observed during the gemcitabine treatment phase. To enhance the model's predictive accuracy, a moving window technique was incorporated, as detailed in the *Materials and Methods* section. Specifically, the window length was set to capture the last $l = 6$ tumor weight measurements.

This side-by-side comparison provides a clear perspective on the ARX (3,3) model's precision in tracing the short-term changes in tumor weight, especially when considering the model's periodic updates with the latest measurements. Table 5.3

Prediction of the cancer patients' response to their therapeutical treatment with non-linear forecasting techniques

Chapter 5: Time series approaches to tumor growth inhibition: ARX modeling and predictive analysis

catalogues the RMSE and MAPE metrics for every prediction interval, offering an in-depth review of the model's prediction fidelity across different forecasting spans. The findings shed light on the proficiency of the ARX (3,3) model in forecasting short-term tumor weight variations. Incorporating both adaptive prediction techniques and the moving window approach, the model's demonstrated statistical robustness could serve as a pivotal tool in refining treatment plans and deepening our understanding of tumor growth dynamics.

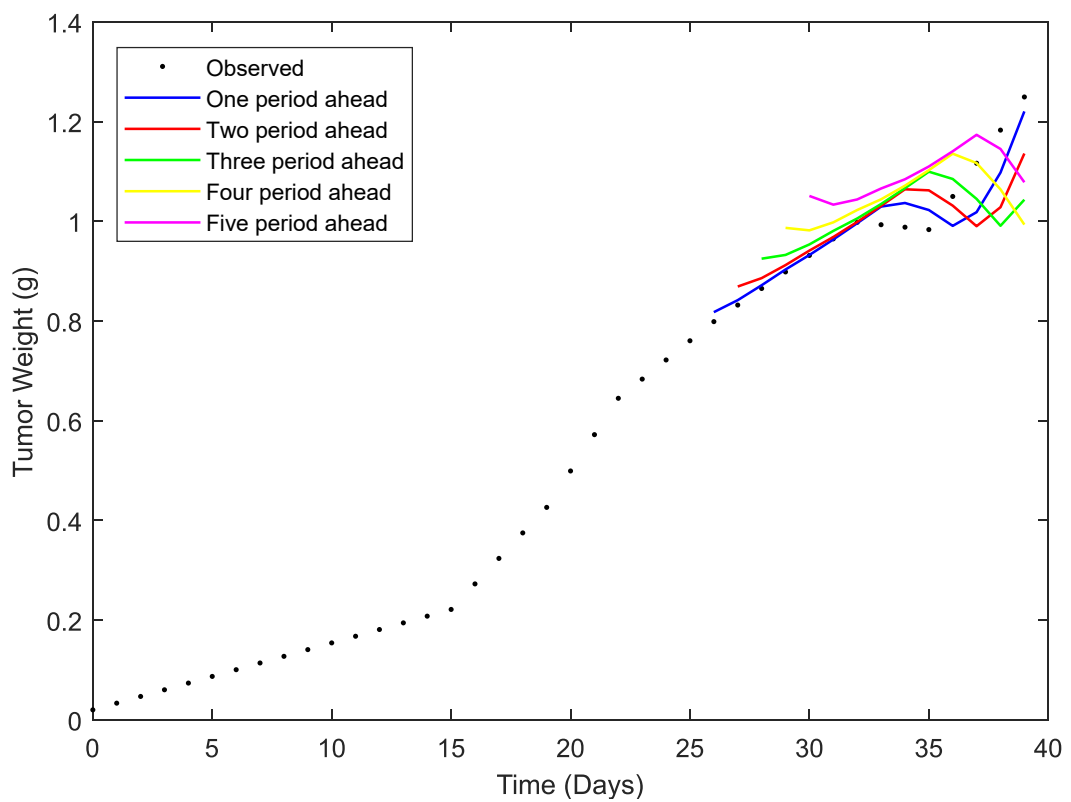


Figure 5.3. Observed and time period (1 to 5 days) ahead adaptive prediction curves of the tumor growth in mice given doses of gemcitabine (100 mg/kg on days 19 and 26). Predictions performed after the 25th day of the experiment using ARX (3,3) model.

Table 5.3. Prediction errors for the time period (1 to 5 days) ahead adaptive tumor growth inhibition prediction in mice given doses of gemcitabine (100 mg/kg on days 19 and 26). Predictions performed with ARX (3,3) model.

	# Time periods ahead				
Evaluation metrics	1	2	3	4	5
RMSE (g)	0.036077	0.056725	0.084136	0.103191	0.109214
MAPE (%)	3.73	5.64	7.56	9.37	10.35

Prediction of the cancer patients' response to their therapeutical treatment with non-linear forecasting techniques

Chapter 5: Time series approaches to tumor growth inhibition: ARX modeling and predictive analysis

The data highlight the incremental increase in errors as the prediction horizon is extended from one to five days ahead. The RMSE values, reveal a progressive escalation from approximately 0.0361 g at a one-day forecast to 0.1092 g for a five-day outlook. Similarly, MAPE, which provides a percentage estimation of prediction accuracy, rises from 3.73% for one day ahead to 10.35% for five days ahead. This trend is somewhat intuitive, as forecasting accuracy typically diminishes the further it projects into the future.

When compared to the predictions (and errors) derived using the Simeoni TGI mathematical model (see Chapter 4), the current results showcase slightly elevated values. This suggests that, while the employed model is competent in predicting short-term tumor growth, the Simeoni TGI model offers marginally higher precision for the given dataset.

5.3.2 Multi-agent ARX-based predictions of tumor inhibition

The effectiveness of the ARX (4,4) model in predicting the short-term tumor weight evolution was also assessed in the context of the adaptive prediction method previously employed for gemcitabine in the single-agent case scenario. From day 17 to day 70 of the experiment, step-ahead predictions of tumor weight were conducted using an ARX (4,4) model. Predictions spanned one to five time periods ahead. After each prediction, the model was updated (i.e., retrained) using the latest $l = 16$ observed measurements, including the most recent tumor weight.

The predicted tumor growth curves for each of the horizons (1 to 5 days) are depicted in Figure 5.4, paired with the actual measured tumor weights observed during the administration of CPT-11 and drug C2. This view facilitates a robust evaluation of the ARX (4,4) model's accuracy in capturing the short-term evolution of tumor weight, considering the continuous updating of the model with the most recent measurements. Table 5.4 presents the RMSE and MAPE values for each prediction time period, providing a comprehensive assessment of the model's predictive accuracy across the various forecast horizons.

Prediction of the cancer patients' response to their therapeutical treatment with non-linear forecasting techniques

Chapter 5: Time series approaches to tumor growth inhibition: ARX modeling and predictive analysis

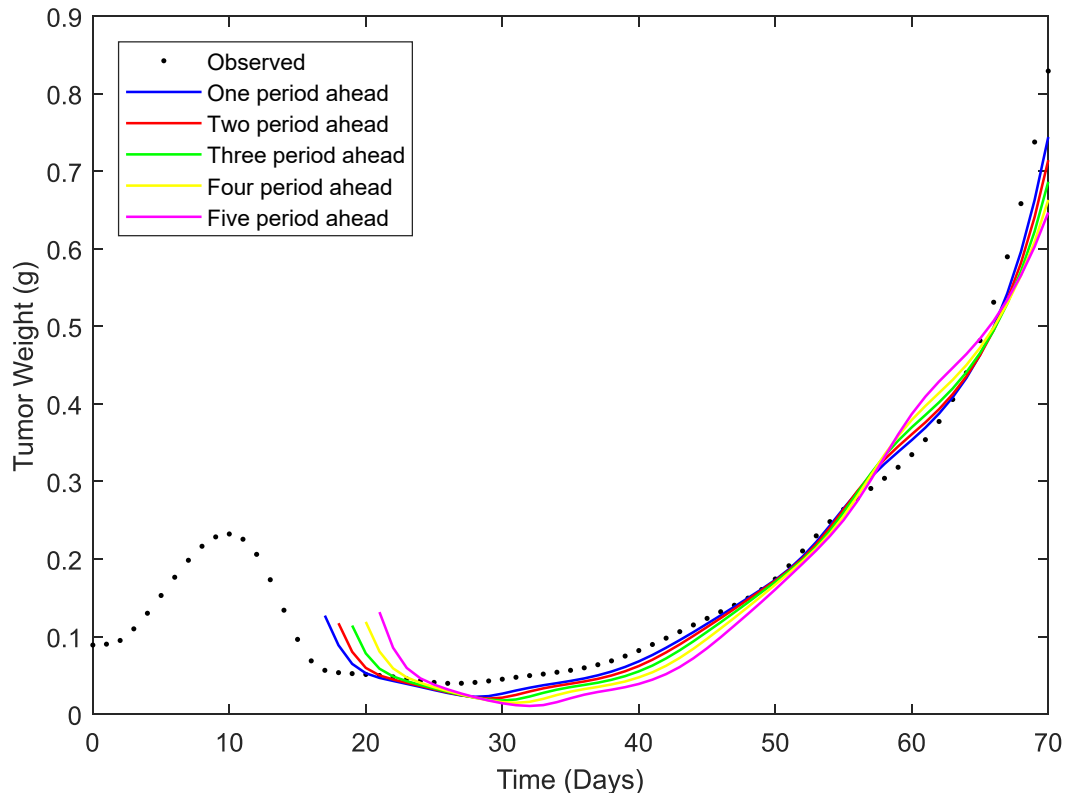


Figure 5.4. Observed curve and time period (1 to 5 days) ahead adaptive predictions of the tumor growth in mice given doses of CPT-11 and drug C2 (45 mg/kg q4dx3 from day 9 and 60 mg/kg on days 10, 11, 12 and 14, 15, 16). Predictions performed after the 16th day of the experiment using ARX (4,4) model.

Table 5.4. Prediction errors for the time period (1 to 5 days) ahead adaptive tumor growth inhibition prediction in mice given doses of CPT-11 and drug C2 (45 mg/kg q4dx3 from day 9 and 60 mg/kg on days 10, 11, 12 and 14, 15, 16). Predictions performed with ARX (4,4) model.

Evaluation metrics	# Time periods ahead				
	1	2	3	4	5
RMSE (g)	0.018599	0.021707	0.025566	0.031446	0.038269
MAPE (%)	15.38	17.93	21.09	25.21	30.47

Reviewing these results, it is evident that there is a progressive increase in error as the forecast extends from one to five days ahead. This trend is not unique to the multi-drug ARX (4,4) model; a similar progressive error increase is observed in the ANFIS models, the TGI Simeoni, as well as in the single-agent ARX (3,3) predictions previously presented. The RMSE values, denoting the model's deviation in grams, climb from 0.0186 g for a one-day ahead forecast to 0.0383 g for five days ahead predictions. This escalation is mirrored also in the MAPE values, which quantify the model's percentage

Prediction of the cancer patients' response to their therapeutical treatment with non-linear forecasting techniques

Chapter 5: Time series approaches to tumor growth inhibition: ARX modeling and predictive analysis

error. Starting at 15.38% for one time period ahead predictions, the MAPE escalates to 30.47% underscoring the complexities in modelling tumor weight dynamics, especially when multiple drugs administrations are involved.

A novel approach to modeling tumor growth under chemotherapy treatment was presented in this chapter. Specifically, an ARX models for cancer growth under chemotherapy, were developed, estimated using laboratory data, and evaluated. These models do not require prior knowledge of the drug's pharmacokinetics, making them easier to implement and use. The results demonstrated an excellent fit to the tumor weight data of [93] and [220], obtained from xenografted chemotherapy treated mice. However, it is crucial to subject the models to extensive testing with additional data sources.

Chapter 6: Tumor growth modelling using adaptive neuron-fuzzy inference system (ANFIS)

6.1 Introduction to ANFIS

Physical systems and processes such as cancer are often hard to describe with equations. Due to the existence of processes which involve complex phenomena and strong non-linearities, it is rather difficult and time consuming to obtain a mathematical model. Over the last decades, fuzzy logic and systems have been commonly used, especially in control systems, as they provide solutions to possible system uncertainties and noisy data. Using if-then rules and membership functions fuzzy estimation systems can be formed to perform a non-linear input-output mapping. The adaptive neuro-fuzzy inference system (ANFIS) is one of the most famous neuro-fuzzy systems to fit input-output data.

A common ANFIS structure usually includes 5 layers. Figure 6.1 shows an ANFIS architecture with 2 rules for a multi-input, single output (MISO) system consisting of 1 output f (e.g., the tumor growth in g) and 2 inputs x and y (e.g., the time in days and the dose level of the chemotherapy drug in mg/kg).

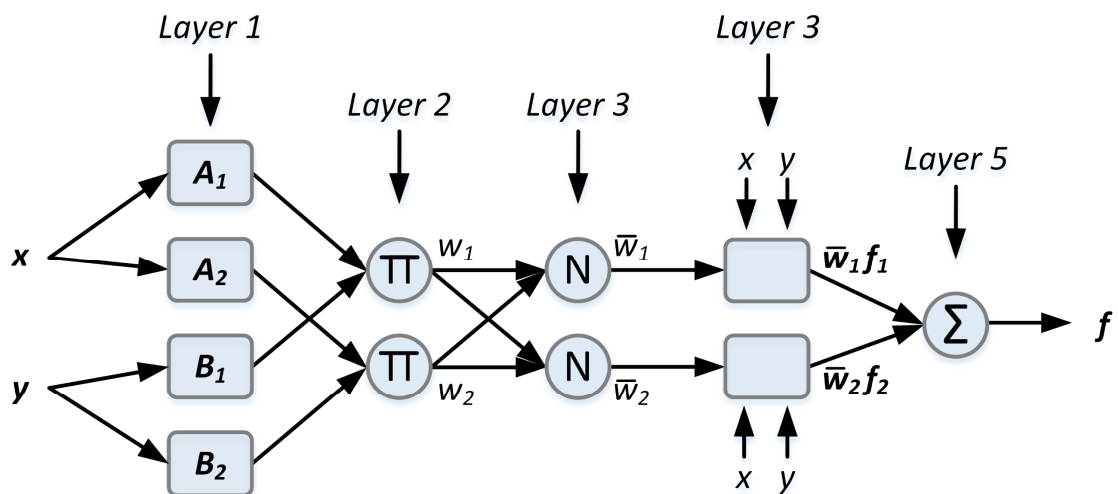


Figure 6.1. Representation of an adaptive neuro fuzzy inference system (ANFIS) structure with two rules, for a system of one output (f) and two inputs (x and y).

A typical set of fuzzy if-then rules of Takagi-Sugeno-Kang's (TSK) type are described below [234]:

Prediction of the cancer patients' response to their therapeutical treatment with non-linear forecasting techniques

Chapter 6: Tumor growth modelling using adaptive neuron-fuzzy inference system (ANFIS)

Rule 1: if x is A_1 and y is B_1 , then $f_1 = p_1x + q_1y + r_1$,

Rule 2: if x is A_2 and y is B_2 , then $f_2 = p_2x + q_2y + r_2$

where x, y are the premise variables, A_1, A_2, B_1 and B_2 are the premise parameters and p_1, p_2, q_1, q_2, r_1 and r_2 are the consequence parameters of the fuzzy rules. By using the linear combinations of the consequent parameters (i.e., the functions f_1 and f_2) the output of the system is calculated. Figure 6.2 below illustrates the related fuzzy inference method for the TSK model.

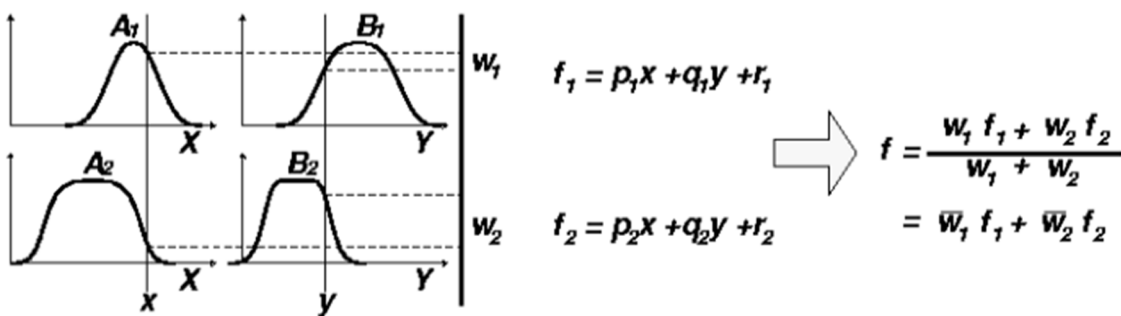


Figure 6.2. Illustration of the TSK fuzzy inference method.

Each layer of an ANFIS is composed of several nodes described by a node function. There are two types of nodes, the adaptive nodes which represent the sets of parameters that are adjustable, and the fixed which represent the fixed parameter sets. In the ANFIS of Figure 6.1 the adjustable nodes are denoted by squares whereas the fixed nodes denoted by circles.

A brief description of the ANFIS framework is presented below [235]:

Layer 1. This is the layer where the fuzzification process takes place. Each node i is an adaptive (square) node with a node function:

$$\begin{aligned} O_{1,i} &= \mu_{A_i}(x), & \text{for } i = 1,2, \text{ or} \\ O_{1,i} &= \mu_{B_{i-2}}(y), & \text{for } i = 3,4 \end{aligned} \tag{6.1}$$

where $\mu_{A_i}(x)$ and $\mu_{B_{i-2}}(y)$ are the membership functions (MFs) of the inputs x and y , respectively, for each node i . A_i and B_{i-2} represent the linguistic labels associated with this node function. It must be also noted that $O_{1,i}$ specifies the degree to which a given input x or y satisfies A_i and B_i , respectively. Generally, there are several types of MFs

Prediction of the cancer patients' response to their therapeutical treatment with non-linear forecasting techniques

Chapter 6: Tumor growth modelling using adaptive neuron-fuzzy inference system (ANFIS)

which can be used as membership function of A [235]. One of the most common is the generalized bell-shaped MF with a minimum and a maximum equal to 0 and 1, respectively, is calculated according to the function below:

$$\mu(x) = \frac{1}{1 + \left| \frac{x-c}{a} \right|^{2b}}, \quad (6.2)$$

where a , b and c are the parameters of the bell function. As shown in Figure 6.3, the parameter a represents the width of the membership function, where an increased value results in a broader membership function. The parameter b defines the shape of the curve at the two sides of the central plateau, with a greater value leading to a steeper transition. Both a and b define the gradient (i.e., gradient = $-\frac{b}{2a}$) of the curve. Finally, c is the center (or midpoint) of the membership function. Different combinations of these parameters can lead to various form of bell-shaped membership functions.

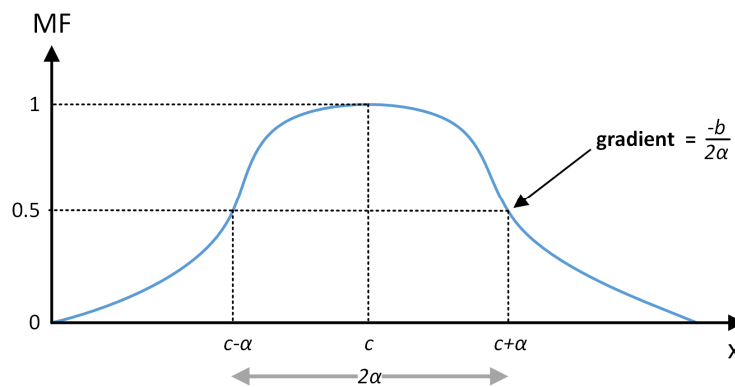


Figure 6.3. A generalized bell-shaped membership function for fuzzy sets [236].

Layer 2. In contrast to the first layer of the ANFIS (i.e., Layer 1), this layer (also called the membership layer) consists of fixed nodes labeled Π . The output of each node, which indicates the weight of membership functions, is calculated as the product of all the incoming signals supplied from Layer 1:

$$O_{2,i} = \omega_i = \mu_{A_i}(x)\mu_{B_i}(y), \quad i = 1,2. \quad (6.3)$$

The output of every node is also called the firing strength of the rule.

Prediction of the cancer patients' response to their therapeutical treatment with non-linear forecasting techniques

Chapter 6: Tumor growth modelling using adaptive neuron-fuzzy inference system (ANFIS)

Layer 3. This is where the normalization process takes place. The nodes of this layer are also fixed nodes, and they are labeled N. Each node i calculates the ratio of the i th rule's firing strength to the sum of all rules' firing strengths:

$$O_{3,i} = \bar{\omega}_i = \frac{\omega_i}{\omega_1 + \omega_2}, \quad i = 1,2. \quad (6.4)$$

Each output $O_{3,i}$ is called normalized firing strength.

Layer 4. Each node i in the fourth layer is an adaptive (square) node with node function:

$$O_{4,i} = \bar{\omega}_i f_i = \bar{\omega}_i (p_i x + q_i y + r_i), \quad i = 1,2. \quad (6.5)$$

where p_i , q_i and r_i are the parameters of this node and $\bar{\omega}_i$ is the output of the previous layer (i.e., Layer 3). This layer is also called the defuzzification layer and its parameters are referred to as consequent parameters.

Layer 5. This is the final or the output layer of the ANFIS. It is also called the summation layer as it sums up all the incoming signals and produces the overall output of the model. It consists of a single, fixed (circle) node labeled Σ :

$$output_{ANFIS} = O_{5,1} = \sum_{i=1}^2 \bar{\omega}_i f_i = \frac{\sum_{i=1}^2 \omega_i f_i}{\sum_{i=1}^2 \omega_i}. \quad (6.6)$$

In this chapter, a new approach on solid tumor growth modelling is introduced. More specifically, ANFIS architecture is used to model the tumor growth under the effect of single or multi-agent chemotherapy in human-to-mouse xenografts. The prediction ability of the ANFIS models is investigated through step ahead predictions of the tumor growth inhibition. Results are presented and discussed while important conclusions are drawn.

6.2 ANFIS models for tumor growth inhibition modelling

The present chapter aims to investigate the application of ANFIS models in describing tumor growth inhibition. The integration of artificial intelligence techniques with fuzzy inference systems has been demonstrated to provide a powerful tool for modelling complex systems. In this study, three ANFIS models were developed and evaluated for the description of tumor growth inhibition under different chemotherapy regimens (ANFIS TGI models). Specifically, the first model for the case of single agent

Prediction of the cancer patients' response to their therapeutical treatment with non-linear forecasting techniques

Chapter 6: Tumor growth modelling using adaptive neuron-fuzzy inference system (ANFIS)

chemotherapy was developed using tumor weight data from mice administered gemcitabine. The other two models are for cases where two anticancer drugs were administered in combination (CPT-11 and Drug C2, and 5-FU and Drug C2). More details about the datasets used in this chapter are shown in *Materials and Methods*. The models' ability to perform accurate short-term step ahead predictions of tumor growth under chemotherapy was also explored. A trial-and-error process was conducted to select the appropriate ANFIS structure along with its parameters, such as the number of MFs and the number of training epochs, to ensure the best fit to the experimental tumor growth curves.

6.2.1 An ANFIS TGI model for single-agent chemotherapy

In the case of single agent chemotherapy treatment three parameters were considered for the ANFIS. The time (in days) and the chemotherapy drug dosage (in mg/kg) administered to the mice represent the 1st and 2nd input of the ANFIS, respectively whereas the tumor mass (in g) is considered the output of the model (see Table 6.1).

Table 6.1. Inputs and outputs of the ANFIS tumor growth inhibition model for the case of single agent chemotherapy (gemcitabine i.p.).

ANFIS model	Unit
A. Inputs	
Time	day
Chemotherapy drug dosage	mg/kg
B. Outputs	
Tumor mass	g

To find the most effective ANFIS model, which best fits the tumor growth curve, several modifications were made on the model structure. The number of membership functions for the input variables is a very important factor, hence it must be chosen carefully. The ANFIS structure configurations tested included 2, 3, and 4 membership functions for the input variables, with a generalized bell-shaped membership function type for all cases, and step size of 0.10, decrease rate of 0.90 and increase rate of 1.10 for all cases. The number of 100 epochs was used to train the model. The characteristics of the structure of the ANFIS architectures that were tested are illustrated in the Table 6.2 below.

Table 6.2. Configurations of the tested ANFIS structures for the case of single agent chemotherapy (gemcitabine i.p.).

Parameters	Case 1	Case 2	Case 3
Membership functions (MF)	2	3	4
Type of MF	Generalized bell-shaped	Generalized bell-shaped	Generalized bell-shaped
Epochs	100	100	100
Step size	0.10	0.10	0.10
Decrease rate	0.90	0.90	0.90
Increase rate	1.10	1.10	1.10

Simulation results for each ANFIS configuration tested indicate that all models accurately captured the tumor growth dynamics. The accuracy of the models was confirmed by the low values of the fitting errors such as RMSE and MAPE, which demonstrate the convergence of the fitted tumor growth curve to the observed tumor weight data points. The training total runtime (s) and the evaluation metrics MSE (g^2), RMSE (g) and MAPE (%), are provided in Table 6.3. The fitted tumor growth curves for each ANFIS model configuration, obtained in mice given i.p. doses of gemcitabine (100 mg/kg on Days 19 and 26), are compared to the observed/interpolated tumor weight data in Figures Figure 6.4, Figure 6.5 and Figure 6.6), highlighting the high accuracy of all three models. Moreover, the curve fitting errors by iteration (100 epochs) are presented in the same figures. Of the three cases tested, the ANFIS with three MFs had the lowest fitting errors with a MAPE of less than 1%).

Table 6.3. Evaluation (i.e., fitting errors to the tumor growth experimental curve) of the ANFIS model for different structure configurations for the case of single agent chemotherapy (gemcitabine i.p.).

Evaluation metrics	Case 1	Case 2	Case 3
Total runtime (s)	1.469	3.295	8.123
MSE (g^2)	4.5e-4	2.0e-4	1.0e-5
RMSE (g)	0.0214	0.0131	0.0036
MAPE (%)	2.21	2.54	0.73

Prediction of the cancer patients' response to their therapeutical treatment with non-linear forecasting techniques

Chapter 6: Tumor growth modelling using adaptive neuron-fuzzy inference system (ANFIS)

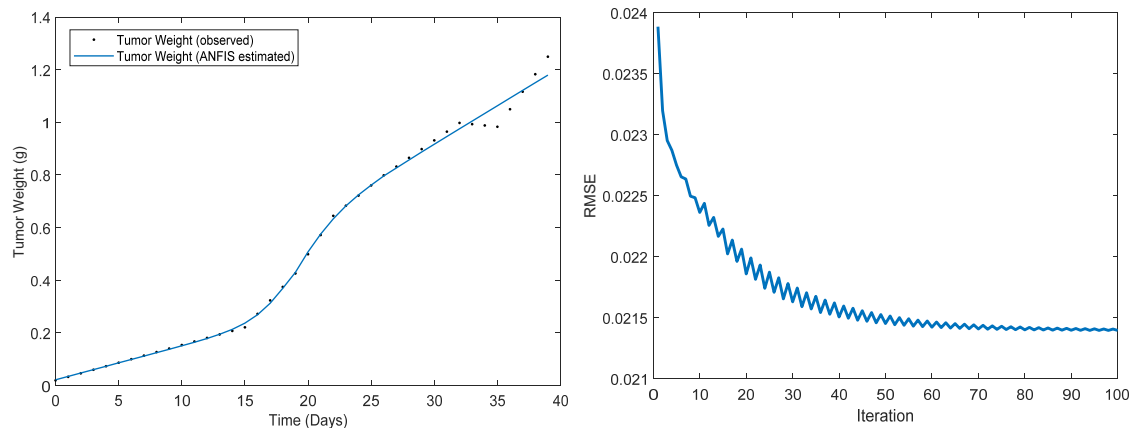


Figure 6.4. Case 1 – (Left) Observed/interpolated (*) and ANFIS model fitted tumor growth curves (in g) obtained in mice given i.p. doses of gemcitabine (100 mg/kg on Days 19 and 26). (Right) Curve fitting error by iteration.

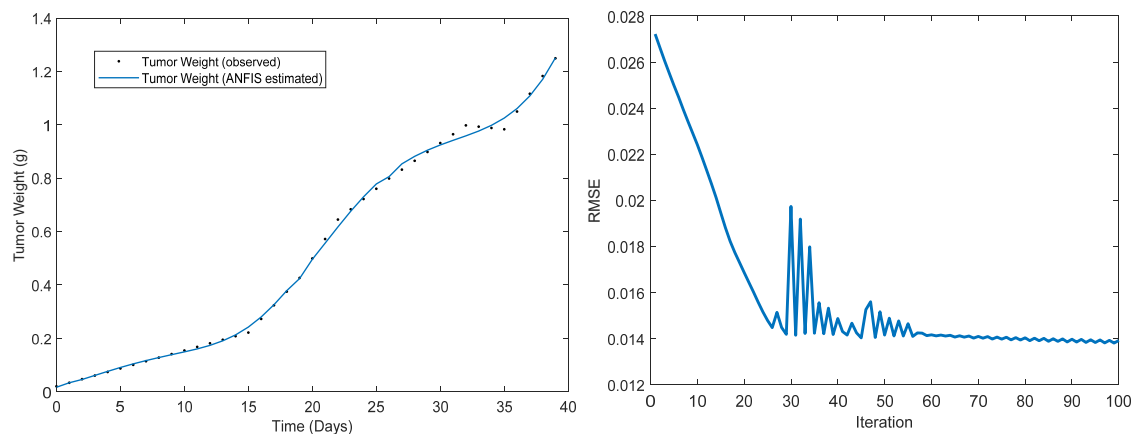


Figure 6.5. Case 2 – (Left) Observed/interpolated (*) and ANFIS model fitted tumor growth curves (in g) obtained in mice given i.p. doses of gemcitabine (100 mg/kg on Days 19 and 26). (Right) Curve fitting error by iteration.

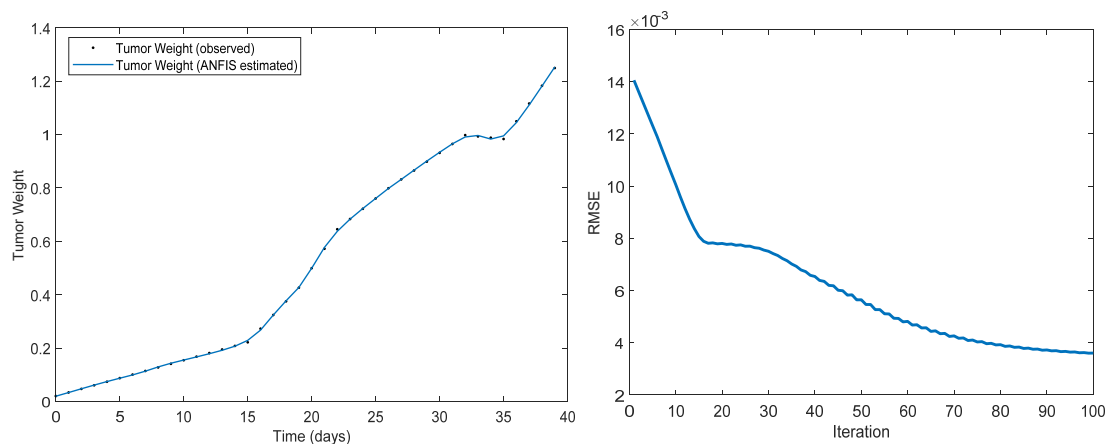


Figure 6.6. Case 3 – (Left) Observed/interpolated (*) and ANFIS model fitted tumor growth curves (in g) obtained in mice given i.p. doses of gemcitabine (100 mg/kg on Days 19 and 26). (Right) Curve fitting error by iteration.

However, this came at the cost of the longest training runtime. On the other hand, the ANFIS with two MFs had a slightly higher fitting errors but had significantly shorter runtime. Thus, this highlights the trade-off between fitting errors and runtime when choosing the number of MFs for ANFIS models.

6.2.2 ANFIS TGI models for multi-agent chemotherapy treatments

In comparison to the single agent case, in the cases of multi-agent chemotherapy treatment (i.e., CPT-11 with drug C2 and 5-FU with drug C2) four parameters were considered for the ANFIS model. The multi-agent ANFIS takes into account the time (in days) and the chemotherapy drug dosages (in mg/kg) of each drug administered to the mice. These are the inputs to the model. The tumor mass (in g) is considered the target variable, i.e., the output of the model. The input and output variables of the multi-agent ANFIS tumor growth inhibition model are shown in Table 6.4.

Table 6.4. Inputs and outputs of the ANFIS tumor growth inhibition model for the case of multi-agent chemotherapy.

ANFIS model	Unit
A. Inputs	
Time	day
Chemotherapy drug A dosage	mg/kg
Chemotherapy drug B dosage	mg/kg
B. Outputs	
Tumor mass	g

As in the single agent case several modifications on the structure of the model can be made in order to find the most effective ANFIS formulation, which best describes the experimental growth curves when tumors are treated using combination chemotherapy. The structure configurations tested included 2, 3, and 4 membership functions for the input variables, with a generalized bell-shaped membership function type for all cases. The step size was set at 0.10 with a decrease rate of 0.90 and increase rate of 1.10 for all cases. Moreover, a constant number of 100 epochs was used to train the model for each case. The characteristics of the structure of the ANFIS architectures that were tested are described in the Table 6.5 below.

Table 6.5. Configurations of the tested ANFIS structures ANFIS for the cases of multi-agent chemotherapy treatment.

Parameters	Case 1	Case 2	Case 3
Membership functions (MF)	2	3	4
Type of MF	Generalized bell-shaped	Generalized bell-shaped	Generalized bell-shaped
Epochs	100	100	100
Step size	0.10	0.10	0.10
Decrease rate	0.90	0.90	0.90
Increase rate	1.10	1.10	1.10

6.2.2.1 CPT-11 administered in combination with drug C2

The fitting errors (using the RMSE (g) and MAPE (%) metrics) to the experimental tumor growth curves and the total training runtime using the above ANFIS configurations are presented in Table 6.6. The ANFIS fitted tumor growth curves for each model configuration against the observed/interpolated tumor weight data obtained in mice given doses of CPT-11 and drug C2 (45 mg/kg q4dx3 from day 9 and 60 mg/kg on days 10, 11, 12 and 14, 15, 16) are shown in Figure 6.7, Figure 6.8 and Figure 6.9, below. These figures also present the curve fitting errors by iteration (100 epochs).

Table 6.6. Evaluation (i.e., fitting errors to the tumor growth experimental curve) of the ANFIS model for different structure configurations for the case of CPT-11 given with drug C2.

Evaluation metrics	Case 1	Case 2	Case 3
Total runtime (s)	5.35	41.58	219.0
MSE (g²)	8.0e-4	2.8e-4	1.0e-5
RMSE (g)	0.0285	0.0167	0.0032
MAPE (%)	19.24	12.89	2.79

Prediction of the cancer patients' response to their therapeutical treatment with non-linear forecasting techniques

Chapter 6: Tumor growth modelling using adaptive neuron-fuzzy inference system (ANFIS)

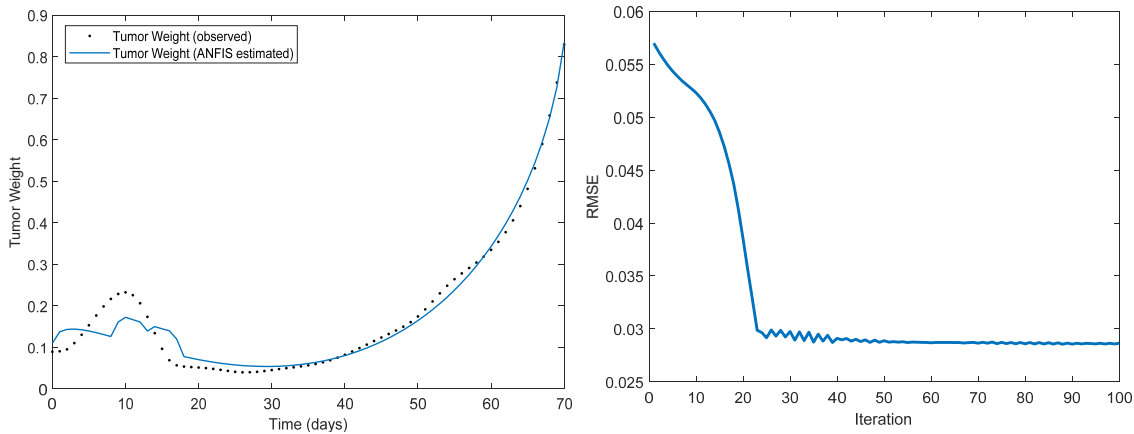


Figure 6.7. Case 1 – (Left) Observed/interpolated (*) and ANFIS model fitted tumor growth curves (in g) obtained in mice given doses of CPT-11 and drug C2 (45 mg/kg q4dx3 from day 9 and 60 mg/kg on days 10, 11, 12 and 14, 15, 16). (Right) Curve fitting error by iteration.

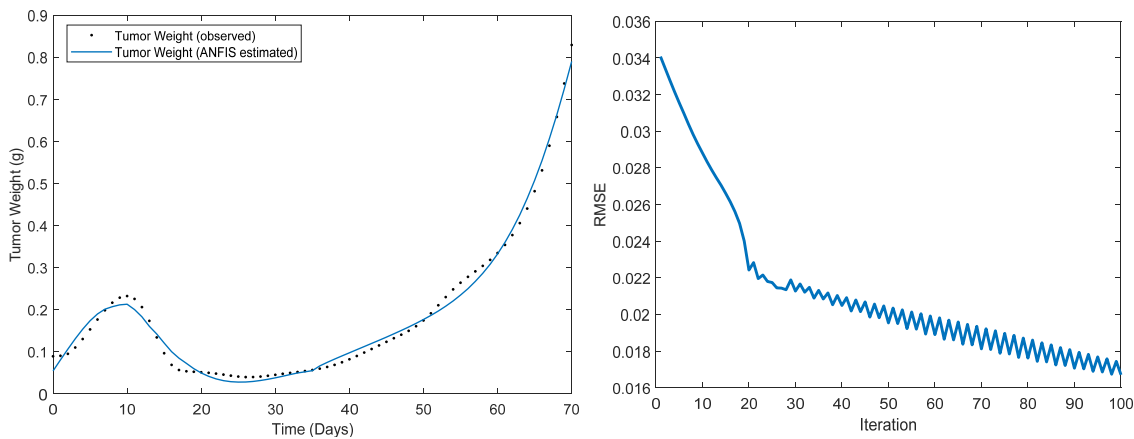


Figure 6.8. Case 2 – (Left) Observed/interpolated (*) and ANFIS model fitted tumor growth curves (in g) obtained in mice given doses of CPT-11 and drug C2 (45 mg/kg q4dx3 from day 9 and 60 mg/kg on days 10, 11, 12 and 14, 15, 16). (Right) Curve fitting error by iteration.

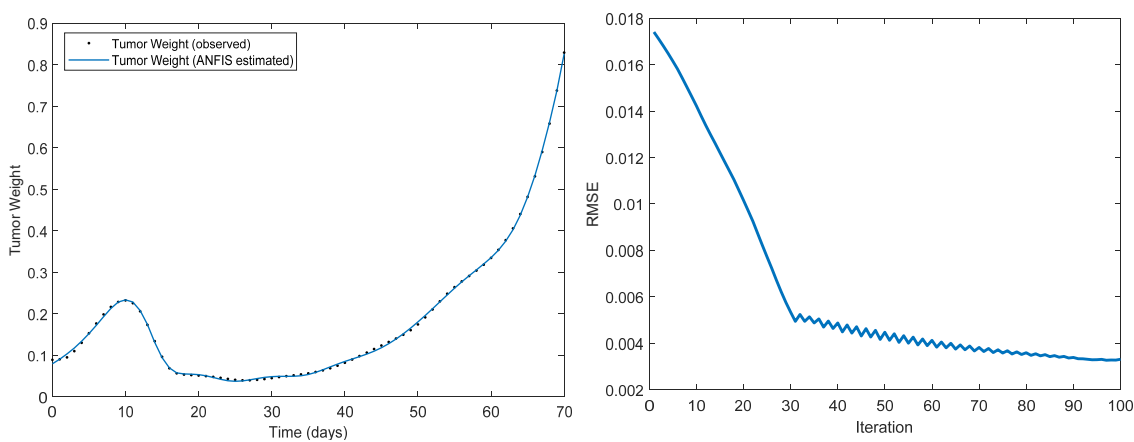


Figure 6.9. Case 3 – (Left) Observed/interpolated (*) and ANFIS model fitted tumor growth curves (in g) obtained in mice given doses of CPT-11 and drug C2 (45 mg/kg q4dx3 from day 9 and 60 mg/kg on days 10, 11, 12 and 14, 15, 16). (Right) Curve fitting error by iteration.

Prediction of the cancer patients' response to their therapeutical treatment with non-linear forecasting techniques

Chapter 6: Tumor growth modelling using adaptive neuron-fuzzy inference system (ANFIS)

6.2.2.2 5-FU administered in combination with drug C2

The performance of the ANFIS models was evaluated based on the RMSE (g) and MAPE (%) metrics. The fitting errors to the experimental tumor growth curves along with the total runtime are presented in Table 6.7. The ANFIS fitted tumor growth curves obtained in mice given doses of 5-FU and drug C2 (50 mg/kg q4dx3 from day 9 and 60 mg/kg on days 10, 11, 12 and 14, 15, 16) for each model configuration against the observed/interpolated tumor weight data are shown in the figures below (see Figure 6.10, Figure 6.11 and Figure 6.12). The curve fitting errors by iteration (100 epochs) are also shown in the same figures. The ANFIS models tested in both multi-agent cases effectively captured the tumor growth dynamics, as demonstrated by the low fitting errors and the close convergence to the observed tumor weight data points. The inclusion of additional MFs in each model improved the overall accuracy of the models, as demonstrated by the evaluation metrics and figures. However, as observed also in the single agent case of gemcitabine, the training runtime was significantly prolonged with the increase in the number of MFs.

Table 6.7. Evaluation (i.e., fitting errors to the tumor growth experimental curve) of the ANFIS model for different structure configurations for the case of 5-FU given with drug C2.

Evaluation metrics	Case 1	Case 2	Case 3
Total runtime (s)	6.67	46.70	219.1
MSE (g²)	4.0e-4	1.5e-4	2.4e-5
RMSE (g)	0.0200	0.0124	0.0049
MAPE (%)	9.87	4.14	3.23

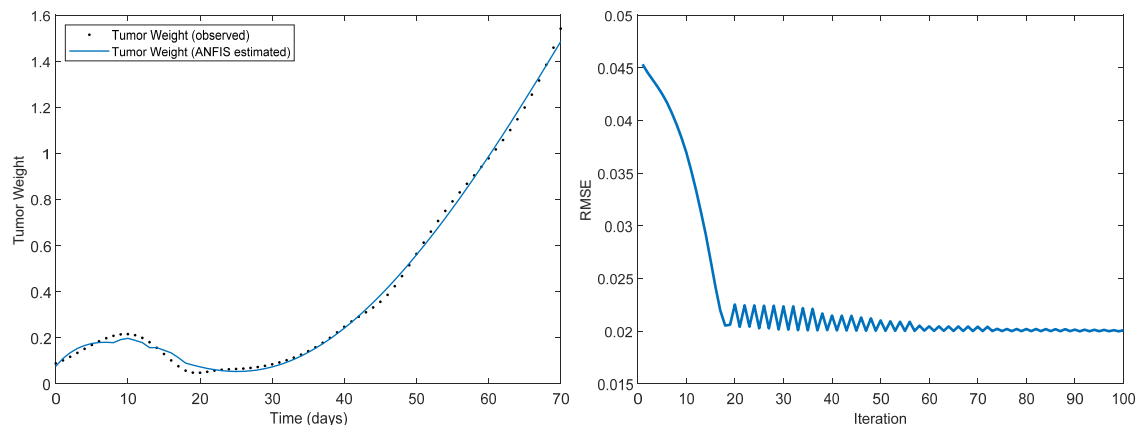


Figure 6.10. Case 1 – (Left) Observed/interpolated (*) and ANFIS model fitted tumor growth curves (in g) obtained in mice given doses of 5-FU and drug C2 (50 mg/kg q4dx3 from day 9 and 60 mg/kg on days 10, 11, 12 and 14, 15, 16). (Right) Curve fitting error by iteration.

Prediction of the cancer patients' response to their therapeutical treatment with non-linear forecasting techniques

Chapter 6: Tumor growth modelling using adaptive neuron-fuzzy inference system (ANFIS)

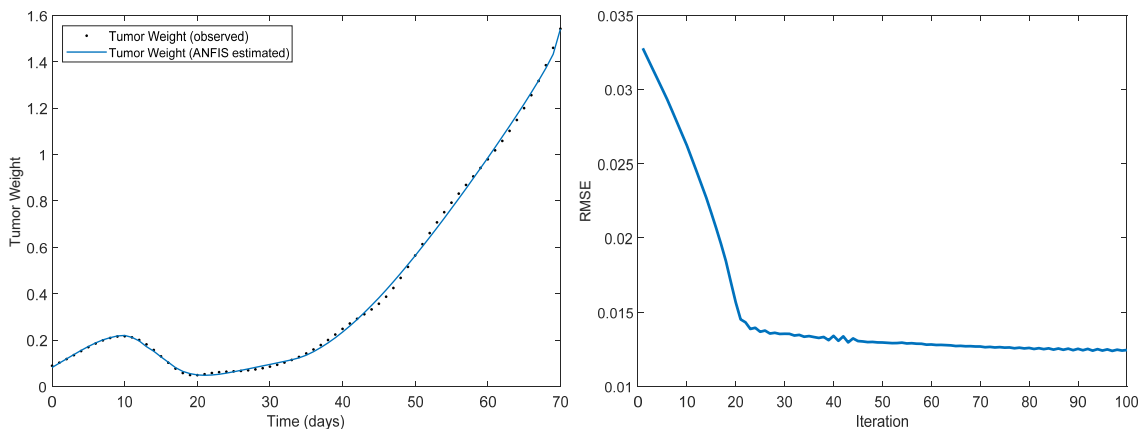


Figure 6.11. Case 2 – (Left) Observed/interpolated (*) and ANFIS model fitted tumor growth curves (in g) obtained in mice given doses of 5-FU and drug C2 (50 mg/kg q4dx3 from day 9 and 60 mg/kg on days 10, 11, 12 and 14, 15, 16). (Right) Curve fitting error by iteration.

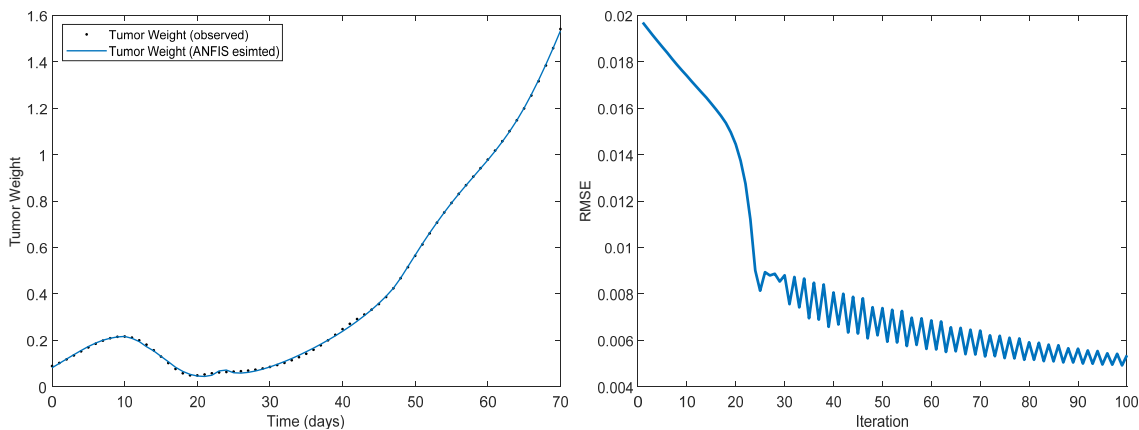


Figure 6.12. Case 3 – (Left) Observed/interpolated (*) and ANFIS model fitted tumor growth curves (in g) obtained in mice given doses of 5-FU and drug C2 (50 mg/kg q4dx3 from day 9 and 60 mg/kg on days 10, 11, 12 and 14, 15, 16). (Right) Curve fitting error by iteration.

6.3 Evaluation of ANFIS models short-term ahead predictions of TGI

Simply describing the solid tumor growth under treatment is not sufficient. Predictions can provide valuable insight into the future progression of a tumor's size, and ultimately aid in the design and refine of the treatment strategy and its fine tuning. In this study, the ANFIS model's ability to make accurate short-term prediction is explored by using the same short-term adaptive prediction process outlined in the Material and Methods section, as previously applied in Chapter 4. The ANFIS ability to perform short-term future predictions of the tumor growth is evaluated in three different scenarios: tumor growth by single chemotherapy drug administration (gemcitabine i.p.), and multi-drug

Prediction of the cancer patients' response to their therapeutical treatment with non-linear forecasting techniques

Chapter 6: Tumor growth modelling using adaptive neuron-fuzzy inference system (ANFIS)

administration (CPT-11 and 5-FU with drug C2). In all scenarios, the tumor growth predictions were made for one, two, three, four and five time periods (days) ahead.

6.3.1 Single-drug chemotherapy – Predictions of TGI under gemcitabine

Using the same adaptive prediction method described in Chapter 4, statistically accurate forecasts were made to evaluate efficacy of ANFIS models in predicting short-term tumor weight evolution. For the case of single agent administration (100 mg/kg of gemcitabine given i.p. on days 19 and 26), a three-MFs ANFIS model was trained for 100 epochs, ANFIS (3,100). Step ahead predictions of the tumor weight were performed starting from day 25 after inoculation to day 39 of the experiment. After each tumor weight prediction, the ANFIS model was retrained using the measured tumor weights up to day 25. For example, to predict tumor weight on day 26 of the experiment, the model was trained with all the available data (e.g., tumor weight observations, gemcitabine dosages) up to day 25. Then, to predict tumor growth on day 27, the model was fine-tuned with all data up to day 26. The procedure is described in detail in the Material and Methods and Chapter 4. The prediction tumor growth curves, for one, two, three, four and five time periods ahead, against the measured tumor weight is presented in Figure 6.13. Prediction errors are shown in Table 6.8.

To enhance the model's performance, a moving window of measurements was established for fitting the ANFIS. The moving window allows the ANFIS to be trained with a sliding window of data, rather than all data available up to the prediction time, improving the model's ability to capture changes in the tumor weight over time, leading to more accurate predictions. The efficacy of this approach can be confirmed by the improved fit of the ANFIS predicted tumor weight curves to the observed/experimental data points, as well as by the reductions in the prediction errors (RMSE and MAPE). Specifically, the use of moving windows of $l = 20$ measurements improved the accuracy of the predictions (for five time periods ahead) by 26.4% when compared to the non-window case. By reducing the window length by five measurements, from $l = 20$ to $l = 15$, the performance of the model was significantly improved. A 303% reduction of the prediction error was achieved when compared to the non-window case. In both cases (i.e., window sizes of $l = 20$ and $l = 15$), ANFIS models of three MFs was trained for 50

Prediction of the cancer patients' response to their therapeutical treatment with non-linear forecasting techniques

Chapter 6: Tumor growth modelling using adaptive neuron-fuzzy inference system (ANFIS)

epochs, ANFIS (3,50). The tumor growth curves as well as the prediction errors for these cases are plotted in Figure 6.15, Figure 6.14 and Table 6.9, Table 6.10, respectively. In conclusion, the ANFIS model has been found to provide accurate predictions of the tumor growth under gemcitabine while the use of a moving window approach enhanced the model's performance, leading to more accurate forecasts of the tumor growth over time.

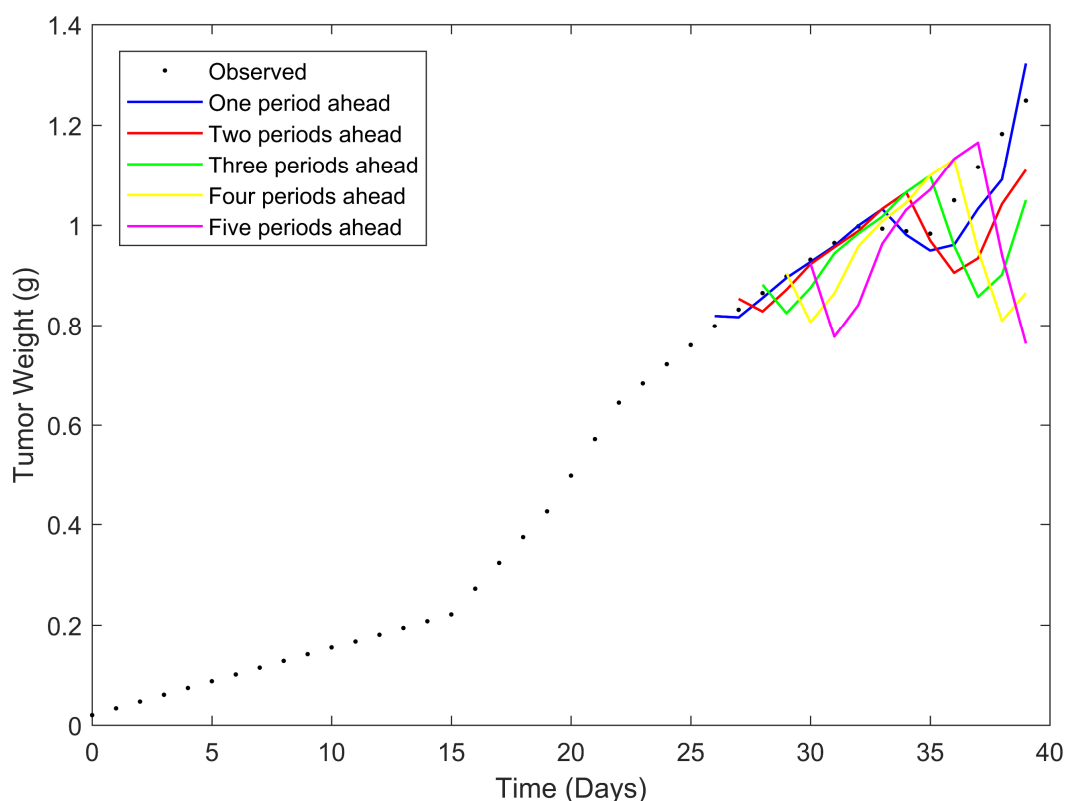


Figure 6.13. Observed and time period (1 to 5 days) ahead adaptive prediction curves of the tumor growth in mice given i.p. doses of gemcitabine (100 mg/kg on days 19 and 26). Predictions performed after the 25th day of the experiment using ANFIS model (3,100) without moving window.

Table 6.8. Prediction errors for the time period (1 to 5 days) ahead adaptive tumor growth inhibition prediction in mice given i.p. doses of gemcitabine (100 mg/kg on days 19 and 26). Predictions performed with ANFIS model (3,100) without using moving window.

	# Time periods ahead				
Evaluation metrics	1	2	3	4	5
RMSE (g)	0.047902	0.089165	0.136458	0.182297	0.193423
MAPE (%)	3.20	6.06	9.44	12.06	12.39

Prediction of the cancer patients' response to their therapeutical treatment with non-linear forecasting techniques

Chapter 6: Tumor growth modelling using adaptive neuron-fuzzy inference system (ANFIS)

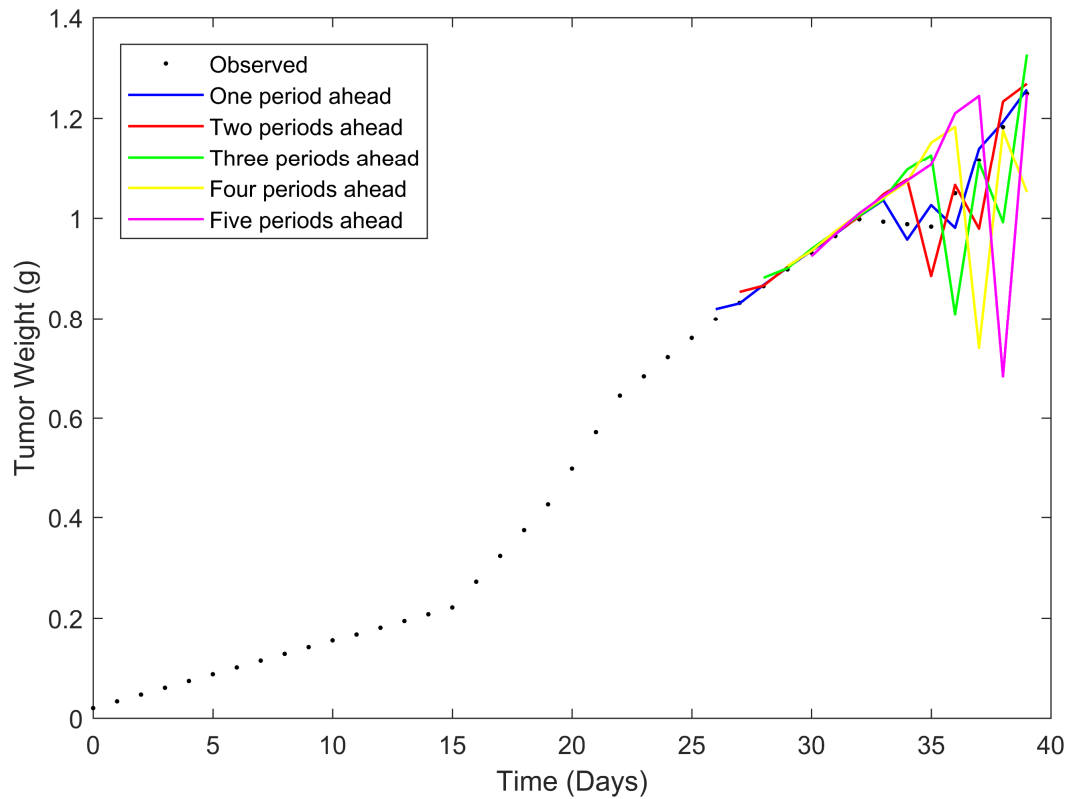


Figure 6.14. Observed curve and time period (1 to 5 days) ahead adaptive predictions of the tumor growth in mice given i.p. doses of gemcitabine (100 mg/kg on Days 19 and 26). Predictions performed after the 25th day of the experiment using ANFIS model (3,50) with moving window of $l=20$ measurements.

Table 6.9. Prediction errors for the time period (1 to 5 days) ahead adaptive tumor growth inhibition prediction in mice given i.p. doses of gemcitabine (100 mg/kg on Days 19 and 26). Predictions performed with ANFIS model (3,50) with moving window of $l=20$ measurements.

Evaluation metrics	# Time periods ahead				
	1	2	3	4	5
RMSE (g)	0.027481	0.057566	0.106060	0.146427	0.178117
MAPE (%)	1.91	3.78	6.70	8.75	9.80

Prediction of the cancer patients' response to their therapeutical treatment with non-linear forecasting techniques

Chapter 6: Tumor growth modelling using adaptive neuron-fuzzy inference system (ANFIS)

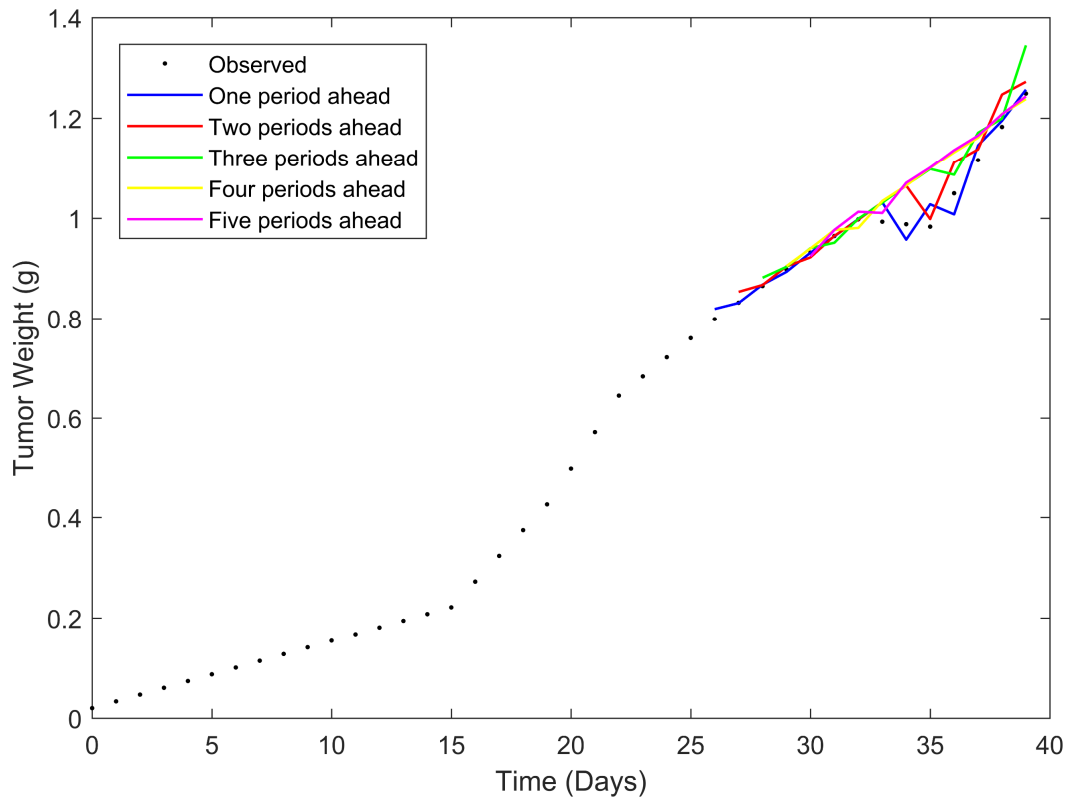


Figure 6.15. Observed curve and time period (1 to 5 days) ahead adaptive predictions of the tumor growth in mice given i.p. doses of gemcitabine (100 mg/kg on Days 19 and 26). Predictions performed after the 25th day of the experiment using ANFIS model (3,50) with moving window of $l = 15$ measurements.

Table 6.10. Prediction errors for the time period (1 to 5 days) ahead adaptive tumor growth inhibition prediction in mice given i.p. doses of gemcitabine (100 mg/kg on Days 19 and 26). Predictions performed with ANFIS model (3,50) with moving window of $l = 15$ measurements.

Evaluation metrics	# Time periods ahead				
	1	2	3	4	5
RMSE (g)	0.023504	0.036396	0.054110	0.053542	0.056606
MAPE (%)	1.68	2.63	4.00	3.94	4.09

6.3.2 Multi-drug chemotherapy – Predictions of TGI in combination chemotherapy scenarios

Chemotherapy drug combination comprises a standard treatment strategy to halt the tumor growth and eventually lead to the eradication of it. Therefore, it is important to test the prediction ability of ANFIS also in the multi-agent cases, where two or more antineoplastic drugs are delivered. Applying the same adaptive prediction technique as in the single drug case, ANFIS performance was evaluated in the terms of its ability to predict the future progression of the tumor growth in mice. Predictions were performed

Prediction of the cancer patients' response to their therapeutical treatment with non-linear forecasting techniques

Chapter 6: Tumor growth modelling using adaptive neuron-fuzzy inference system (ANFIS)

on the CPT-11 and 5-FU with drug C2 tumor growth datasets, described in the previous sections. In both cases, the ANFIS models were trained including tumor weight data of 0 to 16th day of each experiment. After this time point, one, two, three, four and five step (days) ahead predictions of the tumor weight were performed, until the 70th and 55th days of the experiment, respectively.

In the first case, 5-FU administered in combination with drug C2, a three-membership function ANFIS model was structured and trained for 100 epochs, ANFIS (3,100). On the dataset of CPT-11 and drug C2, a more complex ANFIS model of five MFs was required, mainly due to the complexity of the dataset. The model was also trained for 100 epochs ANFIS (5,100). It is important to note that in comparison to the single case, no moving windows were used in any of the two multi-agent cases studied. The prediction tumor growth curves for the cases of drugs administered in combination, i.e., CPT-11 with drug C2 and 5-FU with C2, are presented in Figure 6.16 and Figure 6.17, respectively. Prediction errors are shown in Table 6.11 and Table 6.12, below.

As seen from the figures in both cases the ANFIS models provided a good fit to the experimental data, as evidenced by the low RMSE and MAPE values. The ANFIS models' predictions were found to be in close agreement with the observed tumor weight data. This can be observed in Figure 6.16 and Figure 6.17, where the predicted tumor growth curves are found to closely follow the measured data points.

However, as the time periods ahead increase from one to two, two to three, etc., the prediction error also increases, indicating a decrease at the models' accuracy as the prediction horizon becomes longer. This phenomenon repeats itself in both cases studied. For example, in the case of 5-FU and drug C2, the prediction MAPE increases from 3% in the one-time period ahead to almost 20% in the five-time periods ahead predictions. The prediction error increases as the time steps ahead increase due to the model attempting to make predictions further into the future, where there is more uncertainty. The uncertainty in values of variables, such as chemotherapy drug dosages, can potentially impact the outcome, i.e., tumor growth.

Prediction of the cancer patients' response to their therapeutical treatment with non-linear forecasting techniques

Chapter 6: Tumor growth modelling using adaptive neuron-fuzzy inference system (ANFIS)

Nevertheless, the prediction errors for three-time periods ahead predictions of the tumor weight were lower than 12%, both in the 5-FU and drug C2, and CPT-11 and drug C2 cases. When performing five-step ahead predictions, both models achieved a MAPE lower than 28%.

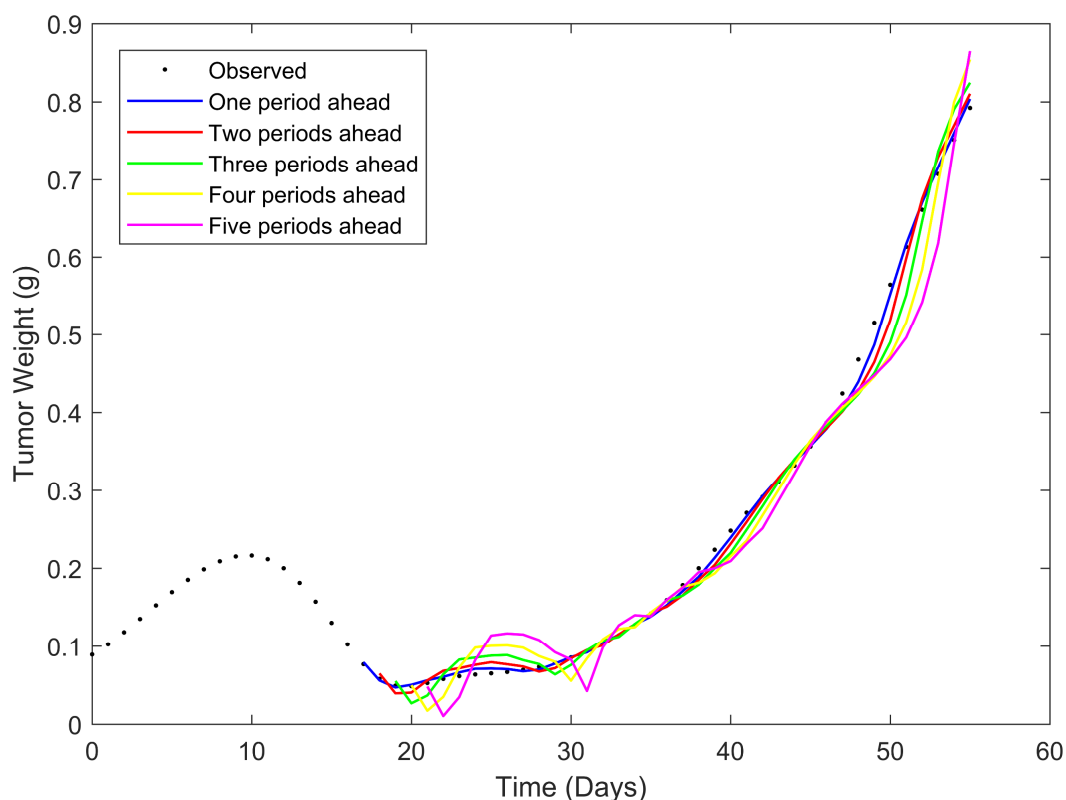


Figure 6.16. Observed curve and time period (1 to 5 days) ahead adaptive predictions of the tumor growth in mice given doses of 5-FU and drug C2 (50 mg/kg q4dx3 from day 9 and 60 mg/kg on days 10, 11, 12 and 14, 15, 16). Predictions performed after the 16th day of the experiment using ANFIS model (3,100).

Table 6.11. Prediction errors for the time period (1 to 5 days) ahead adaptive tumor growth inhibition prediction in mice given 5-FU and drug C2 (50 mg/kg q4dx3 from day 9 and 60 mg/kg on days 10, 11, 12 and 14, 15, 16). Predictions performed with ANFIS model (3,100).

Evaluation metrics	# Time periods ahead				
	1	2	3	4	5
RMSE (g)	0.009202	0.016895	0.026370	0.036939	0.047050
MAPE (%)	3.33	7.07	11.36	15.61	20.02

Prediction of the cancer patients' response to their therapeutical treatment with non-linear forecasting techniques

Chapter 6: Tumor growth modelling using adaptive neuron-fuzzy inference system (ANFIS)

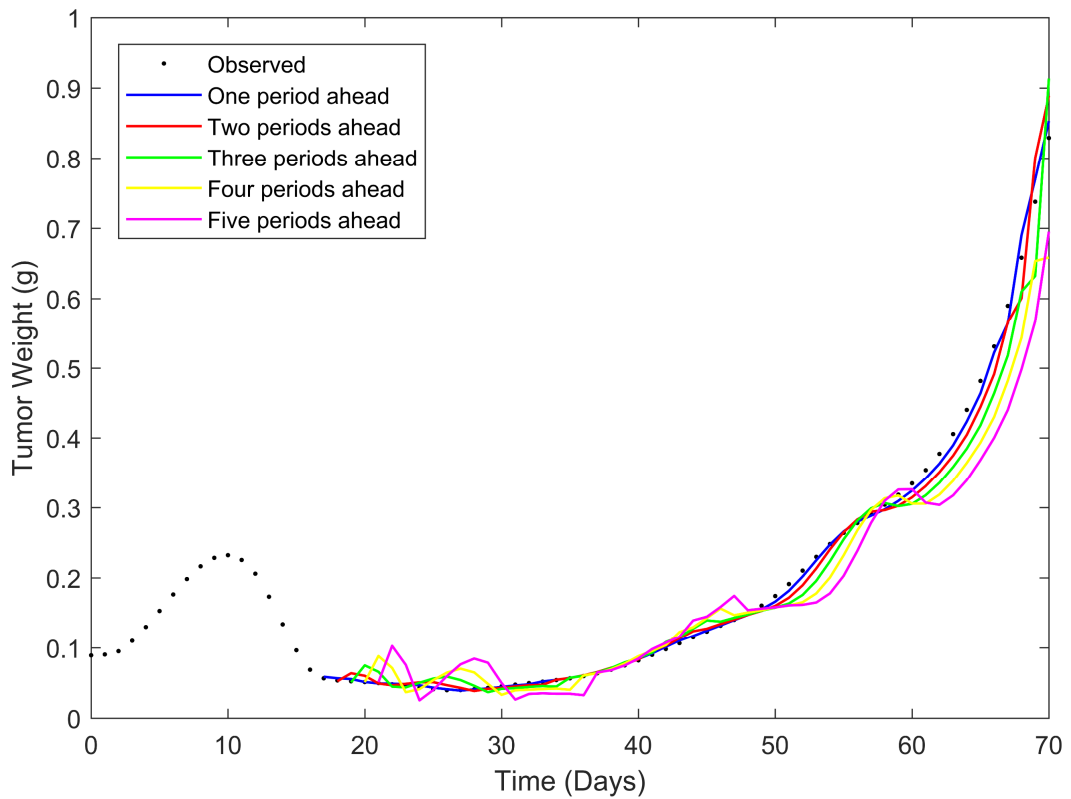


Figure 6.17. Observed curve and time period (1 to 5 days) ahead adaptive predictions of the tumor growth in mice given doses of CPT-11 and drug C2 (45 mg/kg q4dx3 from day 9 and 60 mg/kg on days 10, 11, 12 and 14, 15, 16). Predictions performed after the 16th day of the experiment using ANFIS model (5,100).

Table 6.12. Prediction errors for the time period (1 to 5 days) ahead adaptive tumor growth inhibition prediction in mice given CPT-11 and drug C2 (45 mg/kg q4dx3 from day 9 and 60 mg/kg on days 10, 11, 12 and 14, 15, 16). Predictions performed with ANFIS model (5,100).

Evaluation metrics	# Time periods ahead				
	1	2	3	4	5
RMSE (g)	0.009792	0.019767	0.031182	0.046882	0.193423
MAPE (%)	2.66	6.29	11.37	17.83	27.73

It is important to highlight that the ANFIS models for multi-agent tumor growth prediction achieved lower prediction errors when compared to the TGI_{add} models of [237]. The bar plots in Figure 6.18 and Figure 6.19 below, offer a clear visualization of the performance of the ANFIS models for multi-agent tumor growth predictions in contrast to the TGI_{add} models. To be more specific, the ANFIS models exhibited notably lower residuals across all test cases. This demonstrates a significant enhancement in the accuracy of predictions, particularly in situations where the tumor growth is erratic and

Prediction of the cancer patients' response to their therapeutical treatment with non-linear forecasting techniques

Chapter 6: Tumor growth modelling using adaptive neuron-fuzzy inference system (ANFIS)

less predictable. This improvement is evidenced by the smaller MAPE values for the ANFIS models when compared to the TGI_{add} models. For instance, in the case of 5-FU and drug C2, the ANFIS model three steps ahead forecasts achieved MAPE of 11.37%, compared to a MAPE of 15.62% for the TGI_{add} model. Similarly, for CPT-11 with drug C2, the ANFIS model yielded a MAPE of 11.37%, whereas the TGI_{add} model returned a MAPE of 17.68%. In the first case, the ANFIS model achieved a 27.21% reduction on the prediction error, while in the second case of CPT-11 with drug C2, it did achieve an astonishing 35.69% reduction of the MAPE.

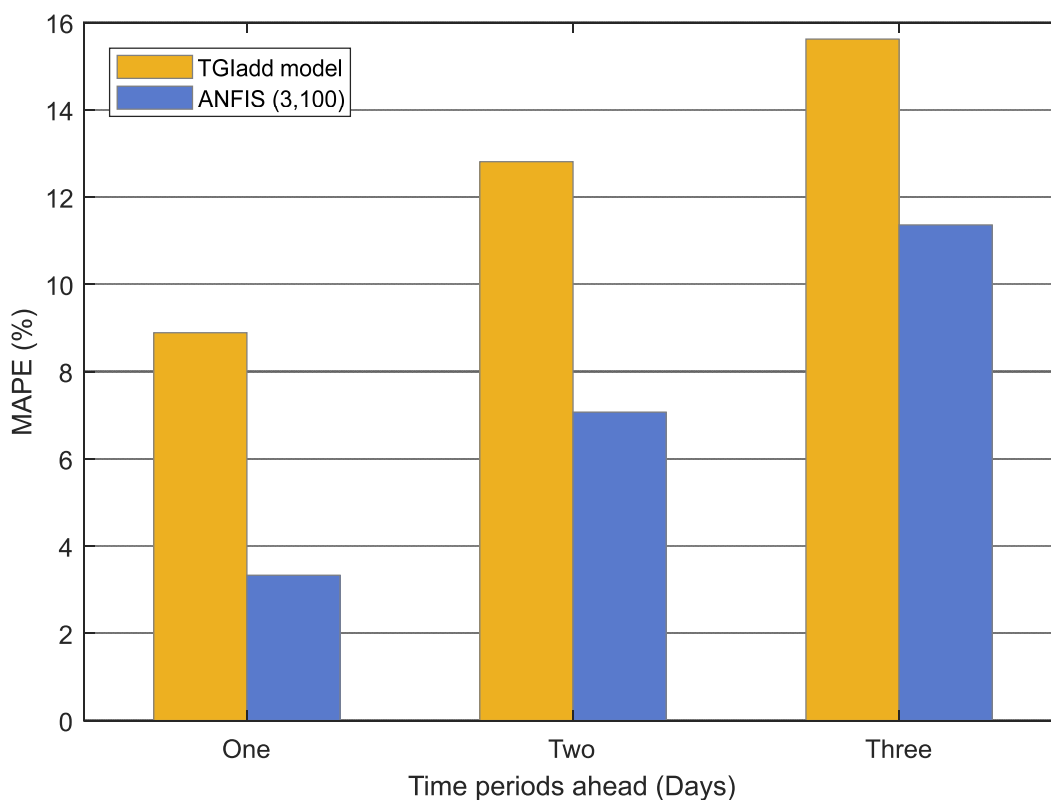


Figure 6.18. Prediction errors (MAPE %) for the time period ahead tumor growth inhibition predictions in mice given 5-FU and drug C2: TGI_{add} and ANFIS models. One, two and three time periods ahead.

Prediction of the cancer patients' response to their therapeutical treatment with non-linear forecasting techniques

Chapter 6: Tumor growth modelling using adaptive neuron-fuzzy inference system (ANFIS)

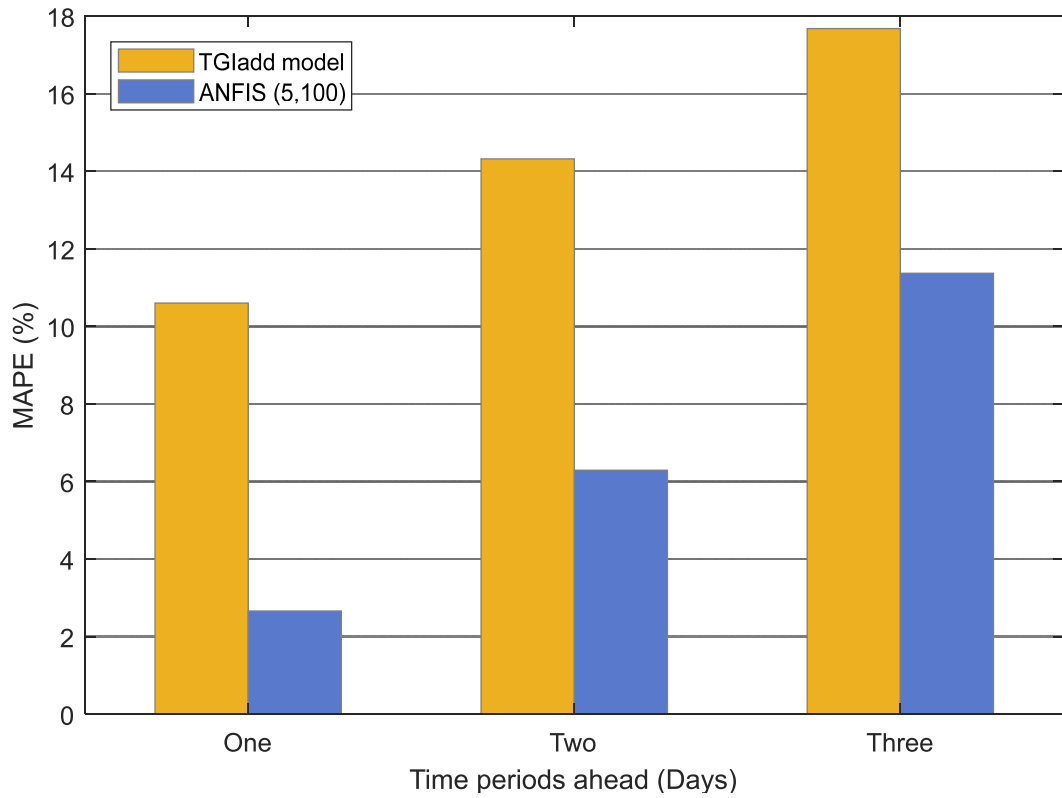


Figure 6.19. Prediction errors (MAPE %) for the time period ahead tumor growth inhibition predictions in mice given CPT-11 and drug C2: TGI_{add} and ANFIS models. One, two and three time periods ahead.

PART II

Efficient tumor eradication based on optimal control methods

Chapter 7: Non-linear optimal control for efficient tumor growth eradication

Traditional cytotoxic cancer chemotherapeutic regimens are often based on the MTD schedule, which can result in significant host toxicity and create windows for tumor vasculature regrowth and the emergence of drug-resistant cell populations during extended drug-free recovery periods. In contrast, metronomic treatment protocols adopt a different approach by administering chemotherapy drugs at lower doses than conventional MTD regimens. These lower doses are delivered at a more frequent rate, and in some cases, on a continuous, daily schedule, thereby reducing the overall burden of toxicity on the host. Optimal control could be used to describe treatment protocols which have the potential to be more efficient than the standard periodic protocols that are currently in use. Therefore, formulating this as an optimal control problem allows not only to investigate the tumor growth dynamics and minimize its size at some of end-time but at the same time optimize the application of the control such that the quantity of the treatment (e.g., gemcitabine doses) is minimum. This results in avoiding high toxicity levels and adverse effects due to treatment. To determine the optimal dose level, the Simeoni *et al.* TGI model was further extended, forming the *augmented TGI model*. Specifically, an additional state q corresponding to the one-compartment PK model was added (see (4.5)). Therefore, the Simeoni *et al.*'s TGI model now becomes:

$$\begin{aligned}
 \frac{dz_0(t)}{dt} &= \frac{\lambda_0 \cdot z_0(t)}{\left[1 + \left(\frac{\lambda_0}{\lambda_1} \cdot w(t)\right)^\psi\right]^{\frac{1}{\psi}}} - k_2 \cdot \frac{q(t)}{V} \cdot z_0(t) \\
 \frac{dz_1(t)}{dt} &= k_2 \cdot \frac{q(t)}{V} \cdot z_0(t) - k_1 \cdot z_1(t) \\
 \frac{dz_2(t)}{dt} &= k_1 \cdot [z_1(t) - z_2(t)] \\
 \frac{dz_3(t)}{dt} &= k_1 \cdot [z_2(t) - z_3(t)] \\
 \frac{dq(t)}{dt} &= -k_{10}q(t) + u(t) \\
 w(t) &= z_0(t) + z_1(t) + z_2(t) + z_3(t)
 \end{aligned} \tag{7.1}$$

Prediction of the cancer patients' response to their therapeutical treatment with non-linear forecasting techniques

Chapter 7: Non-linear optimal control for efficient tumor growth eradication

where $u(t)$ is the chemotherapy drug dose in mg/kg and the control input at each time instance t . The initial conditions (at $t = 0$) of the augmented mathematical model (7.1) are $[z_0(0), z_1(0), z_2(0), z_3(0), q(0)] = [0,0,0,0,0]$.

The aim of chemotherapy is to use the right drug doses during treatment to bring the system to a tumor-free equilibrium point $[z_0, z_1, z_2, z_3, q] = [0,0,0,0,0]$, where the tumor mass is reduced to zero. Since this equilibrium point in the case of Simeoni TGI model is located at the origin, there is no need to employ error states to shift the point.

Due to the non-linear nature of the problem, the State Dependent Coefficient (SDC) form was used to capture the system non linearities into a pseudo-linear system matrix, which is used then to derive the SDRE based optimal control for tumor growth. The (7.1) equations must be factorized into a SDC form of:

$$\dot{\underline{x}} = A(\underline{x})\underline{x} + B(\underline{x})u \quad (7.2)$$

where $\underline{x} = [x_1, x_2, x_3, x_4, x_5]^T = [z_0, z_1, z_2, z_3, q]^T$ is the state vector, $u \geq 0$ is the input (i.e., gemcitabine dose levels) while $A(\underline{x}) \in \mathbb{R}^{5 \times 5}$ and $B(\underline{x}) \in \mathbb{R}^{5 \times 1}$ matrices are the pseudo-linear system matrices in the SDC form.

The initial values of the system states (at $t = 0$) for the pseudo-linear system of $[x_1(0), x_2(0), x_3(0), x_4(0), x_5(0)] = [0,0,0,0,0]$. However, the parameterization is not unique, and to preserve the dependency of terms that contain two or more states (e.g., $\frac{q(t)}{V} z_0(t)$), free designs parameters (θ) are introduced. For more information on SDC parameterization, please refer to the "SDC parameterization" section in the Appendix. Using θ , a family of SDC parameterizations of (7.1) can be constructed. More specifically, a set of vectors of different values of $\theta_i \in [0,1]$, for $i = 1,2$ was used to identify the vector $\theta = [\theta_1, \theta_2]$ which maximizes the pointwise controllable space.

The SDC parameterization of the system (7.1) by using θ is described through (7.3) and (7.4) below. The sets of θ values that were tested against the TGI model states are shown in Table 7.1 below.

Prediction of the cancer patients' response to their therapeutical treatment with non-linear forecasting techniques

Chapter 7: Non-linear optimal control for efficient tumor growth eradication

$$A(x, \theta) = \begin{bmatrix} a_{11} & 0 & 0 & 0 & a_{15} \\ a_{21} & a_{22} & 0 & 0 & a_{25} \\ 0 & a_{32} & a_{33} & 0 & 0 \\ 0 & 0 & a_{43} & a_{44} & 0 \\ 0 & 0 & 0 & 0 & a_{55} \end{bmatrix} \text{ and } B = \begin{bmatrix} 0 \\ 0 \\ 0 \\ 0 \\ 1 \end{bmatrix} \quad (7.3)$$

where

$$\begin{aligned} a_{11} &= \frac{\lambda_0}{\left[1 + \left(\frac{\lambda_0}{\lambda_1} \cdot w(t)\right)^\psi\right]^{\frac{1}{\psi}}} - (1 - \theta_1)k_2 \frac{x_5}{V}, \\ a_{15} &= -\theta_1 k_2 x_1 \frac{1}{V}, \\ a_{21} &= (1 - \theta_2)k_2 \frac{x_5}{V}, \\ a_{22} &= -k_1, \\ a_{25} &= \theta_2 k_2 x_2 \frac{1}{V}, \\ a_{32} &= k_1, \quad a_{33} = -k_1, \\ a_{43} &= k_1, \quad a_{44} = -k_1, \\ a_{55} &= -k_{10} \end{aligned} \quad (7.4)$$

Table 7.1. Sets of the free design parameters θ values. Tested against the augmented TGI model states to identify the vector $\theta = [\theta_1, \theta_2]$ which maximizes the pointwise controllable space.

θ set	θ_1	θ_2	θ_1	θ_2	θ_1	θ_2	θ_1	θ_2
1	0.0	0.0	0.5	0.0	0.75	0.0	1.0	0.0
2	0.0	0.5	0.5	0.5	0.75	0.5	1.0	0.5
3	0.0	0.75	0.5	0.75	0.75	0.75	1.0	0.75
4	0.0	1.0	0.5	1.0	0.75	1.0	1.0	1.0

In Figure 7.1, the absolute value of the determinant of the state-dependent controllability matrix $M_c(z)$, $|\det(M_c)|$ for the tumor dynamics is plotted against state $x_2 = z_1$ of the TGI model, for the values of θ . For the given parameter set of Simeoni TGI model, presented in Table 4.4, the largest value of $|\det(M_c)|$ was obtained by

Prediction of the cancer patients' response to their therapeutical treatment with non-linear forecasting techniques

Chapter 7: Non-linear optimal control for efficient tumor growth eradication

choosing the vector $\theta = [\theta_1, \theta_2] = [1,1]$ (see Figure 7.1), which ensures that the pair $A(x, \theta), B$ is pointwise controllable and therefore stabilizable.

To prevent side effects, such as acute toxicity of the host cells resulting from the action of chemotherapy drug, hard constraints were introduced on the control input, i.e., the dose level. When the suggested dose level exceeds a predefined threshold, the control signal is constrained using predefined inequalities. Since the control input cannot be negative, a minimum value (u_{min}) of zero was considered for the administered drug dose. In addition, a maximum dose (u_{max}) of 200 mg/kg was also applied to balance toxicity and chemotherapy efficacy. Thus, at any time instance t the control input u is constrained within the bounds:

$$u_{min} \leq u(t) \leq u_{max} \tag{7.5}$$

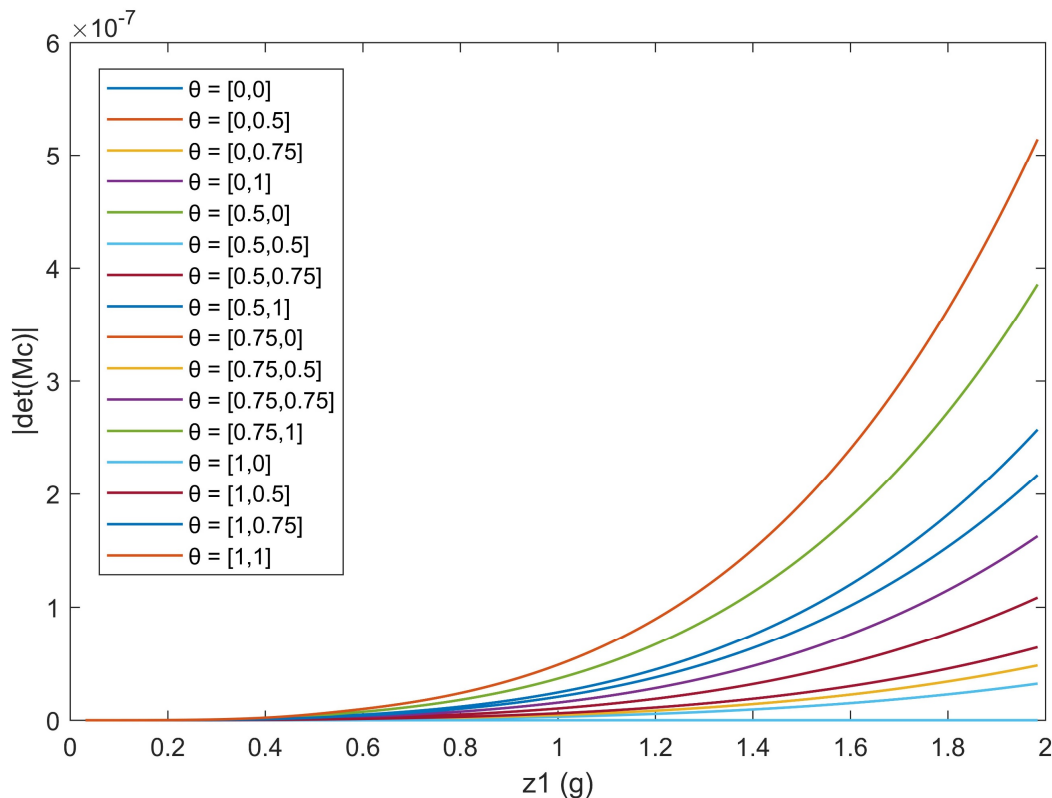


Figure 7.1. The absolute determinant of the state-dependent controllability matrix $M_c(x)$ against $x_2 = z_1$ (g) state of the augmented Simeoni's TGI model for various free design parameters θ .

where $u_{min} = 0$ mg/kg and $u_{max} = 200$ mg/kg. Of course, the solutions derived under these constraints possibly yield suboptimal control, as they might not strictly minimize

the original objective but do so under the imposed constraints, ensuring a balance between optimality and feasibility.

The SDRE controller for the augmented Simeoni TGI model was designed and developed in MathWorks MATLAB and SIMULINK [238] platform where optimal chemotherapy drug doses for several periodic and intermittent chemotherapy treatment schedules were computed. The goal of non-linear optimal regulation using the SDRE method is to drive all system states to the tumor-free equilibrium with the lowest cost. In other words, the objective is to eradicate tumor by administering minimum doses of gemcitabine. For this purpose, the controller was designed to minimize a cost functional J_{TGI} :

$$J_{TGI} = \frac{1}{2} \int_0^{\infty} (\underline{x}^T Q(\underline{x}) \underline{x} + R(\underline{x}) u^2) dt \quad (7.6)$$

where Q and R are the state and input weighting matrices.

Their values were selected through trial-and-error experiments using “good” initial values as $Q = \text{diag}(1e3, 1e3, 1e3, 1e3, 0.04)$ and $R = 25$. The methods for selecting these values are described in detail in the Appendix D.

$$Q = \begin{bmatrix} 1e3 & 0 & 0 & 0 & 0 \\ 0 & 1e3 & 0 & 0 & 0 \\ 0 & 0 & 1e3 & 0 & 0 \\ 0 & 0 & 0 & 1e3 & 0 \\ 0 & 0 & 0 & 0 & 0.04 \end{bmatrix} \text{ and } R = 25. \quad (7.7)$$

Optimal drug doses extracted both for periodic and intermittent chemotherapy treatment schedules, with all simulations performed using an incremental time step of 0.001 days and a final time $t_f = 100$ days. To evaluate each drug delivery scenario, certain metrics were calculated. These metrics provide important insights into the ability of each drug delivery scenario to control tumor growth while at the same time minimizing the total amount of drug needed to achieve this goal. Specifically, the total dose of the administered drug (u_{total} in mg/kg) until the end of the simulation at $t = t_f$,

as well as the maximum weight of the tumor reached (w_{max} in g) during the same period were calculated. The equations below describe how these metrics were calculated:

$$u_{total} = \sum_{t=0}^{t_f} u(t) \quad (7.8)$$

$$w_{max} = \max_{0 \leq t \leq t_f} w(t) \quad (7.9)$$

Here, $u(t)$ represents the dose of the administered drug as proposed by the controller at each time point t , and $w(t)$ represents the weight of the tumor at time t . u_{total} can also be referred also as the total control effort.

Monitoring the mouse weight loss is crucial in clinical settings as it serves as a vital indicator of treatment-related side effects and overall well-being, aiding in the assessment of the treatment tolerability and the overall health during chemotherapy. However, in this study, the measurement of weight loss is not conducted as it focuses on theoretical simulations rather than real clinical observations.

7.1 Optimized chemotherapy dosages in periodic treatment scenarios using the augmented TGI model and SDRE optimal control

This study divided the periodic treatment schedules into five distinct cases. For each case, the SDRE controller suggested optimal i.p. doses of gemcitabine. In the first case, i.e., Case 1, gemcitabine was administered daily or continuously at the optimal dosage. This aims to objectively analyze the immediate and consistent impacts of the drug and investigate how a persistent drug presence affects the tumor growth. The rest of the cases, i.e., Cases 2-5, cover periodic treatment schedules commonly used in clinical practice, which include drug administration every 2, 3, 5, and 7 days, respectively, as outlined in Table 7.2. The purpose of investigating these intervals is to determine the trade-offs between dosing frequency, patient comfort, and the drug's effectiveness in treating tumors. Prolonged time intervals may increase patient comfort and reduce side effects, although they may also impact the drug's effectiveness.

Optimum gemcitabine dosages and the corresponding metrics, such as u_{total} and w_{max} , for each case, are listed in Table 7.2. This table can also serve as a reference point for comparing the results of the different treatment regimens, thereby aiding in the

Prediction of the cancer patients' response to their therapeutical treatment with non-linear forecasting techniques

Chapter 7: Non-linear optimal control for efficient tumor growth eradication

decision-making process when selecting the most efficient and effective treatment plan. The suboptimal drug delivery protocols related to the SDRE control for the periodic cases are depicted in Figure 7.2 - Figure 7.6, below.

Table 7.2. Periodic SDRE treatment results (dose schedules and metrics) across Cases 1 to 5.

Cases	Dose schedule	u_{total} (mg/kg)	w_{max} (g)	w_{zero} (days)
Case 1	Continuous	3234.63	0.4957	>100
Case 2	every 2 days	3062.82	0.5188	>100
Case 3	every 3 days	3002.18	0.5447	>100
Case 4	every 5 days	2844.42	0.5970	>100
Case 5	every 7 days	2705.71	0.5486	>100

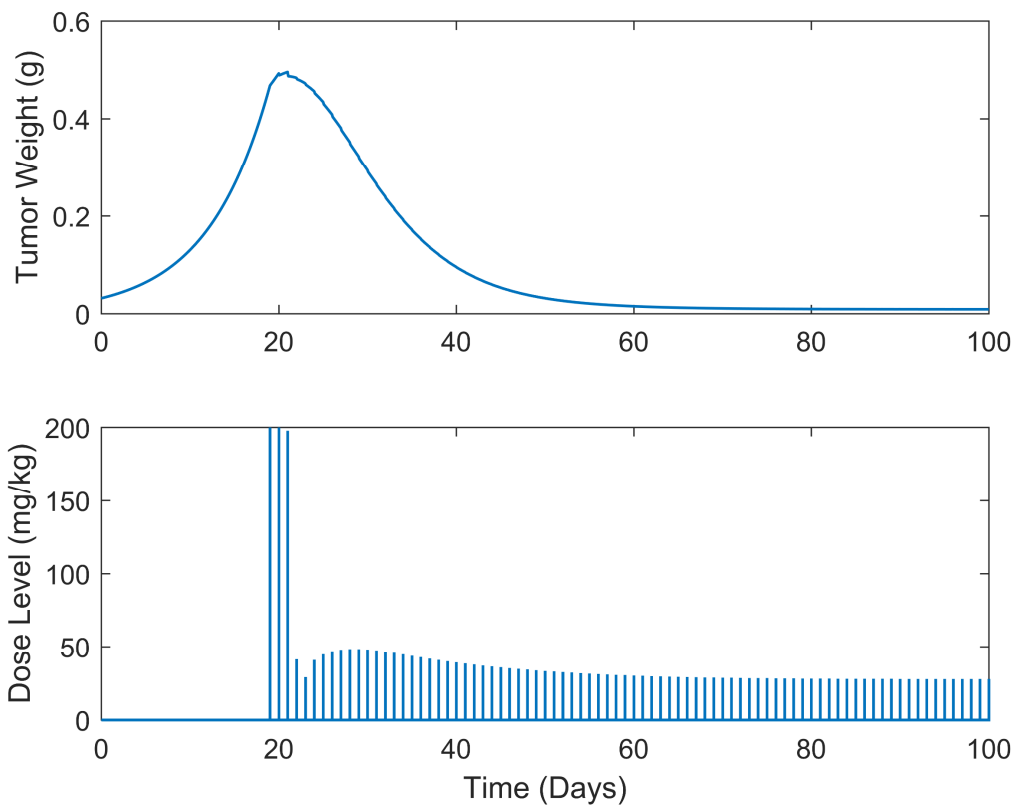


Figure 7.2. Augmented TGI system's response (i.e., tumor weight) and optimal control input (i.e., dose level). Continuous treatment: daily dose administration (Case 1).

In all treatment schedules, the proposed doses of gemcitabine doses highly effective in reducing tumor growth. Specifically, in cases 1 – 3, the tumor weight reached values on the scale of $1e-2$ g or less. Such values are below the tumor weight w_0 at the time of inoculation $t = 0$. Thus, they can be described as undetectable. However, it was observed that the drug dosages suggested by the SDRE were not zero. This observation

Prediction of the cancer patients' response to their therapeutical treatment with non-linear forecasting techniques

Chapter 7: Non-linear optimal control for efficient tumor growth eradication

suggests that the controller may have tried to maintain the tumor at a low level rather than eradicating it completely. This is the case in each periodic treatment scheduled explored. The tumor weight is rapidly reduced, and it is stabilized to a certain weight at days 70 to 80 of the simulations. Such behavior could result from the objective function used to optimize drug doses or even from the selection of the state-dependent weighting matrices Q and R . Another potential factor may be the dose intervals. Longer intervals could act as rest periods, allowing the tumor to recover slightly and requiring subsequent doses. The maximum tumor weight reached is lower than 0.5 g. Nonetheless, as the interval of the doses increases, an increase in the maximum tumor weight is observed during the simulations. This increase in the maximum tumor weight, w_{max} , observed when the dosing intervals becomes longer may confirm this hypothesis.

In all cases the suggested doses start aggressively at the onset of the treatment, beginning with 200 mg/kg of gemcitabine, reaching the predefined upper dose limit. As the drug takes effect on the tumor, the SDRE suggests progressively lower doses.

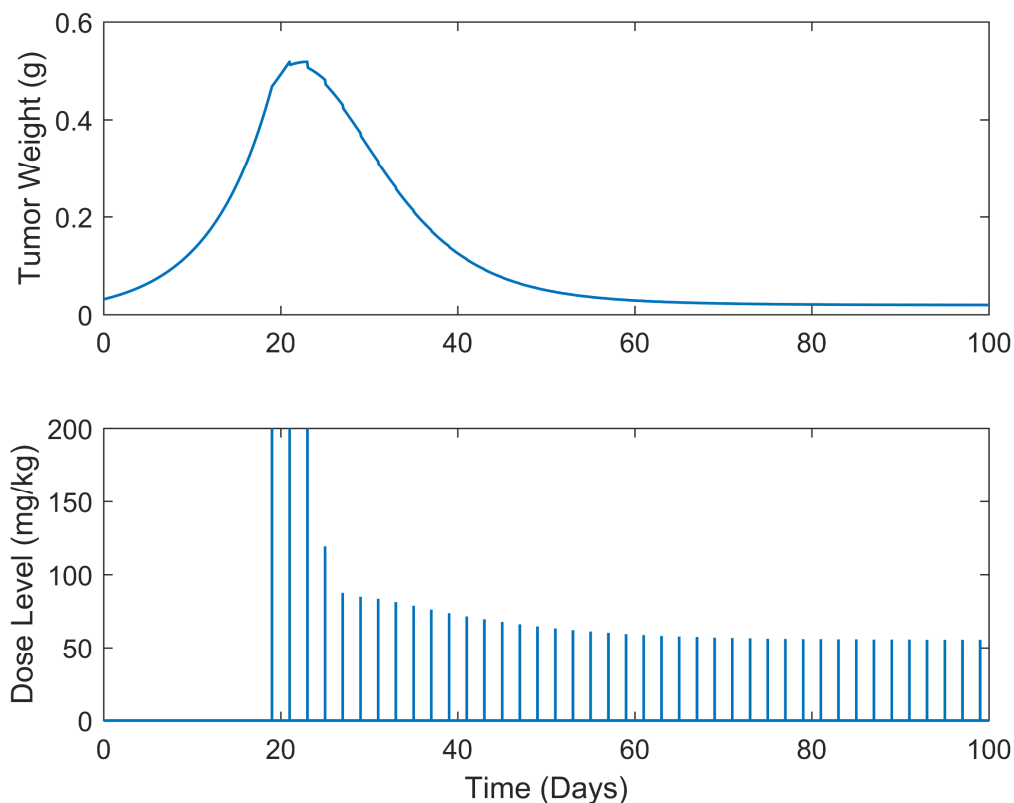


Figure 7.3. Augmented TGI system's response (i.e., tumor weight) and optimal control input (i.e., dose level). Periodic treatment: dose administration every 2 days (Case 2).

Prediction of the cancer patients' response to their therapeutical treatment with non-linear forecasting techniques

Chapter 7: Non-linear optimal control for efficient tumor growth eradication

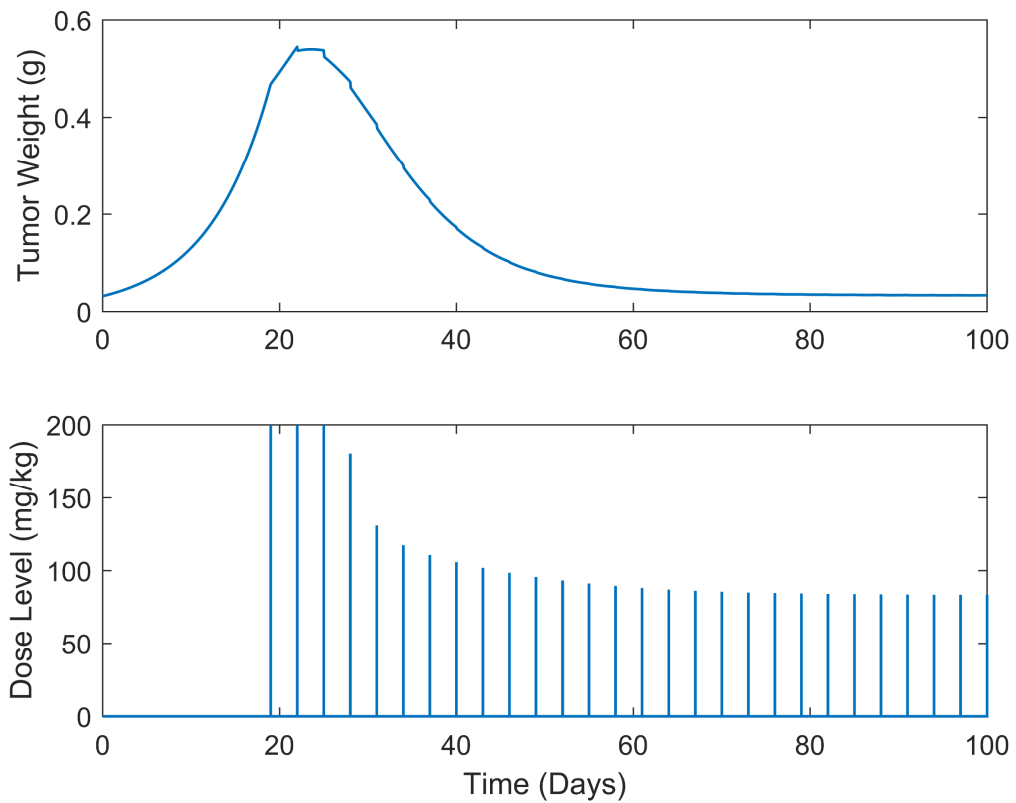


Figure 7.4. Augmented TGI system's response (i.e., tumor weight) and optimal control input (i.e., dose level). Periodic treatment: dose administration every 3 days (Case 3).

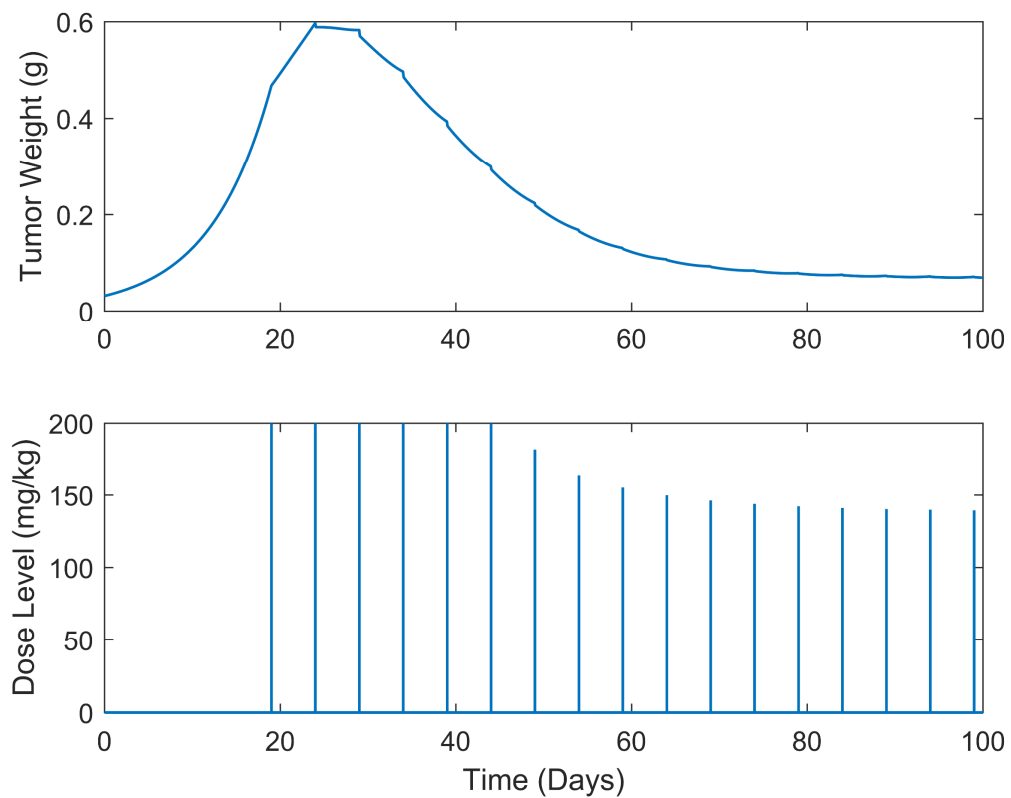


Figure 7.5. Augmented TGI system's response (i.e., tumor weight) and optimal control input (i.e., dose level). Periodic treatment: dose administration every 5 days (Case 4).

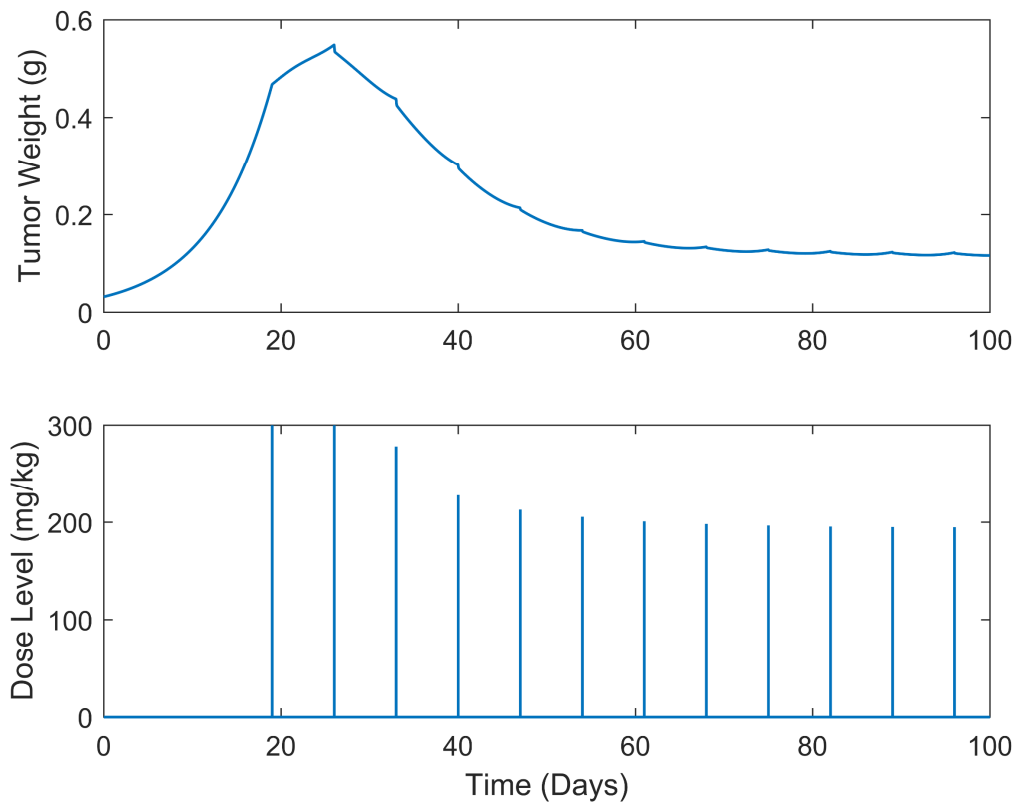


Figure 7.6. Augmented TGI system's response (i.e., tumor weight) and optimal control input (i.e., dose level). Periodic treatment: dose administration every 7 days (Case 5).

To determine whether non-zero drug doses are necessary to maintain the desired tumor size, future work could involve modifying the objective function and further optimizing the SDRE controller to reduce drug doses while maintaining tumor control. Overall, the results demonstrate the effectiveness of the optimal drug doses proposed by the SDRE method in reducing tumor growth to low levels. Further investigation into the underlying mechanisms of the controller may lead to improvements in drug dosing strategies for cancer treatment.

7.2 Optimized chemotherapy dosages in intermittent treatment cases using the augmented TGI model and SDRE optimal control

Whereas in the abovementioned cases the tumor was successfully eliminated, chemotherapy resistant scenarios might occur due to the long exposure to the drug. Cancer chemotherapy resistance is a phenomenon where the neoplastic cells develop the ability to evade the effects of the chemotherapeutic treatment, leading to failure in drug response [239], [240]. To this direction, optimal drug dosages for intermittent chemotherapy schedules were also explored. To be more precise, optimal dosages for

Prediction of the cancer patients' response to their therapeutical treatment with non-linear forecasting techniques

Chapter 7: Non-linear optimal control for efficient tumor growth eradication

two cases of different intermittent treatment schedules were investigated. In both cases chemotherapy was administered every 3 days for five times, i.e., q3dx5. Then, to avoid toxicity and drug resistance, the treatment paused for a period of $tr_p = 7$ (Case 6) and 10 days (Case 7), respectively. Finally, it is restarted with dose administrations every 5 days for five times, i.e., q5dx5.

The nature of intermittent dosing introduced new dynamics and responses into the system, requiring an adjustment in the control strategy. To address the changes in state regulation and control effort priorities under this new paradigm, modifications to the Q and R weighting matrices were deemed essential. Periodic and intermittent dosing represent different operational scenarios, each with unique challenges and objectives.

A summary of the results is presented in Table 7.3 below, while the tumor weight curves and the optimal drug dosages are illustrated in Figure 7.7 and Figure 7.8.

Table 7.3. Intermittent SDRE treatment results (dose schedules and metrics) across Cases 6 and 7.

Cases	Dose schedule	tr_p (days)	u_{total} (mg/kg)	w_{max} (g)	w_{zero} (days)
Case 6	q3dx5, q5dx5	7	2804.91	0.5447	>100
Case 7	q3dx5, q5dx5	10	2714.38	0.5447	>100

In examining the results presented in Table 7.3 , a striking observation is the efficacy of the intermittent SDRE treatment schedules in both cases 6 and 7. Over approximately 100 days, tumor size was stabilized at about 0.067 g, a weight close to the initial, at the inoculation time, for Case 6, and at about 0.089 g for Case 7, demonstrating the potential of these treatment strategies. The proposed drug doses in both cases start aggressively, with initial doses close to 200 mg/kg, and average 156 mg/kg in Case 6 and 170 mg/kg in Case 7. A comparison between the two cases reveals a direct correlation between the length of the chemotherapy holidays, denoted by tr_p , and the total amount of drug administered, u_{total} . Specifically, Case 7, which had longer chemotherapy holidays, required 3.34% lower total amount of drug than Case 6. This reduction total amount of drug also resulted in faster tumor eradication.

Prediction of the cancer patients' response to their therapeutical treatment with non-linear forecasting techniques

Chapter 7: Non-linear optimal control for efficient tumor growth eradication

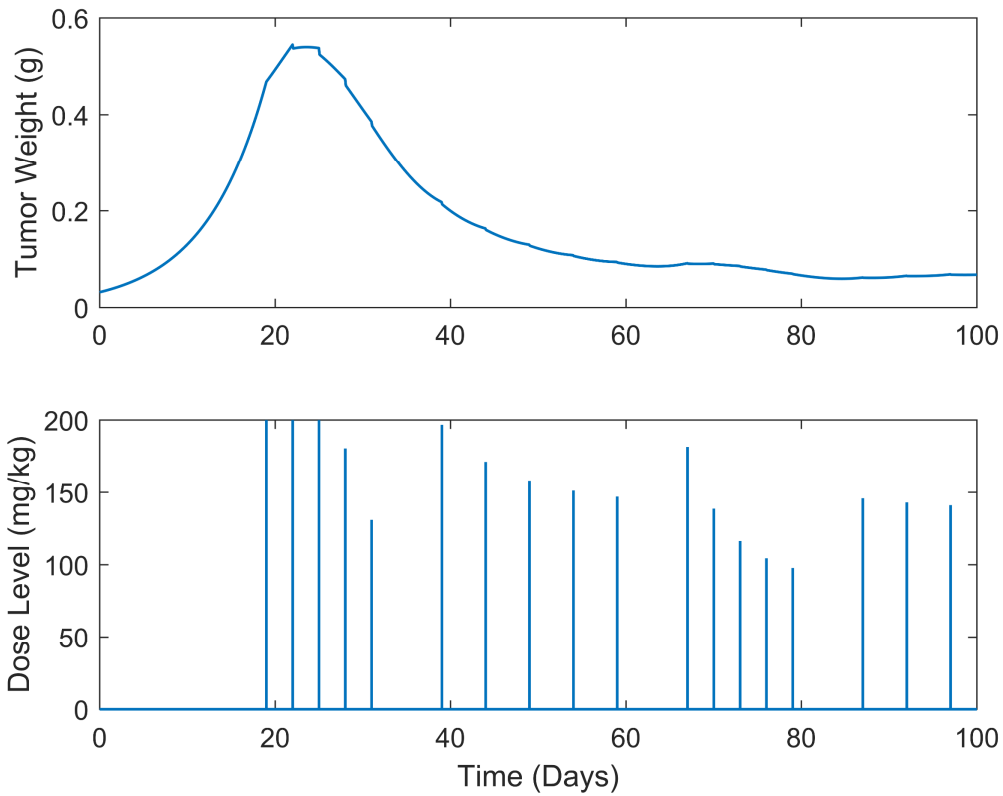


Figure 7.7. Augmented TGI system's response (i.e., tumor weight) and optimal control input (i.e., dose level). Intermittent: $q3dx5$, $q5dx5$ dose administrations with 7 days pauses (Case 6).

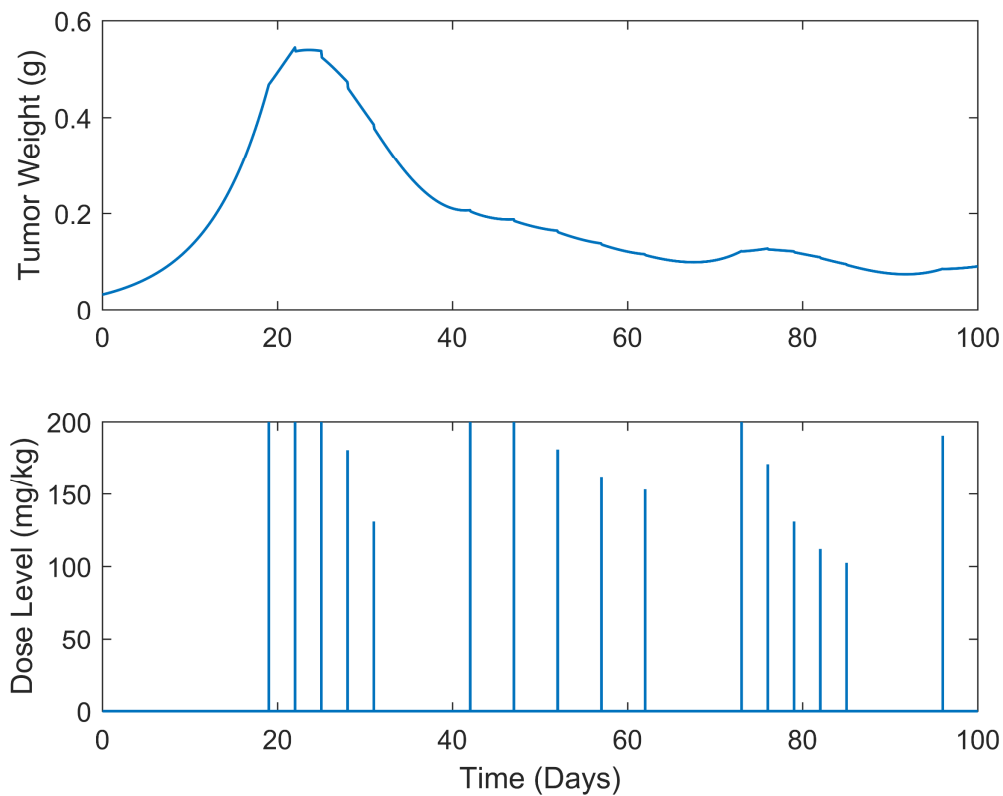


Figure 7.8. Augmented TGI system's response (i.e., tumor weight) and optimal control input (i.e., dose level). Intermittent: $q3dx5$, $q5dx5$ dose administrations with 10 days pauses (Case 7).

Chapter 8: Linear quadratic control (LQC) applied for effective tumor growth eradication

The optimal administration of chemotherapy drugs is a challenging problem. While in complex, non-linear mathematical models, such as the Simeoni *et al.*'s TGI model, through its augmented form, the SDRE method is a very good sub-optimal solution to discover optimal dose levels in periodic and intermittent chemotherapy schedules, when it comes to linear problems, LQC through methods like LQR can provide optimally controlled feedback gains and therefore an optimal solution to the problem. Through linear state feedback, LQR can achieve closed-loop optimal control of the anti-cancer drug dose levels while at the same time eliminate the tumor.

To do that, liner models such as the ARX models developed in Chapter 5 are necessary to be converted in a state-space form. This is feasible by calculating its transfer function $H(z)$. Generally, the transfer function of a system can be transformed to a non-unique state-space representation using a discrete-time realization algorithm (DRA) [241].

The transfer function of the single-agent ARX model (5.2) can be calculated as follows:

$$w[k] = a_1 w[k-1] + a_2 w[k-2] + a_3 w[k-3] + b_1 u[k-1] + b_2 u[k-2] + b_3 u[k-3]$$

$$W(z) = W(z)(a_1 z^{-1} + a_2 z^{-2} + a_3 z^{-3}) + U(z)(b_1 z^{-1} + b_2 z^{-2} + b_3 z^{-3})$$

$$H(z) = \frac{W(z)}{U(z)} = \frac{b_1 z^{-1} + b_2 z^{-2} + b_3 z^{-3}}{1 - a_1 z^{-1} - a_2 z^{-2} - a_3 z^{-3}} \quad (8.1)$$

$$H(z) = \frac{6.7573 z^{-5} - 5.8769 z^{-2} - 8.7736 z^{-3}}{1 + 2.9653 z^{-1} - 2.9456 z^{-2} + 0.9851 z^{-3}}$$

Among several equivalent state-space forms of the above transfer function, the observable canonical form ensures the observability of the derived system [241] (see more in the Appendix E). The state-space representation of (8.1) in the observable canonical form is described by the equations below:

$$\begin{aligned} x[k+1] &= A x[k] + B u[k] \\ y[k] &= C x[k] + D u[k] \end{aligned} \quad (8.2)$$

where

Prediction of the cancer patients' response to their therapeutical treatment with non-linear forecasting techniques

Chapter 8: Linear quadratic control (LQC) applied for effective tumor growth eradication

$$A = \begin{bmatrix} -a_1 & 1 & 0 \\ -a_2 & 0 & 1 \\ -a_3 & 0 & 0 \end{bmatrix}, \quad B = \begin{bmatrix} b_1 \\ b_2 \\ b_3 \end{bmatrix}, \quad C = [1 \quad 0 \quad 0], \quad D = 0$$

with

$$x[k] = [x_1 \quad x_2 \quad x_3]^T$$

Although the derived state-space system is not stable, it is both observable and

controllable. This means that the observability matrix $\mathcal{O} = \begin{bmatrix} C \\ CA \\ CA^2 \end{bmatrix}$ and the controllability

matrix $\mathcal{C} = [B \quad AB \quad A^2B]$ are full column and row rank, respectively. Therefore, the initial conditions may be calculated from the output $y[k]$ and input $u[k]$.

Generally, for a n -order system, if $\mathcal{O} = \begin{bmatrix} C \\ CA \\ \vdots \\ CA^{n-1} \end{bmatrix}$ is full-rank (i.e., observable) or

nonsingular, $x[0]$ may be reconstructed with any $y[k]$, $u[k]$ as shown below:

$$\begin{aligned} y[k] &= Cx[k] + Du[k] \\ y[0] &= Cx[0] + Du[0] \\ y[1] &= C [Ax[0] + Bu[0]] + Du[1] \\ y[2] &= C [A^2x[0] + ABu[0] + Bu[1]] + Du[2] \\ &\vdots \\ y[n-1] &= C [A^{n-1}x[0] + A^{n-2}Bu[0] + \dots + Bu[n-1]] + Du[n-1] \end{aligned} \tag{8.3}$$

The above can be written in a vector form as follows:

$$\begin{bmatrix} y[0] \\ y[1] \\ \vdots \\ y[n-1] \end{bmatrix} = \underbrace{\begin{bmatrix} C \\ CA \\ \vdots \\ CA^{n-1} \end{bmatrix}}_{\mathcal{O}} x[0] + \underbrace{\begin{bmatrix} D & 0 & \dots & 0 \\ CB & D & \dots & 0 \\ CAB & CB & \dots & 0 \\ \vdots & \vdots & \ddots & D \end{bmatrix}}_{\mathcal{T}} \begin{bmatrix} u[0] \\ u[1] \\ \vdots \\ u[n-1] \end{bmatrix} \tag{8.4}$$

Prediction of the cancer patients' response to their therapeutical treatment with non-linear forecasting techniques

Chapter 8: Linear quadratic control (LQC) applied for effective tumor growth eradication

So,

$$x[0] = \mathcal{O}^{-1} \left[\begin{array}{c} y[0] \\ y[1] \\ \vdots \\ y[n-1] \end{array} \right] - \mathcal{T} \left[\begin{array}{c} u[0] \\ u[1] \\ \vdots \\ u[n-1] \end{array} \right]. \quad (8.5)$$

For the specific case studied in this work, the initial conditions of the systems are calculated through the following equation:

$$x[0] = \mathcal{O}^{-1} \left[\begin{array}{c} y[0] \\ y[1] \\ y[2] \end{array} \right] - \mathcal{T} \left[\begin{array}{c} u[0] \\ u[1] \\ u[2] \end{array} \right]. \quad (8.6)$$

Using (8.6) and the laboratory measurements of the tumor growth for $w_{k=0} = y[k=0]$, $w_{k=1} = y[k=1]$ and $w_{k=2} = y[k=2]$, the initial values of the states x of the (8.2) state-space system were calculated as:

$$x[0] = \begin{bmatrix} x_1[0] \\ x_2[0] \\ x_3[0] \end{bmatrix} = \begin{bmatrix} 0.0200 \\ -0.0259 \\ 0.0066 \end{bmatrix}. \quad (8.7)$$

As previously mentioned, it was determined that the inherent dynamics exhibit unstable behavior. Nevertheless, a thorough examination confirmed that the system possesses both controllability and observability properties. This combination of attributes offers a promising avenue for stabilization. Specifically, the LQR approach is employed to counteract the system's inherent instability. Given the controllability of the system, the LQR method has the potential to not only stabilize the system but also optimize its performance under specified criteria.

Given observability and controllability of the system, the use of LQR optimal control was considered feasible. Based on the theory presented in [242] (see the Appendix for details), an initial selection was made for the weighting matrices Q_p and R_p as $\text{diag}\{14 \ 14 \ 14\} \cdot 10^{-4}$ and $343 \cdot 10^2$, respectively, serving as a "good" start for daily dose administrations (see Figure 8.1). However, for chemotherapy schedules that extend to doses administered every 2, 3, 5, and 7 days, these matrices required

Prediction of the cancer patients' response to their therapeutical treatment with non-linear forecasting techniques

Chapter 8: Linear quadratic control (LQC) applied for effective tumor growth eradication

adjustments. Consequently, a series of refinements to Q_p and R_p were made through a trial-and-error approach to better accommodate to these extended dosing intervals.

While there are numerous possible combinations that can be used, the weighting matrices Q_p and R_p were chosen to be $\text{diag}\{42 \ 42 \ 42\} \cdot 10^{-4}$ and 1700, respectively:

$$Q_p = \begin{bmatrix} 42 & 0 & 0 \\ 0 & 42 & 0 \\ 0 & 0 & 42 \end{bmatrix} \cdot 10^{-4} \quad \text{and} \quad R_p = 1700.$$

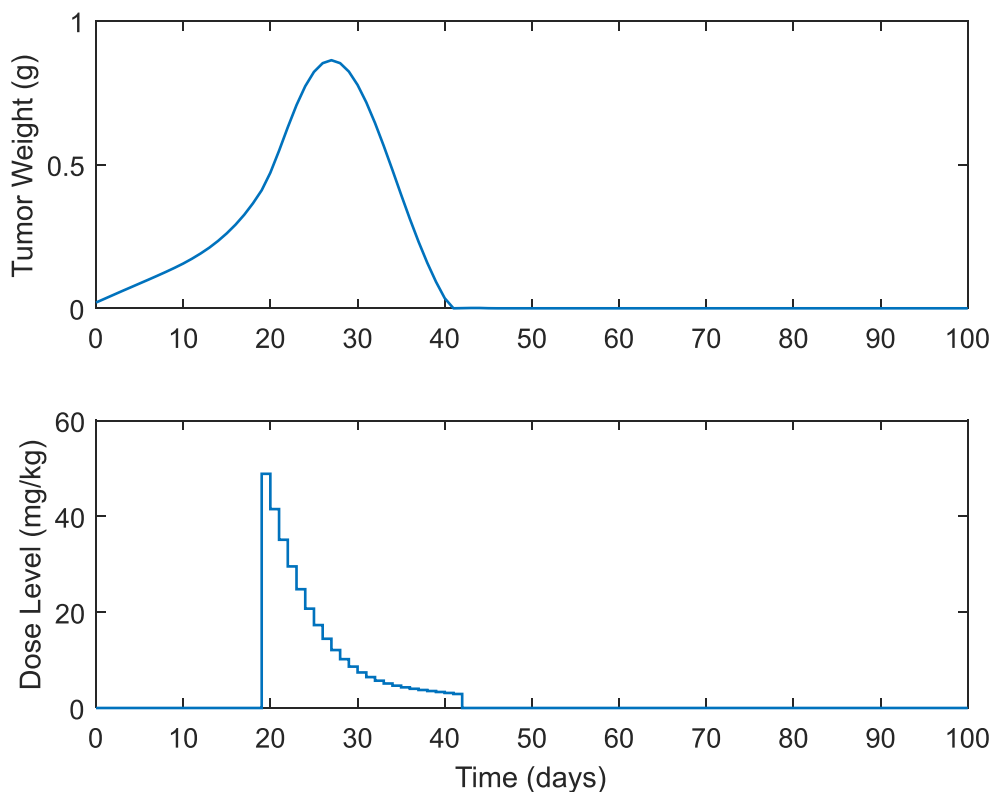


Figure 8.1. ARX system's response (i.e., tumor weight) and optimal control input (i.e., dose level) utilizing the initial "good" Q and R weights. Continuous treatment (daily drug administration starting from day 19).

While the primary objective of the optimal control problem is to eradicate the tumor, it is particularly important this to be done with the minimum cost, i.e., minimal side effects. High dose levels may lead to acute toxicity on healthy cells and severe side effects. To avoid such phenomena, it is necessary to impose "hard" constraints on the system's control variable u , i.e., the chemotherapy dosage. Therefore, when the dose level proposed by the LQR controller surpasses a predefined threshold, the control signal adheres to the following inequality:

$$u_{min} \leq u \leq u_{max}$$

where $u_{min} = 0$ and u_{max} represent the minimum and the maximum allowable dose levels, respectively. To balance toxicity and the chemo treatment efficacy, u_{max} was set at 5.4 mg for mice body weight of approximately 27 g, which translates to 200 mg/kg.

To employ LQR control, an optimal feedback gain must be computed. For this reason, MATLAB's *dlqr* function [238] was utilized. The *dlqr* function is used to design optimal state-feedback controllers for discrete-time linear systems. It calculates the optimal gain matrix by minimizing a quadratic cost function J representing the trade-off between control effort and system performance. The optimal feedback gain matrix K as derived by MATLAB, is shown below:

$$K_p = [-0.1394, -0.1165, -0.0956].$$

It also is important to note that in order to simulate more realistic clinical scenarios, control inputs were not initiated from day 0 but from day 19 of the experiments, in full accordance with the Simeoni *et al.*'s TGI SDRE optimal control cases, presented in Chapter 7. In addition, tumor weights below 10^{-3} g were considered negligible and thus set to zero in all simulations. This threshold was set because such small tumor masses are often undetectable and may have limited clinical relevance in terms of therapeutic intervention.

8.1 ARX and LQR-based gemcitabine dosage optimization for periodic treatment schedules

Several cases of different periodic treatment schedules were examined. Specifically, optimal doses of gemcitabine i.p. for five different treatment schedules were explored (as in Section 7.1.1). In the first case, i.e., Case 1, the controller calculated doses for continuous (i.e., every day) drug administration. For the rest of the cases, i.e., cases 2, 3, 4 and 5 the controller calculated optimal drug doses for periodic treatments (see Table 8.1). Gemcitabine was administered every 2, 3, 5 and 7 days for the Cases 2, 3, 4 and 5, respectively, until the tumor's eradication achievement. Importantly, longer intervals between treatments often allow tumor regrowth. For this reason, intervals longer than a week (7 days) have not been explored. The response of the state-space

Prediction of the cancer patients' response to their therapeutical treatment with non-linear forecasting techniques

Chapter 8: Linear quadratic control (LQC) applied for effective tumor growth eradication

system (i.e., the tumor growth in g) along with the optimal control input (i.e., the gemcitabine dose levels in mg/kg) for each case are shown in Figure 8.2 - Figure 8.6.

To understand better the proposed optimal treatment schedules and to evaluate their effectiveness in controlling tumor growth some descriptive statistics were also calculated and are presented in Table 8.1. u_{total} denotes the cumulative drug intake (i.e., the total dose administered) while y_{max} represents the maximum tumor weight observed during the simulation period. Both metrics were calculated based on (7.8) and (7.9). In addition, y_{zero} represents the time duration, in days, required for tumor eradication, indicating the efficacy of the treatment in eliminating the tumor.

In all cases, the chemotherapy treatment is started on day 19 with dose administrations ranging from 130 to 140 mg/kg. Then, the estimated dose levels are gradually decreased until the tumor is completely eradicated— as late as day 300+ in Case 5. In Case 4, shown in Figure 8.5, there is noticeable fluctuation in the suggested doses, starting high, below the predefined upper limit of 200 mg/kg, and then fluctuating until the tumor is eradicated. In contrast, Case 5, shown in Figure 8.6, starts with a high dosage that steadily decreases until the tumor is completely eradicated.

In addition, as the intervals between doses increase, both the cumulative amount of drug required to suppress tumor growth, u_{total} , and the duration of treatment, y_{zero} , increase. These increases are particularly pronounced when the intervals exceed 3 days, as observed in cases 4 and 5. It is also worth mentioning that in none of the cases did the weight of the tumor exceed 0.75 g.

Table 8.1. Periodic LQR treatment results (dose schedules and metrics) across Cases 1 to 5.

Cases	Dose schedule	u_{total} (mg/kg)	y_{max} (g)	y_{zero} (days)
Case 1	continuous	241.93	0.7325	33
Case 2	every 2 days	230.96	0.7428	35
Case 3	every 3 days	227.59	0.7522	37
Case 4	every 5 days	437.21	0.7591	148
Case 5	every 7 days	1296.45	0.7523	>300

Prediction of the cancer patients' response to their therapeutical treatment with non-linear forecasting techniques

Chapter 8: Linear quadratic control (LQC) applied for effective tumor growth eradication

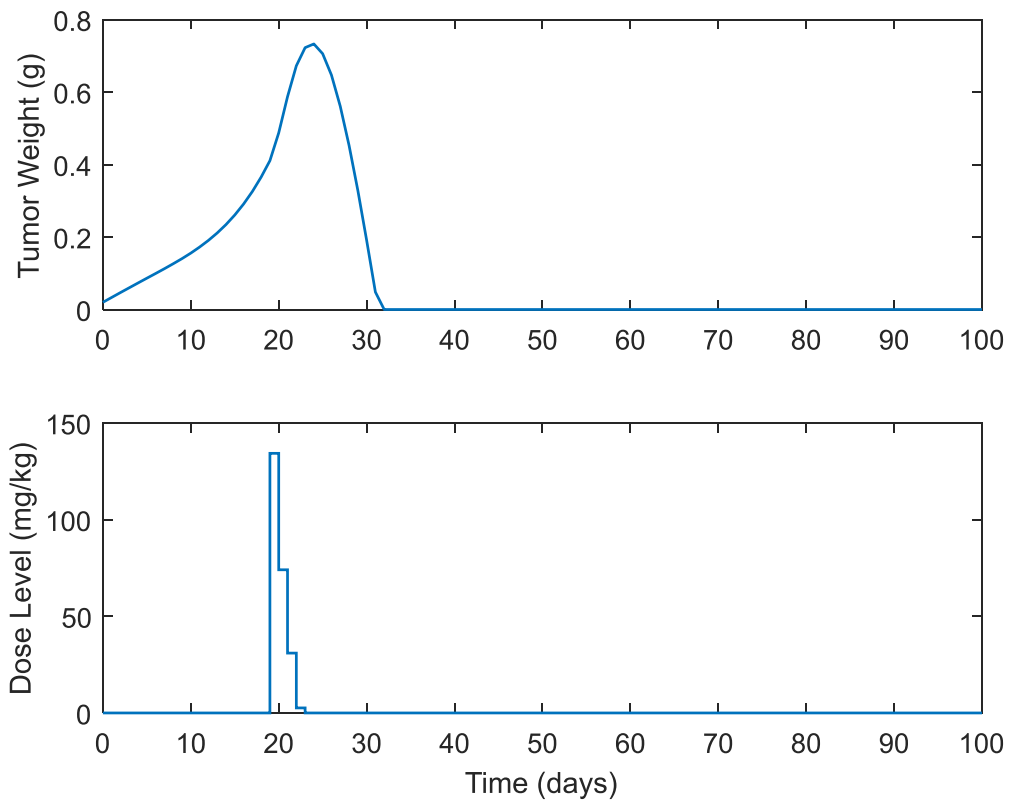


Figure 8.2. ARX system's response (i.e., tumor weight) and optimal control input (i.e., dose level). Continuous treatment: daily dose administration (Case 1).

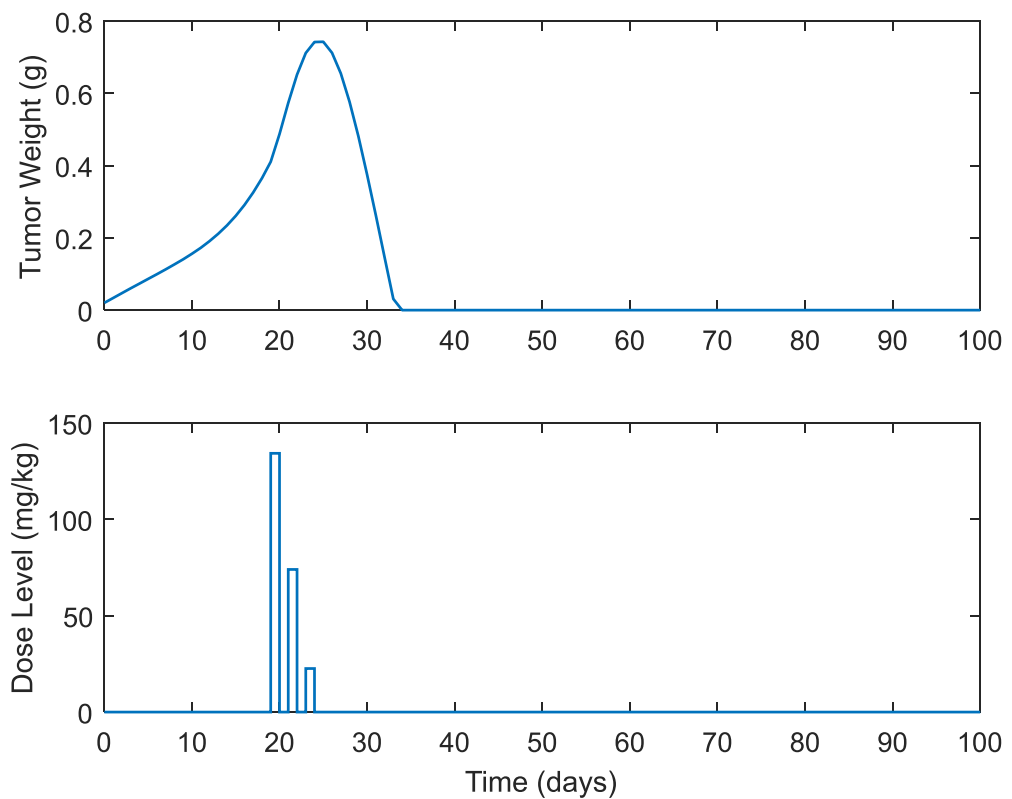


Figure 8.3. ARX's response (i.e., tumor weight) and optimal control input (i.e., dose level). Periodic treatment: dose administration every 2 days (Case 2).

Prediction of the cancer patients' response to their therapeutical treatment with non-linear forecasting techniques

Chapter 8: Linear quadratic control (LQC) applied for effective tumor growth eradication

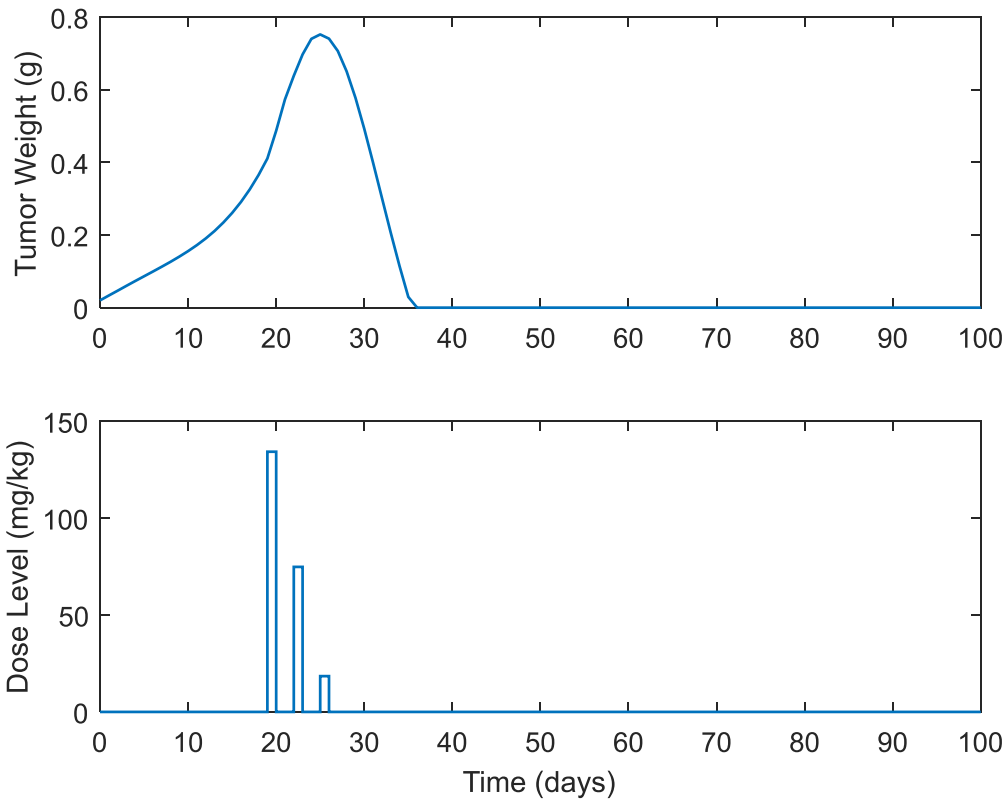


Figure 8.4. ARX's response (i.e., tumor weight) and optimal control input (i.e., dose level). Periodic treatment: dose administration every 3 days (Case 3).

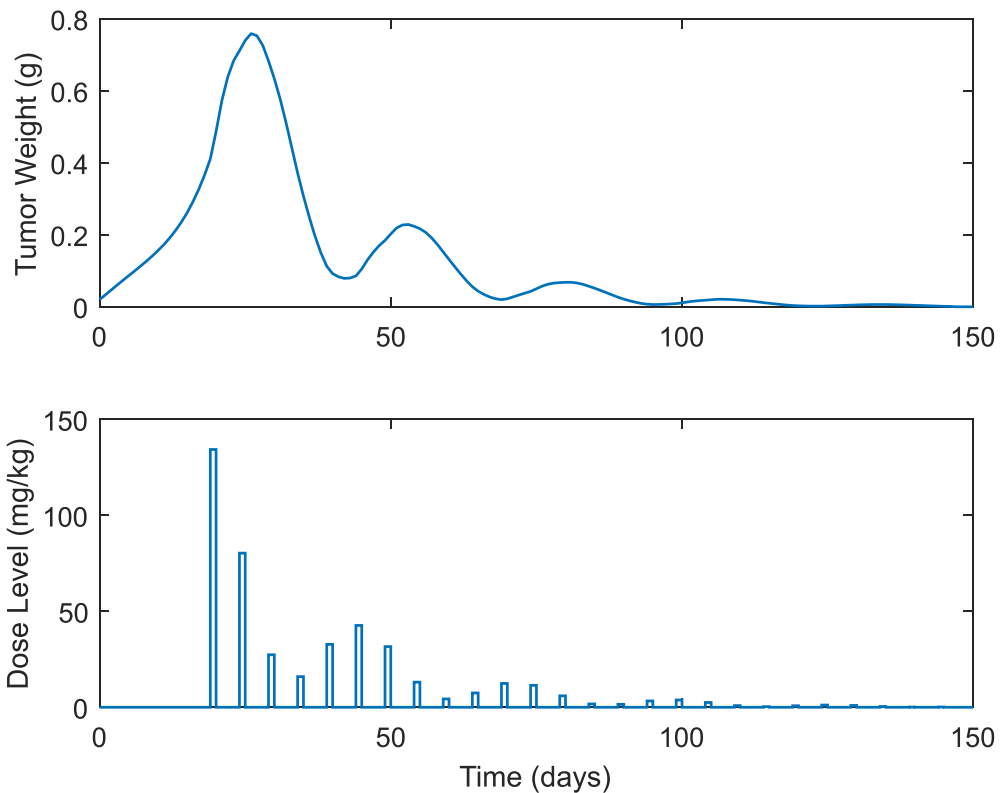


Figure 8.5. ARX's response (i.e., tumor weight) and optimal control input (i.e., dose level). Periodic treatment: dose administration every 5 days (Case 4).

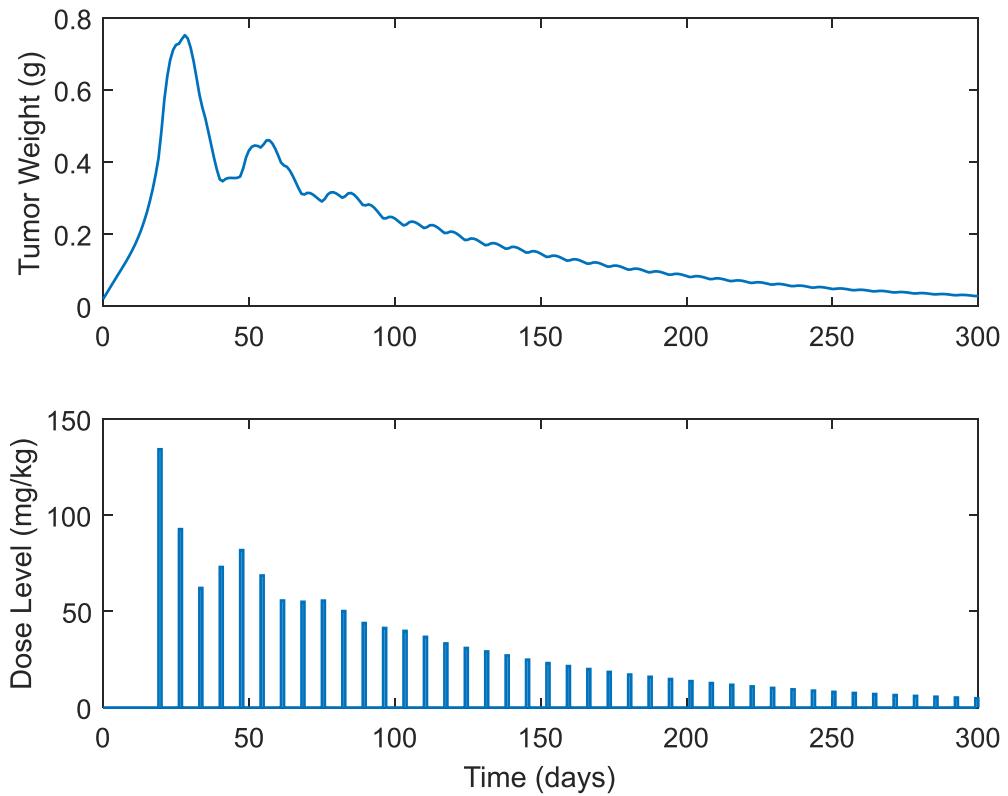


Figure 8.6. ARX's response (i.e., tumor weight) and optimal control input (i.e., dose level). Periodic treatment: dose administration every 7 days (Case 5).

8.2 Optimal gemcitabine dosages for intermittent treatment schedules using ARX and LQR

Whereas in the abovementioned scenarios the tumor was successfully eliminated, chemotherapy resistant scenarios might occur due to the long exposure to the drug. Cancer chemotherapy resistance is a phenomenon where the neoplastic cells develop the ability to evade the effects of the chemotherapeutic treatment, leading to failure in drug response [239], [240]. To this direction, optimal drug dosages for intermittent chemotherapy schedules were also explored.

To be more precise, optimal dosages for two cases of different intermittent treatment schedules were investigated. In both cases chemotherapy was administered every 3 days for five times, i.e., q3dx5. Then, to avoid toxicity and drug resistance, the treatment paused for a period of $tr_p = 7$ (Case 6) and 10 days (Case 7), respectively. Finally, it is restarted with dose administrations every 5 days for five times, i.e., q5dx5.

The nature of intermittent dosing introduced new dynamics and responses into the system, requiring an adjustment in the control strategy. To address the changes in state

Prediction of the cancer patients' response to their therapeutical treatment with non-linear forecasting techniques

Chapter 8: Linear quadratic control (LQC) applied for effective tumor growth eradication

regulation and control effort priorities under this new paradigm, modifications to the Q and R weighting matrices were deemed essential. Periodic and intermittent dosing represent different operational scenarios, each with unique challenges and objectives. While periodic dosing emphasizes regularity and consistent response, intermittent dosing may prioritize minimizing cumulative effects or addressing the unique pharmacodynamics of spaced administrations. As a result, the optimization criteria captured by the Q_P and R_P matrices have been adapted to ensure that the control strategy aligns with the specific requirements and desired outcomes of intermittent dosing. The weighting matrices Q and R were chosen to be $\text{diag}\{48\ 48\ 48\} \cdot 10^{-4}$ and 3430, respectively:

$$Q_I = \begin{bmatrix} 48 & 0 & 0 \\ 0 & 48 & 0 \\ 0 & 0 & 48 \end{bmatrix} \cdot 10^{-4}$$

and

$$R_I = 3430$$

while the optimal feedback gain matrix K as derived by MATLAB, is shown below:

$$K_I = [-0.1190, -0.1005, -0.0835].$$

A summary of the results is presented in Table 8.2 below, while the tumor weight curves and the optimal drug dosages are illustrated in Figure 8.7 and Figure 8.8.

In examining the results presented in Table 8.2, a striking observation is the efficacy of the intermittent LQR treatment schedules in both cases 6 and 7. Over approximately 120 days, tumor size was effectively minimized, demonstrating the potential of these treatment strategies.

The proposed drug doses in both cases start aggressively, with initial doses close to 100 mg/kg, and average 25.46 mg/kg in Case 6 and 38.82 mg/kg in Case 7. A comparison between the two cases reveals a direct correlation between the length of the chemotherapy holidays, denoted by tr_p , and the total amount of drug administered, u_{total} . Specifically, Case 7, which had longer chemotherapy holidays,

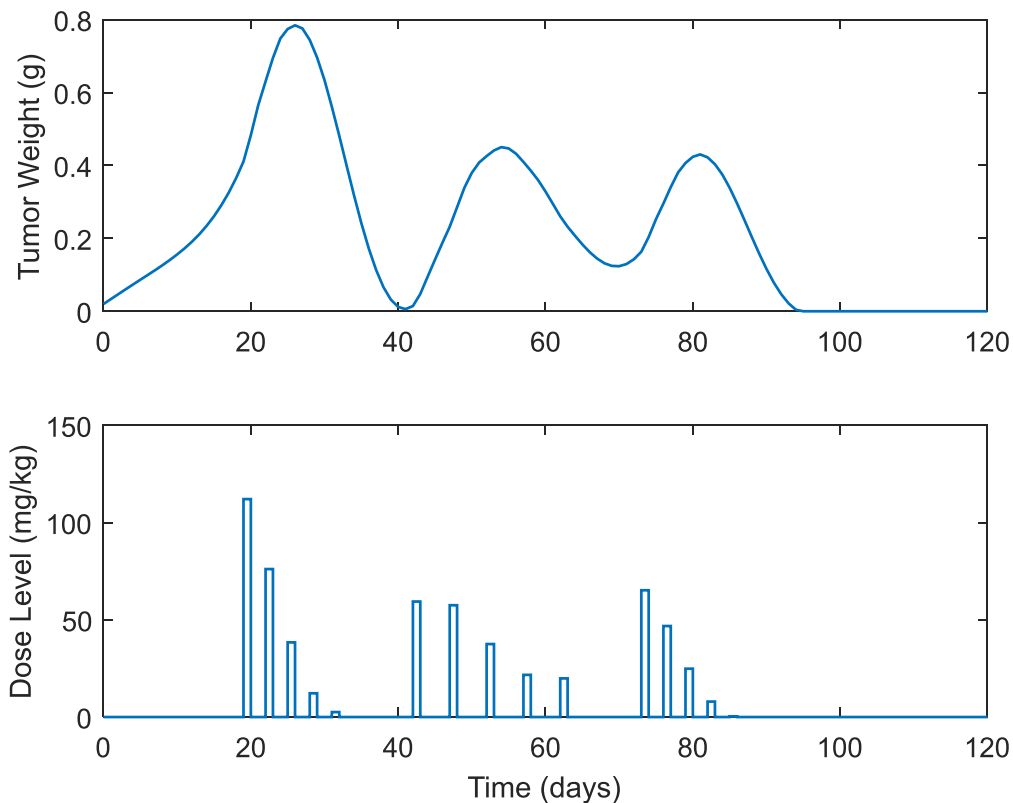


Figure 8.8. ARX's response (i.e., tumor weight) and optimal control input (i.e., dose level). Intermittent treatment: q3dx5, q5dx5 dose administrations with 10 days pauses (Case 7).

8.3 Multi-agent chemotherapy optimal control of tumor growth: The case of CPT-11 administered in combination with drug C2

The administration of chemotherapy often involves the complex decision-making process of selecting the most effective drug regimen for a given patient. In many cases, oncologists opt for a combination chemotherapy approach, in which multiple drugs are administered. This combination strategy is favored for several reasons. Firstly, each drug in the combination can target a different pathway or mechanism of the tumor, increasing the chances of successfully hindering its growth or killing it altogether. This multi-faceted attack can also reduce the chances of the tumor developing resistance to a single agent. In addition, by using drugs with non-overlapping side effects, the therapeutic window can potentially be broadened to maximize the anticancer effects while minimizing the damage to healthy cells.

Combination chemotherapy is common in clinical practice, especially when dealing with aggressive or advanced-stage cancers. However, a significant challenge lies in determining the optimal dosing for each drug in the combination to achieve the desired therapeutic effect without exacerbating toxicity. This is where control strategies, such

Prediction of the cancer patients' response to their therapeutical treatment with non-linear forecasting techniques

Chapter 8: Linear quadratic control (LQC) applied for effective tumor growth eradication

as the LQR, can have an impact. By using LQR, feedback controls can be derived ensuring that the system, in this case, the tumor's response to drugs, stays as close as possible to a desired state, while penalizing excessive drug use.

In this context, multi-input ARX models become particularly relevant. As described and identified in Chapter 5, these models can capture the complex dynamics between multiple chemotherapy drugs and their combined effects on tumor growth. By transforming these models into a state-space form suitable for LQR, we can extract optimal drug doses for each agent. This provides a robust and systematic way to improve the effectiveness of combination chemotherapy regimens and individualize treatment based on the patient's unique response dynamics.

As with the single-drug case involving gemcitabine, it is essential to convert the multi-input ARX models into a state-space representation in order to utilize the LQR method. Here, the case of CPT-11 with drug C2, which is modeled using an ARX (4,4) is explored. The transfer function H_m for the ARX system described by (5.3) (5.2) can be derived by applying inverse Z-transformation, which is described in detail as follows:

$$H_m(z) = H_1(z) + H_2(z)$$

$$H_1(z) = \frac{W_m(z)}{U_1(z)} = \frac{b_{1,1}z^{-1} + b_{1,2}z^{-2} + b_{1,3}z^{-3} + b_{1,4}z^{-4}}{1 - a_{m1}z^{-1} - a_{m2}z^{-2} - a_{m3}z^{-3} - a_{m4}z^{-4}} \quad (8.8)$$

$$H_2(z) = \frac{W_m(z)}{U_2(z)} = \frac{b_{2,1}z^{-1} + b_{2,2}z^{-2} + b_{2,3}z^{-3} + b_{2,4}z^{-4}}{1 - a_{m1}z^{-1} - a_{m2}z^{-2} - a_{m3}z^{-3} - a_{m4}z^{-4}}$$

For the given transfer function, multiple state-space representations are possible [241]. The state-space representation of (8.8) in observable canonical form ensures that the observability can be portrayed by the following equations:

$$x_m[k + 1] = A_m x_m[k] + B_m u_m[k]$$

$$y_m[k] = C_m x_m[k] + D_m u_m[k] \quad (8.9)$$

where

$$A_m = \begin{bmatrix} A_{m1} & 0 \\ 0 & A_{m2} \end{bmatrix}, \quad B_m = \begin{bmatrix} B_{m1} & 0 \\ 0 & B_{m2} \end{bmatrix}, \quad C_m = [1 \quad 0 \quad 0 \quad 0], \quad D_m = 0$$

Prediction of the cancer patients' response to their therapeutical treatment with non-linear forecasting techniques

Chapter 8: Linear quadratic control (LQC) applied for effective tumor growth eradication

with

$$A_{m1} = A_{m2} = \begin{bmatrix} -a_{m1} & 1 & 0 & 0 \\ -a_{m2} & 0 & 1 & 0 \\ -a_{m3} & 0 & 0 & 1 \\ -a_{m4} & 0 & 0 & 0 \end{bmatrix}, B_{m1} = \begin{bmatrix} b_{1,1} \\ b_{1,2} \\ b_{1,3} \\ b_{1,4} \end{bmatrix} \text{ and } B_{m2} = \begin{bmatrix} b_{2,1} \\ b_{2,2} \\ b_{2,3} \\ b_{2,4} \end{bmatrix}$$

and

$$x_m[k] = [x_{m1} \quad x_{m2} \quad \dots \quad x_{m8}]^T$$

$$u_m[k] = [u_1 \quad u_2].$$

with

$$\begin{bmatrix} a_{m1} \\ a_{m2} \\ a_{m3} \\ a_{m4} \end{bmatrix} = \begin{bmatrix} -1.6640 \\ 0.2182 \\ 0.1082 \\ 0.3594 \end{bmatrix}, \begin{bmatrix} b_{1,1} \\ b_{1,2} \\ b_{1,3} \\ b_{1,4} \end{bmatrix} = \begin{bmatrix} -9.1822 \\ 10.8916 \\ -9.9531 \\ 5.0423 \end{bmatrix} \text{ and } b_{2,j} \begin{bmatrix} b_{2,1} \\ b_{2,2} \\ b_{2,3} \\ b_{2,4} \end{bmatrix} = \begin{bmatrix} -20.1489 \\ 1.9032 \\ 1.9030 \\ 24.1672 \end{bmatrix}, \text{ as calculated in}$$

Chapter 5.

Chapter 9: Discussion and conclusions

Cancer, with its multifaceted nature, has always posed a challenge to the understanding of its complex dynamics and, consequently, to its treatment. While medicine has been the primary focus in the fight against this disease, the importance of a multidisciplinary approach cannot be overemphasized. Mathematical tumor modeling emerges as a powerful tool in this context, providing insights into the puzzling behavior of tumors and guiding the optimization of therapeutic interventions.

Within this study, three major topics are studied. The first and foremost is the description of the dynamics of tumor growth. To achieve this, both linear and non-linear mathematical models were employed. Specifically, three distinct model types were explored, identified, and used to describe the tumor growth inhibition. Two when a single drug is administered and one when combination treatments with two or more anticancer drugs are applied. Specifically, these models were identified, and their parameters were estimated for the cases of intraperitoneously administration of gemcitabine to xenografted mice [220], of CPT-11 given in combination with drug C2 and of 5-FU also administered to mice in combination with the drug C2 [93].

The TGI mathematical model, introduced by Simeoni *et al.* in 2004 [226], is the first model used in this study to describe tumor dynamics. It is a well-established, non-linear input-output PK-PD mathematical model that accurately describes tumor dynamics under the effects of single-agent chemotherapy. This model is based on ODEs with parameters that capture the pharmacodynamics of the tumor. The model parameters were estimated using data from xenografted mice, demonstrating a strong fit to the experimental data (MAPE < 10%). This confirms both the effectiveness of the proposed parameter estimation method and the algorithm used (NNA) and the ability of the model to capture tumor dynamics.

In the field of tumor growth modeling, the challenge often lies in striking the right balance: capturing the essential dynamics without introducing undue complexity. In contrast to complex non-linear systems such as TGI models, ARX models offer a compelling solution to this challenge. Their primary advantage stems from their dependency on prior observations (e.g., tumor weight) and input terms (e.g., drug

doses) to predict tumor growth. In scenarios where the available data are limited and deep insights into pharmacokinetics and pharmacodynamics are lacking, ARX models provide a robust framework. They simplify the analysis by focusing on observable growth patterns instead of getting deep into intricate physiological interactions. For this reason, linear mathematical models of cancer growth under single and multi-drug administrations were developed, fitted to the experimental tumor growth curves, and assessed. Three novel *ARX TGI* models – each tailored to the single and multi-drug scenarios mentioned above – are presented. The results showed an excellent agreement to the tumor weight data, with MAPE less than 3% for gemcitabine and 12% in the case of CPT-11 administered in combination with drug C2.

The third category of models pertains to the ANFIS approach. The ANFIS combines the benefits of fuzzy logic systems with the learning capability of neural networks. This integration allows for the modeling of complex, non-linear systems in a way that's both intuitive and adaptive. The introduction, for the first time in this study, of ANFIS models in the context of tumor growth provides a more flexible alternative to traditional modeling methods, enabling the inclusion of nuanced interactions and subtle variations observed in experimental data. Specifically, three novel *ANFIS TGI* models were developed to address both single and multi-agent chemotherapy scenarios. Each of these models was trained using the same experimental tumor growth datasets as were used for the *ARX TGI* models. Again, the models indicate a promising potential in describing tumor growth trajectories, especially when faced with the complexities and variations associated with multiple chemotherapy regimens.

It's worth pointing out that the *ANFIS TGI* models demonstrated greater robustness when it came to accounting for the complexities and variability inherent in multi-agent tumor growth. These models effectively leveraged fuzzy logic principles to address uncertainties and nonlinearities within the data, thereby offering a more reliable prediction tool for clinical applications. The clear performance advantage demonstrated by the ANFIS models suggests that they might be useful for deployment in clinical environments where multi-agent tumor growth predictions are required. However, this conclusion should be contextualized within the limitations of the current study and additional testing should be carried out.

Prediction of the cancer patients' response to their therapeutical treatment with non-linear forecasting techniques

Chapter 9: Discussion and conclusions

The second area of focus is centered on prediction. The prediction ability of each model type (namely Simeoni *et al.*'s TGI, ANFIS TGI and ARX TGI models) for single and multi-agent chemotherapy treatment schedules was explored, tested, and evaluated. By applying an adaptive prediction procedure, the models were tested on forecasting tumor growth under treatment over five time periods (days). Each model demonstrated accuracy in predicting the future course of the tumor. Such a method holds significant promise as a tool to predict tumor growth trajectories, potentially aiding in the development of more personalized and efficacious chemotherapy regimens. By utilizing a moving window technique on the experimental data, short-term predictions of tumor growth for up to five days in advance were achieved. This important outcome arises because each model's parameters are continuously re-fitted to the actual tumor growth curves, updating whenever a new laboratory or clinical data becomes available. As anticipated, the accuracy of the prediction tends to diminish as the prediction horizon lengthens. Yet, even for prediction periods spanning to five days, the error margin remained low (below 11%), highlighting the robust predictive capabilities of these models and the adaptive methodology.

For the single drug case (i.e., gemcitabine i.p. administration) the ANFIS model outperformed both the Simeoni *et al.*'s TGI mathematical model and the ARX (3,3) TGI model, achieving 3.31% and 6.26% lower MAPE, respectively (as illustrated in the bar plot of Figure 9.1). A reduced prediction error, such as that of ANFIS, suggests that it is potentially more reliable in predictions. Finally, the TGI model, although it is not achieved the best results, it still performs better than the ARX model by approximately 2.95 percentage points. A similar trend is observed also in the multi-agent cases (see Figure 9.2). It is also important to note that when re-fitting the model using the moving window of the last l measurements instead of all the available data points, found to improve the prediction performance of the models in the single agent cases of gemcitabine as well as in the multi-agent cases (when using ARX models).

However, the complexity and the resource requirements of each model should also be considered when comparing the models. Even though the ARX models have the highest errors, they are linear models with a small number of parameters to estimate. As a

result, they are much simpler and faster to deploy, making them preferable in situations where rapid approximation is more valuable than precision.

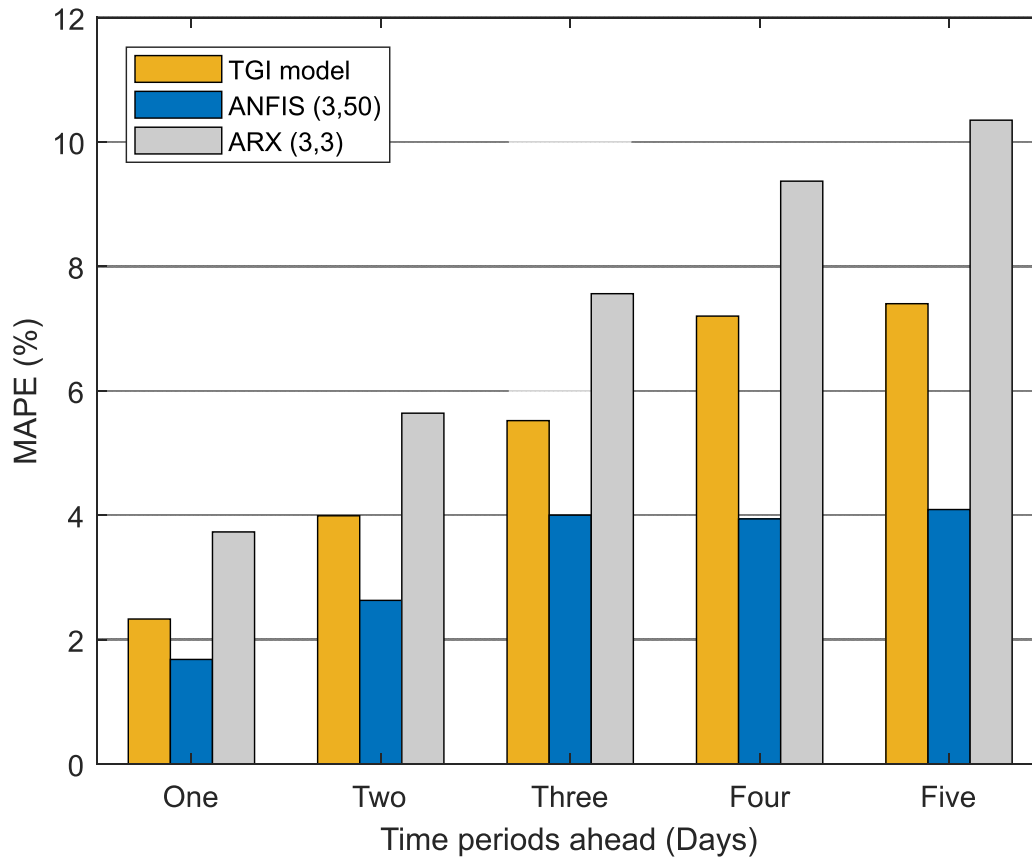


Figure 9.1. Prediction errors (MAPE %) for the time period ahead tumor growth inhibition predictions in mice given gemcitabine i.p.: A comparison of Simeoni et al.'s TGI, ANFIS (3,50) and ARX (3,3) TGI models. One, two, three, four and five time periods ahead.

To solidify these findings and expand the use of ANFIS and ARX models in clinical decision making, further research and validation using larger and more diverse datasets is imperative. By incorporating a broader range of data, these studies can improve the reliability and generalizability of ARX models, ultimately enhancing their utility in informing clinical practice and treatment strategies. To further enhance the predictive capabilities of such models and optimize its forecasting accuracy, it is worthwhile to further explore and test models of a variety of orders and different window sizes. For example, by considering more complex ARX models and varying the size of the data window, better results may be derived, enabling improved prediction, and forecasting of tumor growth inhibition.

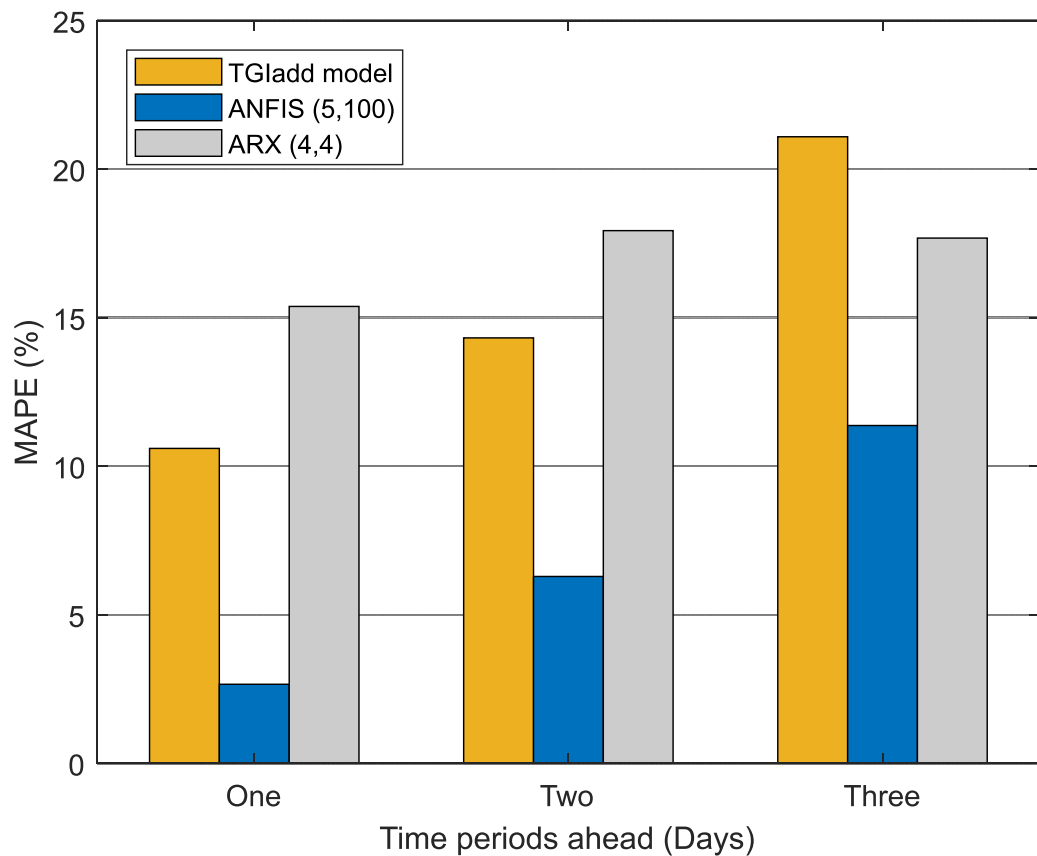


Figure 9.2. Prediction errors (MAPE %) for the time period ahead tumor growth inhibition predictions in mice given CPT-11 and drug C2: A comparison of TGladd, ANFIS (5,100) and ARX (4,4) TGI models. One, two and three time periods ahead.

Anti-cancer chemotherapy is an intensive systemic treatment. This means that chemotherapy drugs circulate through the patient's blood stream, potentially affecting not just the cancerous cells at the tumor site, but also healthy cells. Therefore, prolonged exposure, especially at high drug concentrations, can lead to acute toxicity and side effects. Applying mathematical modeling of tumor growth and optimal control theory might offer a solution to this challenge. This marks the third and concluding area of focus for this study.

Two well-established optimal control methods, SDRE and LQR, are utilized to determine optimal dose regimens that can minimize the tumor size. Optimal control-suggested drug dosages are presented and assessed. In the first approach, the non-linear nature of the Simeoni *et al.*'s TGI model makes the SDRE method particularly suitable. To apply the SDRE, the model had to be converted to a pseudo-linear form. However, before the model transformation to the pseudo-linear form its state vector was expanded (augmented) to include a one-compartment PK model, to accurately capture the PKs of

the administered drug dosages, forming an *augmented TGI* model. In the second approach, the LQR method is combined with the ARX model to determine optimal regimens. Here, it was essential to transform the ARX model into a state-space representation. In both cases, periodic and intermittent treatment schedules were extensively explored.

To mitigate excessive toxicity, hard bounds were set on drug dosages suggested by the controllers. In all examined scenarios, including continuous, periodic and intermittent drug administration with treatment “holidays”, the tumor size was reduced. Adopting such intermittent treatment schedules could serve as a potential alternative, aiming to decrease toxicity and enhance the patient's overall quality of life.

In the case of ARX and LQR the tumor weight was minimized. On the other hand, when utilizing the TGI model with the SDRE the tumor weight is reduced but it is not ground to zero. Instead, it is stabilized on a value around the tumor weight at the inoculation time. Moreover, the SDRE suggested optimal dose levels are higher than those calculated by the LQR. The difference of the methods as well as the simplification on modeling tumor growth dynamics with an ARX model maybe the cause of these differences on the results (i.e., the tumor weight eradication and the suggested optimal doses). Nevertheless, prolonged treatments with high dosage levels may result in severe side effects for the patient.

The presented methodologies can provide oncologists with computational tools to design optimal and patient-personalized chemotherapy schedules to confront cancer successfully, while improving the quality of life of the patients. Studies have shown that mCHT (i.e., the continuous or frequent administration of chemo drugs at low dosages) may be a promising strategy to control successfully tumor growth [245]–[247]. For this reason, scientists should focus on the identifying optimal metronomic schedules using not only optimal control but also artificial intelligence and machine learning algorithms [247].

Moreover, the importance of delving deeper into optimal treatment schedules extends beyond just chemotherapy. There is a growing interest in combination therapies, such as chemo-immunotherapy, which have shown effectiveness. Thus, continuous efforts to

Prediction of the cancer patients' response to their therapeutical treatment with non-linear forecasting techniques

Chapter 9: Discussion and conclusions

integrate mathematical modeling with advanced control strategies, including LQR and SDRE, are essential. This cross-disciplinary effort has the potential to enhance the efficacy of chemotherapy while reducing its systemic impact. In addition, the rise of artificial intelligence and machine learning techniques offers new avenues for optimizing mCHT schedules, personalized to each patient's unique profile, and should be a focal point of future investigations. Ultimately, as we advance in our understanding of the intricate dynamics of cancer and the potential of multi-drug regimens, comprehensive research efforts aimed at identifying optimal treatment strategies will remain critical in the ongoing battle against this complex disease.

In conclusion, more studies are needed towards this direction, but ultimately, the choice of the antitumor drug doses for each patient could be significantly and more efficiently improved by properly integrating similar mathematical/computational approaches such as these described herein in the clinical practice.

References

- [1] M. Knowles, P. Selby, M. Knowles, and P. Selby, "Introduction to the Cellular and Molecular Biology of Cancer," Fourth Edition, Fourth Edition., Oxford, New York: Oxford University Press, 2005, p. 61.
- [2] R. Sever and J. S. Brugge, "Signal transduction in cancer.," *Cold Spring Harb. Perspect. Med.*, vol. 5, no. 4, p. a006098, Apr. 2015, doi: 10.1101/cshperspect.a006098.
- [3] D. Hanahan and R. A. Weinberg, "The hallmarks of cancer: Perspectives for cancer medicine," in *Oxford Textbook of Oncology*, Oxford University Press, 2016, pp. 3–10. doi: 10.1093/med/9780199656103.003.0001.
- [4] M. L. Martins, S. C. Ferreira, and M. J. Vilela, "Multiscale models for the growth of avascular tumors," *Phys. Life Rev.*, vol. 4, no. 2, pp. 128–156, Jun. 2007, doi: 10.1016/j.plrev.2007.04.002.
- [5] Nature.com and Nature, "Cell Division and Cancer." Accessed: Mar. 20, 2023. [Online]. Available: <https://www.nature.com/scitable/topicpage/cell-division-and-cancer-14046590/>
- [6] B. S. C. and S. National Institutes of Health (US), *NIH Curriculum Supplement Series*. Bethesda (MD): National Institutes of Health (US), 2007. [Online]. Available: <https://www.ncbi.nlm.nih.gov/books/NBK20362/>
- [7] Mayo Clinic Staff, "Cancer." Accessed: Jan. 25, 2023. [Online]. Available: <https://www.mayoclinic.org/diseases-conditions/cancer/symptoms-causes/syc-20370588>
- [8] M. Jakóbiak, W. Lasek, and J. Gołąb, "Natural mechanisms protecting against cancer," *Immunol. Lett.*, vol. 90, no. 2, pp. 103–122, 2003, doi: <https://doi.org/10.1016/j.imlet.2003.08.005>.
- [9] L. Liverpool, "Antibodies," *New Scientist*. Accessed: Mar. 03, 2022. [Online]. Available: <https://www.newscientist.com/definition/antibodies/>
- [10] R. A. Weinberg, *The Biology of Cancer*, 2nd ed. Taylor & Francis Ltd., 2013. [Online]. Available: https://www.ebook.de/de/product/39326482/robert_a_weinberg_the_biology_of_cancer.html
- [11] N. S. W.) U. S.-S. I. W. on Mathematical Modeling of Tumor-Immune Dynamics (2013 Sydney, *Mathematical Models of Tumor-Immune System Dynamics*. Springer New York, 2014. doi: <https://doi.org/10.1007/978-1-4939-1793-8>.
- [12] P. Eissmann, "Natural Killer Cells." Accessed: Mar. 03, 2022. [Online]. Available: <https://www.immunology.org/public-information/bitesized-immunology/cells/natural-killer-cells>

Prediction of the cancer patients' response to their therapeutical treatment with non-linear forecasting techniques

References

- [13] E. Wissinger, "CD8+ T Cells." Accessed: Mar. 03, 2022. [Online]. Available: <https://www.immunology.org/public-information/bitesized-immunology/cells/cd8-t-cells>
- [14] J. Masrour-Roudsari and S. Ebrahimpour, "Casual role of infectious agents in cancer: An overview," *Casp. J. Intern. Med.*, vol. 8, no. 3, pp. 153–158, 2017, doi: 10.22088/cjim.8.3.153.
- [15] G. S. Goldberg and R. Airley, *Cancer Chemotherapy: Basic Science to the Clinic: Basic Science to the Clinic*, 2nd ed. Wiley-Blackwell, 2020. [Online]. Available: https://www.ebook.de/de/product/37930272/cancer_chemotherapy_basic_science_to_the_clinic.html
- [16] L. J. Kleinsmith, *Principles of cancer biology*. San Francisco: San Francisco, CA: Pearson Benjamin Cummings, 2006.
- [17] Mayo Clinic Staff, "Cancer surgery: Physically removing cancer." Accessed: Dec. 14, 2022. [Online]. Available: <https://www.mayoclinic.org/diseases-conditions/cancer/in-depth/cancer-surgery/art-20044171>
- [18] J. DePolo, "Understanding Your Pathology Report." Accessed: May 10, 2021. [Online]. Available: <https://www.breastcancer.org/pathology-report>
- [19] Cancer.Net, "What is Radiation Therapy?," Cancer.Net. Accessed: May 10, 2021. [Online]. Available: <https://www.cancer.net/navigating-cancer-care/how-cancer-treated/radiation-therapy/what-radiation-therapy>
- [20] V. T. DeVita and E. Chu, "A History of Cancer Chemotherapy," *Cancer Res.*, vol. 68, no. 21, pp. 8643–8653, Oct. 2008, doi: 10.1158/0008-5472.can-07-6611.
- [21] U.S. National Institutes of Health, National Cancer Institute, "SEER Training Modules, Types of Chemotherapy Drugs." Accessed: Feb. 18, 2022. [Online]. Available: <https://training.seer.cancer.gov/treatment/chemotherapy/types.html>
- [22] R. Vardanyan and V. Hruby, "Antineoplastic Agents," in *Synthesis of Best-Seller Drugs*, Elsevier, 2016, pp. 495–547. doi: 10.1016/b978-0-12-411492-0.00028-6.
- [23] Drugs.com, "Antimetabolites." Accessed: Feb. 18, 2022. [Online]. Available: <https://www.drugs.com/drug-class/antimetabolites.html>
- [24] G. J. Peters, "Novel Developments in the Use of Antimetabolites," *Nucleosides Nucleotides Nucleic Acids*, vol. 33, no. 4–6, pp. 358–374, Apr. 2014, doi: 10.1080/15257770.2014.894197.
- [25] L. Falzone, S. Salomone, and M. Libra, "Evolution of Cancer Pharmacological Treatments at the Turn of the Third Millennium," *Front. Pharmacol.*, vol. 9, 2018, doi: 10.3389/fphar.2018.01300.
- [26] Drugs.com, "Alkylating agents." [Online]. Available: <https://www.drugs.com/drug-class/alkylating-agents.html>

Prediction of the cancer patients' response to their therapeutical treatment with non-linear forecasting techniques

References

- [27] Y. Gao *et al.*, "Antibiotics for cancer treatment: A double-edged sword," *J. Cancer*, vol. 11, no. 17, pp. 5135–5149, 2020, doi: 10.7150/jca.47470.
- [28] K. Nurgali, R. T. Jagoe, and R. Abalo, "Editorial: Adverse Effects of Cancer Chemotherapy: Anything New to Improve Tolerance and Reduce Sequelae?," *Front. Pharmacol.*, vol. 9, Mar. 2018, doi: 10.3389/fphar.2018.00245.
- [29] Cancer.Net, "Side Effects of Chemotherapy." Accessed: Feb. 18, 2022. [Online]. Available: <https://www.cancer.net/navigating-cancer-care/how-cancer-treated/chemotherapy/side-effects-chemotherapy>
- [30] R. Maiti, "Metronomic chemotherapy," *J. Pharmacol. Pharmacother.*, vol. 5, no. 3, pp. 186–192, Jul. 2014, doi: 10.4103/0976-500x.136098.
- [31] C. Simsek, E. Esin, and S. Yalcin, "Metronomic Chemotherapy: A Systematic Review of the Literature and Clinical Experience," *J. Oncol.*, vol. 2019, pp. 1–31, Mar. 2019, doi: 10.1155/2019/5483791.
- [32] S. Krajnak *et al.*, "Explorative Analysis of Low-Dose Metronomic Chemotherapy with Cyclophosphamide and Methotrexate in a Cohort of Metastatic Breast Cancer Patients," *Breast Care*, vol. 13, no. 4, pp. 272–276, 2018, doi: 10.1159/000487629.
- [33] G. Bocci and R. S. Kerbel, "Pharmacokinetics of metronomic chemotherapy: a neglected but crucial aspect," *Nat. Rev. Clin. Oncol.*, vol. 13, no. 11, pp. 659–673, May 2016, doi: 10.1038/nrclinonc.2016.64.
- [34] R. S. Kerbel and B. A. Kamen, "The anti-angiogenic basis of metronomic chemotherapy," *Nat. Rev. Cancer*, vol. 4, no. 6, pp. 423–436, Jun. 2004, doi: 10.1038/nrc1369.
- [35] L. G. de Pillis, W. Gu, and A. E. Radunskaya, "Mixed immunotherapy and chemotherapy of tumors: modeling, applications and biological interpretations," *J. Theor. Biol.*, vol. 238, no. 4, pp. 841–862, Feb. 2006, doi: 10.1016/j.jtbi.2005.06.037.
- [36] S. A. Rosenberg, "IL-2: The First Effective Immunotherapy for Human Cancer," *J. Immunol.*, vol. 192, no. 12, pp. 5451–5458, Jun. 2014, doi: 10.4049/jimmunol.1490019.
- [37] T. Jiang, C. Zhou, and S. Ren, "Role of IL-2 in cancer immunotherapy," *Oncol Immunology*, vol. 5, no. 6, p. e1163462, Apr. 2016, doi: 10.1080/2162402x.2016.1163462.
- [38] Mayo Clinic Staff, "Monoclonal antibody drugs for cancer: How they work." Accessed: Feb. 19, 2022. [Online]. Available: <https://www.mayoclinic.org/diseases-conditions/cancer/in-depth/monoclonal-antibody/art-20047808>
- [39] D. Zahavi and L. Weiner, "Monoclonal Antibodies in Cancer Therapy," *Antibodies Basel*, vol. 9, no. 3, p. 34, Jul. 2020, doi: 10.3390/antib9030034.

Prediction of the cancer patients' response to their therapeutical treatment with non-linear forecasting techniques

References

- [40] M. Morotti *et al.*, "Promises and challenges of adoptive T-cell therapies for solid tumours," *Br. J. Cancer*, vol. 124, no. 11, pp. 1759–1776, Mar. 2021, doi: 10.1038/s41416-021-01353-6.
- [41] A. N. Miliotou and L. C. Papadopoulou, "CAR T-cell Therapy: A New Era in Cancer Immunotherapy," *Curr. Pharm. Biotechnol.*, vol. 19, no. 1, pp. 5–18, May 2018, doi: 10.2174/1389201019666180418095526.
- [42] Cancer Research, "CAR T-cell therapy." Accessed: Feb. 20, 2022. [Online]. Available: <https://www.cancerresearchuk.org/about-cancer/cancer-in-general/treatment/immunotherapy/types/CAR-T-cell-therapy>
- [43] K. J. Mahasa *et al.*, "A combination therapy of oncolytic viruses and chimeric antigen receptor T cells: a mathematical model proof-of-concept," *Math. Biosci. Eng.*, vol. 19, no. 5, pp. 4429–4457, 2022, doi: 10.3934/mbe.2022205.
- [44] L. Galluzzi *et al.*, "Classification of current anticancer immunotherapies," *Oncotarget*, vol. 5, no. 24, pp. 12472–12508, 2014, doi: <https://doi.org/10.18632/oncotarget.2998>.
- [45] S. Cara and I. F. Tannock, "Retreatment of patients with the same chemotherapy: Implications for clinical mechanisms of drug resistance," *Ann. Oncol.*, vol. 12, no. 1, pp. 23–27, Jan. 2001, doi: 10.1023/a:1008389706725.
- [46] I. F. Tannock, "Tumor Physiology and Drug Resistance," *Cancer Metastasis Rev.*, vol. 20, no. 1, pp. 123–132, Nov. 2001, doi: 10.1023/A:1013125027697.
- [47] A. Fjelstul, "Overcoming Resistance: A Review on Chemotherapy Resistance in Cancer," Department of Biomedical Sciences, Iowa State University, Ames, Iowa, USA, 2020. [Online]. Available: <https://dr.lib.iastate.edu/handle/20.500.12876/17059>
- [48] X. Wang, H. Zhang, and X. Chen, "Drug resistance and combating drug resistance in cancer," *Cancer Drug Resist.*, vol. 2, no. 2, pp. 141–160, Jun. 2019, doi: 10.20517/cdr.2019.10.
- [49] R. Bai *et al.*, "Mechanisms of Cancer Resistance to Immunotherapy," *Front. Oncol.*, vol. 10, p. 1290, Aug. 2020, doi: 10.3389/fonc.2020.01290.
- [50] M. Castells, B. Thibault, J.-P. Delord, and B. Couderc, "Implication of Tumor Microenvironment in Chemoresistance: Tumor-Associated Stromal Cells Protect Tumor Cells from Cell Death," *Int. J. Mol. Sci.*, vol. 13, no. 8, pp. 9545–9571, Jul. 2012, doi: 10.3390/ijms13089545.
- [51] D. B. Longley and P. G. Johnston, "Molecular mechanisms of drug resistance," *J. Pathol.*, vol. 205, no. 2, pp. 275–292, Jan. 2005, doi: <https://doi.org/10.1002/path.1706>.
- [52] K. J. Mahasa, R. Ouifki, A. Eladdadi, and L. de Pillis, "Mathematical model of tumor-immune surveillance," *J. Theor. Biol.*, vol. 404, pp. 312–330, Sep. 2016, doi: 10.1016/j.jtbi.2016.06.012.

Prediction of the cancer patients' response to their therapeutical treatment with non-linear forecasting techniques

References

- [53] D. A. Yardley, "Drug Resistance and the Role of Combination Chemotherapy in Improving Patient Outcomes," *Int. J. Breast Cancer*, vol. 2013, pp. 1–15, 2013, doi: 10.1155/2013/137414.
- [54] Q. Hu, W. Sun, C. Wang, and Z. Gu, "Recent advances of cocktail chemotherapy by combination drug delivery systems," *Adv. Drug Deliv. Rev.*, vol. 98, pp. 19–34, Feb. 2016, doi: <https://doi.org/10.1016/j.addr.2015.10.022>.
- [55] H. Funahashi *et al.*, "Successful combination chemotherapy with irinotecan hydrochloride and cisplatin for primary gastric small cell carcinoma: report of a case," *World J. Surg. Oncol.*, vol. 11, no. 1, p. 263, Oct. 2013, doi: 10.1186/1477-7819-11-263.
- [56] R. González-Pastor *et al.*, "Combination Chemotherapy with Cisplatin and Chloroquine: Effect of Encapsulation in Micelles Formed by Self-Assembling Hybrid Dendritic–Linear–Dendritic Block Copolymers," *Int. J. Mol. Sci.*, vol. 22, no. 10, p. 5223, May 2021, doi: 10.3390/ijms22105223.
- [57] Y. Xue *et al.*, "Combination chemotherapy with Zyflamend reduced the acquired resistance of bladder cancer cells to cisplatin through inhibiting NFκB signaling pathway," *OncoTargets Ther.*, vol. 11, pp. 4413–4429, Jul. 2018, doi: 10.2147/ott.s162255.
- [58] S. Yamada *et al.*, "Phase I/II study of adding intraperitoneal paclitaxel in patients with pancreatic cancer and peritoneal metastasis," *Br. J. Surg.*, vol. 107, no. 13, pp. 1811–1817, Jul. 2020, doi: <https://doi.org/10.1002/bjs.11792>.
- [59] D. Salas-Benito *et al.*, "Paradigms on Immunotherapy Combinations with Chemotherapy," *Cancer Discov.*, vol. 11, no. 6, pp. 1353–1367, Mar. 2021, doi: 10.1158/2159-8290.cd-20-1312.
- [60] S. Zhu *et al.*, "Combination strategies to maximize the benefits of cancer immunotherapy," *J. Hematol. Oncol.*, vol. 14, p. 156, Sep. 2021, doi: 10.1186/s13045-021-01164-5.
- [61] L. Galluzzi, A. Buqué, O. Kepp, L. Zitvogel, and G. Kroemer, "Immunological Effects of Conventional Chemotherapy and Targeted Anticancer Agents," *Cancer Cell*, vol. 28, no. 6, pp. 690–714, Dec. 2015, doi: 10.1016/j.ccell.2015.10.012.
- [62] H. West *et al.*, "Atezolizumab in combination with carboplatin plus nab-paclitaxel chemotherapy compared with chemotherapy alone as first-line treatment for metastatic non-squamous non-small-cell lung cancer (IMpower130): a multicentre, randomised, open-label, phase 3 trial," *Lancet Oncol.*, vol. 20, no. 7, pp. 924–937, Jul. 2019, doi: 10.1016/s1470-2045(19)30167-6.
- [63] P. Schmid *et al.*, "Atezolizumab and Nab-Paclitaxel in Advanced Triple-Negative Breast Cancer," *N. Engl. J. Med.*, vol. 379, no. 22, pp. 2108–2121, Nov. 2018, doi: 10.1056/nejmoa1809615.
- [64] L. Paz-Ares *et al.*, "Durvalumab plus platinum–etoposide versus platinum–etoposide in first-line treatment of extensive-stage small-cell lung cancer (CASPIAN): a randomised, controlled, open-label, phase 3 trial," *The Lancet*, vol.

Prediction of the cancer patients' response to their therapeutical treatment with non-linear forecasting techniques

References

- 394, no. 10212, pp. 1929–1939, Nov. 2019, doi: 10.1016/s0140-6736(19)32222-6.
- [65] T. Powles *et al.*, “Avelumab Maintenance Therapy for Advanced or Metastatic Urothelial Carcinoma,” *N. Engl. J. Med.*, vol. 383, no. 13, pp. 1218–1230, 2020, doi: 10.1056/NEJMoa2002788.
- [66] P. Bonate, “Modeling Tumor Growth in Oncology,” in *Pharmacokinetics in Drug Development*, vol. 3, Springer US, 2011, pp. 1–19. doi: 10.1007/978-1-4419-7937-7_1.
- [67] A. Rivaz, M. Azizian, and M. Soltani, “Various Mathematical Models of Tumor Growth with Reference to Cancer Stem Cells: A Review,” *Iran. J. Sci. Technol. Trans. Sci.*, vol. 43, no. 2, pp. 687–700, Apr. 2019, doi: 10.1007/s40995-019-00681-w.
- [68] M. Simeoni, G. De Nicolao, P. Magni, M. Rocchetti, and I. Poggesi, “Modeling of human tumor xenografts and dose rationale in oncology,” *Drug Discov. Today Technol.*, vol. 10, no. 3, pp. e365-372, Sep. 2013, doi: 10.1016/j.ddtec.2012.07.004.
- [69] A. R. A. Anderson and V. Quaranta, “Integrative mathematical oncology,” *Nat. Rev. Cancer*, vol. 8, no. 3, pp. 227–234, Mar. 2008, doi: 10.1038/nrc2329.
- [70] B. Ribba *et al.*, “A review of mixed-effects models of tumor growth and effects of anticancer drug treatment used in population analysis,” *CPT Pharmacomet. Syst. Pharmacol.*, vol. 3, no. 5, p. e113, Dec. 2014, doi: 10.1038/psp.2014.12.
- [71] A. Yin, D. J. A. R. Moes, J. G. C. van Hasselt, J. J. Swen, and H. Guchelaar, “A Review of Mathematical Models for Tumor Dynamics and Treatment Resistance Evolution of Solid Tumors,” *CPT Pharmacomet. Syst. Pharmacol.*, vol. 8, no. 10, pp. 720–737, Oct. 2019, doi: 10.1002/psp4.12450.
- [72] H. Enderling and M. A. J. Chaplain, “Mathematical modeling of tumor growth and treatment,” *Curr. Pharm. Des.*, vol. 20, no. 30, pp. 4934–4940, 2014, doi: 10.2174/1381612819666131125150434.
- [73] R. Everett *et al.*, “A tutorial review of mathematical techniques for quantifying tumor heterogeneity,” *Math. Biosci. Eng. MBE*, vol. 17, no. 4, pp. 3660–3709, Dec. 2020, doi: 10.3934/mbe.2020207.
- [74] L. A. Harris, S. Beik, P. M. M. Ozawa, L. Jimenez, and A. M. Weaver, “Modeling heterogeneous tumor growth dynamics and cell-cell interactions at single-cell and cell-population resolution,” *Curr. Opin. Syst. Biol.*, vol. 17, pp. 24–34, Oct. 2019, doi: 10.1016/j.coisb.2019.09.005.
- [75] M. Tong *et al.*, “New insights from the widening homogeneity perspective to target intratumor heterogeneity,” *Cancer Commun.*, vol. 38, p. 17, May 2018, doi: 10.1186/s40880-018-0287-y.
- [76] S. Friberg and S. Mattson, “On the growth rates of human malignant tumors: implications for medical decision making,” *J. Surg. Oncol.*, vol. 65, no. 4, pp. 284–

Prediction of the cancer patients' response to their therapeutical treatment with non-linear forecasting techniques

References

- 297, Aug. 1997, doi: 10.1002/(sici)1096-9098(199708)65:4<284::aid-jso11>3.0.co;2-2.
- [77] P. Skehan, "On the normality of growth dynamics of neoplasms in vivo: a data base analysis," *Growth*, vol. 50, no. 4, pp. 496–515, 1986.
- [78] A. K. Laird, "Dynamics of Tumour Growth," *Br. J. Cancer*, vol. 18, no. 3, pp. 490–502, Sep. 1964, doi: 10.1038/bjc.1964.55.
- [79] T. B. L. Kirkwood, "Deciphering death: a commentary on Gompertz (1825) 'On the nature of the function expressive of the law of human mortality, and on a new mode of determining the value of life contingencies,'" *Philos. Trans. R. Soc. Lond. B. Biol. Sci.*, vol. 370, no. 1666, p. 20140379, Apr. 2015, doi: 10.1098/rstb.2014.0379.
- [80] L. Norton, R. Simon, H. D. Brereton, and A. E. Bogden, "Predicting the course of Gompertzian growth," *Nature*, vol. 264, no. 5586, pp. 542–545, Dec. 1976, doi: 10.1038/264542a0.
- [81] L. Norton and R. Simon, "Growth curve of an experimental solid tumor following radiotherapy," *J. Natl. Cancer Inst.*, vol. 58, no. 6, pp. 1735–1741, Jun. 1977, doi: 10.1093/jnci/58.6.1735.
- [82] R. Simon and L. Norton, "The Norton–Simon hypothesis: designing more effective and less toxic chemotherapeutic regimens," *Nat. Clin. Pract. Oncol.*, vol. 3, no. 8, pp. 406–407, Aug. 2006, doi: 10.1038/ncponc0560.
- [83] Y. Wang *et al.*, "Elucidation of relationship between tumor size and survival in non-small-cell lung cancer patients can aid early decision making in clinical drug development," *Clin. Pharmacol. Ther.*, vol. 86, no. 2, pp. 167–174, Aug. 2009, doi: 10.1038/clpt.2009.64.
- [84] K. Park, "A Review of Modeling Approaches to Predict Drug Response in Clinical Oncology," *Yonsei Med. J.*, vol. 58, no. 1, p. 1, Jan. 2017, doi: 10.3349/ymj.2017.58.1.1.
- [85] A. Ouerdani, S. Goutagny, M. Kalamarides, I. F. Trocóniz, and B. Ribba, "Mechanism-based modeling of the clinical effects of bevacizumab and everolimus on vestibular schwannomas of patients with neurofibromatosis type 2," *Cancer Chemother. Pharmacol.*, vol. 77, no. 6, pp. 1263–1273, Jun. 2016, doi: 10.1007/s00280-016-3046-2.
- [86] L.-S. Tham *et al.*, "A pharmacodynamic model for the time course of tumor shrinkage by gemcitabine + carboplatin in non-small cell lung cancer patients," *Clin. Cancer Res. Off. J. Am. Assoc. Cancer Res.*, vol. 14, no. 13, pp. 4213–4218, Jul. 2008, doi: 10.1158/1078-0432.CCR-07-4754.
- [87] L. Claret *et al.*, "Model-based prediction of phase III overall survival in colorectal cancer on the basis of phase II tumor dynamics," *J. Clin. Oncol. Off. J. Am. Soc. Clin. Oncol.*, vol. 27, no. 25, pp. 4103–4108, Sep. 2009, doi: 10.1200/JCO.2008.21.0807.

Prediction of the cancer patients' response to their therapeutical treatment with non-linear forecasting techniques

References

- [88] E. Mandonnet *et al.*, "Continuous growth of mean tumor diameter in a subset of grade II gliomas," *Ann. Neurol.*, vol. 53, no. 4, pp. 524–528, Apr. 2003, doi: 10.1002/ana.10528.
- [89] E. K. Hansson *et al.*, "PKPD Modeling of VEGF, sVEGFR-2, sVEGFR-3, and sKIT as Predictors of Tumor Dynamics and Overall Survival Following Sunitinib Treatment in GIST," *CPT Pharmacomet. Syst. Pharmacol.*, vol. 2, no. 11, p. e84, Nov. 2013, doi: 10.1038/psp.2013.61.
- [90] M. Kim, R. J. Gillies, and K. A. Rejniak, "Current Advances in Mathematical Modeling of Anti-Cancer Drug Penetration into Tumor Tissues," *Front. Oncol.*, vol. 3, p. 278, Nov. 2013, doi: 10.3389/fonc.2013.00278.
- [91] G. Mo, F. Gibbons, P. Schroeder, and W. Krzyzanski, "Lifespan Based Pharmacokinetic-Pharmacodynamic Model of Tumor Growth Inhibition by Anticancer Therapeutics," *PLOS ONE*, vol. 9, no. 10, p. e109747, 2014, doi: 10.1371/journal.pone.0109747.
- [92] G. Koch, A. Walz, G. Lahu, and J. Schropp, "Modeling of tumor growth and anticancer effects of combination therapy," *J. Pharmacokinet. Pharmacodyn.*, vol. 36, no. 2, pp. 179–197, Apr. 2009, doi: 10.1007/s10928-009-9117-9.
- [93] M. Rocchetti *et al.*, "Testing additivity of anticancer agents in pre-clinical studies: a PK/PD modelling approach," *Eur. J. Cancer Oxf. Engl. 1990*, vol. 45, no. 18, pp. 3336–3346, Dec. 2009, doi: 10.1016/j.ejca.2009.09.025.
- [94] N. Terranova, M. Germani, F. Del Bene, and P. Magni, "A predictive pharmacokinetic–pharmacodynamic model of tumor growth kinetics in xenograft mice after administration of anticancer agents given in combination," *Cancer Chemother. Pharmacol.*, vol. 72, no. 2, pp. 471–482, 2013, doi: 10.1007/s00280-013-2208-8.
- [95] S. Piantadosi, "A model of growth with first-order birth and death rates," *Comput. Biomed. Res.*, vol. 18, no. 3, pp. 220–232, Jun. 1985, doi: 10.1016/0010-4809(85)90047-3.
- [96] R. K. Jain *et al.*, *Cancer Modelling and Simulation*. Boca Raton: CRC Press, 2003. doi: 10.1201/9780203494899.
- [97] J. C. Panetta, "A mathematical model of drug resistance: heterogeneous tumors," *Math. Biosci.*, vol. 147, no. 1, pp. 41–61, Jan. 1998, doi: 10.1016/s0025-5564(97)00080-1.
- [98] B. Ribba *et al.*, "A tumor growth inhibition model for low-grade glioma treated with chemotherapy or radiotherapy," *Clin. Cancer Res. Off. J. Am. Assoc. Cancer Res.*, vol. 18, no. 18, pp. 5071–5080, Sep. 2012, doi: 10.1158/1078-0432.CCR-12-0084.
- [99] G.-M. Hu, C.-Y. Lee, Y.-Y. Chen, N.-N. Pang, and W. J. Tzeng, "Mathematical model of heterogeneous cancer growth with an autocrine signalling pathway," *Cell Prolif.*, vol. 45, no. 5, pp. 445–455, Oct. 2012, doi: 10.1111/j.1365-2184.2012.00835.x.

Prediction of the cancer patients' response to their therapeutical treatment with non-linear forecasting techniques

References

- [100] G. Housman *et al.*, "Drug Resistance in Cancer: An Overview," *Cancers*, vol. 6, no. 3, pp. 1769–1792, Sep. 2014, doi: 10.3390/cancers6031769.
- [101] G. Peters, "Cancer drug resistance: a new perspective," *Cancer Drug Resist.*, vol. 1, no. 1, pp. 1–5, Mar. 2018, doi: 10.20517/cdr.2018.03.
- [102] J. Trobia *et al.*, "Mathematical model of brain tumour growth with drug resistance," *Commun. Nonlinear Sci. Numer. Simul.*, vol. 103, p. 106013, Dec. 2021, doi: 10.1016/j.cnsns.2021.106013.
- [103] S. S. Hori *et al.*, "A mathematical model of tumor regression and recurrence after therapeutic oncogene inactivation," *Sci. Rep.*, vol. 11, no. 1, p. 1341, Jan. 2021, doi: 10.1038/s41598-020-78947-2.
- [104] J. M. Greene, C. Sanchez-Tapia, and E. D. Sontag, "Mathematical Details on a Cancer Resistance Model," *Front. Bioeng. Biotechnol.*, vol. 8, p. 501, Jun. 2020, doi: 10.3389/fbioe.2020.00501.
- [105] J. A. Sherratt, "Traveling Wave Solutions of a Mathematical Model for Tumor Encapsulation," *SIAM J. Appl. Math.*, vol. 60, no. 2, pp. 392–407, 1999.
- [106] A. J. Perumpanani, B. P. Marchant, and J. Norbury, "Traveling Shock Waves Arising in a Model of Malignant Invasion," *SIAM J. Appl. Math.*, vol. 60, no. 2, pp. 463–476, Jan. 2000, doi: 10.1137/s0036139998328034.
- [107] T. Roose, S. J. Chapman, and P. K. Maini, "Mathematical Models of Avascular Tumor Growth," *SIAM Rev.*, vol. 49, no. 2, pp. 179–208, Jan. 2007, doi: 10.1137/S0036144504446291.
- [108] A. C. Burton, "Rate of growth of solid tumours as a problem of diffusion," *Growth*, vol. 30, no. 2, pp. 157–176, Jun. 1966.
- [109] J. J. Casciari, S. V. Sotirchos, and R. M. Sutherland, "Mathematical modelling of microenvironment and growth in EMT6/Ro multicellular tumour spheroids," *Cell Prolif.*, vol. 25, no. 1, pp. 1–22, Jan. 1992, doi: 10.1111/j.1365-2184.1992.tb01433.x.
- [110] R. A. Gatenby, "The potential role of transformation-induced metabolic changes in tumor-host interaction," *Cancer Res.*, vol. 55, no. 18, pp. 4151–4156, Sep. 1995.
- [111] R. A. Gatenby and E. T. Gawlinski, "A reaction-diffusion model of cancer invasion," *Cancer Res.*, vol. 56, no. 24, pp. 5745–5753, Dec. 1996.
- [112] M. Papadogiorgaki, P. Koliou, X. Kotsiakos, and M. E. Zervakis, "Mathematical modelling of spatio-temporal glioma evolution," *Theor. Biol. Med. Model.*, vol. 10, p. 47, Jul. 2013, doi: 10.1186/1742-4682-10-47.
- [113] A. R. Anderson and M. A. Chaplain, "Continuous and discrete mathematical models of tumor-induced angiogenesis," *Bull. Math. Biol.*, vol. 60, no. 5, pp. 857–899, Sep. 1998, doi: 10.1006/bulm.1998.0042.

Prediction of the cancer patients' response to their therapeutical treatment with non-linear forecasting techniques

References

- [114] A. R. Kansal, S. Torquato, G. R. Harsh IV, E. A. Chiocca, and T. S. Deisboeck, "Cellular automaton of idealized brain tumor growth dynamics," *Biosystems*, vol. 55, no. 1–3, pp. 119–127, Feb. 2000, doi: 10.1016/s0303-2647(99)00089-1.
- [115] S. Turner and J. A. Sherratt, "Intercellular Adhesion and Cancer Invasion: A Discrete Simulation Using the Extended Potts Model," *J. Theor. Biol.*, vol. 216, no. 1, pp. 85–100, May 2002, doi: 10.1006/jtbi.2001.2522.
- [116] D. Drasdo, S. Hoehme, and M. Block, "On the Role of Physics in the Growth and Pattern Formation of Multi-Cellular Systems: What can we Learn from Individual-Cell Based Models?," *J. Stat. Phys.*, vol. 128, no. 1, pp. 287–345, Jul. 2007, doi: 10.1007/s10955-007-9289-x.
- [117] L. Zhang, Z. Wang, J. A. Sagotsky, and T. S. Deisboeck, "Multiscale agent-based cancer modeling," *J. Math. Biol.*, vol. 58, no. 4–5, pp. 545–559, Apr. 2009, doi: 10.1007/s00285-008-0211-1.
- [118] P. Macklin and M. E. Edgerton, "Discrete cell modeling," in *Multiscale Modeling of Cancer*, J. Lowengrub and V. Cristini, Eds., Cambridge: Cambridge University Press, 2010, pp. 88–122. doi: 10.1017/CBO9780511781452.007.
- [119] T. Saeed, K. Djeddi, J. L. G. Guirao, H. H. Alsulami, and M. S. Alhodaly, "A Discrete Dynamics Approach to a Tumor System," *Mathematics*, vol. 10, no. 10, p. 1774, Jan. 2022, doi: 10.3390/math10101774.
- [120] K. A. Rejniak and A. R. A. Anderson, "Hybrid Models of Tumor Growth," *Wiley Interdiscip. Rev. Syst. Biol. Med.*, vol. 3, no. 1, pp. 115–125, 2011, doi: 10.1002/wsbm.102.
- [121] A. R. A. Anderson, "A Hybrid Multiscale Model of Solid Tumour Growth and Invasion: Evolution and the Microenvironment," A. R. A. Anderson, M. A. J. Chaplain, and K. A. Rejniak, Eds., in *Mathematics and Biosciences in Interaction*, Basel: Birkhäuser, 2007, pp. 3–28. doi: 10.1007/978-3-7643-8123-3_1.
- [122] L. Peng, D. Trucu, P. Lin, A. Thompson, and M. A. J. Chaplain, "A Multiscale Mathematical Model of Tumour Invasive Growth," *Bull. Math. Biol.*, vol. 79, no. 3, pp. 389–429, Mar. 2017, doi: 10.1007/s11538-016-0237-2.
- [123] I. M. Chamseddine and K. A. Rejniak, "Hybrid modeling frameworks of tumor development and treatment," *Wiley Interdiscip. Rev. Syst. Biol. Med.*, vol. 12, no. 1, p. e1461, Jan. 2020, doi: 10.1002/wsbm.1461.
- [124] H. M. Byrne, T. Alarcon, M. R. Owen, S. D. Webb, and P. K. Maini, "Modelling aspects of cancer dynamics: a review," *Philos. Transact. A Math. Phys. Eng. Sci.*, vol. 364, no. 1843, pp. 1563–1578, Jun. 2006, doi: 10.1098/rsta.2006.1786.
- [125] T. S. Deisboeck and G. Stamatakos, Eds., *Multiscale Cancer Modeling*. Boca Raton: CRC Press, 2011. doi: 10.1201/b10407.
- [126] S. Benzekry *et al.*, "Classical Mathematical Models for Description and Prediction of Experimental Tumor Growth," *PLOS Comput. Biol.*, vol. 10, no. 8, p. e1003800, 2014, doi: 10.1371/journal.pcbi.1003800.

Prediction of the cancer patients' response to their therapeutical treatment with non-linear forecasting techniques

References

- [127] E. A. Sarapata and L. G. de Pillis, "A comparison and catalog of intrinsic tumor growth models," *Bull. Math. Biol.*, vol. 76, no. 8, pp. 2010–2024, Aug. 2014, doi: 10.1007/s11538-014-9986-y.
- [128] A. Corthay, "Does the Immune System Naturally Protect Against Cancer?," *Front. Immunol.*, vol. 5, p. 197, May 2014, doi: 10.3389/fimmu.2014.00197.
- [129] S. M. Candeias and U. S. Gaipl, "The Immune System in Cancer Prevention, Development and Therapy," *Anticancer Agents Med. Chem.*, vol. 16, no. 1, pp. 101–107, 2016, doi: 10.2174/1871520615666150824153523.
- [130] C. M. Schooling and J. V. Zhao, "Strengthening the immune system for cancer prevention," *Proc. Natl. Acad. Sci. U. S. A.*, vol. 115, no. 19, pp. E4316–E4317, Dec. 2018, doi: 10.1073/pnas.1802584115.
- [131] G. Sriram *et al.*, "The injury response to DNA damage in live tumor cells promotes antitumor immunity," *Sci. Signal.*, vol. 14, no. 705, p. eabc4764, Oct. 2021, doi: 10.1126/scisignal.abc4764.
- [132] E. D. Tabdanov *et al.*, "Engineering T cells to enhance 3D migration through structurally and mechanically complex tumor microenvironments," *Nat. Commun.*, vol. 12, no. 1, p. 2815, Dec. 2021, doi: 10.1038/s41467-021-22985-5.
- [133] N. Zheng *et al.*, "Induction of tumor cell autosis by myxoma virus-infected CAR-T and TCR-T cells to overcome primary and acquired resistance," *Cancer Cell*, vol. 40, no. 9, pp. 973–985.e7, Sep. 2022, doi: 10.1016/j.ccell.2022.08.001.
- [134] N. Çuburu *et al.*, "Harnessing anti-cytomegalovirus immunity for local immunotherapy against solid tumors," *Proc. Natl. Acad. Sci. U. S. A.*, vol. 119, no. 26, p. e2116738119, Jun. 2022, doi: 10.1073/pnas.2116738119.
- [135] G. Leem *et al.*, "Tumour-infiltrating bystander CD8⁺ T cells activated by IL-15 contribute to tumour control in non-small cell lung cancer," *Thorax*, vol. 77, no. 8, pp. 769–780, Aug. 2022, doi: 10.1136/thoraxjnl-2021-217001.
- [136] J. A. Adam, "The dynamics of growth-factor-modified immune response to cancer growth: One dimensional models," *Math. Comput. Model.*, vol. 17, no. 3, pp. 83–106, Feb. 1993, doi: 10.1016/0895-7177(93)90041-V.
- [137] V. A. Kuznetsov, I. A. Makalkin, M. A. Taylor, and A. S. Perelson, "Nonlinear dynamics of immunogenic tumors: Parameter estimation and global bifurcation analysis," *Bull. Math. Biol.*, vol. 56, no. 2, pp. 295–321, Mar. 1994, doi: 10.1016/S0092-8240(05)80260-5.
- [138] D. Kirschner and J. C. Panetta, "Modeling immunotherapy of the tumor-immune interaction," *J. Math. Biol.*, vol. 37, no. 3, pp. 235–252, Sep. 1998, doi: 10.1007/s002850050127.
- [139] M. Kolev, "Mathematical modelling of the competition between tumors and immune system considering the role of the antibodies," *Math. Comput. Model.*, vol. 37, no. 11, pp. 1143–1152, Jun. 2003, doi: 10.1016/S0895-7177(03)80018-3.

Prediction of the cancer patients' response to their therapeutical treatment with non-linear forecasting techniques

References

- [140] L. G. de Pillis and A. Radunskaya, "A mathematical model of immune response to tumor invasion," Elsevier, 2003, pp. 1661–1668. doi: 10.1016/B978-008044046-0.50404-8.
- [141] M. Kolev, E. Kozłowska, and M. Lachowicz, "A mathematical model for single cell cancer—Immune system dynamics," *Math. Comput. Model.*, vol. 41, no. 10, pp. 1083–1095, May 2005, doi: 10.1016/j.mcm.2005.05.004.
- [142] L. G. de Pillis, A. E. Radunskaya, and C. L. Wiseman, "A validated mathematical model of cell-mediated immune response to tumor growth," *Cancer Res.*, vol. 65, no. 17, pp. 7950–7958, Sep. 2005, doi: 10.1158/0008-5472.CAN-05-0564.
- [143] S. Banerjee and R. R. Sarkar, "Delay-induced model for tumor-immune interaction and control of malignant tumor growth," *Biosystems*, vol. 91, no. 1, pp. 268–288, Jan. 2008, doi: 10.1016/j.biosystems.2007.10.002.
- [144] A. d'Onofrio, F. Gatti, P. Cerrai, and L. Freschi, "Delay-induced oscillatory dynamics of tumour–immune system interaction," *Math. Comput. Model.*, vol. 51, no. 5, pp. 572–591, Mar. 2010, doi: 10.1016/j.mcm.2009.11.005.
- [145] C. Letellier, F. Denis, and L. A. Aguirre, "What can be learned from a chaotic cancer model?," *J. Theor. Biol.*, vol. 322, pp. 7–16, Apr. 2013, doi: 10.1016/j.jtbi.2013.01.003.
- [146] A. Radunskaya, L. de Pillis, and A. Gallegos, "A Model of Dendritic Cell Therapy for Melanoma," *Front. Oncol.*, vol. 3, 2013, Accessed: Mar. 21, 2023. [Online]. Available: <https://www.frontiersin.org/articles/10.3389/fonc.2013.00056>
- [147] A. G. López, J. M. Seoane, and M. A. F. Sanjuán, "A validated mathematical model of tumor growth including tumor-host interaction, cell-mediated immune response and chemotherapy," *Bull. Math. Biol.*, vol. 76, no. 11, pp. 2884–2906, Nov. 2014, doi: 10.1007/s11538-014-0037-5.
- [148] S. Singh, P. Sharma, and P. Singh, "Stability of Tumor Growth Under Immunotherapy: A Computational Study," *Biophys. Rev. Lett.*, vol. 12, pp. 69–85, Jan. 2017, doi: 10.1142/S1793048017500047.
- [149] A. M. A. C. Rocha, M. F. P. Costa, and E. M. G. P. Fernandes, "On a multiobjective optimal control of a tumor growth model with immune response and drug therapies," *Int. Trans. Oper. Res.*, vol. 25, no. 1, pp. 269–294, 2018, doi: 10.1111/itor.12345.
- [150] J.-L. Yu, H.-C. Wei, and S. R.-J. Jang, "A model of tumor-immune system interactions with healthy cells and immunotherapies," *Math. Methods Appl. Sci.*, vol. 45, no. 5, pp. 2852–2870, 2022, doi: 10.1002/mma.7958.
- [151] D. G. Mallet and L. G. De Pillis, "A cellular automata model of tumor-immune system interactions," *J. Theor. Biol.*, vol. 239, no. 3, pp. 334–350, Apr. 2006, doi: 10.1016/j.jtbi.2005.08.002.
- [152] R. Wieland, "Fuzzy Models," in *Encyclopedia of Ecology*, B. Fath, Ed., Oxford: Elsevier, 2019, pp. 93–104. doi: 10.1016/b978-0-12-409548-9.00643-6.

Prediction of the cancer patients' response to their therapeutical treatment with non-linear forecasting techniques

References

- [153] K. Roesch, D. Hasenclever, and M. Scholz, "Modelling lymphoma therapy and outcome," *Bull. Math. Biol.*, vol. 76, no. 2, pp. 401–430, Feb. 2014, doi: 10.1007/s11538-013-9925-3.
- [154] Y. Dong, R. Miyazaki, and Y. Takeuchi, "Mathematical modeling on helper T cells in a tumor immune system," *Discrete Contin. Dyn. Syst. Ser. B*, vol. 1, Jan. 2014, doi: 10.3934/dcdsb.2014.19.55.
- [155] M. Galach, "Dynamics of the tumor-immune system competition - the effect of time delay," *Int. J. Appl. Math. Comput. Sci.*, vol. 13, no. 3, pp. 395–406, 2003.
- [156] L. G. De Pillis and A. Radunskaya, "A Mathematical Tumor Model with Immune Resistance and Drug Therapy: An Optimal Control Approach," *Comput. Math. Methods Med.*, vol. 3, pp. 79–100, 2001, doi: 10.1080/10273660108833067.
- [157] L. G. de Pillis *et al.*, "Chemotherapy for tumors: an analysis of the dynamics and a study of quadratic and linear optimal controls," *Math. Biosci.*, vol. 209, no. 1, pp. 292–315, Sep. 2007, doi: 10.1016/j.mbs.2006.05.003.
- [158] P. Unni and P. Seshaiyer, "Mathematical Modeling, Analysis, and Simulation of Tumor Dynamics with Drug Interventions," *Comput. Math. Methods Med.*, vol. 2019, p. e4079298, Oct. 2019, doi: 10.1155/2019/4079298.
- [159] M. Younus Baba, M. Saleem, M. Noman, and A. Raheem, "A mixed therapy minimal model: Some strategies for eradication or minimization of cancer," *Comput. Methods Programs Biomed.*, vol. 192, p. 105433, Aug. 2020, doi: 10.1016/j.cmpb.2020.105433.
- [160] N. A. Awang, N. Maan, and M. D. Sulain, "Tumour-Natural Killer and CD8+ T Cells Interaction Model with Delay," *Mathematics*, vol. 10, no. 13, p. 2193, Jan. 2022, doi: 10.3390/math10132193.
- [161] D. S. Santurio and L. R. C. Barros, "A Mathematical Model for On-Target Off-Tumor Effect of CAR-T Cells on Gliomas," *Front. Syst. Biol.*, vol. 2, 2022, Accessed: Mar. 21, 2023. [Online]. Available: <https://www.frontiersin.org/articles/10.3389/fsysb.2022.923085>
- [162] L. G. De Pillis and A. Radunskaya, "The dynamics of an optimally controlled tumor model: A case study," *Math. Comput. Model.*, vol. 37, no. 11, pp. 1221–1244, Jun. 2003, doi: 10.1016/S0895-7177(03)00133-X.
- [163] L. Depillis *et al.*, "Optimal control of mixed immunotherapy and chemotherapy of tumors," *J. Biol. Syst.*, vol. 16, p. 51, Mar. 2008, doi: 10.1142/S0218339008002435.
- [164] N. Babaei and M. U. Salamci, "State Dependent Riccati Equation Based Model Reference Adaptive Stabilization of Nonlinear Systems with Application to Cancer Treatment," *IFAC Proc. Vol.*, vol. 47, no. 3, pp. 1296–1301, Jan. 2014, doi: 10.3182/20140824-6-ZA-1003.02282.

Prediction of the cancer patients' response to their therapeutical treatment with non-linear forecasting techniques

References

- [165] N. Babaei and M. U. Salamci, "Personalized drug administration for cancer treatment using Model Reference Adaptive Control," *J. Theor. Biol.*, vol. 371, pp. 24–44, Apr. 2015, doi: 10.1016/j.jtbi.2015.01.038.
- [166] N. Babaei, M. U. Salamci, and T. Çimen, "State Dependent Riccati Equation controlled drug delivery for mixed therapy of cancer treatment," *IFAC-Pap.*, vol. 48, no. 25, pp. 265–270, Jan. 2015, doi: 10.1016/j.ifacol.2015.11.098.
- [167] N. Babaei and M. U. Salamci, "Controller design for personalized drug administration in cancer therapy: Successive approximation approach," *Optim. Control Appl. Methods*, vol. 39, no. 2, pp. 682–719, 2018, doi: 10.1002/oca.2372.
- [168] F. A. Rihan, S. Lakshmanan, and H. Maurer, "Optimal control of tumour-immune model with time-delay and immuno-chemotherapy," *Appl. Math. Comput.*, vol. 353, pp. 147–165, Jul. 2019, doi: 10.1016/j.amc.2019.02.002.
- [169] N. Babaei and M. U. Salamci, "Mixed therapy in cancer treatment for personalized drug administration using model reference adaptive control," *Eur. J. Control*, vol. 50, pp. 117–137, Nov. 2019, doi: 10.1016/j.ejcon.2019.03.001.
- [170] J. A. Adam and N. Bellomo, *A Survey of Models for Tumor-Immune System Dynamics*. Springer Science & Business Media, 1997.
- [171] R. Eftimie, J. L. Bramson, and D. J. D. Earn, "Interactions Between the Immune System and Cancer: A Brief Review of Non-spatial Mathematical Models," *Bull. Math. Biol.*, vol. 73, no. 1, pp. 2–32, Jan. 2011, doi: 10.1007/s11538-010-9526-3.
- [172] L. G. dePilllis, A. Eladdadi, and A. E. Radunskaya, "Modeling cancer-immune responses to therapy," *J. Pharmacokinet. Pharmacodyn.*, vol. 41, no. 5, pp. 461–478, Oct. 2014, doi: 10.1007/s10928-014-9386-9.
- [173] P. M. Altrock, L. L. Liu, and F. Michor, "The mathematics of cancer: integrating quantitative models," *Nat. Rev. Cancer*, vol. 15, no. 12, pp. 730–745, Dec. 2015, doi: 10.1038/nrc4029.
- [174] G. E. Mahlbacher, K. C. Reihmer, and H. B. Frieboes, "Mathematical modeling of tumor-immune cell interactions," *J. Theor. Biol.*, vol. 469, pp. 47–60, Dec. 2019, doi: 10.1016/j.jtbi.2019.03.002.
- [175] M. P. Doogue and T. M. Polasek, "The ABCD of clinical pharmacokinetics," *Ther. Adv. Drug Saf.*, vol. 4, no. 1, pp. 5–7, Feb. 2013, doi: 10.1177/2042098612469335.
- [176] R. Southwood, V. H. Fleming, and G. Huckaby, *Concepts in clinical pharmacokinetics*, 7th ed. Bethesda, MD: ASHP publications, 2018.
- [177] S. B. Mortensen, A. H. Jónsdóttir, S. Klim, and H. Madsen, "Introduction to PK/PD modelling - with focus on PK and stochastic differential equations," Technical University of Denmark, DTU Informatics, Building 321, Lyngby, techreport 2018–16, 2008. [Online]. Available: <https://orbit.dtu.dk/en/publications/introduction-to-pkpd-modelling-with-focus-on-pk-and-stochastic-di>

Prediction of the cancer patients' response to their therapeutical treatment with non-linear forecasting techniques

References

- [178] V. Oikonen, "Pharmacokinetic one-compartment model." [Online]. Available: http://www.turkupetcentre.net/petanalysis/pk_1cm.html
- [179] V. Oikonen, "Pharmacokinetic two-compartment model." [Online]. Available: http://www.turkupetcentre.net/petanalysis/pk_2cm.html
- [180] S. A. Saghir and R. A. Ansari, "Pharmacokinetics," in *Reference Module in Biomedical Sciences*, Elsevier, 2018. doi: 10.1016/b978-0-12-801238-3.62154-2.
- [181] M. Kelly, "An Introduction to Trajectory Optimization: How to Do Your Own Direct Collocation," *SIAM Rev.*, vol. 59, no. 4, pp. 849–904, Jan. 2017, doi: 10.1137/16m1062569.
- [182] R. Bellman, "Dynamic Programming," *Science*, vol. 153, no. 3731, pp. 34–37, Jul. 1966, doi: 10.1126/science.153.3731.34.
- [183] C. HARGRAVES and S. Paris, "Direct Trajectory Optimization Using Nonlinear Programming and Collocation," *AIAA J Guid.*, vol. 10, pp. 338–342, Jul. 1987, doi: 10.2514/3.20223.
- [184] L. S. Pontryagin, *Mathematical Theory of Optimal Processes*. London: Routledge, 2017. doi: 10.1201/9780203749319.
- [185] J. T. Betts, "Survey of Numerical Methods for Trajectory Optimization," *J. Guid. Control Dyn.*, vol. 21, no. 2, pp. 193–207, Mar. 1998, doi: 10.2514/2.4231.
- [186] J.-F. Bonnans, J. C. Gilbert, C. Lemaréchal, and C. A. Sagastizábal, *Numerical optimization: theoretical and practical aspects: Theoretical and Practical Aspects (Universitext)*. Springer Science & Business Media, 2006.
- [187] J. T. Betts, *Practical Methods for Optimal Control and Estimation Using Nonlinear Programming*, 2nd ed. Philadelphia: Society for Industrial and Applied Mathematics, 2009.
- [188] B. de Jager, T. van Keulen, and J. Kessels, *Optimal Control of Hybrid Vehicles*. Springer London, 2013. doi: 10.1007/978-1-4471-5076-3.
- [189] T. J. Böhme and B. Frank, "Direct Methods for Optimal Control," in *Hybrid Systems, Optimal Control and Hybrid Vehicles: Theory, Methods and Applications*, in *Advances in Industrial Control*, Cham: Springer International Publishing, 2017, pp. 233–273. doi: 10.1007/978-3-319-51317-1_8.
- [190] N. Dal Bianco, E. Bertolazzi, F. Biral, and M. Massaro, "Comparison of direct and indirect methods for minimum lap time optimal control problems," *Veh. Syst. Dyn.*, vol. 57, no. 5, pp. 665–696, May 2019, doi: 10.1080/00423114.2018.1480048.
- [191] J. R. Cloutier, "State-dependent Riccati equation techniques: an overview," in *Proceedings of the 1997 American Control Conference (Cat. No.97CH36041)*, IEEE, 1997, pp. 932–936. doi: 10.1109/ACC.1997.609663.

Prediction of the cancer patients' response to their therapeutical treatment with non-linear forecasting techniques

References

- [192] H. T. Banks, B. M. Lewis, and H. T. Tran, "Nonlinear feedback controllers and compensators: a state-dependent Riccati equation approach," *Comput. Optim. Appl.*, vol. 37, no. 2, pp. 177–218, Jun. 2007, doi: 10.1007/s10589-007-9015-2.
- [193] T. Çimen, "State-Dependent Riccati Equation (SDRE) Control: A Survey," *IFAC Proc. Vol.*, vol. 41, no. 2, pp. 3761–3775, 2008, doi: 10.3182/20080706-5-KR-1001.00635.
- [194] I. Mehmet, M. Salamci, and S. Banks, "SDRE optimal control of drug administration in cancer treatment," *Turk. J. Electr. Eng. Comput. Sci.*, vol. 18, Jan. 2010, doi: 10.3906/elk-1001-411.
- [195] U. Ledzewicz and H. Schaettler, *Optimizing Chemotherapeutic Anti-cancer Treatment and the Tumor Microenvironment: An Analysis of Mathematical Models: Quantitative Modeling and Simulations*. in *Advances in Experimental Medicine and Biology*. Cham: Springer London, Limited, 2016. doi: 10.1007/978-3-319-42023-3_11.
- [196] K. Bahrami and M. Kim, "Optimal control of multiplicative control systems arising from cancer therapy," *IEEE Trans. Autom. Control*, vol. 20, no. 4, pp. 537–542, Aug. 1975, doi: 10.1109/TAC.1975.1101019.
- [197] G. W. Swan and T. L. Vincent, "Optimal control analysis in the chemotherapy of IgG multiple myeloma," *Bull. Math. Biol.*, vol. 39, no. 3, pp. 317–337, May 1977, doi: 10.1007/BF02462912.
- [198] G. W. Swan, "Optimal control in some cancer chemotherapy problems," *Int. J. Syst. Sci.*, vol. 11, no. 2, pp. 223–237, Jan. 1980, doi: 10.1080/00207728008967009.
- [199] G. W. Swan, "General Applications of Optimal Control Theory in Cancer Chemotherapy," *Math. Med. Biol.*, vol. 5, no. 4, pp. 303–316, 1988, doi: 10.1093/imammb/5.4.303.
- [200] J. M. Murray, "Optimal control for a cancer chemotherapy problem with general growth and loss functions," *Math. Biosci.*, vol. 98, no. 2, pp. 273–287, Mar. 1990, doi: 10.1016/0025-5564(90)90129-m.
- [201] A. Swierniak, A. Polanski, and M. Kimmel, "Optimal control problems arising in cell-cycle-specific cancer chemotherapy," *Cell Prolif.*, vol. 29, no. 3, pp. 117–139, 1996, doi: 10.1046/j.1365-2184.1996.00995.x.
- [202] J. C. Panetta and K. R. Fister, "Optimal Control Applied to Competing Chemotherapeutic Cell-Kill Strategies," *SIAM J. Appl. Math.*, vol. 63, no. 6, pp. 1954–1971, Jan. 2003, doi: 10.1137/S0036139902413489.
- [203] F. Castiglione and B. Piccoli, "Cancer immunotherapy, mathematical modeling and optimal control," *J. Theor. Biol.*, vol. 247, no. 4, pp. 723–732, Aug. 2007, doi: 10.1016/j.jtbi.2007.04.003.

Prediction of the cancer patients' response to their therapeutical treatment with non-linear forecasting techniques

References

- [204] M. Itik, M. U. Salamci, and S. P. Banks, "Optimal control of drug therapy in cancer treatment," *Nonlinear Anal. Theory Methods Appl.*, vol. 71, no. 12, pp. e1473–e1486, Dec. 2009, doi: 10.1016/j.na.2009.01.214.
- [205] H. Moradi, G. Vossoughi, and H. Salarieh, "Optimal robust control of drug delivery in cancer chemotherapy: A comparison between three control approaches," *Comput. Methods Programs Biomed.*, vol. 112, no. 1, pp. 69–83, Oct. 2013, doi: 10.1016/j.cmpb.2013.06.020.
- [206] A. Ghaffari, M. Nazari, and F. Arab, "Optimal Finite Cancer Treatment Duration by Using Mixed Vaccine Therapy and Chemotherapy: State Dependent Riccati Equation Control," *J. Appl. Math.*, vol. 2014, pp. 1–9, 2014.
- [207] K. S. Kim, G. Cho, and I. H. Jung, "Optimal treatment strategy for a tumor model under immune suppression," *Comput. Math. Methods Med.*, vol. 2014, p. 206287, 2014, doi: 10.1155/2014/206287.
- [208] M. M. Hadjiandreou and G. D. Mitsis, "Mathematical Modeling of Tumor Growth, Drug-Resistance, Toxicity, and Optimal Therapy Design," *IEEE Trans. Biomed. Eng.*, vol. 61, no. 2, pp. 415–425, Oct. 2014, doi: 10.1109/TBME.2013.2280189.
- [209] H. Schättler and U. Ledzewicz, "Optimal Control of Mathematical Models for Antiangiogenic Treatments," in *Interdisciplinary Applied Mathematics*, Springer New York, 2015, pp. 171–235. doi: 10.1007/978-1-4939-2972-6_5.
- [210] S. Wang and H. Schattler, "Optimal control of a mathematical model for cancer chemotherapy under tumor heterogeneity," *Math. Biosci. Eng. MBE*, vol. 13, no. 6, pp. 1223–1240, Dec. 2016, doi: 10.3934/mbe.2016040.
- [211] H. Moore, "How to mathematically optimize drug regimens using optimal control," *J. Pharmacokinet. Pharmacodyn.*, vol. 45, no. 1, pp. 127–137, Feb. 2018, doi: 10.1007/s10928-018-9568-y.
- [212] N. H. Sweilam, S. M. Al-Mekhlafi, T. Assiri, and A. Atangana, "Optimal control for cancer treatment mathematical model using Atangana–Baleanu–Caputo fractional derivative," *Adv. Differ. Equ.*, vol. 2020, no. 1, p. 334, Jul. 2020, doi: 10.1186/s13662-020-02793-9.
- [213] A. M. Jarrett *et al.*, "Optimal Control Theory for Personalized Therapeutic Regimens in Oncology: Background, History, Challenges, and Opportunities," *J. Clin. Med.*, vol. 9, no. 5, p. 1314, May 2020, doi: 10.3390/jcm9051314.
- [214] F. Angaroni *et al.*, "An Optimal Control Framework for the Automated Design of Personalized Cancer Treatments," *Front. Bioeng. Biotechnol.*, vol. 8, 2020, Accessed: Mar. 21, 2023. [Online]. Available: <https://www.frontiersin.org/articles/10.3389/fbioe.2020.00523>
- [215] P. Lecca, "Control Theory and Cancer Chemotherapy: How They Interact," *Front. Bioeng. Biotechnol.*, vol. 8, 2021, Accessed: Mar. 21, 2023. [Online]. Available: <https://www.frontiersin.org/articles/10.3389/fbioe.2020.621269>

Prediction of the cancer patients' response to their therapeutical treatment with non-linear forecasting techniques

References

- [216] M. Bodzioch, P. Bajger, and U. Foryś, "Angiogenesis and chemotherapy resistance: optimizing chemotherapy scheduling using mathematical modeling," *J. Cancer Res. Clin. Oncol.*, vol. 147, no. 8, pp. 2281–2299, Aug. 2021, doi: 10.1007/s00432-021-03657-9.
- [217] G. Haddad *et al.*, "Optimal control model of tumor treatment in the context of cancer stem cell," *Math. Biosci. Eng.*, vol. 19, no. 5, pp. 4627–4642, 2022, doi: 10.3934/mbe.2022214.
- [218] I. S. Mavromatakis, S. G. Liliopoulos, and G. S. Stavrakakis, "Determination of the pharmaceutical treatment-dosage for cancer patients using non-linear optimal control techniques," in *2020 24th International Conference on Circuits, Systems, Communications and Computers (CSCC)*, Chania, Greece: IEEE, Jul. 2020, pp. 106–111. doi: 10.1109/CSCC49995.2020.00026.
- [219] I. S. Mavromatakis, S. G. Liliopoulos, and G. S. Stavrakakis, "Optimized intermittent pharmaceutical treatment of cancer using non-linear optimal control techniques," *WSEAS Trans. Biol. Biomed.*, vol. 17, pp. 67–75, Mar. 2020, doi: 10.37394/23208.2020.17.9.
- [220] P. Bilalis *et al.*, "Self-healing pH- and enzyme stimuli-responsive hydrogels for targeted delivery of gemcitabine to treat pancreatic cancer," *Biomacromolecules*, vol. 19, no. 9, pp. 3840–3852, Aug. 2018, doi: 10.1021/acs.biomac.8b00959.
- [221] P. E. Black, "Optimization problem." Accessed: Jun. 17, 2022. [Online]. Available: <https://xlinux.nist.gov/dads/HTML/optimization.html>
- [222] G. Venter, "Review of Optimization Techniques," in *Encyclopedia of Aerospace Engineering*, R. Blockley and W. Shyy, Eds., John Wiley & Sons, Ltd, 2010. doi: <https://doi.org/10.1002/9780470686652.eae495>.
- [223] A. Sadollah, H. Sayyaadi, and A. Yadav, "A dynamic metaheuristic optimization model inspired by biological nervous systems: Neural network algorithm," *Appl. Soft Comput.*, vol. 71, pp. 747–782, Oct. 2018, doi: 10.1016/j.asoc.2018.07.039.
- [224] P. Singla, M. Duhan, and S. Saroha, "10 - Different normalization techniques as data preprocessing for one step ahead forecasting of solar global horizontal irradiance," in *Artificial Intelligence for Renewable Energy Systems*, A. K. Dubey, S. K. Narang, A. L. Srivastav, A. Kumar, and V. García-Díaz, Eds., in Woodhead Publishing Series in Energy. , Woodhead Publishing, 2022, pp. 209–230. doi: 10.1016/B978-0-323-90396-7.00004-3.
- [225] S. Kim and H. Kim, "A new metric of absolute percentage error for intermittent demand forecasts," *Int. J. Forecast.*, vol. 32, no. 3, pp. 669–679, Jul. 2016, doi: 10.1016/j.ijforecast.2015.12.003.
- [226] M. Simeoni *et al.*, "Predictive pharmacokinetic-pharmacodynamic modeling of tumor growth kinetics in xenograft models after administration of anticancer agents," *Cancer Res.*, vol. 64, no. 3, pp. 1094–1101, Feb. 2004, doi: 10.1158/0008-5472.can-03-2524.

- [227] M. Rocchetti *et al.*, "A pharmacokinetic-pharmacodynamic model for predicting tumour growth inhibition in mice: a useful tool in oncology drug development," *Basic Clin. Pharmacol. Toxicol.*, vol. 96, no. 3, pp. 265–268, 2005, doi: <https://doi.org/10.1111/j.1742-7843.2005.pto960325.x>.
- [228] M. C. Bissery, P. Vrignaud, F. Lavelle, and G. G. Chabot, "Experimental antitumor activity and pharmacokinetics of the camptothecin analog irinotecan (CPT-11) in mice," *Anticancer. Drugs*, vol. 7, no. 4, pp. 437–460, Jun. 1996, doi: 10.1097/00001813-199606000-00010.
- [229] M. Rocchetti, M. Simeoni, E. Pesenti, G. D. Nicolao, and I. Poggesi, "Predicting the active doses in humans from animal studies: A novel approach in oncology," *Eur. J. Cancer*, vol. 43, no. 12, pp. 1862–1868, Aug. 2007, doi: 10.1016/j.ejca.2007.05.011.
- [230] G. Veerman *et al.*, "Antitumor activity of prolonged as compared with bolus administration of 2',2'-difluorodeoxycytidine in vivo against murine colon tumors," *Cancer Chemother. Pharmacol.*, vol. 38, no. 4, pp. 335–342, Jul. 1996, doi: 10.1007/s002800050492.
- [231] G. E. P. Box, G. M. Jenkins, and G. C. Reinsel, *Time Series Analysis: Forecasting and Control*, 5th ed. Hoboken, New Jersey: Wiley, 2015.
- [232] Y. Chakhchoukh, P. Panciatici, and L. Mili, "Electric Load Forecasting Based on Statistical Robust Methods," *IEEE Trans. Power Syst.*, vol. 26, no. 3, pp. 982–991, Dec. 2011, doi: 10.1109/TPWRS.2010.2080325.
- [233] V. Sakkalis *et al.*, "Parametric and Nonparametric EEG Analysis for the Evaluation of EEG Activity in Young Children with Controlled Epilepsy," *Comput. Intell. Neurosci.*, vol. 2008, p. e462593, Aug. 2008, doi: 10.1155/2008/462593.
- [234] T. Takagi and M. Sugeno, "Fuzzy identification of systems and its applications to modeling and control," *IEEE Trans. Syst. Man Cybern.*, vol. SMC-15, no. 1, pp. 116–132, Jan. 1985, doi: 10.1109/TSMC.1985.6313399.
- [235] J.-S. R. Jang, C.-T. Sun, and E. Mizutani, *Neuro-fuzzy and Soft Computing: A Computational Approach to Learning and Machine Intelligence*. Upper Saddle River, NJ: Prentice Hall, 1997.
- [236] M. Hossain *et al.*, "Application of the hybrid ANFIS models for long term wind power density prediction with extrapolation capability," *PLOS ONE*, vol. 13, no. 4, pp. 1–31, Apr. 2018, doi: 10.1371/journal.pone.0193772.
- [237] S. G. Liliopoulos and G. S. Stavrakakis, "Adaptive Short Term Ahead Tumor Growth Inhibition Prediction Subjected in Anticancer Agents Given in Combination," in *2019 IEEE 19th International Conference on Bioinformatics and Bioengineering (BIBE)*, IEEE, Oct. 2019. doi: 10.1109/bibe.2019.00039.
- [238] The MathWorks Inc., "MATLAB 9.7.0.1190202 (R2019b)." The MathWorks Inc., Natick, Massachusetts, United States, 2022. [Online]. Available: <https://www.mathworks.com>

Prediction of the cancer patients' response to their therapeutical treatment with non-linear forecasting techniques

References

- [239] S. Raguz and E. Yagüe, "Resistance to chemotherapy: new treatments and novel insights into an old problem," *Br. J. Cancer*, vol. 99, no. 3, pp. 387–391, Aug. 2008, doi: 10.1038/sj.bjc.6604510.
- [240] K. O. Alfarouk *et al.*, "Resistance to cancer chemotherapy: failure in drug response from ADME to P-gp," *Cancer Cell Int.*, vol. 15, no. 1, p. 71, Jul. 2015, doi: 10.1186/s12935-015-0221-1.
- [241] K. Ogata, *Modern control engineering*, 5th ed. Boston: Prentice-Hall, 2010.
- [242] A. Pouliezios, *Modern Control Theory [Undergraduate textbook]*. Kallipos, Open Academic Editions, Athens, GR, 2015. [Online]. Available: <http://hdl.handle.net/11419/105>
- [243] T. Onishi, T. Sasaki, and A. Hoshina, "Intermittent Chemotherapy Is a Treatment Choice for Advanced Urothelial Cancer," *Oncology*, vol. 83, no. 1, pp. 50–56, 2012, doi: 10.1159/000338770.
- [244] S. R. Berry, R. Cosby, T. Asmis, K. Chan, N. Hammad, and M. K. Krzyzanowska, "Continuous versus intermittent chemotherapy strategies in metastatic colorectal cancer: a systematic review and meta-analysis," *Ann. Oncol.*, vol. 26, no. 3, pp. 477–485, Mar. 2015, doi: 10.1093/annonc/mdu272.
- [245] M. E. Cazzaniga *et al.*, "Treating advanced breast cancer with metronomic chemotherapy: what is known, what is new and what is the future?," *OncoTargets Ther.*, vol. 12, pp. 2989–2997, 2019, doi: 10.2147/OTT.S189163.
- [246] V. Wichmann, N. Eigeliene, J. Saarenheimo, and A. Jekunen, "Recent clinical evidence on metronomic dosing in controlled clinical trials: a systematic literature review," *Acta Oncol.*, vol. 59, no. 7, pp. 775–785, Jul. 2020, doi: 10.1080/0284186X.2020.1744719.
- [247] M. E. Cazzaniga, N. Cordani, S. Capici, V. Cogliati, F. Riva, and M. G. Cerrito, "Metronomic Chemotherapy," *Cancers*, vol. 13, no. 9, p. 2236, Jan. 2021, doi: 10.3390/cancers13092236.
- [248] M. J. Box, "A New Method of Constrained Optimization and a Comparison With Other Methods," *Comput. J.*, vol. 8, no. 1, pp. 42–52, Apr. 1965, doi: 10.1093/comjnl/8.1.42.
- [249] S. S. Rao, *Engineering Optimization Theory and Practice*, 5th ed. Hoboken, NJ, USA: Wiley, 2019. doi: 10.1002/9781119454816.
- [250] R. E. Kalman and R. W. Koepcke, "Optimal Synthesis of Linear Sampling Control Systems Using Generalized Performance Indexes," *J. Fluids Eng.*, vol. 80, no. 8, pp. 1820–1826, Nov. 1958, doi: 10.1115/1.4012899.
- [251] J. D. PEARSON, "Approximation Methods in Optimal Control I. Sub-optimal Control†," *J. Electron. Control*, vol. 13, no. 5, pp. 453–469, Nov. 1962, doi: 10.1080/00207216208937454.

Prediction of the cancer patients' response to their therapeutical treatment with non-linear forecasting techniques

References

- [252] T. Çimen, "Systematic and effective design of nonlinear feedback controllers via the state-dependent Riccati equation (SDRE) method," *Annu. Rev. Control*, vol. 34, no. 1, pp. 32–51, Apr. 2010, doi: 10.1016/j.arcontrol.2010.03.001.
- [253] J. Cloutier and J. Cockburn, *The state-dependent nonlinear regulator with state constraints*, vol. 1. 2001. doi: 10.1109/ACC.2001.945577.
- [254] G. Franklin, *Feedback control of dynamic systems*, 6th ed. Upper Saddle River, N.J: Pearson, 2010.
- [255] R. M. Murray, "Lecture 2 – LQR Control." California Institute of Technology, US, Jan. 2006. Accessed: Oct. 20, 2021. [Online]. Available: <http://www.cds.caltech.edu/~murray/courses/cds110/wi06/lqr.pdf>
- [256] S. J. P. S. Mariano, J. A. N. Pombo, M. R. A. Calado, and L. A. F. M. Ferreira, "Pole-shifting procedure to specify the weighting matrices for a load-frequency controller," in *Melecon 2010 - 2010 15th IEEE Mediterranean Electrotechnical Conference*, IEEE, 2010, pp. 818–823. doi: 10.1109/melcon.2010.5475958.
- [257] S. J. P. S. Mariano, J. Á. N. Pombo, M. do R. A. Calado, and L. A. F. M. Ferreira, "A procedure to specify the weighting matrices for an optimal load-frequency controller," *Turk. J. Electr. Eng. Comput. Sci.*, vol. 20, no. 3, pp. 367–379, 2012.
- [258] M. Abdillah, H. Setiadi, A. B. Reihara, K. Mahmoud, I. W. Farid, and A. Soeprijanto, "Optimal selection of LQR parameter using AIS for LFC in a multi-area power system," *J. Mechatron. Electr. Power Veh. Technol.*, vol. 7, no. 2, pp. 93–104, Dec. 2016, doi: 10.14203/j.mev.2016.v7.93-104.
- [259] J. Cloutier, C. Souza, and C. Mracek, *Nonlinear Regulation and Nonlinear H_∞ Control Via the State-Dependent Riccati Equation Technique: Part1, Theory*. 1996.
- [260] J. Carrasco, "State-Space Control." Oct. 01, 2016. [Online]. Available: https://personalpages.manchester.ac.uk/staff/joaquin.carrasco/SS_notes.pdf

Appendix

Appendix A: Neural Network Algorithm (NNA)

Introduced by Sadollah *et al.* [223], the Neural Network Algorithm (NNA) is an unsupervised non-linear constraint optimization method that searches to achieve the global minimum value of an objective function $J(x_1, \dots, x_n, t)$ subject to n constraints of the form $x_{r,min} \leq x_r \leq x_{r,max}$ where $r = 1, \dots, n$.

$$\begin{aligned} &\text{Minimize } J(x_1, \dots, x_n, t) \\ &\text{Subject to } x_{r,min} \leq x_r \leq x_{r,max} \end{aligned} \quad (\text{A.1})$$

Each “individual” defined as a set containing a numerical value of each optimization variable (unknown parameter) is called “pattern solution” (e.g., in the Genetic Algorithms this vector is called “Chromosome”). In a n dimensional optimization problem, a pattern solution is a vector of $1 \times n$, representing the input data of the method. This matrix is defined as the $\underline{x}^T = [x_1, \dots, x_n]$ above.

To initiate the optimization algorithm, a candidate of pattern solution matrix \mathbf{X} with size $N_{pop} \times n$ is generated. The matrix \mathbf{X} is given as follows:

$$\mathbf{X} = \begin{bmatrix} \underline{x}_1 \\ \underline{x}_2 \\ \vdots \\ \underline{x}_{N_{pop}} \end{bmatrix} = \begin{bmatrix} x_1^1 & x_2^1 & \dots & x_n^1 \\ x_1^2 & x_2^2 & \dots & x_n^2 \\ \vdots & \vdots & \ddots & \vdots \\ x_1^{N_{pop}} & x_2^{N_{pop}} & \dots & x_n^{N_{pop}} \end{bmatrix}, \quad (\text{A.2})$$

where the rows and columns are the population size (N_{pop}) and the dimension size (n), respectively. It should be noted that each matrix value is randomly generated within the range between the lower and upper bounds of each unknown variable (the lower and upper bounds are assumed to be defined by a decision maker).

Next, their objective function J is evaluated following the procedure outlined in Figure 3.6 and described by the equations (3.2) and (3.3), and the initial “target” solution \underline{x}^{target} (i.e., the vector initially assumed to correspond to minimum J value) is determined.

Similar to the population of pattern solutions, a weight matrix \mathbf{W} is also generated:

$$\mathbf{W} = \begin{bmatrix} \underline{w}_1 \\ \underline{w}_2 \\ \vdots \\ \underline{w}_{N_{pop}} \end{bmatrix}' = \begin{bmatrix} w_1^1 & w_1^i & \cdots & w_1^{N_{pop}} \\ w_2^1 & w_2^i & \cdots & w_2^{N_{pop}} \\ \vdots & \vdots & \ddots & \vdots \\ w_{N_{pop}}^1 & w_{N_{pop}}^i & \cdots & w_{N_{pop}}^{N_{pop}} \end{bmatrix}, \quad (\text{A.3})$$

The weights are randomly generated following uniform distribution and must satisfy the constraints imposed by (A.4) below. These constraints are particularly important as they prevent the algorithm from getting “stuck” at a local minimum [223].

$$\sum_{j=1}^{N_{pop}} w_j^i = 1, \quad w_j^i \in U(0,1), \quad i, j = 1, 2, \dots, N_{pop}. \quad (\text{A.4})$$

Based on the previous population of pattern solutions and inspired by the weight summation technique commonly used in ANNs, a new updated \mathbf{X} population is generated, and the weighting matrix \mathbf{W} is updated. The aforementioned procedure is described by the equations (A.5) - (A.7) below:

$$\underline{x}_j^{New}(k+1) = \sum_{i=1}^{N_{pop}} w_j^i(k) \underline{x}_i(k), \quad j = 1, 2, \dots, N_{pop}, \quad (\text{A.5})$$

$$\underline{x}_i(k+1) = \underline{x}_i(k) + \underline{x}_i^{New}(k+1), \quad i = 1, 2, \dots, N_{pop}, \quad (\text{A.6})$$

$$\underline{w}_i^{update}(k+1) = \underline{w}_i(k) + 2 \cdot rand \cdot \left(\underline{w}^{target}(k) - \underline{w}_i(k) \right), \quad (\text{A.7})$$

$$i = 1, 2, \dots, N_{pop}$$

where k is the optimization iteration index.

A common issue that may occur when searching for an optimum is premature convergence of optimization. To prevent the algorithm from an early convergence, a bias strategy (using an operator β) is introduced [223]. A portion of the pattern solutions and the weights generated in the new population are altered, making the bias operator to act as a form of noise in the system and providing the ability to broaden the search space and explore other areas that have not yet been visited by the population. As the iteration index k increases, the likelihood of modifying and generating new pattern solutions using the bias operator decreases. Instead, it is more likely for a solution to be

Prediction of the cancer patients' response to their therapeutical treatment with non-linear forecasting techniques

Appendices

transferred towards the best solution (i.e., the new "target" solution), as described in (A.8) below:

$$\begin{aligned} \underline{x}_i^*(k+1) &= \underline{x}_i(k+1) + 2 \cdot \text{rand} \cdot \left(\underline{x}^{\text{target}}(k) - \underline{x}_i(k+1) \right) \\ i &= 1, 2, \dots, N_{\text{pop}}. \end{aligned} \quad (\text{A.8})$$

The new "target" solution and its weight are then determined, and the above update procedure is repeated until the maximum number of iterations k_{max} is reached. The parameters estimation procedure is then restarted from the converged solution of the previous trial; thus, a "rough check" is performed to see if the solution obtained corresponds to the global minimum of the objective function. A flowchart of the NNA optimization algorithm is provided in the Figure A.1 for a visual representation of the process and steps involved in the optimization.

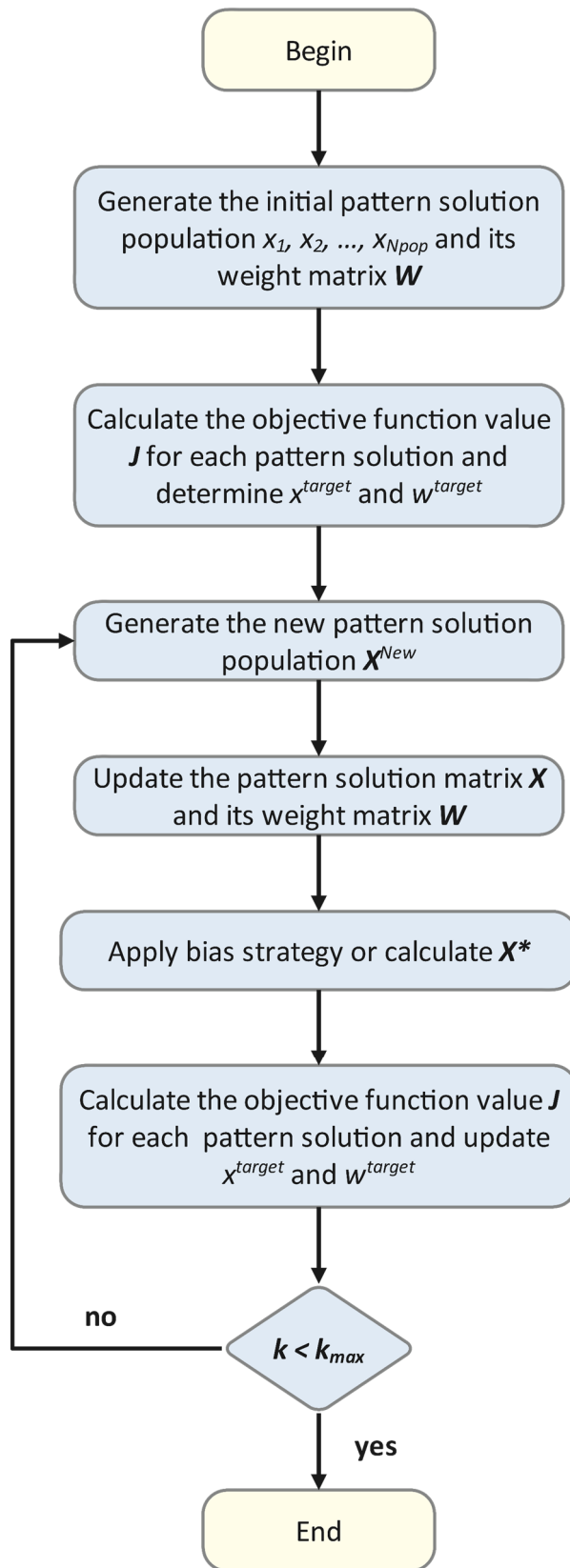


Figure A.1. Flowchart of the NNA optimization algorithm. Visual representation of the process and steps involved in the optimization.

Appendix B: Complex method of Box

The COMPLEX algorithm is a non-linear global constraint optimization technique proposed by M. J. Box in 1965 [245]. The method searches to achieve the minimum value of an objective function $J(x_1, \dots, x_n, t)$ subject to n constraints of the form $x_{r,min} \leq x_r \leq x_{r,max}$, $r = 1, \dots, n$.

$$\begin{aligned} &\text{Minimize} && J(x_1, \dots, x_n, t) \\ &\text{Subject to} && x_{r,min} \leq x_r \leq x_{r,max}, \quad r = 1, \dots, n \end{aligned} \quad (\text{B.1})$$

In the COMPLEX method a set (population) of $N_{pop} \geq 2n + 1$ vectors of the under-estimation parameters with random values of the unknown parameters, but within the value range of each unknown parameter is created. By narrowing down this set of vectors to a very small area in the n^{th} dimensional space, the global minimum of the objective function $J(x_1, \dots, x_n, t)$ can be found. The objective then function is evaluated for each of these “points” in the set, and the “worst point”, i.e., the point with the highest value of the objective function, is replaced by a new one calculated using the equations below:

$$X_r = (1 + \mathbf{a}) \cdot X_o + \mathbf{a} \cdot X_h \quad (\text{B.2})$$

$$X_o = \frac{1}{k-1} \cdot \sum_{i=1}^{N_{pop}-1} X_i \quad (\text{B.3})$$

where X_h is the current “worst point” to be replaced, X_o is the centroid of all vertices except X_h and \mathbf{a} is a constant with an initial value greater than 1. In [248] M. J. Box suggested a value of $\mathbf{a} = 1.3$ as a starting point for the procedure. The steps described above are referred to as a “reflection process” [249].

Whenever a “point” is replaced by a new one, it must be checked to ensure that it does not violate any constraints. If a constraint violation is detected at any stage of the method, the corresponding “point” is moved into the pre-defined boundaries of the under-estimation parameters, as defined by the inequalities in (B.1). The value of the objective function corresponding to the “new point” X_r is then evaluated and if it remains the “worst” of all, the coefficient \mathbf{a} is reduced by half and the process is repeated.

Prediction of the cancer patients' response to their therapeutical treatment with non-linear forecasting techniques

Appendices

This process described above continues until the “worst point” is improved, that is until the corresponding objective function value is no longer the highest. If the value of the objective function is improved, then the convergence of the process is checked by determining if the swarm of the “points” (i.e., vectors of the initially unknown parameters) shrinks to a very small size and if the standard deviation of the objective function value (calculated by the equation below) becomes very small:

$$\left(\frac{1}{N_{pop}} \cdot \sum_{i=1}^{N_{pop}} [J(X_a) - J(x_i)]^2 \right)^{\frac{1}{2}} < \varepsilon \quad (\text{B.4})$$

where X_a is the centroid of all vertices and ε is a very small number (i.e., $\varepsilon = 10^{-15}$). However, if there is no significant improvement in the estimated parameters values and the value of the coefficient \mathbf{a} becomes smaller than a small quantity (i.e., $\mathbf{a} < 10^{-6}$), X_r is discarded completely and the procedure continues with the second “worst point” of the swarm until convergence.

Appendix C: LQR optimal control

The linear quadratic regulator (LQR) is a widely used method that provides optimal state-feedback laws for linear systems. This practically enables closed-loop stability and high-performance design of systems. Given a discrete-time linear system described by the equations below:

$$\begin{aligned}x[k + 1] &= Ax[k] + Bu[k] \\y[k] &= Cx[k]\end{aligned}\tag{C.1}$$

where $A \in \mathbb{R}^{n \times n}$, $B \in \mathbb{R}^{n \times m}$, $C \in \mathbb{R}^{l \times n}$, $x[k] \in \mathbb{R}^n$ is the system state vector, $u[n] \in \mathbb{R}^m$ is the input to this system (i.e., the chemotherapy drug amount) and $y[k] \in \mathbb{R}^l$ is the output (i.e., the tumor weight) at time k , LQR tries to determine a control input that minimizes a performance index. A typical form of this index is the quadratic cost function introduced by Kalman in 1958 [250]. It associates weights with the control input u and with each of the system's states x . It is described by the following equation:

$$J_{LQR} = \sum_{k=0}^{\infty} (x^T[k]Qx[k] + u^T[k]Ru[k])\tag{C.2}$$

where $Q \in \mathbb{R}^{n \times n}$ and $R \in \mathbb{R}^{m \times m}$ are the real positive semi-definite and positive definite weighting matrices for each state x and the control variable u , respectively. The cost function J_{LQR} is minimized using the state-feedback controller described by the equation below:

$$u[k] = -R^{-1}B^T Sx[k] \triangleq -Kx[k]\tag{C.3}$$

where $K = R^{-1}B^T S$ is the optimal feedback gain and S is a positive definite symmetric matrix and the unique solution of the algebraic Riccati equation (ARE), below:

$$A^T S + SA - SBR^{-1}B^T S + Q = 0.\tag{C.4}$$

The uniqueness of the ARE solution is implied by the controllability and observability of (A, B) and (A, C) , respectively.

Controllability: A pair of $\{A, B\}$ is controllable if and only if none of the left eigenvectors of A are orthogonal to all columns of B .

Prediction of the cancer patients' response to their therapeutical treatment with non-linear forecasting techniques

Appendices

Observability: A pair of $\{C, A\}$ is observable if and only if none of the right eigenvectors of A are orthogonal to all rows of C .

Appendix D: SDRE – State-Dependent Riccati Equation

The State-dependent Riccati equation (SDRE), originally introduced in 1962 by Pearson [251], is a powerful tool used to solve optimal control problems for non-linear systems. By transforming the non-linear mathematical model into a pseudo-linear formulation, also referred as extended linear form, the SDRE method treats the transformed system as a sequence of LTI mathematical models. A suboptimal solution is then computed by solving the Riccati equation for each of the LTI models derived in each time step.

In general, a non-linear state-space mathematical model can be represented as:

$$\dot{\underline{x}} = f(\underline{x}(t)) + G(\underline{x}(t))u(t), \quad \underline{x}(0) = \underline{x}_0 \quad (\text{D.1})$$

where $\underline{x} \in \mathbb{R}^n$ is the state vector and $u \in \mathbb{R}^m$ is the input vector. In several cases, the above equation can be written in the pseudo-linear form:

$$\dot{\underline{x}} = A(\underline{x})\underline{x} + B(\underline{x})u \quad (\text{D.2})$$

where $f(\underline{x}) = A(\underline{x})\underline{x}$ and $G(\underline{x}) = B(\underline{x})$, with $A(\underline{x}) \in \mathbb{R}^{n \times n}$ and $B(\underline{x}) \in \mathbb{R}^{n \times m}$ where $B(\underline{x}) \neq 0 \forall \underline{x}$. $A(\underline{x})$ and $B(\underline{x})$ matrices are called state-dependent coefficient (SDC) matrices and the (D.2) is said to be represented in SDC form.

If the non-linear system of (D.1) has an equilibrium point at the origin, so that $f(0) = 0$, then f can be parameterized as $A(\underline{x})\underline{x}$ and the LQR method can be used. There are many alternative parameterizations to choose from when constructing the SDC matrices, but the one which will be chosen must ensure point wise controllability for $\forall \underline{x}$, to apply the SDRE control law. This can be achieved if the state-dependent controllability matrix M_c has full rank (i.e., $\text{rank}(M_c) = n$) for the time segment where the control is applied.

$$M_c = [B(\underline{x}) \quad A(\underline{x})B(\underline{x}) \quad \dots \quad A^{n-2}(\underline{x})B(\underline{x})A^{n-1}(\underline{x})B(\underline{x})] \quad (\text{D.3})$$

SDRE attempts to determine (using LQR) the sub-optimal controller for the state space model (D.2) driving all states to zero by minimizing a cost function J_{SDRE} :

$$J_{SDRE} = \frac{1}{2} \int_0^{\infty} (\underline{x}^T Q(\underline{x}) \underline{x} + u^T R(\underline{x}) u) dt, \quad (D.4)$$

where $Q(\underline{x}) \in \mathbb{R}^{n \times n}$ and $R(\underline{x}) \in \mathbb{R}^{m \times m}$ are state-dependent matrices and determine the weight for each state and the control input, thus $Q(\underline{x}) \geq 0$ and $R(\underline{x}) \geq 0$ for $\forall x$ [192].

When the control is applied, if it is unbounded, the cost function J is minimized using the state-feedback controller:

$$u(\underline{x}) = -R^{-1}(\underline{x})B^T(\underline{x})P(\underline{x})\underline{x} \triangleq -K(\underline{x})\underline{x}, \quad (D.5)$$

where the term

$$K(\underline{x}) = R^{-1}(\underline{x})B^T(\underline{x})P(\underline{x}) \quad (D.6)$$

is referred to as feedback gain matrix and $P(\underline{x}) \in \mathbb{R}^{n \times n}$ is a symmetric, positive definite matrix and the unique solution of the algebraic SDRE:

$$A^T(\underline{x})P(\underline{x}) + P(\underline{x})A(\underline{x}) - P(\underline{x})B(\underline{x})R^{-1}(\underline{x})B^T(\underline{x})P(\underline{x}) + Q(\underline{x}) = 0. \quad (D.7)$$

The dynamics of the pseudo-linearized closed-loop non-linear state mathematical model (D.2) are now described as:

$$\dot{\underline{x}} = (A(\underline{x}) - B(\underline{x})K(\underline{x}))\underline{x}. \quad (D.8)$$

The sub-optimal control input for the state space mathematical model (D.2) in the case of a bounded control represented by:

$$u_{bound}(\underline{x}) = \min(\max(u, u_{min}), u_{max}), \quad (D.9)$$

with u_{min} and u_{max} being the lower and upper bounds.

The above procedure (i.e., the SDRE control law computations) is illustrated by the flowchart in Figure D.1.

D.1 SDC parameterization

SDC parameterization or extended linearization is the process of turning a system of non-linear equations to a linear-like (pseudo-linear) form which includes SDC matrices.

In the scalar case, the SDC parameterization of the function f as $A(\underline{x})\underline{x}$ is unique for every $\underline{x} \neq 0$ and it is obtained as:

$$A(\underline{x}) = \frac{f(\underline{x})}{\underline{x}}. \quad (D.10)$$

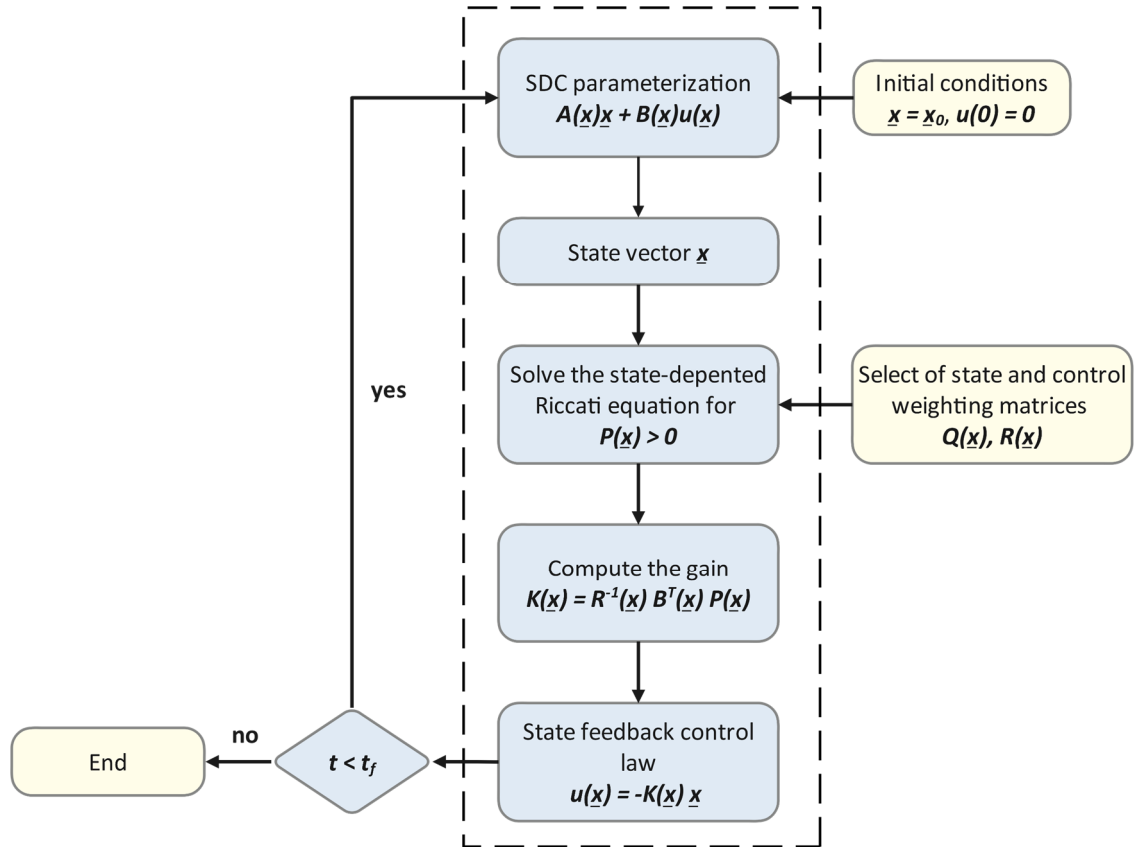


Figure D.1. Flowchart of the SDRE control law computations.

On the other hand, i.e., in multivariate systems, SDC parameterization is not unique and there is an infinite number of them, providing flexibility in the design which potentially could potentially improve the performance of the controller. Using a vector θ of free design parameters, $\theta_i \in \mathbb{R}^n$ with $i \in N$ it is possible to preserve the dependency of terms that contain multiple states (more than 2).

For any vector θ let:

$$A(\underline{x}, \theta_i) = \theta_i A_1(\underline{x}) + (1 - \theta_i) A_2(\underline{x}) \quad (D.11)$$

to represent an infinite number of SDC parameterizations where $A_1(\underline{x})$ and $A_2(\underline{x})$ are two distinct SDC matrices, with $\theta_i \in \mathbb{R}^n$. A rule of thumb through which a good

parameterization of $f(\underline{x})$ can be acquired is by observing the pointwise stability of $(A(\underline{x}), B(\underline{x}))$. More specifically, this can be achieved by maximizing the pointwise controllable and observable spaces of the candidate parameterizations [252]. θ 's and the corresponding SDC parameterizations which give high absolute values of the $\det(M_c)$ can be selected and used in the design process. According to Cimen [252], the selection of this vector θ affects not only the optimality and the stability of the system, but also its flexibility and robustness. More details about this are included in [252].

D.2 Non-affine control

Some control problems involve systems that exhibit nonlinearity in the control input u . This nonlinearity can arise due to constraints, such as hard bounds on the control. When the input cannot be expressed as a linear combination of the system state variables and their derivatives, it becomes challenging to design a control strategy that can properly regulate the system's behavior. These systems are non-affine (non-linear) in the control inputs and can be expressed mathematically as:

$$\dot{\underline{x}} = f(\underline{x}) + g(\underline{x}, u). \quad (\text{D.12})$$

Systems of (D.12) can be brought to the SDRE standard form of (D.1) by introducing integral control [252], [253]:

$$\dot{u} = Cu + D\tilde{u}. \quad (\text{D.13})$$

In the simplest case it is assumed that $C = 0$ and $D = I$, which results in $\dot{u} = \tilde{u}$.

By treating the control input u as a new state variable that is added to the system (D.12), an extended form of the system can be created:

$$\begin{bmatrix} \dot{\underline{x}} \\ \dot{u} \end{bmatrix} = \begin{bmatrix} f(\underline{x}) + g(\underline{x}, u) \\ Cu \end{bmatrix} + \begin{bmatrix} 0 \\ D \end{bmatrix} \tilde{u} \quad (\text{D.14})$$

where \tilde{u} is the pseudo-control input of the augmented system and the actual control input u is an augmented state. Such system conforms to the required SDRE structure, being affine (i.e., linear) in the pseudo-control input \tilde{u} .

D.3 Selection of the Q and R weighting matrices

In most control designs that are based on LQC, weighting (or penalty) matrices Q (i.e., the state weighting matrix) and R (i.e., the control weighting matrix) are design parameters. This means that their values affect the quality of the control design and subsequently the system's performance. Thus, their values need to be chosen carefully. For example, selecting a large value for R it means that the system has to be stabilized with less effort. In reverse, a small value for R means a smaller penalty on the control signal. In the first case an "expensive" control strategy is followed, while in the second case a "cheap" control strategy is applied. Similarly, selecting a large value for Q means that the changes in the system's states will happen faster as they approach to zero. It is important to note that both matrices are real-symmetric, with Q being positive semi-definite and R positive definite in nature. Usually, Q and R are chosen to be diagonal matrices, with the simplest choice to be:

$$Q = I, \quad R = \rho I, \quad (\text{D.15})$$

where ρ is a constant value. However, the selection of Q and R matrices is not unique and there are many combinations that can ensure the stability of the system and optimal closed-loop performance. Commonly, they are selected through trial-and-error, but this can sometimes be time-consuming and therefore techniques such as the one proposed by Pouliezios [242] and Bryson (Bryson's rule) [254] can be useful in this process. According to this rule, Q and R matrices can be selected as diagonal with values for the diagonal elements calculated as:

$$Q_{ii} = \frac{1}{\text{maximum acceptable value of } x_i^2}, \quad i = 1, 2, \dots, l \quad (\text{D.16})$$

$$R_{jj} = \frac{1}{\text{maximum acceptable value of } u_j^2}, \quad j = 1, 2, \dots, k \quad (\text{D.17})$$

The variables that appear in the performance criterion J of the linear or non-linear optimal regulation (discrete or continuous) are scaled to ensure that the maximum value of each term does not exceed one. Even though this rule can provide good results, it is often used as a starting point towards obtaining the pair of Q and R that results in the desired properties for the closed-loop system. Other methods are described in [255]–

Prediction of the cancer patients' response to their therapeutical treatment with non-linear forecasting techniques

Appendices

[258]. Another maybe useful methodology for forming a state-dependent weighting matrix Q in order to find an optimal control solution is proposed by Cloutier *et al.* [259]. However, the application of this methodology it may be difficult for complex systems.

Appendix E: State-space realization in control systems

E.1 Definition and representation

State-space realization offers a matrix-based framework to capture the dynamics of linear time-invariant (LTI) systems. This representation is particularly apt for multi-input, multi-output systems and for contexts where the system's internal dynamics are of interest alongside its input-output behavior.

For a given discrete-time LTI system, the state-space realization can be represented as:

$$\begin{aligned}x[k + 1] &= Ax[k] + Bu[k] \\y[k] &= Cx[k] + Du[k]\end{aligned}\tag{E.1}$$

where $x[k]$ is the state vector at the time instant k , capturing the system's internal states, $u[k]$ denotes the input to the system and $y[k]$ represents the system output at time k . A, B, C and D are matrices that dictate the relationships between the states, inputs, and outputs of the system.

E.2 Transfer function relationship

The relationship between the discrete-time system's state-space representation and its transfer function can be established using the Z-transform. A system with a transfer matrix $H(z)$ has its relationship with state-space matrices A, B, C , and D described as:

$$H(z) = C(zI - A)^{-1}B + D.\tag{E.2}$$

This equation is obtained by applying the Z-transform to the state-space equations and expressing the system's output transform $Y(z)$ as a function of its input transform $U(z)$.

E.3 Minimal Realization

There are an infinite number of possible state-space realizations of any given system, i.e., multiple sets of matrices A, B, C and D can represent the same input-output behavior [241]. However, not all realizations are equally efficient in capturing the system dynamics. A minimal realization refers to the representation where matrix A has the smallest possible dimension while retaining the system's input-output behavior. Such a realization is compact and often preferred for analysis and control purposes, as it eliminates redundant states that do not influence the system's observable behavior. In

essence, a system realization A, B, C, D is termed minimal if there isn't another realization A', B', C', D' such that A' has fewer dimensions than A , but both representations convey identical input-output dynamics.

Within the realm of discrete-time state-space realizations, certain minimal realizations hold particular significance due to their structured representation. These are termed as canonical forms [241]. Canonical forms not only represent the system in its minimal state but also structure the matrices in specific patterns that facilitate certain types of analysis and system manipulations. The observable and controllable canonical forms stand out as standardized system representations that emphasize system observability and controllability, respectively. The controllable canonical form is structured such that its matrices provide clear insight into the system's controllability, ensuring that the system's states can be driven to desired values using suitable inputs. On the other hand, the observable canonical form is tailored to illuminate the system's observability, indicating the system's ability to have its internal states estimated purely based on its outputs [241].

Let a single-input single-output (SISO) system with a transfer function $G(z)$:

$$G(z) = \frac{W(z)}{U(z)} = \frac{b_1 z^{-1} + b_2 z^{-2} + \dots + b_n z^{-n}}{1 - a_1 z^{-1} - a_2 z^{-2} - \dots - a_n z^{-n}} \quad (\text{E.3})$$

The observable canonical form ensures the observability of the derived system. Its state-space representation of (8.1) in canonical form is described by:

$$A_{obs} = \begin{bmatrix} -a_1 & 1 & \dots & \dots & 0 \\ -a_2 & 0 & 1 & \dots & 0 \\ \vdots & \vdots & \vdots & \ddots & 0 \\ -a_{n-1} & 0 & 0 & \dots & 1 \\ -a_n & 0 & 0 & \dots & 0 \end{bmatrix}, \quad B_{obs} = \begin{bmatrix} b_1 \\ b_2 \\ \vdots \\ b_{n-1} \\ b_n \end{bmatrix}, \quad C_{obs} = [1 \ 0 \ \dots \ 0], \quad D_{obs} = 0 \quad (\text{E.4})$$

In the case of multiple-input multiple-output (MIMO) systems, where there are multiple transfer functions the realization can be found trivially by the realization of each element [260].

Let a 2-by-2 system, i.e., two inputs and two outputs. The transfer function of such system is described by a 2-by-2 matrix:

Prediction of the cancer patients' response to their therapeutical treatment with non-linear forecasting techniques

Appendices

$$G_M(z) = \begin{bmatrix} G_1(z) & G_2(z) \\ G_3(z) & G_4(z) \end{bmatrix} \quad (\text{E.5})$$

where $G_i(z) = C_i(zI - A_i)^{-1}B_i + D_i$, for $i = 1,2,3,4$.

The state realization of the system is given by the following matrices:

$$\begin{aligned} A_M &= \begin{bmatrix} A_1 & 0 & 0 & 0 \\ 0 & A_2 & 0 & 0 \\ 0 & 0 & A_3 & 0 \\ 0 & 0 & 0 & A_4 \end{bmatrix}, & B_M &= \begin{bmatrix} B_1 & 0 \\ 0 & B_2 \\ B_3 & 0 \\ 0 & B_4 \end{bmatrix} \\ C_M &= \begin{bmatrix} C_1 & C_2 & 0 & 0 \\ 0 & 0 & C_3 & C_4 \end{bmatrix}, & D_M &= \begin{bmatrix} D_1 & D_2 \\ D_3 & D_4 \end{bmatrix}. \end{aligned} \quad (\text{E.6})$$

where A_i, B_i, C_i and D_i are the realization matrices of each transfer function G_i , for $i = 1,2,3,4$.

These canonical forms not only simplify system representations but also streamline the tasks of analysis, controller design, and observer synthesis by focusing on fundamental system properties. More information can be found on [241] and [260].